The role of *STX6* in sporadic Creutzfeldt-Jakob disease and related neurodegenerative diseases

Emma Louise Jones

Doctor of Philosophy in
Neurodegenerative Diseases

MRC Prion Unit at UCL, Institute of Prion Diseases
University College London

I, Emma Louise Jones, confirm that the work presented in this thesis is my own. Where information has been derived from other sources, I confirm that this has been indicated in the thesis.

Abstract

Sporadic Creutzfeldt-Jakob disease (sCJD) is the most common human prion disease, in which the cellular prion protein (PrP^C) appears to spontaneously misfold and aggregate into a disease-associated form leading to invariably fatal neurodegeneration. Although there is clear genetic control in sCJD, no loci except *PRNP* (encoding PrP^C) have previously been consistently significant in genetic studies. Through international collaboration a two-stage genome wide association study (GWAS) was conducted for sCJD risk analysing a total of 5,208 cases and 511,585 matched control individuals from 11 countries. This thesis describes the first replicated association of two novel loci alongside *PRNP*, with variants in or near *STX6* (encoding syntaxin-6) and *GAL3ST1* (encoding cerebroside sulfotransferase), as conferring risk for sCJD at genome-wide significance in populations with European ancestry. With a focus hereafter on elucidating the casual gene and functional mechanisms at the *STX6* locus, fine-mapping and integration of publically-available expression quantitative trait loci databases provides evidence for increased *STX6* expression in the caudate and putamen as driving this association. RNA silencing in immortalised cell lines and CRISPR-mediated gene knockout in human iPS-derived cortical neurons and mice were used to model the biological mechanism of syntaxin-6 in prion propagation and cell biology with a particular focus on its role in the endolysosomal system. Knockout and hemizygous expression of *Stx6* in C57BL/6 mice modestly extends survival time following inoculation with mouse-adapted scrapie prion strains RML and ME7, supporting the genetic association of *STX6* expression in patients. Identification of non-*PRNP* loci associated with sCJD risk provides new insight into disease mechanisms and offers potential additional targets for therapeutic intervention. Furthermore the previous implication of *STX6* in related neurodegenerative diseases such as the tauopathy progressive supranuclear palsy indicates a possible shared role of syntaxin-6 in the pathobiology of other “prion-like” proteins and disorders.

Impact statement

Prion diseases are a class of neurodegenerative diseases, of which sporadic Creutzfeldt-Jakob disease (sCJD) is the most common, all associated with the misfolding and aggregation of the cellular prion protein into disease-associated forms. Like nearly all others, prion diseases are invariably fatal due to the lack of effective therapeutic treatments available to modify or halt progression. The *PRNP* gene encoding the cellular prion protein is a key genetic determinant of all disease subtypes, however evidence suggests there remains undefined heritable risk factors. Furthermore it is not yet clear whether targeting the prion protein will prove to be an effective therapeutic strategy, and so elucidation of these other genetic modifiers is essential.

This thesis describes the replicable identification of non-*PRNP* genetic risk factors for sCJD through a genome-wide association study (GWAS). Computational post-GWAS analysis restricts putative causal genes at these sites and highlights likely mechanisms driving this association, however to secure these hypotheses, exploration of the role of one of these genes, *STX6*, in vitro, in cell culture models and in vivo provides critical biological evidence to validate the pathogenic association of this gene.

Through classifying unrecognised genes as driving risk for sCJD, this thesis has unveiled new pathways which have not been previously explicitly associated with the disease, including aspects of vesicular protein trafficking and sphingolipid metabolism. This opens up new avenues to be exploited by researchers, with secure genetic association providing implicitly causal evidence and minimising time lost on erroneous leads. Through sharing these results in both publication and at international research conferences, as well as providing open access to datasets online, these new risk factors are now evident to the wider research field accelerating relevant discovery.

The causality of the associations identified in this study, as well as the evidence provided for a protective effect of inhibiting *STX6* in a mouse model of the disease, supports targeting these pathways in clinical treatment for prion diseases, providing an alternative to perturbing the prion protein itself for which success is not guaranteed. Targeting these additional risk factors in combination

with *PRNP* may also increase efficacy or reduce vulnerability to resistance during treatment. Publication of this research in accessible forms, including blogs and podcasts, aimed to impart this hope on individuals suffering as a result of sCJD and other prion diseases.

Finally, increasingly in neurodegenerative disease research, parallels are being drawn between prion diseases and other diseases associated with aberrant protein misfolding. The same genetic association at *STX6* described in this thesis is shared with related neurodegenerative disease, progressive supranuclear palsy, with additional evidence implicating the same signal in Alzheimer's disease. Therefore both the work and models developed to explore the role of *STX6* described in this thesis, as well as the support its discovery lends to a common mechanism in these related diseases, will have broad-ranging applications for the wider neurodegeneration research field.

Table of contents

List of tables

List of figures

List of abbreviations

AD	Alzheimer's disease
ALS	Amyotrophic lateral sclerosis
APP	Amyloid precursor protein
ASCA	Automated scrapie cell assay
BMP	Bone morphogenic protein
BSE	Bovine spongiform encephalopathy
CAA	Cerebral amyloid angiopathy
CAD	Cath.a-differentiated
CADD	Combined annotation dependent depletion
CAVIAR	Causal variants identification in associated regions
CDS	Coding sequence
CFP	Cyan fluorescent protein
CFTR	Cystic fibrosis transmembrane conductance regulator
CHIP	Chromatin immunoprecipitation
CJD	Creutzfeldt-Jakob disease
CLPP	Colocalisation posterior probability
CNS	Central nervous system
CNV	Copy number variant
COG	Conserved oligomeric Golgi complex
CPP	Causal posterior probability
CRISPR	Clustered regularly interspaced short palindromic repeats
CST	Cerebroside sulfotransferase
CWD	Chronic wasting disease
DHS	DNase hypersensitivity site
DRM	Detergent resistant membrane
EARP	Endosome-associated recycling protein complex
EE	Early endosome
EGFR	Epidermal growth factor receptor

ELISA	Enzyme-linked immunosorbent assay
ELISPOT	Enzyme-linked immunospot
EM	Electron microscopy
eQTL	Expression quantitative trait loci
ER	Endoplasmic reticulum
ES	Embryonic stem
FBS	Foetal bovine serum
fCJD	Familial Creutzfeldt-Jakob disease
FFI	Fatal familial insomnia
FRET	Fluorescence resonance energy transfer
FTD	Frontotemporal dementia
FUMA	Functional mapping and annotation of genome-wide association studies
GARP	Golgi-associated retrograde protein complex
gDNA	Genomic DNA
GPI	Glycosylphosphatidylinositol
GSS	Gerstmann-Sträussler-Scheinker disease
GWAS	Genome wide association study
HD	Huntington's disease
HDR	Homology directed repair
ICE	Inference of CRISPR edits
INDEL	Insertion and deletion
IPD	Inherited prion disease
iPK1	RML-infected PK1
iPS	Induced pluripotent stem
KO	Knockout
LD	Linkage disequilibrium
LE	Late endosome
MAF	Minor allele frequency
MRI	Magnetic resonance imaging

MVB	Multivesicular body
NCAM	Neurite cell adhesion molecule
NGF	Nerve growth factor
NHEJ	Non-homologous end joining
NIM	Neural induction media
NMR	Nuclear magnetic resonance
NSF	N-ethylmaleimide sensitive fusion protein
OE	Overexpression
OR	Odds ratio
ORI	Octapeptide repeat insertion
PAM	Protospacer adjacent motif
PD	Parkinson's disease
PK	Proteinase K
PM	Plasma membrane
PMCA	Protein misfolding cyclic amplification
PPS	Pentosan polysulfate
PrP	Prion protein
PrP^{C}	Cellular prion protein
PrP^{Sc}	Scrapie-associated prion protein
PSP	Progressive supranuclear palsy
PWAS	Proteome wide association study
QC	Quality control
QTL	Quantitative trait loci
RE	Recycling endosome
RFP	Red fluorescent protein
RML	Rocky mountain laboratories
RNP	Ribonucleoprotein
RT	Reverse transcription
SCA	Scrapie cell assay

sCJD	Sporadic Creutzfeldt-Jakob disease
SMB	Scrapie-infected mouse brain cells
SNAP	Soluble NSF attachment protein
SNARE	SNAP receptor
SNP	Single nucleotide polymorphism
SNV	Single nucleotide variant
STX6	Syntaxin-6
TCIU	Tissue culture infectious unit
TGN	Trans Golgi network
TM	Transmembrane
TSE	Transmissible spongiform encephalopathy
UTR	Untranslated region
vCJD	Variant Creutzfeldt-Jakob disease
VEP	Variant effect predictor
VPSP	Variably protease-sensitive prionopathy
WAT	White adipose tissue
WGS	Whole genome sequencing
WT	Wildtype
YFP	Yellow fluorescent protein

1. Introduction

1.1. History of prion diseases

It is thought the description of an unusual disease in sheep as early as the 18th century is the first recorded account of a prion disease, which was later designated “scrapie” due to characteristic itching (Stockman, 1913). With increased understanding of biological concepts over the coming centuries the nature of this disease was highly debated with both genetic and infectious origins proposed. In 1936, Cuillé and Chelle first clearly demonstrated the transmissibility of the disease through intraocular inoculation of healthy sheep and goats, classifying scrapie as the prototypical transmissible spongiform encephalopathy (TSE), although the identity of the infectious agent at this stage was unclear (Cuillé & Chelle, 1936).

Nearly 200 years after scrapie was first identified, neurologists Hans Creutzfeldt and Alons Jakob independently described a rapidly progressive neurological disorder in humans, later classified by Walther Spielmeyer as Creutzfeldt-Jakob disease (CJD) (Creutzfeldt, 1920; Jakob, 1921). Some 40 years after this, the first cases were detailed in the literature of another neurological disorder affecting the Fore ethnic group in the highlands of Papua New Guinea called kuru (Gajdusek & Zigas, 1959). In 1959, Hadlow, through a chance visit to an exhibition at the Wellcome Medical Museum in London, started to draw similarities between kuru and scrapie, followed shortly after by Klatzo for kuru and CJD (Hadlow, 1959; Klatzo, Gajdusek, & Zigas, 1959). These observations led to landmark inoculation studies of both kuru and CJD into primates, similar to what was performed decades before for scrapie, definitively demonstrating the transmissible nature of these diseases (Gajdusek, Gibbs, & Alpers, 1966; Gibbs et al., 1968).

Despite the certified infectivity of these TSEs, the exact nature of the infectious agent of was highly contended for decades to follow. Increased scientific awareness of viral replication prompted initial hypotheses. In 1954, Sigurdsson first coined the term ‘slow virus’ to describe the scrapie agent, due to its clear transmissibility (thought to be of viral origin) but long incubation times (Sigurdsson, 1954). This however failed to consider earlier experiments by

Gordon a decade prior demonstrating the resistance of the scrapie agent to formalin inactivation (during vaccine preparation), indicating the infectious agent was distinct from traditional viruses (Gordon, 1946). Nonetheless this remained the primary hypothesis for around a decade until the latter half of the 20th century when a number of studies started to again question the viral origin, due to unsuccessful attempts to remove infectivity with other techniques including radiation, extreme heat and pressure and chemical agents, known to inactivate viruses, or robustly identify nucleic acids in these preparations. Alper was the first to conclude in 1967 that the infectious agent may be devoid of nucleic acid (Alper, Cramp, Haig, & Clarke, 1967). In the same year Griffith made the first proposal of a proteinaceous agent driving infectivity (Griffith, 1967), leading to Prusiner coining the term “prion” (derived from proteinaceous infectious particle) in 1982 (Prusiner, 1982).

Attempts to purify prions through enriching for infectivity in scrapie-infected brain homogenate identified a 27-30 kDa protease-resistant sialoglycoprotein specific to infected brains termed the prion protein (PrP^{27-30}), which could be inactivated by agents specific to protein denaturation (Bolton, McKinley, & Prusiner, 1982; Prusiner, Bolton, et al., 1982). It was initially assumed this PrP protein must be encoded by viral nucleic acids however, through deduction of the mRNA sequence, Chesebro and Race identified transcripts in both infected and uninfected animals indicating PrP was actually a normal cellular component (Chesebro et al., 1985). The host gene, *Prnp*, was identified in the same year by Prusiner and Weissman but was not associated with infectivity, supporting the protein-only nature of the infectious agent (Oesch et al., 1985). Analysis of the primary sequence of the normal protease-sensitive gene product of *Prnp* (later termed cellular PrP or PrP^{C}) and the scrapie-associated PrP (termed PrP^{Sc}) concluded both were derived from the same protein via post-transcriptional processes (Basler et al., 1986). The *Prnp* gene was clearly important for disease however, as early studies identifying a chromosomal region associated with disease incubation time in mice were mapped to the same region (Carlson et al., 1986; Dickinson, Meikle, & Fraser, 1968). Generation of *Prnp* knockout mice by Bueler and colleagues in 1993 confirmed this gene is in fact essential for pathogenesis (Bueler et al., 1993).

Prion diseases are now understood to be invariably fatal neurodegenerative diseases of both humans and animals, characterised by the templated conversion of the cellular prion protein (PrP^{C}) into a number of disease-associated forms, including proteinase K (PK)-resistant scrapie-associated PrP^{Sc}. In humans, prion diseases can be sporadic, acquired or inherited, all characterised by a triad of neuropathological impairments of distinct spongiform vacuolation accompanied by neuronal loss and astrocyte proliferation (Budka et al., 1995). A number of animal prion diseases have also been characterised including scrapie in sheep and goats, chronic wasting disease (CWD) in cervids and bovine spongiform encephalopathy (BSE) in cattle.

1.2. Types of prion disease

1.2.1. Animal prion diseases

As previously mentioned, scrapie has been recorded in Europe for over 200 years. It is therefore often described as the “prototypical” prion disease affecting farmed sheep and goats (McGowan, 1922). Multiple strains of typical scrapie have been described, most commonly presenting with the same intense pruritus as initially reported (prion strains discussed later in section 1.5.3) (Pattison & Millson, 1961). More recently, atypical forms have also been observed, clinically characterised instead by distinct ataxia and incoordination (Benestad et al., 2003).

Since the identification of scrapie, a number of other animal prion diseases have also been recognised, although predominantly still in farmed livestock. Classical BSE was first diagnosed in cattle in 1986 and rapidly led to an epidemic in the UK with over 35,000 new formally diagnosed cases per year at its peak, which is probably a marked underestimate of the true number of cases (Anderson et al., 1996; Wilesmith, Wells, Cranwell, & Ryan, 1988). Surveillance testing has since identified two additional distinct BSE strains denoted as H- and L-type (Biacabe, Laplanche, Ryder, & Baron, 2004; Casalone et al., 2004). Dietary transmission to humans led to the subsequent well-described variant CJD (vCJD) epidemic (described later in section 1.2.2.3). Interestingly, incidence of two other animal prion diseases also overlapped with the BSE epidemic: feline spongiform encephalopathy (FSE) affecting domestic and captive wild cats, and exotic

ungulate encephalopathy (EUE) affecting exotic zoo animals in the Bovidae family (Kirkwood & Cunningham, 1994); investigation of strain properties implicates zoonotic transmission from contaminated feed similar to vCJD (Fraser et al., 1994; Jeffrey, Scott, Williams, & Fraser, 1992). Other prion diseases in captive animals include transmissible mink encephalopathy (TME) in farmed mink and more recently described prion disease in dromedary camel livestock (Babelhadj et al., 2018; Marsh & Hadlow, 1992).

CWD is the only prion disease which has been described in free-ranging animals, affecting both wild and farmed members of the Cervidae family (Williams & Young, 1980). It was first documented in North America but more recently described in South Korea and some countries in the Scandinavian Peninsula. Due to the common consumption of wild deer in some of these regions, CWD poses some public health concerns, however studies have so far suggest the zoonotic potential of this prion disease is limited with no evidence for CWD being able to seed conversion of human PrP either in vitro or in transgenic mice (Kurt, Telling, Zabel, & Hoover, 2009; Sandberg et al., 2010).

1.2.2. Human prion diseases

1.2.2.1. Sporadic

Accounting for approximately 85% of all incidence, sCJD is the most common human prion disease in most populations, with an approximate annual mortality rate of 1-2 deaths per million people (Ladogana et al., 2005). The median age of onset of sCJD is in the seventh decade of life when patients classically present with rapidly progressive dementia (median disease duration 5 months) accompanied by various other neurologic symptoms including myoclonus, ataxia and visual problems (Collins et al., 2006), however there is considerable variation in clinical presentation and disease progression. This can be partially explained by genotype at a common *PRNP* variant at codon 129 (see section 1.4.2) and related PrP^{Sc} subtype (see section 1.5.3). For example, patients homozygous for methionine at codon 129 and type 1 PrP^{Sc} profile generally have the shortest disease duration (Hill et al., 2003).

Less common sporadic prion diseases have been described in addition to sCJD. This includes the most recently identified human prion disease, variably protease-

sensitive prionopathy (VPSPr), characterised by partial PrP^{Sc} protease-sensitivity and a distinct PrP^{Sc} subtype to sCJD (Gambetti et al., 2008). Due to the novelty of this disease, the clinical criteria are less well defined, but has generally been diagnosed in elderly populations with a longer disease duration than sCJD. A small number of cases of sporadic fatal insomnia have also been identified which share many clinical and pathological features with the inherited prion disease (IPD) fatal familial insomnia (FFI; described in the next section) without an identifiable genetic cause (Mastrianni et al., 1999).

For sporadic prion diseases there is no known genetic aetiology or an epidemiological link so are thought to be caused by either a stochastic misfolding event of PrP^{C} or somatic *PRNP* mutation in single cells, although an unidentified iatrogenic source cannot be ruled out.

1.2.2.2. Inherited

Inherited or genetic prion diseases account for 10-15% of annual prion disease in most populations, and are all caused by highly penetrant autosomal dominant mutations in the *PRNP* gene (Ladogana et al., 2005). To date over 60 variants have been identified in *PRNP*, a number of which cause IPD (Figure 1) (Mead, Lloyd, & Collinge, 2019). The frequency and distribution of these varies among populations, for example the V210I mutation is relatively prevalent in European populations but rarely reported in South East Asian populations (C. Chen & Dong, 2016). The age of onset and clinical presentation can be highly variable even within families but generally presents younger than sCJD with often longer disease duration times (Kovacs et al., 2005).

IPDs are classified into three main groups based on clinical presentation and genetic aetiology: genetic CJD (gCJD), FFI and Gerstmann-Sträussler-Scheinker disease (GSS) (Budka et al., 1995; Ladogana & Kovacs, 2018). The largest group is gCJD, characterised by clinical and pathological features similar to sCJD, although again with a generally younger age of onset and longer duration. There are numerous mutations which cause gCJD with E200K being the most common (Kovacs et al., 2005), unlike FFI for which only a single haplotype containing the missense mutation D178N associated with methionine at codon 129 has been described (Medori et al., 1992). Patients with FFI are clinically dissimilar from

gCJD and sCJD characterised instead by severe insomnia and dysautomnia. GSS is also distinct, presenting with as slowly progressive cerebellar degeneration or parkinsonism and more variable neurologic symptoms.

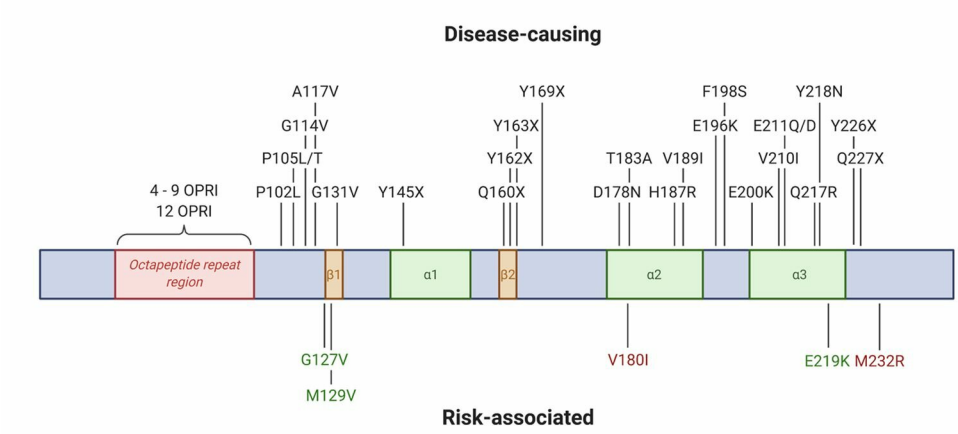

Figure 1: *PRNP* variants associated with IPDs or modifying prion disease risk. The coloured bar represents PrP^C and associated structural features including the octapeptide repeat domain (red), β-strands (orange) and α-helices (green). Definite disease-causing mutations (pathologically confirmed) are listed above and protective variants (green text) or risk factors (red text) listed below. Probable or possible disease-causing mutations not shown. Figure adapted from (Mead et al., 2019).

More recently a novel clinicopathologic phenotype has been described associated with the Y163X truncation mutation (Mead et al., 2013). These patients are unusually characterised with a more peripheral pathology including diarrhea, autonomic neuropathy, and a systemic PrP amyloidosis. Other stop codon mutations have also been attributed to hereditary prion cerebral amyloid angiopathy (Ghetti, Tagliavini, Takao, Bugiani, & Piccardo, 2003).

1.2.2.3. Acquired

Prion diseases appear unique in their ability to efficiently transmit neurodegeneration between organisms, especially between different species. vCJD was first identified in patients in the United Kingdom in 1996, quickly linked to cross-species transmission of BSE through infected meat products (Will et al., 1996). The subsequent epidemic peaked in 2000, with a total of 232 cases identified to date (Creutzfeldt-Jakob Disease International Surveillance Network, 2019). Generally vCJD is distinct from sCJD with a younger age of onset (median age 27 years) and longer disease duration (mean 14.5 months), usually presenting with psychiatric and/or sensory symptoms (Heath et al., 2010).

Although new diagnoses of vCJD are currently extremely rare, the high level of exposure in the population means it is likely that some individuals are harbouring sub-clinical vCJD prions, indicated by the description of abnormal PrP in the appendices of some asymptomatic individuals (Gill et al., 2020). Consequently, vCJD is still monitored as a public health concern especially due to historical long incubation times following exposure (up to decades) and the previously described transmission from infected blood transfusions to three individuals (Gill et al., 2020; Llewelyn et al., 2004). The risks of vCJD however are now currently thought to be minimal.

As previously mentioned, kuru was the first acquired prion disease to be described in humans, originally identified by Gadjusek within the Fore ethnic group in the highlands of Papua New Guinea (Collinge et al., 2006; Gajdusek & Zigas, 1959). This epidemic was driven by the mortuary practice of transumption, leading to increased prevalence of neurological disease characterised by cerebellar ataxia manifesting with tremors, choreiform and athetoid movements. Prohibition of this practice in the mid-1950s led to decline in incidence, however the last cases were not diagnosed until the beginning of the 21st century due to extended incubation periods that may have exceeded 50 years.

Transmission of prions between humans in the form of iatrogenic CJD (iCJD) was first described in 1974 in a patient who received cadaveric corneal transplant from a donor with sCJD (Duffy et al., 1974). Since then over 450 cases of iCJD have been identified, predominantly through historic treatments with either contaminated dura matter grafts (approximately 228 cases) or human cadaveric pituitary growth hormone (approximately 226 cases) (P. Brown et al., 2012). Other sources of transmission have included neurosurgical equipment and intracerebral electrodes. The incubation time and clinical presentation varies with source and route of transmission, with often long incubation times sometimes making attributing an iatrogenic cause difficult and perhaps leading to underestimates of iCJD prevalence.

1.3. Cellular prion protein

1.3.1. Structure

In humans, PrP^C is a 253 amino acid cell surface glycoprotein expressed in most tissues, with high expression in the peripheral and central nervous system (CNS), encoded by the gene *PRNP* on chromosome 20 (Sarnataro, Pepe, & Zurzolo, 2017). Both sequence and structure are highly conserved between mammals (Wopfner et al., 1999). The protein is predominantly α-helical and can be broadly divided into a C-terminal globular domain and a flexible unstructured N-terminal region, as well as an N-terminal signal peptide to direct co-translational translocation into the endoplasmic reticulum (ER) during synthesis (Figure 2) (Riek, Hornemann, Wider, Glockshuber, & Wuthrich, 1997).

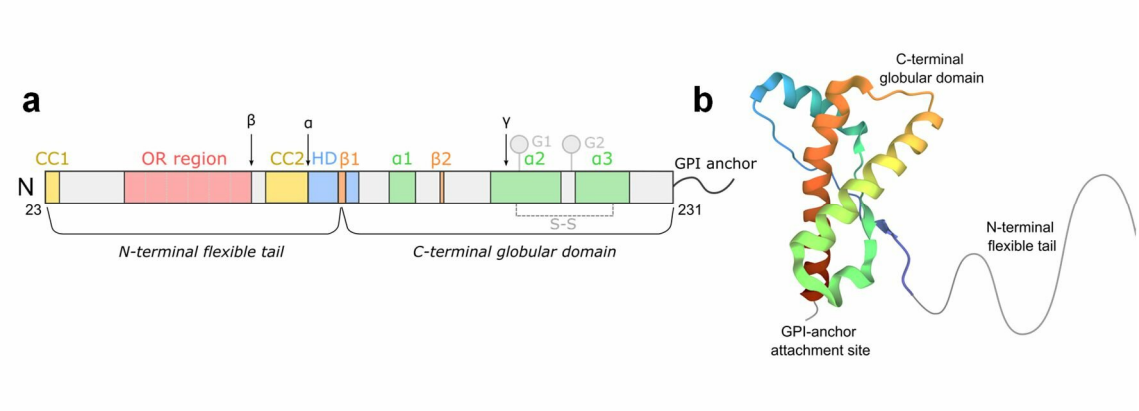

Figure 2: PrP^C structure comprising an α-helical C-terminal globular domain and a flexible N-terminal region.
PrP^C is a 253 amino acid protein (prior to cleavage of N- and C-terminal signal sequences, not shown). (**a**) Primary sequence shows two charged residue clusters (CC1, CC2), a series of octapeptide repeat (OR) sequences and a hydrophobic domain (HD) within the unstructured N-terminal region, and a structured C-terminal comprised of two β-sheets (β1-2) and three α-helices (α1-3) with a disulphide bond (S-S) linking helices 2 and 3, two N-linked glycosylation sites (G1-2) and a glycosylphosphatidylinositol (GPI) membrane anchor. Endoproteolytic processing occurs at three sites (α, β, γ). (**b**) Example X-ray crystal structure of human PrP^C demonstrating predominant α-helical fold, with position of N-terminal flexible tail and GPI-anchor attachment depicted. Structure determined by (S. Lee et al., 2010) obtained from the Protein Data Bank (rcsb.org) (Berman et al., 2000). Figure adapted from (Watts, Bourkas, & Arshad, 2018).

The structure of the globular domain has been studied extensively by X-ray crystallography and nuclear magnetic resonance (NMR) (Knaus et al., 2001; Riek et al., 1997; Zahn et al., 2000). This has consistently described three α-helices (denoted H1-H3) and two short anti-parallel β-sheets, with a critical disulphide

bond linking the H2 and H3 helices. This domain is post-translationally modified with N-linked glycosylation at two sites and addition of a glycosylphosphatidylinositol (GPI) membrane anchor to a signal peptide at the C-terminal (which is subsequently degraded). Glycosylation can occur on one or both sites allowing for three possible glycoforms of PrP^C.

Because of the highly flexible nature of the N-terminal region of PrP, structural information is currently lacking, however the primary amino acid sequence indicates two charged clusters (CC1 and CC2), a glycine-rich octapeptide repeat (OR) region and a hydrophobic domain. Despite its unstructured nature, this region of the protein is vital for function, with the N-terminal predicted to act as a "molecular sensor" for the protein with numerous interactors identified. These include divalent cations like copper (II) ions and other protein partners including oligomeric forms of amyloid-β and other neurodegenerative-disease associated proteins (discussed later in section 1.6.2) (Beland & Roucou, 2012).

PrP^C is processed by multiple endoproteolytic events as part of its normal metabolism, generating various protein fragments which are thought to have independent functions (Haigh & Collins, 2016). This occurs at two main sites termed α- and β-cleavage. The first of these falls within the hydrophobic domain and generates a C-terminal fragment, C1, which remains linked to the membrane, likely releasing the N1 N-terminal fragment into the extracellular space (S. G. Chen et al., 1995). Alternatively β-cleavage occurs at the end of the OR region to generate N2 and C2 fragments; this is generally thought to be a pathogenic process as it increases in frequency during disease and it preserves the likely amyloidogenic region to promote prion conversion. Interestingly, however, both the N1 and N2 fragments have been found to exhibit neuroprotective effects. A third γ-cleavage mechanism has also more recently been described occurring within the globular C-terminal domain, likely therefore to exert distinct functions to α- and β-cleavage fragments although these are yet to be characterised (Lewis et al., 2016). Finally shedding of PrP^C also occurs constitutively via cleavage at the GPI-anchor by metalloproteases, releasing the protein from the cell surface (Parkin, Watt, Turner, & Hooper, 2004).

1.3.2. Trafficking

Studying trafficking of PrP^C and prion aggregates is key to understanding disease biology, particularly due to the hypothesis that either a direct interaction between the cellular form and misfolded protein or via another co-factor underpins prion conversion and disease progression, likely to occur at some point during the normal cellular transport of the two proteins. Additionally, research indicates that the microenvironment of the proteins can contribute to effective prion conversion, something which varies substantially between different subcellular compartments.

1.3.2.1. Secretory pathway

Following synthesis, PrP^C is first translocated into the ER where glycosylation and addition of a GPI anchor occurs, as well as cleavage of the N- and C-terminal peptides (Sarnataro et al., 2017). After correctly folding, the protein is transported through the typical secretory pathway via the Golgi cisternae for further post-translational modifications of the glycosylation sites and GPI anchor, followed by translocation to the plasma membrane where the majority of steady-state PrP^C is located (Figure 3) (Caughey, Race, Ernst, Buchmeier, & Chesebro, 1989; Stahl, Borchelt, Hsiao, & Prusiner, 1987). Within the plasma membrane, the protein is localised specifically within detergent resistant membranes (DRMs) or lipid rafts in all cell types studied (Naslavsky, Stein, Yanai, Friedlander, & Taraboulos, 1997). Multiple lines of evidence indicate cholesterol and sphingolipid levels regulate PrP^C localisation to these domains, with impaired cholesterol synthesis in N2a and epithelial cells preventing association of PrP^C with these DRMs, possibly through preventing Golgi exit or ER maturation (Gilch, Kehler, & Schatzl, 2006; Sarnataro et al., 2004; Sarnataro et al., 2002). Furthermore, induction of ER stress in cell culture also perturbs PrP^C transport through the secretory pathway (Nunziante et al., 2011). Within neurons, PrP^C can be detected on cell surface membranes of all processes (although not in synaptic vesicles), again regulated by both cholesterol and sphingolipids, and undergoes both anterograde and retrograde transport within axons mediated by motor proteins kinesin-1 and cytoplasmic dynein (Encalada, Szpankowski, Xia, & Goldstein, 2011; Galvan, Camoletto, Dotti, Aguzzi, & Ledesma, 2005; Mironov et al., 2003).

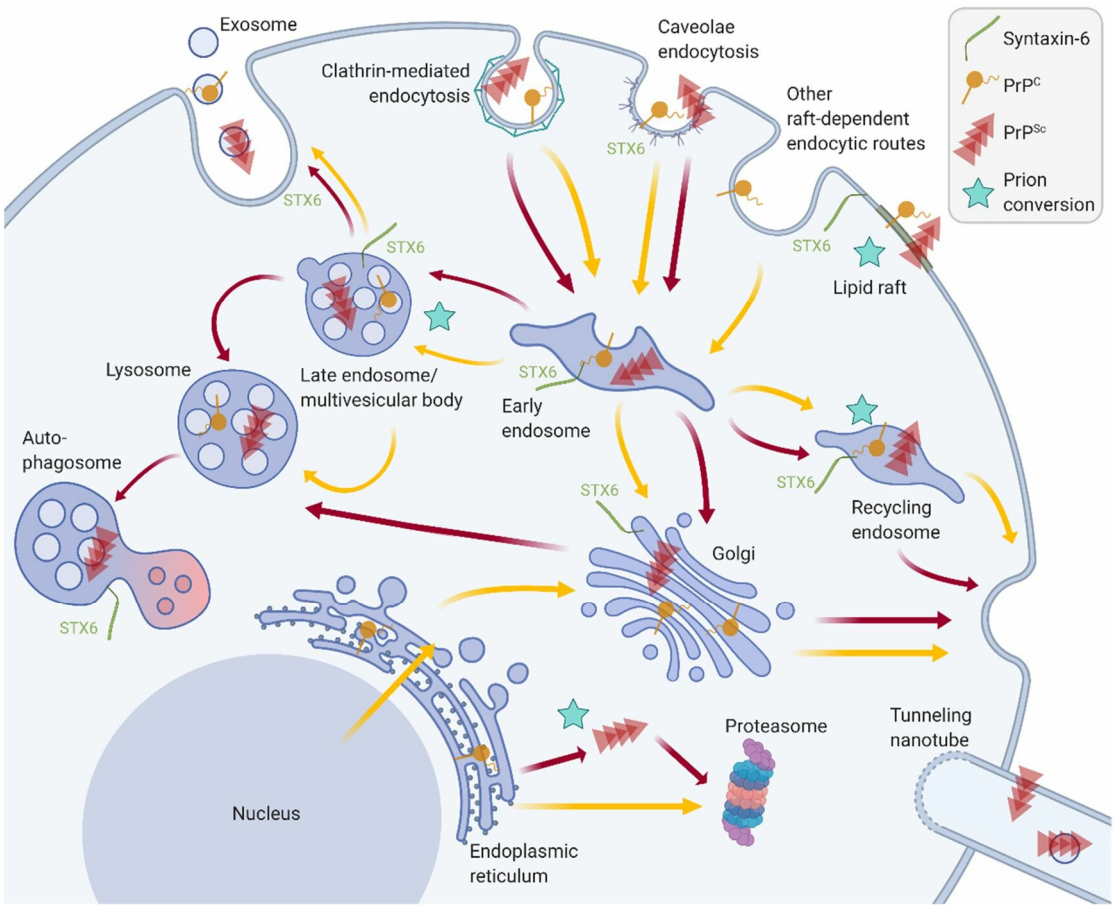

Figure 3: Trafficking of PrP^{Sc} and PrP^{C} through endocytic and secretory pathways and relationship with SNARE protein syntaxin-6.
Both PrP^{C} and PK-resistant aggregates (e.g. PrP^{Sc}) are constitutively trafficked between the plasma membrane (PM) and endocytic compartments in cell models. PrP^{C} (yellow arrows) is synthesised in the ER and trafficked through the Golgi to lipid rafts on the PM. Endocytosis of PrP^{C} occurs via clathrin-, caveolae- or other raft-dependent routes to early endosomes (EE) where it is either recycled back to the PM via retrograde transport through the trans-Golgi network (TGN) or via recycling endosomes (RE). PrP^{C} is alternatively trafficked to late endosomes (LE) and lysosomes for degradation. PrP^{Sc} is primarily formed on the PM (indicated by the star symbol) in association with lipid rafts before internalisation (red arrows) via caveolae- or clathrin-mediated endocytosis to EE. It can then be recycled to the PM via the TGN or RE (where additional conversion may occur), or from TGN or EE to LE/multivesicular body (MVB) (another potential conversion site) and lysosomes and/or autophagosomes. Retrotranslocation from the ER to the cytosol during synthesis may also promote aggregation in the proteasome. Cell-to-cell PrP^{Sc} transmission has been demonstrated through exosomes and tunneling nanotubes. Syntaxin-6 (STX6) is primarily localised to the TGN and EE but has also been detected on PM, RE, LE and autophagosomes. It is further implicated indirectly in exosomal transport and caveolae-mediated endocytosis. Figure generated with biorender.com.

1.3.2.2. Endocytosis

Following secretion to the membrane, the transport of PrP^C through the endolysosomal system has been widely studied and many aspects are still under debate. Multiple different pathways and regulators have been described: in steady-state, PrP^C is most abundant on plasma membranes, but is also detected within a number of membrane bound organelles including the Golgi, early and recycling endosomes, late endosomes, lysosomes and mitochondria indicating numerous potential routes through the cell (prion trafficking summarised in Figure 3) (Faris et al., 2017; Marijanovic, Caputo, Campana, & Zurzolo, 2009). This subcellular localisation appears partially mediated by protein composition including glycosylation state, GPI anchor content and pathological mutations, with abnormal proteins mostly being retained intracellularly (Ivanova, Barmada, Kummer, & Harris, 2001; Puig et al., 2019; Salamat, Dron, Chapuis, Langevin, & Laude, 2011). For example comprehensive exploration by David Harris's group on impaired secretion of mutant PrP (particularly the D178N FFI mutation) in numerous cell lines has demonstrated that this protein accumulates along the secretory pathway and impairs post-Golgi transport of multiple other cargo, including GPI-anchored proteins, as well as impairing functionality of recycling small GTPase Rab11 (Massignan et al., 2010; Restelli et al., 2021). This indicates effective PrP^C transport itself is required for efficient trafficking along related pathways, highlighting a potential pathogenic mechanism in IPDs.

Despite being localised to lipid rafts, the mechanism of PrP^C endocytosis is still somewhat contended. Unexpectedly a clathrin-dependent route has been most widely proposed as the primary mechanism in both cell models and primary neurons due to localisation of PrP^C within coated pits and interaction of the protein with clathrin-associated proteins such as the LRP1 receptor, AP2M1 and Rab5a (Ballmer et al., 2017; Fehlinger et al., 2017; Jen et al., 2010; Parkyn et al., 2008; Show Ling Shyng, Heuser, & Harris, 1994; Sunyach et al., 2003). However a number of studies have been unable to support a relationship between clathrin and PrP^C surface expression, providing evidence for alternative routes including a caveolae-dependent mechanism due to the sensitivity of PrP^C endocytosis to cholesterol, and colocalisation with caveolae-associated proteins and vesicles (Marella, Lehmann, Grassi, & Chabry, 2002; Peters, Mironov, & Peretz, 2003;

Taraboulos et al., 1995). Furthermore, endocytosis of PrP^C via non-clathrin- or caveolae-dependent mechanisms has been demonstrated, for example regulated by Arf6 signalling molecule in N2a cells (in disagreement with previous reports of clathrin-mediated endocytosis) or the DRM endocytic protein flotillin-1 through direct interaction in a human neuroblastoma cell line, independent from the aforementioned canonical pathways (Y. S. Kang, Zhao, Lovaas, Eisenberg, & Greene, 2009; K. Ren et al., 2013). Endocytosis of PrP^C may therefore present an unusual pathway dependent on both clathrin and lipid rafts, however it is likely that the mechanism of endocytosis is highly dependent on cell type studied (Sarnataro et al., 2009). Regardless, effective endocytosis appears to require a complete N-terminal region with deletion mutants of various sections all significantly impeding internalisation in N2a cells, and the process is strongly stimulated by binding of copper (II) ions to this flexible region, potentially contributing to the physiological role of PrP^C (discussed later in section 1.3.3) (Nunziante, Gilch, & Schatzl, 2003; Pauly & Harris, 1998). Although the mechanism of endocytosis is unclear, most PrP^C certainly continuously cycles between the plasma membrane and intracellular compartments. This occurs with an estimated turnover time in N2a cells of around 60 minutes (from internalisation to recycling to the membrane) and a half-life of 2-3 hours (endolysosomal trafficking routes of PrP^C shown in Figure 3) (Nunziante et al., 2003; S. L. Shyng, Huber, & Harris, 1993).

1.3.2.3. Degradation and recycling

Following endocytosis, PrP^C is directed to early endosomes, from which the protein can either be recycled back to the plasma membrane or trafficked for degradation. Both of these pathways have been explored extensively with multiple regulatory partners identified. For example a direct interaction has been described between PrP^C and sortilin, a member of the Vps10 sorting receptor family (interestingly also extensively characterised in the context of APP processing), and perturbation of sortilin function in N2a cells reduced PrP^C sorting to lysosomes (Barthelson, Newman, & Lardelli, 2020; Uchiyama et al., 2017). A similar study also characterised muskelin as coordinating lysosomal degradation via interaction with kinesin and dynein motor proteins, and proteomics analysis in an immortalised murine hippocampal cell line for PrP^C interactors identified

lysosomal Rab7a (although the function of this interaction is not well defined), highlighting lysosomal degradation as a key regulatory pathway (Heisler et al., 2018; Zafar et al., 2011). Lysosomal degradation as well as cell surface expression of PrP^C are modulated by retrograde transport associated proteins VPS35 and mannose-6-phosphate receptor (M6PR), indicating a synergistic relationship between the degradative and recycling pathways in protein regulation (Ballmer et al., 2017). Pharmacological inhibition of proteasome function in cell culture also increases PrP^C expression suggesting this may also contribute to protein degradation although this is less well established (Nunziante et al., 2011). Along with surface expression, cholesterol levels appear to alter the degradation of PrP^C, but it is unclear whether this is due to its hindered transport through the secretory pathway or an independent mechanism (Taraboulos et al., 1995). Interestingly misfolded PrP lacking the disulphide bond (as a proxy for misfolded GPI anchored proteins) appears to still be degraded in the lysosome during ER stress, and not the proteasome as shown for other misfolded ER proteins (Satpute-Krishnan et al., 2014). This occurs via a vesicle-mediated transport pathway in coordination with ER chaperones, thought to prevent accumulation of aberrant proteins in this organelle (Zavodszky & Hegde, 2019). It would be of interest to determine whether this pathway is also used for IPD mutants.

Finally, as previously discussed, PrP^C is constitutively released from cells (see section 1.3.1). This can be occur either as 'shed' protein following endoproteolytic cleavage, which is also regulated by components of the endolysosomal pathway such as SNX33, as well as within exosomes derived from multivesicular bodies during lysosomal maturation (Heiseke et al., 2008). The latter has been observed from multiple cell lines including mouse hippocampal neurons and N2a cells (also regulated by muskelin), as well as RK13 cells and more specialised macrophages and monocytes, indicating a common mechanism potentially contributing to protein function (L. Cheng, Zhao, & Hill, 2018; Heisler et al., 2018; G. Wang, Zhou, Bai, Zhang, & Zhao, 2010; G. H. Wang et al., 2011).

1.3.3. Function

The exact cellular function of PrP^C has been repeatedly investigated although a clear answer is still mostly lacking. Its presence in most vertebrates, with a large

degree of structural conservation, indicates that PrP^C must play a crucial physiological role, and highest expression in the CNS suggests this is likely the primary functional site (Ford, Burton, Morris, & Hall, 2002; Harrison, Khachane, & Kumar, 2010). Attempts to investigate this however have not provided clear answers, especially as the generation of multiple *Prnp* null mouse models and higher species including goats and cattle display no obvious deleterious phenotype (PrP^C functions reviewed in (Watts et al., 2018)). Except complete resistance to prion infection, these animals are developmentally, behaviourally and physiologically normal up to late adulthood.

Although lack of PrP expression does not appear detrimental to survival, more intricate investigations have highlighted potential more subtle functions of PrP, including (but not limited to) a role in neurogenesis, neuroprotection, plasticity, apoptosis and cell-cell adhesion (Watts et al., 2018). The perhaps most convincing phenotype associated with *Prnp* knockout is a chronic demyelinating polyneuropathy in peripheral nerves. This myelination deficit has been observed in multiple knockout mouse lines as well as PrP null goats, suggesting this function is conserved across species (Bremer et al., 2010; Skedsmo et al., 2020). Reassuringly, re-introduction of PrP^C into peripheral neurons appears to rescue this phenotype (Bremer et al., 2010). More recent work by Aguzzi and colleagues has highlighted a putative interaction of PrP^C with the G-protein coupled receptor Adgrg6 in Schwann cells functioning in transcriptional regulation during myelin maintenance, providing a potential mechanism for this (Kuffer et al., 2016). However, even though PrP^C expression is much higher in the CNS than the periphery, a myelination deficit in the brain is not observed, suggesting that PrP^C may play a different role in the two systems.

Despite no obvious neuropathological phenotype in knockout animals, multiple lines of evidence also point towards a role of PrP^C in neurogenesis and neurite outgrowth, concordant with high PrP^C expression in proliferative brain areas during embryonic development (Tremblay, Bouzamondo-Bernstein, Heinrich, Prusiner, & DeArmond, 2007). Both cell culture and mouse models have indicated a direct interaction of PrP^C with the neurite cell adhesion molecule (NCAM), shown to induce neurogenesis through a signalling cascade mediated by the protein kinase Fyn (Mehrabian et al., 2015; Santuccione, Sytnyk,

Leshchyns'ka, & Schachner, 2005; Slapsak et al., 2016). However, a converse study concluded PrP^C/Fyn signalling induces production of reactive oxygen species, indicating this relationship functions instead in a neurotoxic pathway (Schneider et al., 2003). Therefore the exact consequence of PrP in this is unclear, with the possibility for diverse functions in multiple pathways or in different cell types. To this effect, the PrP/NCAM interaction also appears to be required for neuronal differentiation of neural stem cells (Prodromidou, Papastefanaki, Sklaviadis, & Matsas, 2014).

Synaptic signalling and plasticity have been repeatedly implicated in PrP^C function. Electrophysiology studies on organotypic slice cultures obtained from PrP knockout mice initially highlighted a synaptic impairment (Collinge et al., 1994). Similar studies have also observed a specific deficit of NMDA excitotoxicity in these cultures (Gasperini, Meneghetti, Pastore, Benetti, & Legname, 2015). Further investigation suggests a defect in S-nitrosylation of NMDA receptor subunits (required for closure of the ion channels during deactivation) to be the cause, with the authors proposing a mechanism in which binding of PrP^C to copper (II) ions in the synapse, in close proximity to NDMA receptor subunits, acts to provide a crucial electron acceptor for this process. Additionally metabotropic glutamate receptors (mGluRs) have been repeatedly implicated in PrP^C function (specifically the mGluR5 subunit) as well as plasticity signalling via protein kinase A (Beraldo et al., 2011; Caiati et al., 2013; Haas et al., 2016). This suggests PrP^C may act to regulate multiple pathways during synaptic signalling, supported by identification of around 50 differentially expressed genes in a proteomics analysis of primary cerebellar granule neurons from *Prnp* null mice compared to controls, including multiple involved in synaptic vesicle trafficking (Peggion et al., 2018).

It is possible that PrP^C plays a diverse and multi-faceted role in neurons and other cell types, however the frequent use of gene knockouts to study function are unlikely to represent the physiological state. Although more sophisticated methods of perturbation have been developed, including crucial conditional knockouts in adult mouse brain, these have not been any more fruitful for delineating a clear PrP function (Mallucci et al., 2002). It is however highly unlikely that PrP^C has been conserved just to provide susceptibility to prion diseases, so

future studies as gene manipulation technologies progress will hopefully shed more light on this topic.

1.4. Prion genetics

1.4.1. The PRNP gene

In humans *PRNP* is located on chromosome 20 and is formed of two exons, and in mice on chromosome 2 with three exons, encoding a 253 and 254 amino acid protein respectively (prion protein structure discussed in section 1.3.1) (Mead et al., 2019; Oesch et al., 1985). In both cases the whole open reading frame is located within the last larger exon preventing possible additional splicing isoforms. *PRNP* forms part of a small gene family comprising itself and two related genes, *SPRN* ('shadoo' expressed predominantly in brain) and *PRND* ('doppel' expressed in testis), thought to have evolved from a common ZIP-transporter ancestor gene (Schmitt-Ulms, Ehsani, Watts, Westaway, & Wille, 2009). The prion protein is expressed in most vertebrates and often found in multiple copies, with a highly conserved amino acid sequence between mammals indicating gene function is favourably selected during evolution (Tsangaras et al., 2014). Gene and protein expression is highest in the CNS with a specific enrichment on neuronal synaptic membranes, but can also be detected at lower levels in peripheral tissues and immune cells (Ford et al., 2002).

1.4.2. Genetics in human prion diseases

Over 60 variants have been identified in the human *PRNP* gene comprising a variety of single nucleotide polymorphisms (SNPs), missense mutations, alterations in octapeptide repeat number, premature truncations or rarer frame-shift mutations, some of which lead to IPDs (see recent review (Mead et al., 2019)) (Figure 1). A handful of these variants have also been implicated in sporadic and acquired prion disease risk, however the causality of those identified in sCJD patients is less clear due to the possibility of undiagnosed IPD with potentially variable penetrance.

PRNP codon 129 is a primary genetic determinant for all human prion diseases, occupied by either valine or methionine as encoded by the presence of either G or A at the rs1799990 polymorphism. The implication of this variation is thought to relate to differing susceptibility and conformation of prion strains, discussed

later in section 1.5.3. The genotype at this site drives susceptibility for sCJD with both homozygous genotypes increasing disease risk, as well as bringing about distinct clinical phenotypes, for example MM individuals generally progress more rapidly following symptom onset (Palmer, Dryden, Hughes, & Collinge, 1991; Pocchiari et al., 2004).

With acquired prion diseases, the role of codon 129 polymorphisms is somewhat more complex. For example in iCJD the relationship seems to differ substantially between populations, potentially reflecting differing origins of the prion strain, with a temporal change in genotype frequency indicating a possible additional association of codon 129 with incubation time (Collinge, Palmer, & Dryden, 1991; Rudge et al., 2015). Nonetheless, as with sCJD, in all populations studied homozygosity again increases disease risk. Conversely for another acquired prion disease, kuru, codon 129 genotype has a marked influence instead on the age of onset, with a homozygous methionine genotype being largely overrepresented in younger age groups (Collinge et al., 2006). A similar effect is also found in multiple IPDs with heterozygous genotypes displaying a later clinical onset (Mead et al., 2019). The most striking effect however has been observed for vCJD for which, until recently when two patients were diagnosed with a heterozygous genotype, all identified cases have been homozygous for methionine at this site (Kaski et al., 2009; Mead, Poulter, et al., 2009; Mok et al., 2017).

Although variation at codon 129 appears to be the strongest genetic risk factor for human prion disease and the only association implicated in all disease subtypes, a handful of additional variants within *PRNP* have been found to alter disease risk in distinct contexts. The presence of valine at codon 127 appears completely protective against kuru (Mead, Whitfield, et al., 2009). This variant has almost solely been identified in kuru-affected populations (with only one exception identified through the Genome Aggregation Database (gnomAD) (Karczewski et al., 2020)), yet none of the individuals diagnosed with kuru carried this allele, unlike 8% of the unaffected population of the Purosa valley who are predicted to have been exposed to the disease. Furthermore a polymorphism at codon 219 is protective against sCJD in East and South East Asian populations, with the presence of lysine in the heterozygous state conferring reduced disease

risk (Riedel, Straube, Schwarz, Wilske, & Mller, 1998). V180I and M232R likely represent additional uncommon polymorphisms associated with sCJD risk in Japanese populations due to the lack of family history associated with these variants (Beck, Collinge, & Mead, 2012; Qina et al., 2014).

The identification of non-*PRNP* associated genes in human disease has proved more challenging, particularly due to the rarity of human prion diseases hindering sample ascertainment, often limiting power to detect variants with small effect sizes. Prior specification of candidate genes is one way to surmount this, reducing the number of statistical tests required. For example Calero and colleagues genotyped a common polymorphism in *BACE1* previously associated with AD risk (rs638405) in 237 sCJD cases and found a significant association with sCJD susceptibility, particularly in codon 129 methionine homozygotes (Calero et al., 2012), however one must be cautious with interpreting candidate gene studies due to propensity for bias. These results require robust independent replication, as demonstrated by confounding studies of *APOE* genotype in prion diseases (Calero et al., 2011; Pickering-Brown et al., 1995; Salvatore et al., 1995).

In the last two decades advancements in sequencing technologies have accelerated human genetics studies, allowing for increased availability of samples with genome-wide information, thus permitting sufficiently powered studies on diverse populations. This has led to the increased popularity of genome-wide association studies (GWAS) being performed for diseases and quantitative traits. Although the issues with sample ascertainment are still present for human prion diseases, a handful of GWAS have been performed for various disease subtypes. This will be discussed in detail as the subject of a future chapter (see chapter 3, section 3.1). To summarise briefly, previous studies have still been largely underpowered to robustly detect non-*PRNP* risk variants at genome-wide significance, with the unexpected exception of vCJD although the replication evidence here is lacking (Mead, Poulter, et al., 2009; Sanchez-Juan et al., 2012). The current thesis will describe the first GWAS sufficiently powered to identify variants with low effect sizes for sCJD risk, with replication evidence provided for genome-wide significant variants in and around the genes *PRNP*, *STX6* and *GAL3ST1* (Jones et al., 2020).

1.4.3. Genetics in animal prion diseases

The genetics underlying multiple animal prion diseases has been studied extensively in the interest of both furthering our understanding of these debilitating diseases and their occurrence in different populations, but also as a model to aid understanding of human prion diseases.

As expected, due to the strong genetic association of *PRNP* variants in human prion diseases, multiple polymorphisms have been described in this gene in animals (Mead et al., 2019). Ovine PrP is particularly polymorphic with multiple common coding variants described including a subset associated with scrapie: the combination of alleles at codons 136, 154 and 171 define five different risk groups driving differing susceptibility to classical scrapie (Baylis & Goldmann, 2004). This appears strain specific, however the selective breeding and genetic distinction between herds makes interpreting allele frequencies in livestock populations difficult (Luhken et al., 2007). A similar association is found with scrapie in goats, with the additional recent identification of a naturally occurring nonsense mutation at codon 32 preventing full protein translation and driving disease resistance (Benestad, Austbo, Tranulis, Espenes, & Olsaker, 2012; Salvesen et al., 2020). Conversely bovine PrP displays much less common variation possibly due to long term inbreeding, with only a small deletion in the promoter region implicated in disease risk (Haase et al., 2007). Although the overlap with *PRNP* variation in human prion diseases appears surprisingly low, variation at codon 132 in Rocky Mountain elk (equivalent to human codon 129) appears to alter CWD susceptibility, and there are reports of genetic prion disease in cattle associated with a E211K mutation (equivalent to human E200K), indicating some overlap between mechanisms in animal and human prion diseases (O'Rourke et al., 1999; Richt & Hall, 2008).

The natural susceptibility of animals to disease allows researchers the rare opportunity to replicate all characteristics of human diseases in model systems. Studies representing acquired prion diseases in mice have been most common due to the relative feasibility and availability of tools for genetic manipulation (animal models of prion diseases discussed in detail later in chapter 6). The diversity of incubation times between mouse strains following prion inoculation has allowed investigation of associated quantitative trait loci (QTLs). These

studies have been somewhat hindered by large regions of linkage containing hundreds of genes, as well as a general lack of reproducibility between different methodologies, however regions on chromosomes 2, 4 and 11 have been repeatedly implicated (Mead et al., 2019). Attempts to map these areas by studying more genetically diverse heterogeneous stock mice has highlighted the genes *Cpne8* and *Hectd2,* although the underlying mechanisms here are yet to be elucidated (Lloyd, Maytham, Grizenkova, Hummerich, & Collinge, 2010; Lloyd et al., 2009). Nonetheless the latter was also shown to be significantly associated with vCJD and kuru risk, supporting the use of mice as a general prion disease model. Due to the rarity of spontaneous disease in animals, the study of genes directly relevant to sporadic prion diseases is more difficult, for example attempts to study this in cattle and sheep have been insufficiently powered to detect non-*PRNP* associated genes (Moreno et al., 2010; C. Zhang et al., 2004).

1.5. Prions and other disease-associated forms of PrP

1.5.1. Prion mechanism

Shortly after the initial description of protease-resistant proteinaceous material associated with scrapie infectivity (PrP^{Sc}) and the subsequent identification of a chromosomal gene encoding the same amino acid sequence in uninfected animals, the debate on how these particles relate to drive infectivity in prion diseases has been ongoing (prion history previously described in section 1.1) (Basler et al., 1986; Prusiner, 1982). Although the hypothesis of a nucleotide-based infection similar to viruses was held by some researchers for many years, the experimental support for this was clearly lacking (Prusiner, 1991). An increasing body of evidence instead described a post-translational conversion of PrP^{C} into PrP^{Sc}, with the absence of any differences in sequence or known covalent post-translational modifications between the two proteins indicating a purely conformational distinction, provoking alternative hypotheses of a protein only templated conversion (termed the ‘prion hypothesis’) (Caughey & Raymond, 1991; Griffith, 1967; Prusiner, 1991).

Support for the prion hypothesis has expanded over the following decades. The generation of PrP null mice resistant to both prion disease and the accumulation of PrP^{Sc} confirmed that PrP^{C} expression is required for the infectious mechanism

(Bueler et al., 1993). Initial in vitro studies lent support to the prion hypothesis demonstrating seeded aggregation of PrP^C was feasible, with incubation of purified PrP^C and denaturation-resistant PrP resulting in increased PK-resistant PrP aggregates (Kocisko et al., 1994). The efficiency of conversion however was low preventing determination of infectivity and not reflecting the exponential growth that is seen during disease. Subsequent development of the protein misfolding cyclic amplification (PMCA) assay by Claudio Soto's group in 2001 provided the clearest support to the prion hypothesis, demonstrating an exponential increase in authentically infectious prions following co-incubation of prion-infected brain homogenate with uninfected material and multiple rounds of sonication (Castilla, Saa, Hetz, & Soto, 2005; Saborio, Permanne, & Soto, 2001). It is now generally accepted that exponential increases in PrP^{Sc} during disease occurs through interaction of PrP^C with aggregated infectious PrP, nucleating the misfolding and recruitment into the amyloid protein form, followed by dispersion to increase nucleation-competent species for exponential growth (Figure 4).

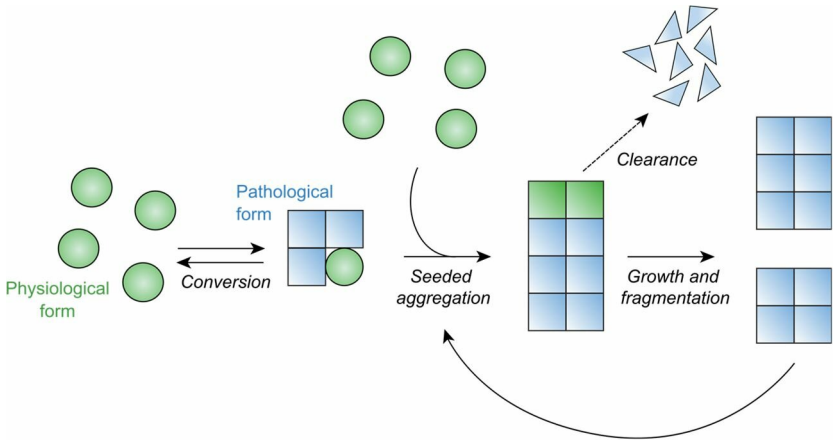

Figure 4: The prion hypothesis.
The hypothesis of protein-only infectivity initially proposed in the context of prion diseases, termed the prion hypothesis, proposes that pathological or infectious protein forms, in this case of PrP^{Sc} (blue), template and recruit the aggregation of the physiological protein (green), PrP^C, in a dynamic reaction. Protein aggregates or fibrils can then either be degraded by cellular mechanisms, or continue to elongate through continuous templated conversion. Fibrils can then be fragmented to nucleate the exponential growth of new aggregates.

Although the templated conversion of PrP^C into prions is now well accepted as an explanation for infectivity, the exact mechanism of how this process occurs in vivo and how this leads to disease is still unclear. It has long been described that both PrP infectivity and neurotoxicity are distinct from the level of PK-resistant PrP (Collinge & Clarke, 2007). This is driven by multiple lines of evidence including: PK-resistant PrP levels do not correlate with infectivity of multiple prion strains; levels of PrP^{Sc} in both mice and humans do not correlate with disease; conditional knockout of PrP in neurons following prion accumulation prevents and even reverses clinical disease in mice (Frigg, Klein, Hegyi, Zinkernagel, & Aguzzi, 1999; Mallucci et al., 2002; Safar et al., 1998; Zerr et al., 1998). A recent sophisticated study performed by Sandberg and colleagues has clearly demonstrated that prion infectivity and toxicity occur in distinct mechanistic phases, with prion titre initially increasing exponentially in a process independent from PrP^C expression, followed by a second phase in which the level of infectivity is stable but the clinical incubation period to onset of disease is dependent on PrP^C expression (Sandberg, Al-Doujaily, Sharps, Clarke, & Collinge, 2011). This suggests an independent, likely PrP-based species drives neurotoxicity, generated following accumulation of infectious PrP^{Sc}, possibly using these aggregates as a catalytic surface. Ongoing development of relevant assays able to distinguish these processes will hopefully allow identification of this toxic PrP species (Benilova et al., 2020). Of note, in the literature, PrP^{Sc} is often used interchangeably to describe PK-resistant PrP and authentically infectious prions; in this thesis, PrP^{Sc} is only used to describe known infectious prion species, to distinguish from proteinase or detergent resistant aggregates of unknown infectivity.

1.5.2. Structure

It is clear that solving the infectious prion structure will be key to determining the molecular basis of prion conversion. Over 35 years ago two publications in short succession independently described fibrillar rod-like structures enriched in prion-infected brain material from multiple sources through negative stain electron microscopy (EM) (Merz, Somerville, Wisniewski, & Iqbal, 1981; Prusiner, Bolton, et al., 1982). Characterisation of these preparations by Prusiner and colleagues described a PK-resistant PrP species of 27-30 kDa specific to these samples

(later understood to be the protease resistant core of PrP^{Sc}) and subsequent investigations indicated that the conversion of PrP^{C} to rod-shaped PrP^{Sc} involves the conversion from a predominant α-helical structure to one with increased β-sheet content (K. M. Pan et al., 1993; Prusiner, Bolton, et al., 1982; Prusiner, Groth, Bolton, Kent, & Hood, 1984). However, despite decades of trying, progress has been slow in delineating the exact molecular structure of infectious prions. This can be attributed to multiple hindering factors including debates over purification artefacts, the propensity for heterogeneous PrP structures both in vitro and ex vivo, and a lack of consistent and specific prion infectivity correlating with purified preparations (Terry & Wadsworth, 2019).

Within recent years significant progress has been made in our understanding of infectious prion structure, driven by cell models enabling quick determination of prion infectivity, advancements in biophysical techniques for studying protein structure and improved purification procedures. Work by the Wadsworth group to develop a robust protocol for specific purification of high-titre prions enabled the first structural characterisation of authentic homogenous prion preparations (Wenborn et al., 2015). Analysis of these structures purified from RML-infected mouse brain in work led by Terry, using a combination of atomic force microscopy, negative stain electron tomography and cryo-EM, described a helical paired-fiber structure of ~20 nm in width, comprising two strands thought to be independent protofilaments separated by a conformationally distinct gap of 8-10 nm containing unspecified biological material (Terry et al., 2019; Terry et al., 2016).

Earlier this year the first near-atomic structure of prions was published through cryo-EM analysis of prion rod structures purified from 263K-infected hamster brain, indicating a parallel in-register intermolecular β-sheet (PIRIBS) conformation with perpendicular rungs to the fibril axis (Kraus et al., 2021). Interestingly atomic reconstruction suggests these rods comprise a single continuous covalently-linked structure, rather than the two independent filaments previously described, with glycans and GPI-anchor extending externally to the filament core. Structural resolution of other related prion strains will support whether these conformational differences between preparations are due to strain characteristics or confounding methodologies. Additionally, further

characterisation of other PrP structures (prevented here by the restrictive requirement for homogenous populations in cryo-EM) including increased understanding of neurotoxic species, will further our understanding of how these structures relate to disease (Sandberg et al., 2014).

1.5.3. Strains

The presence of distinct prion strains has been evident since early studies of scrapie where multiple different isolates induced distinct incubation times and neuropathology in mouse models (Fraser & Dickinson, 1973). However, the discovery of prions as “protein-only” infectious agents led to uncertainty over how proteins consisting of a single primary sequence can lead to distinct diseases.

Isolation of PrP^{Sc} from infected species and studies of disease transmission have led to characterisation of prion strains as PrP structures with distinct biochemical (such as electrophoretic mobility, glycosylation patterns, protease resistance, stability) and clinicopathological (i.e. incubation time, neurological manifestations) properties (Collinge & Clarke, 2007). As the primary sequence is often the same for distinct strains, it is clear that their molecular basis is instead somehow encoded by protein conformation, which is supported by sustained propagation of the aforementioned strain characteristics upon transmission in vitro and in vivo (Bessen et al., 1995; Fraser & Dickinson, 1973). Furthermore, transmission is usually most efficient when matching PrP primary sequences are expressed (i.e. within species), which is often required for effective transmission into mouse models (Prusiner et al., 1990). The effect of primary sequence on prion strain transmission is exemplified by the association of amino acid at codon 129 with human prion diseases (as previously discussed in section 1.4.2) likely regulating permissible prion strains within the host. For example, there is good evidence that PrP^{C} with valine at this position is unable to adopt the vCJD prion conformation preventing transmission to individuals homozygous for this variant (Wadsworth et al., 2004).

Although there is a clear species barrier for transmission of most prion strains, likely driven somewhat by this distinction in primary sequence, it is evident from historic cross-species infection that prion diseases can be zoonotic between organisms expressing different PrP sequences. It has therefore been

hypothesised that each PrP sequence has the capability to acquire multiple PrP^{Sc} structures and an overlap between these is required for inter-species transmission, defined as the conformational selection model (Collinge & Clarke, 2007). However, although the same biochemically characterised strain can be sustained upon this transmission, strain “mutation” can also occur in which a distinct strain is instead propagated (Kimberlin, Cole, & Walker, 1987). The observation of heterogeneous PrP species within the same prion isolate lends support to a hypothesis in which a pool of prions defining the possible conformations permitted by the primary sequence is present at one time within an organism, and the presence of a distinct prion “seed” or favourable microenvironment drives selection and preferable propagation of one of these strains (Polymenidou et al., 2005).

1.5.4. Cell biology

Similar to the cellular protein, the trafficking of prion aggregates has also been extensively studied, with a key focus on identification of the site of conversion and propagation of the misfolded form. Generally the endolysosomal pathway has long been hypothesised as a potential site for this, due to the increased propensity for PrP misfolding and aggregation at low pH (similar to endocytic vesicles) and the sensitivity of PrP^{Sc} formation in cell culture models to changes in temperature (commonly used to modulate trafficking steps in the endolysosomal and secretory pathways) (Arnold et al., 1995; Borchelt, Taraboulos, & Prusiner, 1992; Hornemann & Glockshuber, 1998). PrP aggregates were identified early on within subcellular compartments of the endolysosomal pathway both in cell culture and animal models (Borchelt et al., 1992; Goold et al., 2011). More recently, long recombinant fibrils have also been found to dissociate into shorter protofilaments under conditions mimicking the endocytic pathway, potentially increasing seed capabilities and driving the exponential increase in infectivity seen during disease (X. Qi, Moore, & McGuirl, 2012).

1.5.4.1. Prion conversion

Identifying sites of prion conversion within cells will undoubtedly increase our understanding of this elusive mechanism and allow us to perturb this process more effectively. The availability of cell culture lines able to propagate infectious

prions has allowed researchers to readily study this process in biological systems (discussed later in chapter 4, section 4.1.1). Reports of the steady-state localisation of PrP^{Sc} are variable and often confounding, with localisation reported in nearly all subcellular compartments including the plasma membrane, early and late endosomes, lysosomes, recycling endosomes, Golgi and even the cytosol, therefore not providing any obvious answers to where these are formed (Goold et al., 2013; Mookherjee et al., 2019; Veith, Plattner, Stuermer, Schulz-Schaeffer, & Burkle, 2009; Yamasaki, Baron, Suzuki, Hasebe, & Horiuchi, 2014; Yamasaki et al., 2012). This also suggests the localisation of aggregates is highly dependent on cell type and methodology used. Studies of PrP^{Sc} formation are even further complicated by the lack of antibodies able to distinguish between PrP^{C} and aggregates, requiring harsh denaturation conditions to enrich for PrP aggregates, which is potentially precluding detection of other markers.

Generally, in order to deduce a subcellular compartment for PrP^{Sc} formation, researchers have utilised genetic or chemical perturbation of different trafficking pathways and measured the effect on PK-resistant PrP levels and intracellular localisation of aggregates. For example Marijanovic and colleagues employed genetic manipulation in chronically prion-infected GT1 (mouse neuronal) cells of proteins in the recycling pathway, focussing on recycling endosome protein Rab22a, and found a specific reduction in PK-resistant PrP following inhibition of early endosome to recycling endosome transport (Marijanovic et al., 2009). Conversely however, Yim et al used similar techniques of gene knockdown in infected N2a and SMB cells, this time focussing on the maturation of late endosomes/multivesicular bodies, to alternatively conclude that these are the main site of prion conversion, as inhibition of transport to these compartments (via Rab7) reduced PK-resistant PrP load whereas preventing recycling from here (via retromer component Vps26) had the opposite effect (Yim et al., 2015). These studies highlight the requirement for multiple methodologies and cell lines to draw secure conclusions, as well as the likely heterogeneity in PrP^{Sc} trafficking pathways. Although largely prion formation is thought to occur after trafficking to the plasma membrane of PrP^{C}, similar studies have also highlighted a function of the ER in this, suggesting that transport of PrP^{C} into the cytosol via retrotranslocation can lead to unglycosylated detergent insoluble aggregates

(Borchelt et al., 1992; Branger & Mang, 2002; Ma & Lindquist, 2002). The relevance of these to infectious PrP^{Sc} is however debated and may instead be protective during ER stress (S. W. Kang et al., 2006; Roucou, Guo, Zhang, Goodyer, & LeBlanc, 2003).

Development of more sophisticated cell models has allowed direct visualisation of conversion to aggregated forms in a temporal manor. In a study led by Goold, aggregation-permissive epitope-tagged PrP was expressed in N2a cells able to propagate infectious murine prions (Goold et al., 2011). In this work, aggregation of de novo denaturation-resistant PrP aggregates was instead observed on the plasma membrane within minutes of prion exposure, which was rapidly internalised towards the perinuclear region, forming a steady state here within two hours (Goold et al., 2013; Goold et al., 2011). Unfortunately, cell culture models are currently limited to modelling acquired prion disease with no published system shown to spontaneously accumulate PrP^{Sc}, therefore this plasma membrane prion conversion may be limited to templated aggregation and not initial prion formation. However independent studies including in vitro evidence does support a role of lipid raft components in prion aggregation (Abid, Morales, & Soto, 2010). Of course, prion conversion sites are not necessarily exclusive and these studies may highlight multiple associated potentialities.

1.5.4.2. Prion trafficking

PrP^{Sc}, like PrP^{C}, cycles dynamically between the plasma membrane and perinuclear region and once internalised has, like PrP^{C}, been identified in the majority of intracellular compartments (see Figure 3) (Yamasaki et al., 2014). Various trafficking pathways must therefore be involved in moving aggregates throughout the cell. Like other membrane proteins, PrP^{Sc} is generally thought to be endocytosed to early endosomes, where it is either recycled to the plasma membrane or trafficked for degradation (Veith et al., 2009).

Similar to PrP^{C}, the mechanism by which PrP^{Sc} is endocytosed is also unclear. PrP^{Sc} has been identified in membrane fractions suggestive of caveolae-mediated endocytosis in both cell models and isolated synaptic membranes indicating caveolae- or at least raft-dependent endocytosis (Goold et al., 2013; Vey et al., 1996). Additionally, perturbation of clathrin- or dynamin-dependent

endocytosis had little effect on PrP^{Sc} uptake in N2a cells (Goold et al., 2011). However fluorescently labelled ex vivo prion fibrils appear to compete for the same LRP1-modulated pathway as PrP^{C} in mouse sensory neurons, indicating an association instead with clathrin vesicles (Jen et al., 2010). More recent work led by Fehlinger simultaneously explored the differential role of each endocytic route during the infection of a L929 mouse fibroblast cell line with both RML and 22L prions (Fehlinger et al., 2017). In this study the authors found that, although both strains required caveolae for sustained propagation, knockdown of caveolae had no effect on productive infection, whereas clathrin was required specifically for RML infection. Interestingly there was no significant effect of perturbation of any pathway on PrP^{Sc} internalisation. This lends support to variable pathways for different strains and point of infection, with possibility to utilise multiple pathways depending on availability, likely also dependent on cell type. Evidence also suggests aggregate internalisation is dependent on fibril size, which may modulate the route of internalisation (Magalhes et al., 2005; Rouvinski et al., 2014).

Recycling to the plasma membrane can generally be mediated either by direct trafficking to recycling endosomes or via retrograde transport to the Golgi. Both pathways have been implicated in the transport of PrP^{Sc}, described in the relevant subcellular compartments in cell culture models and shown to follow similar transport routes to canonical cargo of both pathways (i.e. cholera toxin B (CTxB) and transferrin (Tfn) respectively), mediated by regulatory proteins including the retromer complex and rab GTPase Rab9 (Goold et al., 2013; Yamasaki et al., 2014; Yamasaki, Suzuki, Hasebe, & Horiuchi, 2018; Yamasaki et al., 2012; Yim et al., 2015).

Degradation of prions is clearly of interest in disease biology. As expected due to the well characterised transport of PrP^{Sc} through the endolysosomal system, degradation by lysosomes has been established, with lyososmal inhibition in multiple experiments leading to detergent- or PK-resistant PrP accumulation in enlarged LAMP1-positive lysosomes (Goold et al., 2013; Uchiyama et al., 2017; Yamasaki et al., 2014). This is supported by the observed increased expression and abnormal distribution of lysosomal protease cathepsin D in CJD patients and ME7-inoculated mouse brain tissue (Kovacs et al., 2007; Xiang et al., 2004). An

increasing body of evidence also describes a role of autophagy in the degradation of prion aggregates, with similar studies using small molecules to regulate autophagic flux showing modulated PK-resistant PrP expression (Homma et al., 2014; Phadwal et al., 2018; Thellung et al., 2018). Furthermore, there is some suggestion of a role of proteasome-mediated degradation although this is likely restricted to rarer cytosolic PrP forms (Goold et al., 2013; Nunziante et al., 2011).

Related trafficking pathways may also influence the cell-to-cell spread of prions: multiple studies have described the presence of different infectious PrP^{Sc} strains within exosomes (derived from late endosomes prior to lysosomal maturation) in various cell culture models, with strain-effects on exosome release potentially contributing to tropism in disease (Abdulrahman, Abdelaziz, & Schatzl, 2018; Arellano-Anaya et al., 2015; Fevrier et al., 2004). Additionally PrP^{Sc} transport through actin-containing membrane connections termed tunnelling nanotubes has been described in CAD5 cells in association with endosomal vesicles, providing another route of cell-to-cell spread (Victoria & Zurzolo, 2017).

Although it is highly likely protein trafficking through the secretory and endolysosomal pathways impacts prion propagation and disease progression, the disease itself appears to have a reciprocal effect on normal cell physiology. Prion infection in disease models sequesters ER proteins disrupting organelle integrity and inducing ER stress, reduces maturation of lysosomes via perturbation of Rab7 localisation, disturbs post-Golgi protein transport and induces autophagic and proteasomal flux (Mookherjee et al., 2019; Otero et al., 2021; Shim, Karri, Law, Schatzl, & Gilch, 2016; Thellung et al., 2018; Uchiyama et al., 2013). Furthermore studies of altered gene and protein expression in sCJD brain have demonstrated enrichment of secretory pathway and intracellular transport genes, including multiple SNARE proteins or interaction partners, retromer components and Rab proteins Rab7a, Rab9 and Rab5, as well as decreased expression of synaptic vesicle proteins (Bartoletti-Stella et al., 2019; Ferrer, Rivera, Blanco, & Mart, 1999; Kovacs et al., 2007; Zafar et al., 2017). A number of these have been found to correlate with disease stage, strain type or codon 129 genotype (Kovacs et al., 2007; Zafar et al., 2017). Although cause and effect are hard to delineate in these studies, it is possible that perturbation of

normal trafficking pathways during infection may induce a positive feedback mechanism contributing to the exponential spread through the brain.

Although a vast amount of research into the role of intracellular trafficking pathways in prion diseases has been performed, there still remains a lot of questions. The disagreement within the literature likely comes down to a sensitivity to experimental set up including cell model and prion strain studied. A significant issue in studying the sporadic disease also comes from the requirement in all models for seeding with infectious proteins to induce misfolding, a mechanism which may not represent the spontaneous establishment of the disease in sCJD patients. Therefore better disease models will be required to fully understand this aspect of prion biology (as discussed in 5, section 5.1.2).

1.6. Relationship with other neurodegenerative diseases

1.6.1. Prion-like diseases

Most adult neurodegenerative diseases are associated with protein aggregation and deposition in the brain similar to PrP in prion diseases, including Alzheimer's disease (AD; tau and β-amyloid), Parkinson's disease (PD; α-synyclein), frontotemporal dementia (FTD; TDP-43, tau and FUS) and amyotrophic lateral sclerosis (ALS; TDP43) (recently reviewed in (Jaunmuktane & Brandner, 2020)). These proteins often share commonalities with PrP, notably a similar amyloid structure (cross β-sheet). However, in more recent years, other similarities to prions have been described, leading to the increasing use of the term "prion-like" or "prionoid" disorders. Most frequently this designation is driven by the apparent ability of disease-associated aggregates to induce the self-templated conversion of cellular proteins similar to prions (see section 1.5.1).

The ability of pathological aggregates to template conversion in prion diseases is typically studied using both in vitro assays (i.e. through measuring increase in aggregates following addition of seeding competent material to cellular protein) and in vivo assays (i.e. deposition of protein aggregates and subsequent histopathological disease following inoculation of seed material into host species). Both in vitro and in vivo studies have successfully demonstrated the ability for the aforementioned disease-associated proteins to induce aggregation

of cellular forms, supporting this common mechanism at least under experimental conditions (Jaunmuktane & Brandner, 2020). However the relevance of this to real world aetiology is unclear and there is limited evidence to support human transmission, with the exception of β-amyloid; Collinge and colleagues first published observational reports of frequent β-amyloid pathology in the brains of individuals diagnosed with iCJD, as a result of treatment with prion-contaminated cadaveric human growth hormone (iCJD described in section 1.2.2.3), indicative of pre-clinical cerebral amyloid angiopathy (CAA), suggesting possible concurrent transmission of β-amyloid pathology from this treatment (Jaunmuktane et al., 2015). They have recently gone on to show that the same CAA pathology could be transmitted from the original growth hormone preparations to mice expressing humanised amyloid precursor protein (APP), strongly supporting the presence of contaminating seeding-competent β-amyloid driving pathology in these patients (Purro et al., 2018).

Along with templated aggregation, there are other defining features which should be considered when comparing other diseases to canonical prion diseases. This includes the presence of different strains with distinct structural and clinical definitions. The hypothesis that different strains also define alternative clinicopathological phenotypes within other neurodegenerative disease classes is being increasingly explored. For example there is now comprehensive evidence from both cell-based and mouse models that different tauopathies, including progressive supranuclear palsy (PSP), corticobasal degeneration and argyrophilic grain disease, are able to induce relevant neuropathological features upon transmission and present distinct biochemical characteristics which can be serially propagated (reviewed in (Vaquer-Alicea, Diamond, & Joachimiak, 2021)). Landmark studies have now resolved high resolution structures obtained by cryo-EM of tau fibrils from multiple tauopathies highlighting clear structural differences, supporting the presence of alternative tau conformations and thus strains in disease (Falcon et al., 2018; Falcon et al., 2019; Fitzpatrick et al., 2017).

Although the term “prion” was originally defined only as a disease in which protein is an essential component, the since characterisation of prion diseases as transmissible and infectious neurodegenerative diseases means caution must be taken when making these comparisons, especially due to the public health

concerns associated with prion diseases. Future research will determine whether an ability to seed protein aggregation equates to undiagnosed human transmission for other neurodegenerative diseases, and consequentially how "prion-like" these diseases are.

1.6.2. Interaction with PrP

The requirement of PrP^C for infectivity and neurotoxicity mediated by disease-associated PrP aggregates in prion diseases is now well-established. However more recent studies have also implicated a role of PrP^C in the pathogenesis of related neurodegenerative diseases, which, similarly to PrP aggregates, also seems to be mediated predominantly by a direct protein interaction (reviewed in (Legname & Scialo, 2020)). An interaction of PrP^C with β-amyloid was first highlighted in an expression cloning screen of adult mouse brain cDNAs for putative interactors of synthetic oligomers (namely amyloid-β-derived diffusible ligands (ADDLs)) in COS-7 cells (Lauren, Gimbel, Nygaard, Gilbert, & Strittmatter, 2009). This high affinity interaction with the PrP^C N-terminal is now widely appreciated and has been shown to mediate at least some of β-amyloid's neurotoxic effects in vitro and in vivo, including long-term potentiation deficits, dendritic loss and memory impairments (Corbett et al., 2020; Freir et al., 2011; Gimbel et al., 2010). Interestingly there is also converse evidence to suggest shed PrP and N1 α-cleavage fragments are protective against toxic β-amyloid, potentially by reducing surface PrP^C expression as a toxic receptor, or to inhibit extracellular aggregates prior to binding at the cell surface (Fluharty et al., 2013; Scott-McKean et al., 2016).

The identification of PrP^C as a toxic receptor for pathological β-amyloid has since driven similar studies of other neurodegeneration-associated protein aggregates. A direct interaction of PrP^C with tau and α-synuclein oligomers has been repeatedly described in vitro and in vivo, thought to occur at the same site as β-amyloid (Corbett et al., 2020). This interaction contributes again to some of the neurotoxic effects of these preparations, including synaptic plasticity and behavioural defects (Corbett et al., 2020; D. G. Ferreira et al., 2017; Ondrejcak et al., 2018). A recent publication has also implicated PrP^C in TDP-43 pathology but this requires further exploration (Scialo et al., 2021). For these intracellular aggregates, cell culture-based studies have highlighted a putative role of PrP^C in

the uptake of these pathological proteins into cells, potentially mediating this neurotoxicity (Aulic et al., 2017; De Cecco et al., 2020; Scialo et al., 2021). Although further studies are required to determine whether the toxic mechanism associated with this interaction is the same in all instances, the direct implication of PrP^C in multiple neurodegenerative diseases highlights the exciting possibility of a common therapeutic intervention for these untreatable disorders.

1.7. Syntaxin-6

This thesis describes the identification of non-*PRNP* risk factors for sCJD through a replicated GWAS (section 1.4.2). This and subsequent exploration highlights *STX6* as a risk gene associated with this disease. *STX6* encodes syntaxin-6 on chromosome 1, a 255 amino-acid SNARE protein implicated in vesicle trafficking, primarily during retrograde transport between early endosomes and the Golgi.

1.7.1. Syntaxin-6 as a retrograde transport SNARE

1.7.1.1. Identification of syntaxin-6

The requirement of vesicular structures for protein transport has long been appreciated since the first studies of organelles by George Palade in the 1960s, however at this point the mechanisms underlying transport between specific cellular compartments was not clear (Palade, 1975). Pioneering work by James Rothman over the succeeding three decades led to the identification of multiple key components of the vesicle docking and fusion machinery. Reconstitution of vesicle transport in a cell-free environment and its sensitivity to alkylating reagent N-ethylmaleimide led to identification of N-ethylmaleimide sensitive fusion protein (NSF) and binding partner synaptosomal-associated protein (SNAP) as fundamental components of the trafficking machinery (Figure 5) (Block, Glick, Wilcox, Wieland, & Rothman, 1988; Clary, Griff, & Rothman, 1990). The cytosolic nature of these proteins drove further explorations for an integral membrane protein thought to be required to drive fusion. Purification of “SNAP receptors” (SNAREs) from brain homogenate in 1993 through specific binding to ATP-bound NSF and α-SNAP (denoted the 20S complex) led to classification of previously identified syntaxin, SNAP-25 (localised to plasma membranes) and VAMP (localised to synaptic vesicles) as SNARE proteins and proposal of the SNARE hypothesis of membrane fusion (Sollner et al., 1993).

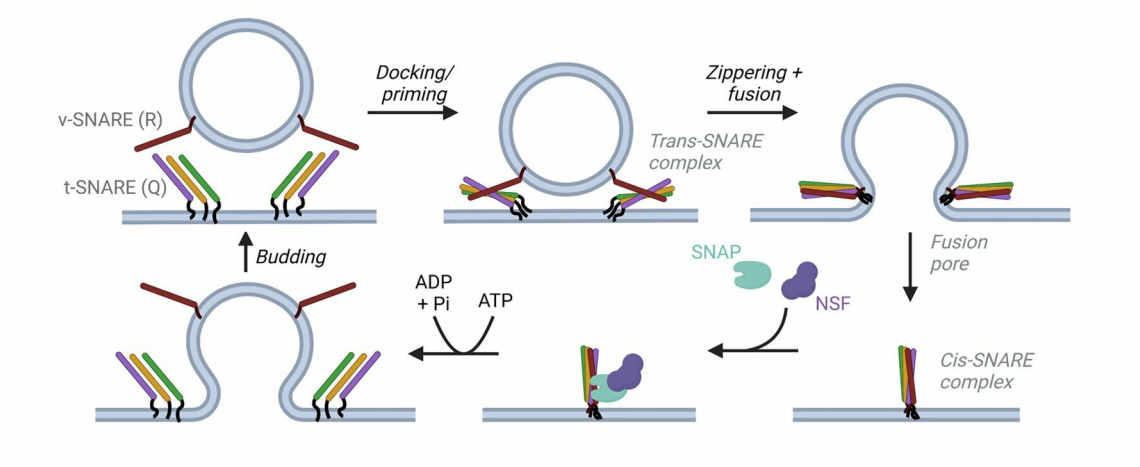

Figure 5: Mechanism of SNARE-mediated vesicle docking and fusion. During transport, SNARE proteins within the membrane bilayer of vesicles (v-SNAREs or R-SNAREs) interact with SNARE proteins on the membrane of their intended target compartment (t-SNAREs or Q-SNAREs). Zippering of corresponding SNARE domains in a highly energetic conformational rearrangement brings membranes in sufficiently close proximity for bilayer fusion, generating a fusion pore allowing protein transport between compartments. The resulting cis-SNARE complex is released with the scaffolded recruitment of NSF (*N*-ethyl-maleimide-sensitive fusion protein) ATPase by α-SNAP (soluble NSF attachment protein) adaptor protein, releasing the complex and allowing SNAREs to be recycled for successive fusion events. Figure adapted from (Rizo & Sudhof, 2002). Figure generated with biorender.com.

Syntaxin-6 was first identified in 1996 by Bock and colleagues due to its sequence homology to a yeast syntaxin Pep12p with a role in Golgi to vacuole transport (Bock, Lin, & Scheller, 1996). Analysis of the 255 amino acid sequence predicted structures similar to other mammalian syntaxins, including a C-terminal hydrophobic region (residues 235-255) likely to form an integral membrane anchor, as well as two sequences computationally predicted to form coiled-coil structures at distinct ends of the protein (resides 47-71 and 166-225). SNARE protein identity was confirmed with binding to canonical partners including α-SNAP.

Alongside this initial characterisation, Bock et al also confirmed syntaxin-6 to localise to Golgi structures in cell culture due its colocalisation with known Golgi resident proteins, supported the following year by immuno-EM demonstrating syntaxin-6 in clathrin-coated Golgi structures, as well as to a lesser extent in various smaller peripheral vesicles outside of the perinuclear region (Bock, Klumperman, Davanger, & Scheller, 1997; Bock et al., 1996). This led to the proposal of a role of syntaxin-6 in the transport of proteins between the trans-

Golgi network (TGN) and endosomes, supported subsequently by live imaging of labelled vesicles trafficking between these two compartments in NRK cells. Later demonstration of the requirement of syntaxin-6 for the transport of canonical retrograde cargo such shiga toxin and TGN38 from early endosomes to the TGN, which have since been robustly replicated in multiple cell lines, securing a common role of syntaxin-6 in retrograde protein transport (Chao et al., 1999; Kuliawat et al., 2004; Lieu et al., 2007; Mallard et al., 2002).

1.7.1.2. Syntaxin-6 structure

The common structure of the SNARE proteins with an integral membrane domain and an extension into the cytoplasm indicated that an interaction between corresponding cytoplasmic domains may drive vesicle docking and subsequent fusion. Landmark realisation of a SNARE complex structure by Brunger and Jahn in 1998 using X-ray crystallography lent support to this hypothesis, as they demonstrated a “pin-like” structure of four parallel α-helices, suggesting that the intertwining of complementary SNARE proteins drives bilayer fusion. Since, a number of SNARE protein complexes have been described acting in different subcellular compartments, including a canonical SNARE complex of syntaxin-6 at the TGN with Vti1a, VAMP4 and syntaxin-16 in both peripheral and neuronal cell lines and in murine brain tissue, with evidence of additional enrichment in synaptic regions (Feldmann, Winterstein, White, Trotter, & Kramer-Albers, 2009; Kreykenbohm, Wenzel, Antonin, & Atlachkine, 2002; Steegmaier, Klumperman, Foletti, Yoo, & Scheller, 1999; Xu et al., 1998).

With the description of increasing numbers of SNARE proteins, a conserved 70 coiled-coil amino acid motif was described and denoted the “SNARE motif”, subsequently confirmed to mediate interactions to drive membrane fusion (Weimbs et al., 1997). This led to the classification of syntaxin-6 in the SNAP25-C family of SNARE proteins due to sequence homology of this critical domain (Bock, Matern, Peden, & Scheller, 2001; Misura, Bock, Gonzalez, Scheller, & Weis, 2002). SNARE proteins can also be classified as Q- or R-SNAREs based on the presence of a key glutamine or arginine residue in the SNARE helix, with Q-SNAREs further denoted as Qa, Qb or Qc depending on their localisation within the four-helix bundle (Fasshauer, Sutton, Brunger, & Jahn, 1998). Due its SNAP25-C homology, syntaxin-6 is classed as a Qc-SNARE.

Soon after the initial SNARE structure was realised, high resolution crystal structures were obtained for the N-terminal region of syntaxin-6 (residues 1-113) (Misura et al., 2002). Here Misura et al demonstrated a three-helical anti-parallel bundle (denoted Habc: a (4–32), b (38–60), c (92–109)) structurally equivalent to that for syntaxin-1a, surprising due to weak sequence homology (Figure 6). However, unlike syntaxin-1a and other SNARE proteins, this N-terminus did not show evidence of regulatory interactions with the SNARE domain. Instead this region likely regulates protein function distinctly, via interactions with other proteins such as α-SNAP, and contributes to its localisation (Bock et al., 1996); syntaxin-6 N-terminal region is required to direct localisation of reconstituted liposomes to Golgi-derived vesicles (Koike & Jahn, 2019). An additional YGRL motif located between the N-terminal helices and the SNARE motif additionally contributes to TGN localisation, at least in adipocytes (Watson & Pessin, 2000).

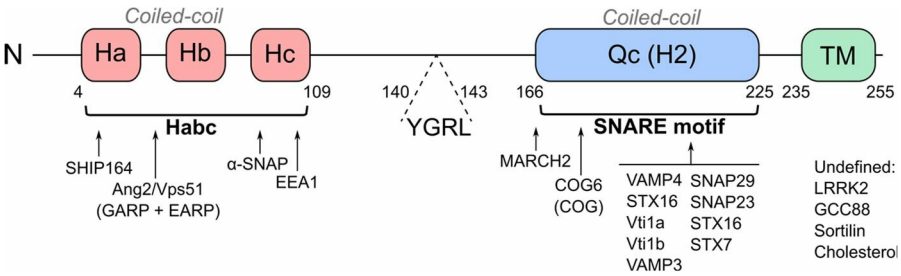

Figure 6: Structure of syntaxin-6 SNARE protein and putative interactors.
Syntaxin-6 is a 255 amino acid protein comprised of two coiled-coil regions, one within the N-terminus constituting three independent helices (Ha-c; red) termed the Habc domain, and another within the SNARE motif (also called H2, classified as Qc due to a conserved glutamine residue; blue). A hydrophobic region at the C-terminal acts as a transmembrane anchor (TM; green). The presence of YGRL motif in the middle region is thought to be functionally important for localisation. A number of binding partners have been described as indicated below, including a number of different SNARE complexes and others where no binding site has been defined (undefined). GARP: Golgi-associated retrograde protein complex; EARP: endosome-associated recycling protein complex; COG: conserved oligomeric Golgi complex. Figure adapted from (Jung, Inamdar, Tiwari, & Choudhury, 2012).

1.7.1.3. Regulation at the trans-Golgi network (TGN)

Over the last few decades, further exploration of the function of syntaxin-6 at the TGN has identified a number of networks which likely contribute to its role in retrograde transport. Firstly, multiple studies have demonstrated an interaction between syntaxin-6 and members of the Golgi-associated retrograde protein

(GARP) complex, a multi-subunit tethering complex comprised of four subunits (Vps51/Ang2, Vps52, Vps53 and Vps54) required for retrograde transport from both late and early endosomes to the TGN (Conibear & Stevens, 2000). In yeast a two-hybrid screen and in vitro experiments identified Tlg1p (syntaxin-6 homologue) as an interactor of GARP subunit Vps51, since characterised in human cells as an interaction between Ang2 (mammalian Vps51 homologue) with the N-terminal Habc domain of syntaxin-6 (Abascal-Palacios, Schindler, Rojas, Bonifacino, & Hierro, 2013; Conibear, Cleck, & Stevens, 2003; Perez-Victoria & Bonifacino, 2009; Perez-Victoria et al., 2010). This interaction recruits and stabilises the canonical syntaxin-6 SNARE complex at the TGN both in cell models and reconstituted systems (Koike & Jahn, 2019; Perez-Victoria & Bonifacino, 2009). Additional interactors of both syntaxin-6 and the GARP complex including SHIP164 (uncharacterised protein complex regulated by syntaxin-6 expression), the conserved oligomeric Golgi (COG) complex (COG6 and COG8, another mutli-subunit Golgi tethering complex) and leucine-rich repeat kinase 2 (LRRK2, diverse function in the endolysosomal system) suggest a complex network of two-way interactions regulating protein function and vesicle trafficking to this site (Beilina et al., 2020; Laufman, Hong, & Lev, 2011; Otto, Razi, Morvan, Stenner, & Tooze, 2010; Willett et al., 2013). Coordination of syntaxin-6 by additional resident proteins including golgin GCC88 and sortilin help delineate the complexity of this regulatory pathway (Hatakeyama & Kanzaki, 2011; Lieu et al., 2007). Finally, evidence suggests cholesterol also modulates syntaxin-6 localisation to the TGN, with one study repeatedly demonstrating reduced Golgi cholesterol (through accumulation in late endosomes) reduces syntaxin-6 localisation at the this site (Reverter, Rentero, Garcia-Melero, & Hoque, 2014). These diverse and numerous regulatory mechanisms indicate the role of syntaxin-6 at the TGN is a critical component of endolysosomal vesicle trafficking.

Some evidence suggests syntaxin-6 plays a cooperative role at the TGN with its presence not only regulated by Golgi interactions, but also itself modulating some additional Golgi functions aside from retrograde protein transport. There is limited evidence to suggest a function in maintaining the Golgi membrane structure for example, with knockdown of syntaxin-6 and it’s canonical SNARE partners in

Hela cells inducing some dispersal of other resident Golgi proteins and modified stack morphology (Shitara et al., 2013). Additionally its relationship with cholesterol transport is potentially synergistic, with evidence to suggest syntaxin-6 modulates cholesterol transport back to the ER with some support for a direct interaction in HeLa cells, although this requires further validation due to inconsistent results and a multitude of proteins studied (Hulce, Cognetta, Niphakis, Tully, & Cravatt, 2013; Urano et al., 2008). Further lipid-protein interactions including sulfatide and multiple phosphoinositides in the same cell line may also contribute to syntaxin-6 regulation in membranes (Kabeiseman, Cichos, & Moore, 2014).

1.7.2. Syntaxin-6 as a promiscuous SNARE protein

1.7.2.1. Endosomes

Despite its clear role in retrograde transport, the description of syntaxin-6 as a "promiscuous" SNARE protein in a review two decades ago already highlighted the diverse functions of this protein in vesicle biology (see Figure 3, page 24) (Hohenstein & Roche, 2001). The early description of syntaxin-6 on peripheral vesicles in addition to the TGN led to the identification of a non-canonical syntaxin-6 SNARE complex on these structures, comprising syntaxin-13 in place of syntaxin-16 (Brandhorst et al., 2006; I. G. Mills, Urbe, & Clague, 2001). Support of its role on endosomes comes from evidence of regulation of homotypic endosome fusion in both cell culture and cell-free systems. Additionally reconstituted liposomes consisting solely of syntaxin-6 are directed to Golgi-derived vesicles, however the addition of syntaxin-13 re-directs transport to endosomal vesicles, indicating syntaxin-6 has the ability to direct vesicle transport in a combinatorial manor with differing SNARE proteins (Koike & Jahn, 2019).

Similar to studies on retrograde transport, identification of a role of syntaxin-6 in early endosomes led to exploration of potential interactors at this site. The N-terminal Habc domain of syntaxin-6 has been repeatedly demonstrated to interact with the C-terminal domain of EEA1, an early endosome tethering molecule (I. G. Mills et al., 2001; Otto et al., 2010; Simonsen, Gaullier, D'Arrigo, & Stenmark, 1999). Another endosomal tethering complex termed the endosome-associated recycling protein (EARP) complex, highly related to the GARP complex sharing three out of four common subunits (Vps52, Vps53 and Vps51/Ang2 with

additional syndetin), has also been demonstrated to interact with syntaxin-6 on Rab4-positive early endosomes, likely via the previously described Ang2 interaction (Schindler, Chen, Pu, Guo, & Bonifacino, 2015). Due to the distinct trafficking routes of syntaxin-6 vesicles in combination with syntaxin-13, researchers aimed to identify a specific interactor of these proteins in combination (Koike & Jahn, 2019). This work highlighted Vps13b, although the exact role of this protein is yet to be characterised. It is likely sytanxin-6 localisation is driven by distinct interactions at differing subcellular compartments to regulate multiple trafficking pathways in the endolysosomal network.

1.7.2.2. Protein recycling

At the early endosome, proteins face a fate decision of recycling (either directly to the plasma membrane, via recycling endosomes and the endocytic recycling compartment, or via the TGN) or degradation. Consequently, the function of syntaxin-6 in endosomes appears to extend to regulation of the recycling pathway. The role of syntaxin-6 may be both at the early endosome, with syntaxin-6 and the EARP contributing to plasma membrane recycling of transferrin receptor (TfnR), as well as the recycling endosomes (Schindler et al., 2015). Multiple studies using a variety of cell lines have demonstrated an interaction of syntaxin-6 with a distinct SNARE protein, VAMP3, which has been well characterised in recycling endosomes, potentially in a complex with syntaxin-16 and Vti1a or Vti1b but this requires further investigation (Mallard et al., 2002; Nozawa, Minowa-Nozawa, Aikawa, & Nakagawa, 2017; Riggs et al., 2012). As a result, manipulation of syntaxin-6 in cell culture has led to the observed perturbation of plasma membrane expression for a diverse range of proteins, including growth factor receptors VEGFR-2 and IGF-1R, integrins constituting α3, α5 and β1 subunits, the cystic fibrosis transmembrane conductance regulator (CFTR) and Met kinase, as well as lipid-raft associated proteins such as Cav-1, GM1-ganglioside and GPI-anchored proteins in human cells, implicating an additional role of syntaxin-6 in caveolae-mediated endocytosis (J. Cheng, Cebotaru, Cebotaru, & Guggino, 2010; Choudhury, Marks, Proctor, Gould, & Pagano, 2006; Garca-Melero et al., 2016; Grassi et al., 2015; Manickam et al., 2011; Reverter et al., 2014; Riggs et al., 2012; Tiwari et al., 2011; Y. Zhang, Shu, & Chen, 2008; Zhu et al., 2016). Furthermore syntaxin-6 clearly contributes to

plasma membrane transport from distinct responsive compartments in specialised cells, such as the transport of GLUT4 and IRAP from the insulin responsive compartment in both adipocytes and muscle cells (Foley & Klip, 2014; Kumudu et al., 2003; Watson, Hou, & Pessin, 2008). These studies clearly secure a role of syntaxin-6 in plasma membrane protein transport under specific conditions, however a more non-biased approach would be interesting to determine the extent of syntaxin-6 recycling cargo.

1.7.2.3. Secretion

Further to trafficking between different subcellular compartments, vesicles are also utilised for secretion of proteins and molecules into the extracellular space. Protein secretion can occur via the secretory pathway following synthesis (where molecules are transported either direct from the TGN to the plasma membrane or are stored in secretory vesicles to be released when required) or can be diverted from the endolysosomal system for release, either within extracellular vesicles (such as exosomes derived from multivesicular bodies) or non-membrane bound (such as lysosomal exocytosis). Due the well-described functions of syntaxin-6 in the endolysosomal system, a role in the latter pathway is perhaps more obvious. This has been eluded to on a couple of occasions with syntaxin-6 knockdown reducing exosome release in a cell model for drug resistance in prostate cancer, and evidence for syntaxin-6 modulating uptake of tau into non-descript vesicles (reconstituted liposomes) and secretion from HEK293T cells (W. S. Lee et al., 2021; Peak, Panigrahi, et al., 2019). However, a role in regulated secretion in specialised secretory cells is better established. For example a number of immune cells use secretion to initiate chain reactions within the immune response, and a role of syntaxin-6 in the degranulation of neutrophils (where it is interestingly detected on the plasma membrane in complex with SNARE SNAP-23) and cytokine secretion (TNF-α) in activated macrophages (in complex with syntaxin-7 and Vti1b) has been described (Martin-Martin, Nabokina, Blasi, Lazo, & Mollinedo, 2000; Murray, Wylie, Khromykh, Hume, & Stow, 2005). Furthermore syntaxin-6 modulates homotypic fusion of immature secretory granules in pancreatic β-cells potentially regulating secretory granule maturation prior to insulin release (Klumperman, Kuliawat, Griffith, Geuze, & Arvan, 1998; Wendler, Page, & Urb, 2001). Cholesterol and other lipids

have again been associated with syntaxin-6 function in these specialised compartments possibly modulating the return of relevant proteins to the TGN (Bogan, Xu, & Hao, 2012; Foley & Klip, 2014). With the presence of syntaxin-6 in diverse SNARE complexes it is likely the role of this protein is distinctly regulated in these specialised cell types.

1.7.2.4. Degradation

Protein degradation is vital for cell function to remove unwanted molecules (i.e. due to errors in synthesis, or from invasion of foreign pathogens) as well as for regulation of protein expression. As previously mentioned the endosomes provide a diverging point for proteins to either be recycled or degraded in lysosomes and related organelles. As well as a role in recycling, modulation of syntaxin-6 function also appears to impact the lysosomal degradation of multiple proteins in different cell lines, such as CFTR in HEK293T and COS7 cells, VEGFR2 and α5β1-integrins in HUVECs and Semliki Forest Virus in pancreatic β-cells (J. Cheng et al., 2010; Kuliawat et al., 2004; Manickam et al., 2011; Tiwari et al., 2011). Interaction of syntaxin-6 H2/SNARE domain with two related ubiquitin ligases, MARCH-II and MARCH-III, provides some indication of its function in this pathway (Fukuda, Nakamura, & Hirose, 2006; Nakamura, 2005). For example a MARCH-II/syntaxin-6 complex regulates CFTR levels, with syntaxin-6 enhancing MARCH-II mediated-ubiquitination of the protein, marking it for degradation (J. Cheng & Guggino, 2013; Fukuda et al., 2006; Nakamura, 2005).

Syntaxin-6 has additionally been implicated in targeting and degradation of invading pathogens. The YGRL motif of syntaxin-6 (shown to generally localise the protein to the TGN) drives localisation to membrane inclusions following *Chlamydia trachomatis* infection (Kabeiseman et al., 2014; Moore, Mead, Dooley, Sager, & Hackstadt, 2011). Similarly there is increased colocalisation with recycling endosomes and autophagosomes with Group A Streptococcus (GAS) infection in culture (Nozawa et al., 2017). A suggestive interaction of syntaxin-6 with autophagy associated proteins LC3B and GABARAP, via putative LC3 interacting motifs in the Habc domain, support this role in autophagy, however this warrants further investigation as this conclusion was not supported with endogenous proteins (Gu et al., 2019). However, these studies indicate syntaxin-

6 acts in the decision at endosomes as to whether proteins are retrieved for recycling to the plasma membrane, or remain in these structures for maturation and degradation in lysosomes and related pathways.

1.7.2.5. Cell physiology

Due to these diverse functions of syntaxin-6, it is no surprise that this protein has been associated with a number of broader physiological properties of cells in culture. With multiple studies describing the perturbations of plasma membrane protein trafficking of key proteins such as integrins, growth factor receptors (VEGFR2, EGFR2) and signalling kinases (Met, focal adhesion kinase) when syntaxin-6 function is modified, it is likely these are driving the phenotypic changes observed by researchers in cell culture, including adhesion to extracellular matrix models, proliferation, migration (in response to growth factor stimulation), spreading (including angiogenesis) and apoptosis (J. Du, Liu, Wu, Zhu, & Tang, 2016; Y. Du et al., 2014; Manickam et al., 2011; Riggs et al., 2012; Tiwari et al., 2011; Y. Zhang et al., 2008). The role of syntaxin-6 in maintaining normal cell biology is supported with syntaxin-6 repeatedly implicated in cancer biology, being the most frequently upregulated SNARE in these diseases (J. Du et al., 2016; Peak, Panigrahi, et al., 2019; Peak, Su, Chapple, Chyr, & Deep, 2019; Riggs et al., 2012; Y. Zhang et al., 2008). Although the vast majority of studies on syntaxin-6 function have been performed either in vitro or in tissue culture models, limiting their applicability to human physiology, the diverse range of cell types and mechanisms studied is reassuring that syntaxin-6 is fundamental to vesicle biology. The variation in phenotypes observed also highlights the need for careful consideration when designing experiments as the role of syntaxin-6 maybe cell type specific.

1.7.3. Role of syntaxin-6 in the brain

1.7.3.1. Neuronal physiology

During their initial characterisation of syntaxin-6, Bock and colleagues established that the expression of this protein was particularly high in brain tissues (Bock et al., 1996). Although its primary function is thought to be in the Golgi and perinuclear region, the canonical syntaxin-6 SNARE complex was also promptly described in synaptosomes isolated from rat brain preparations (Kreykenbohm et al., 2002). More recent characterisation of these regions

suggests a number of endosomal SNAREs can be found in the synaptic bouton and within the active zone, although at low numbers with only approximately 120 copies of syntaxin-6 per synapse (compared to ~120,000 for predominantly synaptic SNARE protein syntaxin 1) (Wilhelm et al., 2014). The exact role of syntaxin-6 in synaptic vesicle trafficking is unclear as both SNARE complexes with syntaxin-16 and syntaxin-13 have been identified in synaptic regions, however it is thought to contribute to fusion between synaptic vesicles and early endosomes during recycling and/or release from the readily releasable pool, with only moderate evidence of mobilisation during full neuron depolarisation suggesting it does not contribute to neurotransmitter release (Hoopmann et al., 2010; Ramirez, Khvotchev, Trauterman, & Kavalali, 2012; Rizzoli et al., 2006).

Neurons are highly polarised cells and this polarisation is key to both development and function. As previously mentioned, syntaxin-6 regulates the transport of a multitude of proteins to the surface, which also applies to neuronal cells. One of these effectors, IGF-1R, plays a key step in the establishment of neuronal polarity with its enrichment at future axons required for development (Grassi et al., 2015). Knockdown of syntaxin-6 in primary hippocampal neurons therefore prevents axon elongation and polarisation, with evidence indicating a direct interaction with both IGFR-1 and axonal motor protein KIF5C mediates this polarised transport (Grassi et al., 2015). Preliminary evidence also suggests a role of syntaxin-6 in nerve growth factor induced neurite outgrowth in PC12 cells, however appropriate controls (overexpression of a dominant negative protein not comparable to endogenous expression) and additional models are required to confirm this (Kabayama, Tokushige, Takeuchi, & Mikoshiba, 2008).

1.7.3.2. Neurodegeneration

Both syntaxin-6 protein and gene function have already been implicated in a number of other related neurodegenerative diseases, making the identification of this gene in sCJD (the focus of this thesis) especially intriguing (Jones et al., 2020). In a two-stage GWAS comparing a total of 2,165 individuals with tauopathy PSP to neurologically healthy controls, SNPs in *STX6* were robustly associated with disease risk, which has since been replicated in further pathologically confirmed cases securing this locus as a genetic risk factor for PSP (Hoglinger et al., 2011; Sanchez-Contreras et al., 2018). Although these variants do not appear

to modify other disease parameters including cognition, age of onset, survival time and tau histopathological phenotypes, these variants do modify both *STX6* expression and brain volume in a number of brain regions including the white matter and striatum, posing a potential mechanism for *STX6* driving risk at this locus (to be discussed later in chapter 3, section 3.3) (Ferrari et al., 2014; Gerstenecker et al., 2017; Jabbari et al., 2020; Kouri et al., 2021; Litvan et al., 2021; Zhao et al., 2019). Interestingly, PSP has been previously associated with a smaller brain volume in multiple brain regions relative to healthy non-neurological disease controls or patients with PD (Messina et al., 2011). Furthermore, a direct protein-protein interaction between syntaxin-6 and tau has been recently identified in HEK293T cells with suggestion of a role in tau secretion, providing a potential cellular mechanism for the association of *STX6* with PSP risk (W. S. Lee et al., 2021). Syntaxin-6 has also been repeatedly implicated in the function of NPC1, a protein involved in the export of cholesterol from late endosomes and lysosomes to other intracellular compartments, in which mutations lead to Niemann-Pick disease type C (NPC) (Reverter et al., 2014; Rogers et al., 2020). Individuals who present with late-onset NPC have been repeatedly reported to display a PSP-like syndrome (Kresojevic et al., 2020).

More recently *STX6* has been additionally genetically implicated in AD, the most commonly diagnosed neurodegenerative disease associated with both tau and β-amyloid pathologies. Through integrating proteome data from 152 dorsolateral prefrontal cortex samples with a large GWAS of AD risk (n = 455,258) in a proteome wide association study (PWAS), the modified expression of syntaxin-6 in this brain region was causally associated with the disease (Wingo et al., 2021). The authors go on to perform a similar exploration with 888 frontal cortex transcriptomes, through which they conclude that modified *STX6* mRNA expression is driving this protein association. Performing this kind of functional analysis enriches GWAS results, highlighting causal genes and putative mechanisms that weren't significant in the original study, as is the case here. Limited data indicates this association is not reflected in an AD mouse model (APP23) but further studies are warranted in better models and patients (APP23 mice bare limitations with overexpression artefacts and limited neuropathology) (Koldamova et al., 2014).

Unlike AD and PSP, PD is traditionally characterised by pathologies thought to be distinct to tau with the accumulation of α-synuclein-containing Lewy bodies. Despite this, syntaxin-6 has also been implicated in PD aetiology, albeit more indirectly. A recent meta-analysis of PD GWAS totalling 56,306 cases (or first-degree relatives as proxies) identified 90 independent risk loci (Nalls et al., 2019). This included variants around *VAMP4,* a SNARE partner for syntaxin-6 in most identified SNARE complexes. However, due to the single stage study design and multitude of associations, this requires independent replication and further analysis to confirm *VAMP4* as the causal gene at this locus. Nonetheless a recent analysis of association of these common variants with PD phenotypes implicated *VAMP4* in occurrence of sleep apnea as a comorbidity in PD patients (Markopoulou et al., 2021). Analysis of protein interaction networks (using STRING) of all genes associated with a PD clinical phenotype and subsequent exploration of gene ontology pathways secured the strong relationship with VAMP4 and syntaxin-6, with the top 5 networks implicated in PD phenotypes all containing *STX6.* Furthermore a recent study aiming to identify LRRK2 interactors (a gene robustly associated with both sporadic and familial PD risk) characterised a complex of syntaxin-6 and VAMP4 with this protein, in association with Vps52 (subunit of the GARP and EARP complexes on TGN and early endosomes) in neurons, suggesting syntaxin-6 and LRRK2 work in coordination to regulate retrograde transport (Beilina et al., 2020). Although PD is traditionally described as a synucleinopathy, GWAS has now repeatedly highlighted *MAPT* as a risk gene for the disease, and multiple in vitro and in vivo experiments have started to implicate tau in disease pathology (recently reviewed in (L. Pan, Meng, He, & Zhang, 2021)). Therefore whether the role of syntaxin-6 and related pathways in these neurodegenerative diseases is all via a common effect on tau biology, or whether there are distinct perturbations of tau, β-amyloid, α-synuclein and PrP functions, will be a fascinating route for future research.

1.8. SNAREs and vesicle trafficking in neurodegeneration

Beyond prion diseases, protein trafficking and the endolysosomal system have been repeatedly implicated in the aetiology of multiple different neurodegenerative diseases. For example, endosomal abnormalities are now

appreciated to be a key pathological hallmark of AD, with enlargement of early endosomes even preceding detectable β-amyloid deposition in the brain (Cataldo et al., 2000). This pathology is associated with increased activity of rab GTPase Rab5, previously attributed to aberrant processing of APP by β-secretase BACE1 (specifically the β-C-terminal fragment) driving Rab5 recruitment (S. Kim et al., 2016). However, a recent study in which researchers overexpressed neuronal Rab5 in mice indicates this alone is sufficient to drive a neurodegenerative phenotype (Pensalfini et al., 2020). This study highlights the potential synergistic relationship between trafficking dysfunctions in neurodegeneration, implicating defective processing in both cause and effect. This is supported by the increasing association of vesicle trafficking genes with both familial and sporadic neurodegenerative diseases, including familial (e.g. *VPS35, DNAJC6, LRRK2*) and sporadic (e.g. *GBA, LRRK2, TMEM175*) PD, late-onset AD (e.g. *SORL1, BIN1, PICALM, SNX1, TMEM106B, GRN)* and FTD (e.g. *GRN, TMEM106B, CHMP2B)* (Baker et al., 2006; Bellenguez et al., 2020; Edvardson et al., 2012; Nalls et al., 2019; Rogaeva et al., 2007; Skibinski et al., 2005; Van Deerlin et al., 2010; Vilarino-Guell et al., 2011; Zimprich et al., 2004). A comprehensive review of the extensive literature on protein and vesicle trafficking in neurodegeneration is beyond the scope of this introduction, but a number of recent reviews have highlighted the breadth of literature on this topic, including repeated implications of endosomal, lysosomal, recycling, autophagy, secretory and exososomal pathways in these diseases (Nixon, 2017; Root, Merino, Nuckols, Johnson, & Kukar, 2021; Smolders & Van Broeckhoven, 2020; Vella, Hill, & Cheng, 2016; X. Wang, Huang, Bu, & Xu, 2014).

In addition to the previously described associations of syntaxin-6 with neurodegeneration (see section 1.7.3.2), the functions of other SNARE proteins have also been implicated in related diseases (recently reviewed in (Margiotta, 2021)). The canonical SNARE complex driving exocytic fusion of synaptic vesicles constitutes syntaxin-1a, VAMP2 and SNAP-25, which are all expressed at high levels in these regions (Wilhelm et al., 2014). Therefore it is not surprising that the function of these SNAREs has been associated with neuronal pathology. A marked increase in SNAP-25 levels in the cerebrospinal fluid of individuals with AD and mild-cognitive impairment (MCI) is thought to indicate synaptic damage,

preceding neuronal loss in patients and potentially even exploitable as a neurodegenerative biomarker (Agliardi et al., 2019; H. Zhang et al., 2018). Conversely the expression of these three SNARE proteins appears reduced in end-stage AD patient brains (Pham et al., 2010). Syntaxin-1a displays propensity to interact with both β-amyloid monomers and oligomers in vitro via the SNARE domain, inhibiting complex assembly, however whether this contributes to the same process in vivo requires further investigation (Yang et al., 2015). Furthermore α-synuclein colocalises with this complex in neurons via direct interaction with VAMP2 promoting SNARE complex assembly, however different aggregated protein states and concentrations appear to have converse effects, so the impact of this interaction during disease requires further investigation (Burre, Sharma, & Sudhof, 2014; Burre et al., 2010; Choi et al., 2013). Nonetheless the emerging role of α-synuclein at synaptic membranes is fascinating, with evidence to show that this alone is sufficient to drive membrane tubulation and curvature in vitro, as well as acting as a tether to independently dock vesicles at the inner leaflet (Fusco et al., 2016; Varkey et al., 2010). The common implication of synaptic vesicle SNAREs may highlight a related mechanism of neurotoxicity in both AD and synucleinopathies.

SNARE proteins not traditionally associated with synaptic vesicles have also been implicated in neurodegeneration, similar to syntaxin-6. For example, a role of syntaxin-5, a SNARE regulating fusion at the ER and Golgi, has been described in the pathogenic processing of APP and subsequent β-amyloid secretion in relation to ER stress (Hernandez-Zimbron & Rivas-Arancibia, 2016; Suga, Saito, Mishima, & Akagawa, 2015). Other SNARE proteins have also been implicated in the secretion of tau from cells in culture including syntaxin-6, as well as VAMP8 and syntaxin-8 (W. S. Lee et al., 2021; Pilliod et al., 2020), highlighting a potential common role of the SNARE protein family in the pathogenic cell-to-cell spread of disease-associated proteins. Finally, a relationship between syntaxin-17-mediated fusion of mitochondria derived vesicles and the PINK1/parkin pathway (two mitochondrial proteins associated with familial PD) has also been described in PD pathogenesis, potentially contributing to the mitochondrial dysfunction seen in this disease (McLelland, Lee, McBride, & Fon, 2016).

The frequent description of SNARE protein function in neurodegeneration is just an example of the types of trafficking proteins that have been repeatedly associated, highlighting the vital role in effective protein and vesicle transport in maintaining cell function, and the detrimental effects perturbation has in disease. The complex and entwined nature of the pathways and proteins that constitute the secretory and endolysosomal networks mean further work is still required to fully understand the consequences of these associations, but expanding research in this field will undoubtedly secure this as a key target in disease.

1.9. Project outline and pre-summary

The identification of genetic risk factors for disease provides the rare opportunity for unbiased identification of implicitly causal mechanisms. Although *PRNP* is clearly a strong genetic determinant for sCJD risk and the role of PrP^C is evident, the utility of this as a therapeutic target is yet to be confirmed. Therefore the identification of non-*PRNP* genes associated with sCJD is essential, to expand our knowledge of fundamental disease biology, as well as to broaden the availability of valid therapeutic targets. However, although GWAS is a powerful tool for identifying disease-associated variants and loci, follow up analysis is key to understand the implication of these. This includes identification of the causal gene driving this genetic association, as well as using relevant models and functional genetics tools to build a fundamental understanding of gene function in disease biology and to explore its utility as a therapeutic target.

The main aims of this thesis were therefore to:

1. Secure association of variants associated with sCJD risk through GWAS (chapter 3)
2. Identify causal genes and variants at associated loci (chapter 3)
3. Develop appropriate cell-based models to investigate the role of associated gene(s) in prion propagation (chapters 4 and 5)
4. Test role of associated gene(s) in vivo including disease survival time in a mouse bioassay for prion infectivity (chapter 6)

2. Materials and Methods

2.1. GWAS

2.1.1. Sample collection

Samples were collected from specialist national surveillance centres from multiple countries of predominantly European ancestry from patients with a diagnosis of definite or probable sCJD according to widely-accepted diagnostic criteria (Zerr et al., 2009). Approval for genetics studies was granted by local ethics committees and consent for genetics research obtained for each sample.

2.1.2. Discovery phase

Genotyping, QC and association test were performed by James Uphill and Holger Hummerich. All visualisations and explorations generated by myself. Cases were genotyped using the Illumina Omniexpress array and validation performed using hydrolysis probes for a selection of SNPs. Various quality control (QC) measures were applied including genotyping rate (>99%), minor allele frequency (>=0.01), Hardy Weinberg disequilibrium in controls (>0.0001) and removal of cryptic duplicates and relatedness. Publicly available control data matched for population were used. Further genotypes were imputed using the Michigan Imputation Server. A frequentist association test was performed assuming an additive allelic model using SNPTEST. Following imputation QC, 6,314,525 SNPs were used in the analysis.

2.1.3. Replication phase

Genotyping of SNPs for the replication phase was performed using the following commercially available TaqMan SNP Genotyping Assays (Applied Biosystems; 4351379) according to manufacturer's protocol: C___1413892_1_ (rs3747957); C___7524681_10 (rs9065); C__33826387_20 (rs34783346); C___2969398_10 (rs1799990); C___2629047_1_ (rs2267161). 1-20 ng DNA was mixed with 5 µl TaqMan GTXpress Master Mix (Applied Biosystems; 4401892) and 0.5 µl SNP genotyping assay (20X) to a volume of 10 µl. qPCR was performed on QuantStudio 12K Flex Real-Time PCR System with Fast 96-well block (Applied Biosystems) (60^{o}C 30 secs; 95^{o}C 20 secs; 40 cycles x 95^{o}C 1 sec, 60^{o}C 20 secs; 60^{o}C 30 secs) and genotype assignment performed using QuantStudio 12K Flex software v1.3. Additional publically available control data was imputed using the

Michigan Imputation Server as previous and genotypes for replication SNPs called with genotyping quality threshold 0.85. Association analysis was performed using PLINK (v1.90) using allele-based χ^2 tests for each case-control cohort matched for population and subsequent fixed-effects meta-analysis performed on summary statistics (Purcell et al., 2007).

2.2. Fine-mapping

2.2.1. CAVIAR

CAVIAR utilises summary statistics to model association at a locus and estimates the posterior probability of a variant to be causal through modelling distribution conditional on the set of causal SNPs (Hormozdiari, Kostem, Kang, Pasaniuc, & Eskin, 2014). GWAS loci were defined as 100 SNPs upstream and downstream of the SNP with the highest association. A linkage disequilibrium (LD) matrix was calculated from sCJD GWAS data using PLINK --r2 function and GWAS z-scores defined as β-value over standard error. CAVIAR was run with an undefined number of causal variants and causal set probability set at 95%.

2.2.2. eCAVIAR

eCAVIAR is an extension of the CAVIAR framework to estimate the posterior probability of the same variant being causal in both GWAS and expression quantitative trait loci (eQTL) datasets (Hormozdiari, van de Bunt, & Segr, 2016). The *STX6* locus was defined as 100 variants upstream and downstream of rs11586493. SNPs were pruned with variant inflation factor of 5 to extract distinct signals and LD matrix calculated from sCJD GWAS data using PLINK as previous. We obtained eQTL data for 48 tissues included in the GTEx portal (v7). eQTLs for these 46 pruned variants with nominal $P \leq 10^{-5}$ were defined as eGenes and eCAVIAR performed for each in its target tissue from summary statistics (z-scores calculated as the slope of the logistic regression over standard error). Resulting colocalisation posterior probability (CLPP) was ranked to identify target gene and tissue. The data used for the analyses described in this thesis were obtained from the GTEx Portal on 4th February 2020 (GTEx Consortium, 2015).

2.2.3. PAINTOR

PAINTOR analysis performed in collaboration with Holger Hummerich. PAINTOR utilises a Bayesian probabilistic framework to integrate GWAS summary statistics and LD data with functional genomic annotation including regulatory datasets such as FANTOM (Fantom Consortium and the RIKEN PMI and CLST et al., 2014) and ENCODE (Encode Project Consortium, 2012) to calculate a posterior probability of a variant being causal and generates a credible causal set (Kichaev et al., 2014). The software was run using default parameters with variants 100 kb around the lead GWAS SNP (rs11586493) with all brain tissue annotations (n = 587).

2.2.4. FUMA

FUMA (v1.3.6a) is a web-based application for post-GWAS analysis which integrates numerous functional annotations with GWAS summary statistics including positional, expression and regulatory datasets to aid hypothesis generation and highlight putative causal genes and variants (Watanabe, Taskesen, van Bochoven, & Posthuma, 2017). This software was run with default parameters using all available input software and datasets: MAGMA (v1.08) (de Leeuw, Mooij, Heskes, & Posthuma, 2015), ANNOVAR (K. Wang, Li, & Hakonarson, 2010), CADD (v1.4) (Kircher et al., 2014), RegulomeDB (v1.1) (Boyle et al., 2012), 15-core chromatin state and enhancer and promoter regions (Roadmap Consortium) (Roadmap Epigenomics Consortium et al., 2015), GTEx (v6/v7/v8) (GTEx Consortium, 2015), Blood eQTL browser (Westra et al., 2013), BIOS QTL browser (Zhernakova et al., 2017), BRAINEAC (Ramasamy et al., 2014), MuTHER (Grundberg et al., 2012), xQTLServer (Ng et al., 2017), CommonMind Consortium (Fromer et al., 2016), eQTLGen (Võsa et al., 2018), DICE (Schmiedel et al., 2018), PsychENCODE (D. Wang et al., 2018), eQTL catalogue (various), FANTOM5 (Fantom Consortium and the RIKEN PMI and CLST et al., 2014), Hi-C (adult and fetal cortex) (Giusti-Rodríguez et al., 2019), MsigDB v7.0 (Liberzon et al., 2011).

2.3. Cell lines and plasmid constructs

PK1 and iPK1 cells were obtained from Emma Quarterman and cultured in Opti-MEM (Gibco; 31985-047) with 10% fetal bovine serum (FBS, Gibco; 41965-039)

and 1% penicillin-streptomycin (Gibco; 15140-122) (complete Opti-MEM). Phoenix-ECO cells (ATCC; CRL-3214) were cultured in Dulbecco's Modified Eagle Medium (Gibco; 41965-039) with 10% FBS and 1% penicillin-streptomycin. CAD5 cells were obtained from Parmjit Jat and cultured in Opti-MEM with bovine growth serum (Cytiva; SH30541.03HI) and 1% penicillin-streptomycin. Cells were stored in an incubator at 37°C/5% CO_2 and passaged twice-weekly by trituration. Other cell lines used are described in relevant sections. *Stx6*-targeting 29-mer shRNA sequences in pRetroSuper vector were purchased from Insight Biotechnology (Table 1): STX6_A (TG517176A), STX6_B (TG517176B), STX6_C (TG517176C), STX6_D (TG517176D). *Prnp*-targeting shRNA (PRNP) was previously cloned into pRetroSuper vector (Goold et al., 2011). Scrambled and *Rfp*-targeting shRNAs were also purchased from Insight Biotechnology as controls: Non-sil (TR30013), shRFP (TR30017). *Stx6* cDNA in pEZ-Lv122 vector was purchased from GeneCopeia (EX-Mm08004-Lv122) with empty vector control (EX-NEG-Lv122).

Construct	Sequence (5' – 3')
STX6_A	CAGATGTCAGCTTCATCTGTGCAGGCACT
STX6_B	GGAGAGGTACAGAAAGCAGTCAACACTGC
STX6_C	CCAGTGGTGTGCCATAGCCATCCTCTTCG
STX6_D	TGGAATGCTGGAGTGGCAGATCGCTATGG
PRNP	GAGACAATCTAAACATTCT
Non-sil	GCACTACCAGAGCTAACTCAGATAGTACT
shRFP	CTTCAAGACCACATACAGATCCAAGAAAC

Table 1: shRNA construct sequences

2.4. Generation of stable knockdown PK1 and CAD5 cells

2.4.1. Optimisation of Stx6 knockdown in PK1 cells

For initial screening, Phoenix-ECO cells were plated at 2 x 10^6 cells per 10 cm dish ~18 h prior to transfection. 12 µl FuGENE 6 transfection reagent (Promega; E2691) was diluted in 100 µl Opti-MEM, incubated for 5 min and 3 µg of plasmid DNA added before applying dropwise to cells. 24 h post-transfection, a complete media change was performed. 48 h post-transfection viral supernatant was

collected and filtered through 0.45 µm syringe filter. PK1 cells were plated at 5 x 10^5 cells per 10 cm dish 24 h prior to transduction with 2 ml fresh filtered viral supernatant in complete Opti-MEM with 8 µg/ml polybrene (Merck; TR-1003-G). Complete media change was performed after 4-5 h. After 3 days transduced cells were selected using media supplemented with 2 µg/ml puromycin (Gibco; A1138-047). Cells were grown in puromycin selection media for at least 2 weeks before gene expression measured. During optimisation 5 µg plasmid DNA was used for transfection and puromycin concentration between 2 – 4 µg/ml.

2.4.2. Generation of final Stx6 knockdown PK1 and CAD5 cells

For PK1 cells single cell cloning and initial RT-qPCR screening was performed in collaboration with Emmanuelle Viré; for CAD5 cells this was performed by myself. Cells were plated at 5 x 10^5 cells per well in a 6-well plate 24 h prior to transfection. 3.5 µg plasmid DNA diluted into 175 µl Opti-MEM with 3.5 µl PLUS reagent (Invitrogen; A12621) was added to 150 µl Opti-MEM with 6 µl Lipofectamine LTX Reagent (Invitrogen; A12621). Transfection mix was incubated for 5 min at room temperature before 250 µl was added dropwise to cells (2.5 µg DNA final). 24 h post-transfection cells were split into a 10 cm dish to promote shRNA integration. 48 h post-transfection transfected cells were selected with 3 µg/ml puromycin (Gibco; A1138-047) in complete Opti-MEM. Cells were grown for up to 2 weeks before single clones were separated and screened for knockdown by RT-qPCR.

2.4.3. RT-qPCR

Cells were resuspended in Dulbecco's phosphate-buffered saline (DPBS, Gibco; 1490-094) and pelleted at 400 x g for 5 min. Pellets were lysed in 300 µl TRI Reagent (Zymo Research; R2050-1-200) and RNA extracted using Direct-zol RNA Miniprep (Zymo Research; R2052) according to manufacturer's instructions. Briefly, an equal volume of ethanol was added to each lysate, mixed thoroughly and loaded onto the RNA-binding column. Columns were treated with DNase I (0.0625 U/µl final) for 15 min, washed and RNA eluted in 30 µl nuclease-free water. Reverse transcription was performed using QuantiTect Reverse Transcription Kit (Qiagen; 205311) according to protocol. 200 ng RNA was diluted in nuclease-free water with gDNA wipe-out and incubated at 42ºC for 2 min to eliminate genomic DNA. Reverse transcriptase mix containing dNTPs, RNase

inhibitor, Mg^{2+} and universal primers was added to each sample and incubated at 42°C for 15 min followed by 95°C for 3 min for enzyme inactivation. qPCR reactions comprised of 10 µl Fast SYBR Green Master Mix (Applied Biosystems; 4385612) and 2 µl QuantiTect Primer Assay (Qiagen; *Stx6*: Mm_Stx6_1_SG, QT01061760; *Prnp*: Mm_Prnp_1_SG, QT00101080; *Gapdh*: Mm_Gapdh_3_SG, QT01658692, *Actb*: Mm_Actb_1_SG, QT00095242) and 2 µl cDNA (diluted 1:4 in nuclease-free water) were performed on QuantStudio 12K Flex Real-Time PCR System with Fast 96-well block (Applied Biosystems) (95°C 20 secs; 40 cycles x 95°C 1 sec, 60°C 20 secs; melt curve: 95°C 15 secs, 60°C 1 min, 95°C 15 secs).

2.4.4. Bradford assay

Cells were resuspended in DPBS and pelleted at 400 x g for 5 min. Pellets were lysed using RIPA buffer (50 mM Tris-HCl pH 8, 150 mM NaCl, 1% NP-40, 0.5% sodium deoxycholate, 0.1% SDS) with protease inhibitors (Roche; 11873580001) using a 26 G needle. Lysates were diluted 1:8 into DPBS and 5 µl dispensed into a 96-well plate in triplicate with 250 µl Bradford reagent (Sigma; B6916). Bovine serum albumin (BSA, Thermo Scientific; 23210) standards were prepared with 2-fold serial dilution series (2 – 0.0125 mg/ml). Absorbance was measured at 595 nm using a plate reader (Tecan; Infinite F200 Pro).

2.4.5. Immunoblot

Lysates were diluted in DBPS with 4X SDS sample buffer (250 mM Tris base, 40% glycerol, 8% SDS, 0.04% bromophenol blue) and boiled at 95°C for 5 min. 65 µg of total protein was loaded onto a 4-12% Bis-Tris polyacrylamide gel (Invitrogen; NP0336BOX) with Chameleon Duo Pre-stained Protein Ladder (LI-COR; 928-60000) and electrophoresed at 180 V for 1 h then electroblotted to a nitrocellulose membrane (Invitrogen; LC2001) at 35 V for 2 h. Membranes were blocked in Odyssey Blocking Buffer (LI-COR; 927-40000) for 1 h at room temperature, probed with monoclonal anti-PrP antibody (clone ICSM18; 1:500; D-Gen Ltd; Table 2) or anti-syntaxin-6 (clone C34B2; 1:500; Table 2) overnight at 4°C. Membranes were washed with 0.05% Tween-20 (Sigma; P9416) in PBS (PBST) for 3 x 5 min with agitation and incubated with anti-β actin (1:1000 rabbit polyclonal or 1:5000 mouse monoclonal (Table 2)). After washing as previously described, membranes were probed with fluorophore-conjugated secondary

antibodies IRDye 800CW Donkey anti-rabbit IgG (1:4000, LI-COR; Table 3) and IRDye 680RD goat anti-mouse IgG (1:4000, LI-COR; Table 3) for 1 h at room temperature. Membranes were washed again and imaged with Odyssey Gel Documentation System (LI-COR; Model 9120).

Target	Host species	Dilution	Supplier	Catalogue number	Method
PrP	Mouse	1:500	D-Gen Ltd	NA (clone ICSM18)	WB, DB
PrP	Mouse	1:500	Sigma	P0110 (clone 8H4)	IF
PrP	Mouse	1:10,000 (IF) 1:20,000 (ELISA)	BioLegend	808003 (clone 6D11)	IF, ELISA
PrP	Mouse	1:1000	D-Gen Ltd	NA (clone ICSM35)	IHC
Syntaxin-6	Rabbit	1:500 (WB, DB) 1:200 (ELISA)	Cell Signaling	2869S (clone C34B2)	WB, DB, ELISA
Syntaxin-6	Mouse	1:500	Abcam	Ab12370 (clone 3D10)	IF
Syntaxin-6	Rabbit	1:100	Atlas Antibodies	HPA038558	IHC
β-actin	Mouse	1:5000	Sigma	A5441	WB
β-actin	Rabbit	1:1000	Sigma	A2066	WB
Oct4	Goat	1:300	Abcam	Ab27985	IF
Tra-1-60	Mouse	1:200	Abcam	Ab16288	IF
Pax6	Rabbit	1:300	Biolegend	901302	IF
Ki-67	Mouse	1:50	Abcam	Ab8191	IF
Tuj1	Rabbit	1:500	Biolegend	802001	IF
Tbr1	Rabbit	1:200	Abcam	Ab31940	IF
Ctip2	Rat	1:200	Abcam	18465	IF
Map2	Chicken	1:5000	Abcam	Ab5392	IF
Goraps2 (GRAPS55)	Rabbit	1:1000	ProteinTech	10598-1-AP	IF
Iba1	Rabbit	1:250	AlphaLaboratories	019-19741	IHC
GFAP	Rabbit	1:1000	Dako (Agilent)	Z0334	IHC

Table 2: Primary antibodies.
WB = Western blot; DB = Dot blot; IF = Immunofluorescence; IHC = Immunohistochemistry.

Target	Host species	Conjugate	Dilution	Supplier	Catalogue number	Method
Rabbit IgG (H + L)	Donkey	IRDye 800CW	1:4000	LI-COR	926-32213	WB, DB
Mouse IgG (H + L)	Goat	IRDye 680RD	1:4000	LI-COR	925-68070	WB, DB
Mouse IgG (Fab specific)	Goat	Peroxidase	1:25,000	Sigma	A2304	ELISA
Rabbit IgG (Whole molecule)	Goat	Peroxidase	1:25,000	Sigma	A0545	ELISA
Mouse IgG (Fcγ subclass 1)	Goat	Alexa Fluor 647	1:1000	Jackson ImmunoResearch	115-605-205	IF
Mouse IgG (Fcγ subclass 2b)	Goat	Rhodamine Red-X	1:1000	Jackson ImmunoResearch	115-605-207	IF
Mouse IgG (Fcγ subclass 2a)	Goat	Rhodamine Red-X	1:1000	Jackson ImmunoResearch	115-605-206	IF
Goat IgG (H + L)	Donkey	Alexa Fluor 488	1:500	Invitrogen	A-11055	IF
Mouse IgG (H + L)	Donkey	Alexa Fluor 568	1:500	Invitrogen	A-10037	IF
Mouse IgG (H + L)	Donkey	Alexa Fluor 488	1:500	Invitrogen	A-21202	IF
Rabbit IgG (H + L)	Donkey	Alexa Fluor 546	1:500	Invitrogen	A-10040	IF
Rabbit IgG (H + L)	Donkey	Alexa Fluor 488	1:500	Invitrogen	A-21206	IF
Rat IgG (H + L)	Goat	Alexa Fluor 568	1:500	Invitrogen	A-11077	IF
Chicken IgY (H + L)	Goat	Alexa Fluor 647	1:500	Invitrogen	A-21449	IF

Table 3: Secondary antibodies.
WB = Western blot; DB = Dot blot; IF = Immunofluorescence.

2.4.6. Growth rate

Cell lines were seeded into a T25 flask (Thermo Scientific; 12034917) at a consistent density and grown for 3 to 4 days. Cells were resuspended in 5 ml complete Opti-MEM. 10 µl cell suspension was mixed 1:2 with 0.4% Trypan blue stain (Invitrogen; T10282) and cell count was measured using the Countess II FL Automated Cell Counter (Invitrogen; AMQAF1000). Cell doubling time was calculated using the following equation, where N_t = end point cell number, N_0 = start point cell number and t = time (days).

$$Doubling\ time\ (days) = \frac{t}{\log_2 \frac{N_t}{N_0}}$$

2.4.7. Automated Scrapie Cell Assay

Automated Scrapie Cell Assays (ASCA) were performed by Christian Schmidt, George Thirlway and Parvin Ahmed as previously described (Klohn, Stoltze, Flechsig, Enari, & Weissmann, 2003). Each cell line was seeded at 1.8 x 10^4 cells per well in a 96-well plate 24 h prior to infection with 10% (w/v) RML brain homogenate at 3 x 10^{-6}, 1 x 10^{-6}, 3 x 10^{-7}, 1 x 10^{-7}, 3 x 10^{-8} and 1 x 10^{-8} dilutions with 12 wells per condition. Cells were split 1:8 every 3 to 4 days using an automated liquid handling robot (Biomek FX liquid handling robot; Beckman Coulter) and assayed after the 3rd and 4th splits. 25,000 cells were plated on ELISpot IP Filter Plates (PVDF membrane, 0.45 µm, Merck; MSIPN4550) and fixed at 50°C for 1 h before treatment with 1 µg/ml proteinase K (PK; Roche; 3115828001) in lysis buffer (50 mM Tris HCl pH 8, 150 mM NaCl, 0.5% (w/v) sodium deoxycholate, 0.5% (v/v) Triton X-100) at 40°C for 1 h. Plates were washed and treated with 3M guanidine thiocyanate (Melford; G54000) for decontamination and antigen retrieval before blocking with SuperBlock blocking buffer (Thermo; 37545). Staining was performed using anti-PrP antibody (clone ICSM18; D-Gen Ltd; Table 2) followed by detection with alkaline phosphatase-linked anti-IgG1 antiserum (Southern Biotech; 1070-04). Spots were visualised with alkaline phosphatase conjugate substrate (Bio-Rad; 170-6432) and PK-resistant PrP infected cells counted using the Bioreader 5000-Eβ (BioSys Karben, Germany).

2.4.8. Immunofluorescence for syntaxin-6 and PrP in PK1 cells

Cells were seeded at 3.5 x 10^4 cells per well into 8-well glass chamber slides (Thermo Scientific; 155411) and incubated at 37°C/5% CO_2 for 3 days. Cells were rinsed twice with DPBS and fixed for 15 min at RT with 3.7% formaldehyde (Sigma; F8775) diluted in DPBS. After washing 3 x DPBS, cells were permeabilised using 0.04% Triton X-100 (Sigma; T9284) in DPBS for 10 min at RT. Cells were washed again as previous and incubated with anti-syntaxin-6 (clone 3D10, 1:500; Table 2) or anti-PrP (clone 8H4, 1:500; Table 2) primary antibodies in 0.25 X SuperBlock (Thermo Scientific; 37545) overnight at 4°C. The following day cells were washed again and incubated with IgG-specific fluorophore-conjugated secondary antibodies (Jackson ImmunoResearch; Table 3) in 0.25 X SuperBlock overnight at 4°C. Antibodies were removed and nuclei stained with DAPI (1:5000; Merck; D9542) for 15 min in DPBS at RT before washing and imaging using a confocal microscope (Zeiss; LSM 710) at 63X objective.

2.4.9. Image quantification

Image analysis was performed using Columbus Image Data Storage and Analysis System (Perkin Elmer) on 3-5 images per independent replicate. Nuclei and cell boundaries were identified through DAPI staining and used to define the nuclei, cytoplasmic and membrane boundaries (Figure 7). Objects were defined as individual cells. For analysis of protein colocalisation, masks were generated for each channel within the cytoplasm region and overlaid onto the alternative channel and area and intensity within this mask quantified. For analysis of PrP localisation within cells the area and intensity within each cell region was determined. Total protein was calculated as intensity (average per pixel) multiplied by area (pixels^2). Proportions were calculated as total protein per cell region per object over total protein per object.

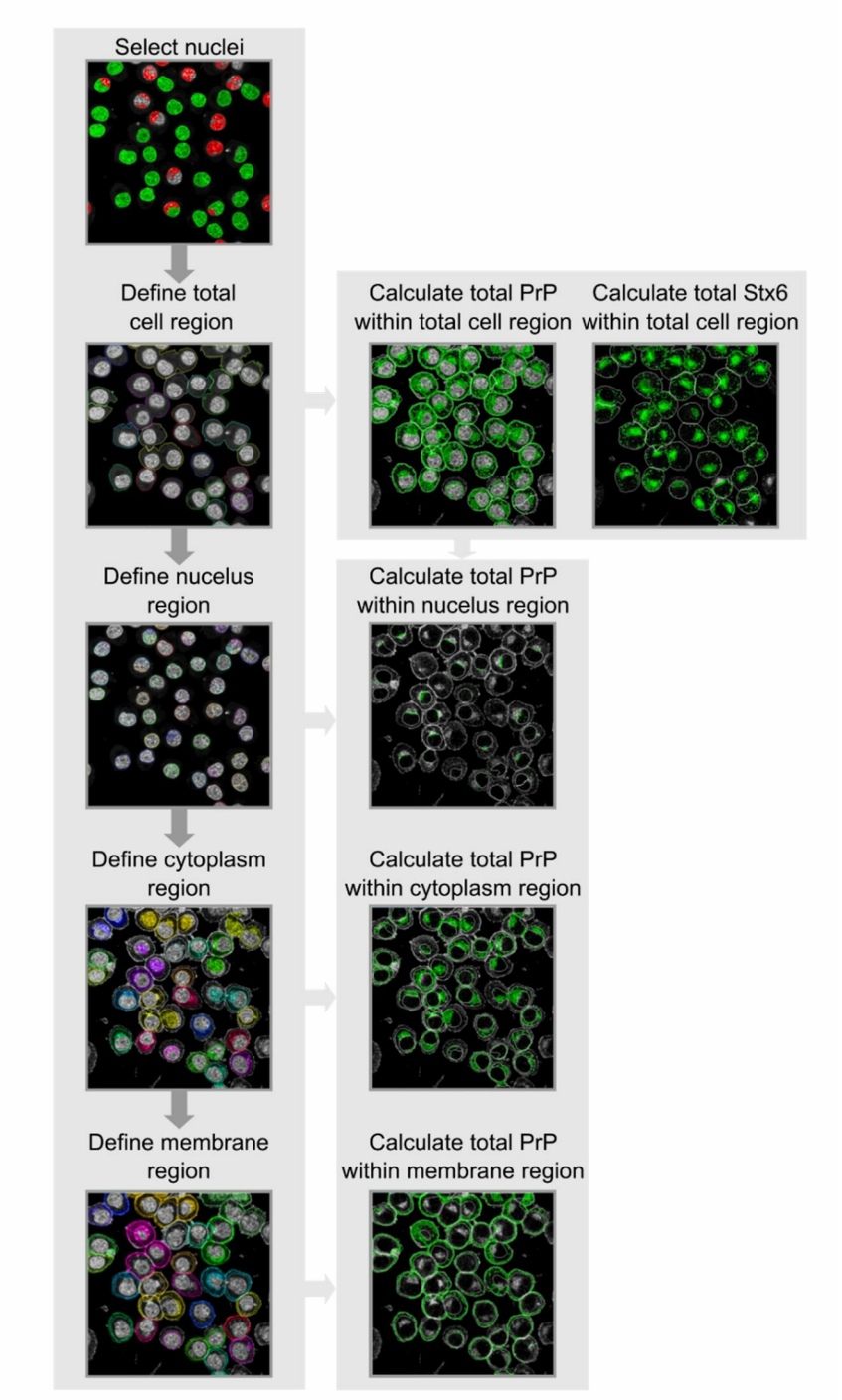

Figure 7: Quantification of PrP localisation in PK1 and iPK1 cells using Columbus.

2.5. Manipulation of gene expression in iPK1 cells

2.5.1. Transient transfection of iPK1 cells

iPK1 cells were plated at 1.5 x 10^4 cells per well in a 96-well plate ~6 h prior to transfection in complete Opti-MEM. 25 ng of each *Stx6*-targeting shRNA plasmid (A-D) was diluted with Opti-MEM and 0.1 µl PLUS reagent (Invitrogen; A12621) to a final volume of 5 µl per well. 100 ng Non-sil or PRNP plasmid were prepared in the same way. 0.5 µl Lipofectamine LTX transfection reagent (Invitrogen; A12621) was diluted into 4.5 µl Opti-MEM. DNA mix was added to the transfection reagent mix and incubated for 5 min at room temperature before adding to cells. A complete media change was performed ~18 h post-transfection. For RT-qPCR analysis cells were detached with 0.05% trypsin/EDTA after 48 and 72 h and 3 wells pooled. RT-qPCR was performed as previously described (see section 2.4.3). Cells were lysed at 72 h post-transfection for dot blot immunoassay (see section 2.4.5).

2.5.2. Generation of stable iPK1 cell lines

iPK1 cells were seeded at 5 x 10^5 cells per well in a 6-well plate ~6 h prior to transfection as previous (see section 2.4.2). After 24 h cells were split into 10 cm dish and after 48 h transfected cells were selected with 3 µg/ml puromycin (Gibco; A1138-047) in complete Opti-MEM. Cells were grown as populations for at least 2 weeks before gene expression measured. Growth rate was measured as previously described (section 2.4.6).

2.5.3. Dot blot immunoassay

250 µl ice-cold lysis buffer (50 mM Tris pH 7.4, 150 mM NaCl, 0.5% sodium deoxycholate, 0.5% triton-X 100) was added to each well or to pelleted cells at a final cell density of 250,000 cells per ml of lysis buffer and incubated on ice for 20 min. Nitrocellulose membrane (GE Healthcare; 45004002) was pre-soaked in lysis buffer for 5 min before assembly into the Bio-Dot Microfiltration Apparatus (Bio-Rad; 170-6545). After pre-washing with lysis buffer, 100 µl cell lysate was loaded into well, lysates applied to membrane using vacuum and washed twice with lysis buffer. Membranes were removed from the apparatus for further processing. For detection of PK-resistant PrP, membranes were incubated with 5 µg/ml PK (Merck; 539480) for 1 h at 37°C with agitation before 10 min incubation with 4 mM 4-(2-Aminoethyl)-benzenesulfonyl fluoride (AEBSF,

Meflord; MB2003) to inactivate the enzyme. All membranes were treated with 3 M guanidine thiocyanate for 10 min at room temperature for decontamination and antigen retrieval and washed 3 x 5 min with ddH_2O. Blocking, immunodetection and imaging were performed as previously described (see section 2.4.5 for immunoblotting; Table 2). Staining with anti-β actin antibodies was performed after imaging initial primary antibody to prevent undetectable cross-reactivity.

2.5.4. Immunofluorescence for syntaxin-6 and prion aggregates in iPK1 cells

iPK1 cells were plated, fixed and permeabilised as described previously (see section 2.4.8). Following permeabilisation, cells were treated with 3.5 M guanidine thiocynate diluted in ddH_2O for 10 min at RT. To remove residual guanidine cells were washed thoroughly with 5 x DPBS before staining with anti-syntaxin-6 (clone 3D10, 1:500; Table 2) or anti-PrP (clone 6D11, 1:10,000; Table 2) in 0.25X SuperBlock ON at 4^oC. The following day cells were washed 3 x DPBS and incubated with IgG-specific fluorophore-conjugated secondary antibodies (Jackson ImmunoResearch; Table 3) in 0.25X SuperBlock ON at 4^oC. Antibodies were removed and nuclei stained with DAPI (1:5000; Merck; D9542) for 15 min in PBS at RT before washing and imaging using a confocal microscope (Zeiss; LSM 710) at 63 X objective.

2.5.5. Prion release into culture media

iPK1 cells were seeded at 1 x 10^6 cells into 10 cm culture dishes in 10 ml complete Opti-MEM (without puromycin selection) and incubated for 48 h at 37^oC/5% CO_2. Cells were then rinsed in DBPS and 10 ml fresh media added and placed back into the incubator overnight (~16 h). Media was then collected, centrifuged at 3000 x g for 10 min and supernatant filtered using 0.45 µm PES membrane (Starlab; E4780-1226) to remove any remaining cells. Culture media was then either frozen at -80^oC or used fresh in the ASCA as previous (see section 2.4.7) across 5 x 10^{-1} to 8 x 10^{-4} dilution range. Tissue culture infectious units per ml sample (TCIU) were calculated relative to a standard curve of RML-infected brain homogenate.

2.6. ELISA for PrP/syntaxin-6 interaction

2.6.1. Preparation of recombinant proteins

Recombinant proteins were prepared by Mark Batchelor as previously described with amendments (Jackson et al., 1999). DNA encoding human PrP residues 23-231 (huPrP$^{23-231}$) in pTrcHisB vector or human syntaxin-6 residues 1-255 (huStx6$^{1-255}$) in pQTEV vector were transformed into BL21 (DE3) competent cells. Cultures were grown in LB medium with 100 µg/ml ampicillin or 60 mg/ml carbenicillin. At optical density (OD) 0.55 – 0.9 protein expression was induced with 1 mM IPTG (Melford; I56000) and incubated at 37^{o}C ON with shaking. The following day protein was purified from inclusion bodies using a Ni-NTA column (Ni Superflow Resin) under denaturing conditions with oxidative refolding using an AKTA pure (GE Healthcare Life Sciences) and eluted using an imidazole gradient. For huPrP$^{23-231}$ the histidine tag was cleaved using 2.5 mM $CaCl_2$/50 U thrombin (VWR) and Ni-NTA purification repeated. Both proteins were then dialysed for >4 h against 20 mM Bis-Tris (pH 6.5) or 20 mM Tris/2 mM EDTA/10 mM DTT/200mM NaCl (pH. 8.0) for huPrP$^{23-231}$ and huStx6$^{1-255}$ respectively. Final protein concentration was measured by absorbance at 280 nm (molar extinction coefficients: huPrP$^{23-231}$ 56667 M^{-1} cm^{-1}; huStx6$^{1-255}$ 31970 M^{-1} cm^{-1}) and stored at -80^{o}C until use.

2.6.2. Protein interaction ELISA

96-well plates (Thermo Scientific; 439454) were coated with 50 µl/well of 100 µg/ml huPrP$^{23-231}$ or 100 µg/ml huStx6$^{1-255}$ in carbonate/bicarbonate buffer (0.057 M $NaHCO_3$, 0.0034 M Na_2CO_3; pH 9.6) for 1.5 h at room temperature. Plates were washed with 4 x 100 µl/well 0.05% PBST using a microplate washer (Thermo Scientific Wellwash; MK4) and blocked using 150 µl/well SuperBlock Blocking Buffer (Thermo; 37545) for 1 h at 37^{o}C with gentle agitation. Plates were washed as previous and where applicable incubated with 50 µl/well of huStx6$^{1-255}$ in a 3-fold serial dilution from 100 to 0.412 µg/ml or carbonate/bicarbonate buffer alone for 1 h at 37^{o}C with gentle agitation. After washing, plates were incubated with 50 µl/well anti-syntaxin-6 (clone C34B2; 1:200; Table 2) or anti-PrP (clone 6D11, 1:20,000; Table 2) in 2% milk (Sigma; 70166) for 1 h at 37^{o}C with gentle agitation. During optimisation additional primary antibodies were tested; anti-syntaxin-6 (clone 3D10, 1:1000), anti-PrP (clone ICSM18; 1:1000).

Plates were again washed before incubation with peroxidase-conjugated secondary antibodies (Sigma; Table 3) in 0.05% PBST for 1 h at 37°C with gentle agitation. After final washing as previous, equal volumes of room temperature TMB solutions A and B (BD Biosciences; 555214) were mixed, 50 µl added to each well and incubated for 10 min at room temperature in the dark. To stop the reaction, 25 µl of 3 M H_2SO_4 was added to each well. Assay plates were read at 450 nm using a plate reader (Tecan; Infinite F200 Pro).

2.7. HEK293T tau biosensor assay

2.7.1. HEK293T tau biosensor cell line

HEK283T tau biosensor cells were previously generated by Marc Diamond to express P301S tau repeat domain fused to CFP and YFP (Holmes et al., 2014) and obtained from Julia Ravey. Cells were cultured in 10 cm dishes in DMEM (Gibco; 41966-029) supplemented with 10% foetal bovine serum (FBS; Gibco; 10500064), 1% penicillin-streptomycin, 1% GlutaMax (Gibco; 35050061) and maintained at 37°C/5% CO_2. Cells were passaged at 1:10 to 1:15 dilution every 3 to 4 days using 0.05% trypsin (Gibco; 25300054).

2.7.2. siRNA transfection

STX6-targeting (Horizon; L-017164-00-0005) or non-targeting (Horizon; D-001810-10-05) OnTarget PLUS siRNA SMART pool were resuspended in ddH_2O to a stock concentration of 20 µM and stored at -20°C. For transfection optimisation, cells were seeded in antibiotic-free media at 380,000 cells/well in a 12-well plate 4-6 hours prior to transfection with 20-40 pmol siRNA and 2-3 µl Lipofectamine 2000 (Invitrogen; 11668030) diluted in Opti-MEM according to manufacturer's protocol. Complexes were incubated for 20 min at RT before addition to the cells. Cells were collected in DPBS, pelleted at 400 x g for 5 min and lysed in 300 µl TRI Reagent for qPCR analysis (see section 2.4.3) or 120 µl RIPA buffer (see section 2.4.5) for Western blot analysis. For seeding assays cells were plated in antibiotic-free media at 35,000 cells per well in a 96-well plate 4-6 hours prior to transfection with 2 pmol siRNA using 0.3 µl lipofectamine. Media was changed the following morning for complete culture media. Knockdown efficiency was measured by RT-qPCR (see section 2.4.3) (primer

details: *STX6*: Hs_STX6_2_SG, *GAPDH*: Hs_GAPDH_1_SG) and immunoblotting (see section 2.4.5).

2.7.3. Seeding assay

Treatment with tau seeds was performed at 24-hours post-siRNA transfection (6-8 hours following complete media change) at approximately 60% cell confluency as previously described (Holmes et al., 2014). Heparin-induced tau fibrils were previously generated from tau441 monomer using agitation in sodium acetate buffer by Julia Ravey. 1.5 µl tau fibrils were incubated with 1.25 µl per well of Lipofectamine 2000 diluted in Opti-MEM for 20 min on ice before addition to culture media to a final 1:100 seed dilution. Plates were incubated for 72 h Incucyte S3 Live-Cell Analysis System (Sartorius; 4647) (37°C, 5% CO_2).

2.7.4. Image analysis

Image acquisition and analysis utilised the Incucyte S3 Software, set to acquire 4 images per well every 3 h at 20 X objective in the phase and green channels for > 72 h. Phase images were used to generate a confluence mask. Tau aggregates denoted by small, bright puncta in the green channel were selected using size (15 to 70 μm^2), eccentricity (≥ 0.3) and mean intensity (≥ 27.0) filters. Mean aggregate count and standard error per well was normalised to percentage confluence and arbitrary values calculated relative to the maximum aggregate count per replicate to enable comparison between replicates. Mean aggregate levels during the plateau phase (30 to 50 h) were compared using Student's t-test.

2.8. Knockout of *STX6* in iPS cells

2.8.1. iPS cell lines

Imputed genotypes for control human iPS cell lines (male, age 60-69, feeder-free) were downloaded from the human pluripotent stem cell initiative (HipSci) catalogue and genotypes extracted from .vcf files. Two cell lines with A/A at rs1799990 and differing homozygous genotypes at rs3747957 (A/A, HPSI1013i-pamv_1, "PAMV1"; G/G, HPSI0215i-oilg_3, "OLIG3") were purchased from Public Health England's European Collection of Authenticated Cell Cultures (ECACC) (Table 4). iPS cells were cultured on 6-well plates (Thermo Fisher; 140675) in Essential 8 medium (Gibco; A1517001). Plates were coated with

Geltrex-coated (1:100; Gibco; A1413302) for >1 h before use. At 80% confluency cells were passaged at 1:3 to 1:6 ratio by incubation with 0.2 µm filter-sterilised 0.05% EDTA (Invitrogen; 15575020) for 3-4 min at 37ºC, aspiration of EDTA and trituration with 2 ml fresh Essential 8. Multi-guide synthetic single guide RNAs (sgRNAs) targeting human *STX6* (Gene Knockout Kit v2) and *TRAC* (Transfection Optimisation Kit) were purchased from Synthego (Table 5). sgRNA pools were resuspended in nuclease-free TE buffer to a final 100 µM stock concentration and stored at -20ºC.

Donor	**HPSI-oilg**	**HPSI-pamv**
Cell line	**HPSI0215i-oilg_3 (OLIG3)**	**HPSI1013i-pamv_1 (PAMV1)**
STX6 (rs3747957)	G/G	A/A
PRNP (rs1799990)	A/A	A/A
Disease status	Normal	Normal
Age	65-69	65-69
Ethnicity	White - White British	White - White British
Sex	Male	Male
Biosample	SAMEA3249666	SAMEA2398790
Tissue Provider	Cambridge BioResource	Cambridge BioResource
Banking status	ECACC, EBiSC as WTSIi191-A	ECACC, EBiSC as WTSIi025-A
Source material	Skin tissue	Skin tissue
Method of derivation	CytoTune 1	CytoTune 1
Date of derivation	2015-05-28	2014-02-13
Culture conditions	Feeder-free when banked	Feeder-free when banked
Pluripotency score	15.115	36.475
Novelty score	1.402	1.344
Number of regions different from primary tissue	1	1
Length of differences from primary tissue	2 Mbp	1 Mbp

Table 4: Details of iPS cell lines used in this study.

Construct	Description	Sequence (5' – 3')
STX6 G1	sgRNA	AUAACCUCCGGAGCAUAGAG
STX6 G2	sgRNA	UUGUUGCUGUGGAGGGGUCC
STX6 G3	sgRNA	AAAGCAGUCAACACUGCCCA
TRAC G1	sgRNA	CUCUCAGCUGGUACACGGCA
TRAC G2	sgRNA	GAGAAUCAAAAUCGGUGAAU
TRAC G3	sgRNA	ACAAAACUGUGCUAGACAUG
TRAC PCR F	Primer	TCAGGTTTCCTTGAGTGGCAGG
TRAC PCR R	Primer	TAAGGCCGAGACCACCAATCAG
TRAQ SEQ	Primer	CTGGCCGTGAACGTTCACTGAAATCATGGC
STX6 PCR1 F	Primer	ACCAAGTGGAAGCATGTGGGAA
STX6 PCR1 R	Primer	TGACTCCAGGGTCCACAGTCAT
STX6 PCR2 F	Primer	TGGGAATGGTGGTTGCTGAGGA
STX6 PCR2 R	Primer	CCGAATGGCACAGACACCACAG
STX6 SEQ	Primer	TGGCTATTGTATTCCAAGCATCAG

Table 5: CRISPR sgRNA and primer sequences

2.8.2. CRISPR RNP transfection

One day prior to transfection, OLIG3 iPS cells were seeded at 4 x 10^4 cells per well into a 24-well plate (Thermo Scientific; 142475) in 500 µl Essential 8 medium supplemented with with 10 µM ROCK inhibitor (Y-27632 dihydrochloride; Merck; Y0503) following passage as previously described and trituration through P1000 pipette to disperse cell clumps. Transfection was performed using Lipofectamine CRISPRMAX Cas9 Transfection Reagent (Invitrogen; CMAX00008) according to manufacturer's instructions. Briefly, the ribonucleoprotein (RNP) complex was prepared by mixing 1500 ng Cas9 nuclease (20 µM stock concentration; Synthego), 10 pmol sgRNA and 3 µl Cas9 Plus Reagent in 25 µl Opti-MEM reduced serum medium (Gibco; 31985-047) in a sterile RNase-free tube (Invitrogen; AM12400). In a separate tube 1.5 µl Lipofectamine CRIPSRmax reagent was added to 25 µl Opti-MEM. The RNP complex was added to the transfection reagent and incubated for 5 min at room temperature before adding 55 µl to each well. 6 h post-transfection a complete media change was performed for Essential 8 without ROCK inhibitor. Optimisation was performed as described in Table 6 using Transfection Optimisation Kit (Synthego).

	sgRNA (ng/pmol)	Cas9 (ng/pmol)	sgRNA:Cas9 ratio (mol)	Lipofectamine (ul)	PLUS reagent	Reference
A	**250**/7.7	**1000**/6.2	1.25	1.5	6	CRISPRmax
B1	1943/**60**	1296/**8**	7.5	1.5	3	Synthego
B2	1943/**60**	1296/**8**	7.5	3	6	Synthego
C	324/**10**	**1500**/9.3	1.07	1.5	3	Invitrogen

Table 6: CRISPR optimisation conditions

2.8.3. Screening CRIPSR knockout by sequencing

DNA extraction was performed using quick-DNA miniprep kit (Zymo; D3024) according to manufacturer's protocol. During transfection optimisation cells were lysed 4 days post-transfection by adding 250 µl Genomic Lysis Buffer to each well. For analysis of *STX6* knockout cells were passaged into a 12-well plate (Thermo; 150628) and 250 µl Genomic Lysis Buffer added to confluent cells. DNA was eluted in 50 µl nuclease-free water. For PCR amplification 100 ng DNA was added to PCR mix (500 nM forward primer, 500 nM reverse primer (Table 5; TRAC PCR, STX6 PCR1), 2 mM $MgCl_2$, 0.2 mM each dNTP, 1.25 U GoTaq G2 Hot Start Polymerase (Promega; M7401), 1X GoTaq Flexi Buffer (Promega; M890A)) in 50 µl final volume and amplified as follows: *TRAC* (2 min 94^{o}C; 35 cycles x 30 secs 94^{o}C, 30 secs 55^{o}C, 45 secs 72^{o}C; 5 min 72^{o}C), *STX6* (2 min 94^{o}C; 35 cycles x 30 secs 94^{o}C, 30 secs 65^{o}C, 50 secs 72^{o}C; 5 min 72^{o}C). 12.5 µl PCR products were run on a 1% agarose gel (Invitrogen; 16500-500) for 1.5 h at 65 V to confirm amplification before PCR clean-up using Genomic DNA Clean & Concentrator (Zymo; D4011) according to manufacturer's protocol. DNA sequencing was performed by Source Bioscience (Table 5; TRAC SEQ, STX6 SEQ) and analysed using Inference of CRISPR Edits (ICE) tool (Synthego).

2.8.4. Single cell cloning

Following ICE analysis, homogenous colonies of OLIG3 iPS cells transfected with *STX6*-targetting RNPs were isolated. To generate a single cell suspension, cells were detached using accutase (Gibco; A11105-01) for 5-10 min at 37^{o}C until completely detached from plate, suspension washed with DPBS and centrifuged at 200 x g for 5 min and pellet resuspended in 1 ml Essential 8 with 10 µM ROCK inhibitor and counted using a haemocytometer (NanoEntek; DHC-N01). 50,000 cells were plated in a Geltrex-coated 10 cm plate in 10 ml Essential 8 with 10 µM

ROCK inhibitor. Media was gently changed after 24 h to remove the ROCK inhibitor. After 1 week, colonies were selected in DPBS following 5 min incubation with 0.05% EDTA and transferred to a Geltrex-coated 96-well plate (Corning; 3595) in Essential 8 with 10 µM ROCK inhibitor. Media was again gently changed after 24 h to remove the ROCK inhibitor.

2.8.5. Colony screening by PCR

During the first passage in the 96-well plate format, 10 µl cell suspension was removed for screening by PCR. Crude lysates were generated by incubating the cell suspension with 10 µl 2X lysis buffer (2X GoTaq Flexi Buffer (Promega; M890A), 0.2 mg/ml PK (Invitrogen; AM2546), 1% NP40 (Thermo Fisher; J19628.AP) in a PCR plate (Thermo Scientific; AB-0800) at 55ºC for 45 min followed by 95ºC for 10 min using an Alpha Cycler 4 thermocycler (PCRmax). 5 µl lysates were then added to 7 µl PCR mix (500 nM forward primer, 500 nM reverse primer (Table 5; STX6 PCR 2), 2.5 mM $MgCl_2$, 5% DMSO (Thermo Scientific; 85190), 0.2 mM each dNTP, 1.25 U GoTaq G2 Hot Start Polymerase (Promega; M7401), 1X GoTaq Flexi Buffer (Promega; M890A)) in 12 µl final volume and amplified as follows: 2 min 95ºC; 38 cycles x 45 secs 95ºC, 45 secs 63ºC, 30 secs 72ºC; 5 min 72ºC. PCR products were run on a 2% agarose gel at 200 V for 2 h with 100 bp DNA molecular weight marker (Bioline; BIO-33056). Required clones were expanded for cryopreservation in 10% DMSO/Essential 8.

2.8.6. Karyotyping

Karyotyping of most common iPS chromosomal abnormalities was performed using hPSC Genetic Analysis Kit (Stem Cell Technologies; 07550) according to manufacturer's protocol. DNA was extracted from cells as described previously (see section 2.8.3) and 300 ng used for analysis. qPCR reactions were prepared in MicroAmp Optical 384-Well Reaction Plates (Applied Biosystems; 4309849) and amplification was performed on QuantStudio 12K Flex Real-Time PCR System with 384-well block (Applied Biosystems) and analysed using the Genetic Analysis Application (Stem Cell Technologies).

2.8.7. Growth rate analysis

STX6 knockout iPS clones were passaged using accutase as described previously (see section 2.8.5) to enable counting and seeded at 85,000 cells per well into a Geltrex-coated 12-well plate in Essential 8 with 10 µM ROCK inhibitor.

Plates were incubated in the IncuCyte S3 Live-Cell Analysis System (Sartorius; 4647) (37°C, 5% CO_2) for 4 days. The IncuCyte S3 Software (2019B) was set up to acquire 25 images per well in the phase channel every 4 hours at 20X objective. Media was replaced after 24 hours to remove ROCK inhibitor. Growth rate was calculated as previously described (see section 2.4.6).

2.8.8. Whole exome sequencing

Whole exome sequencing (WES) was performed by Novogene as per their standard pipeline. Following gDNA extraction as previously described (see section 2.8.3) DNA quality was measured by ratio of absorbance at 260/280 nm (>1.8) and concentration measured using Qubit fluorometer. Samples were prepared as >1 µg DNA at >20 ng/µl in ddH_2O and transferred on dry ice to Novogene for analysis. Briefly the Novogene WES pipeline is as follows: libraries were prepared by sonication prior to exonuclease digestion to generate blunt ends and ligation of adapter sequences; exomes were hybridised with biotin-labelled probes and captured with streptavidin-conjugated magnetic beads, purified and sequenced on the Illumina PE150 platform; QC was performed on sequencing results (i.e. for artefacts, adapter contamination, low-quality reads) and aligned to the reference genome (GRCh38) to identify germline single nucleotide variants (SNVs), copy number variants (CNVs) and insertions/deletions (indels).

'Somatic' mutations were identified by comparing CRISPR cell clones to the untransfected parent line (OLIG3). For analysis of CRISPR off-target effects, predicted cut sites by Cas9 endonuclease up to 4 mismatches between sgRNA and target were obtained for each sgRNA sequence from the Guide Verification Tool (Synthego) adapted from a publication by Doench et al (Doench et al., 2016). Somatic mutations were extracted within 100 kb upstream and downstream of each predicted cut-site.

2.8.9. Differentiation into cortical neurons

iPS cells were differentiated into cortical neurons using dual SMAD inhibition as previously described with modifications (Shi, Kirwan, & Livesey, 2012). Cells were passaged into Geltrex-coated (1:100) 12-well plates at a ratio of 2.5 wells/6-well to 1 well/12-well to achieve 100% confluence after 24-48 h. To induce

differentiation culture media was exchanged for NB27 media (1:1 N2 (1X N2 (Gibco; 17502-048), 5 µg/ml insulin (Sigma; I9278), 1 mM L-glutamine (Gibco; 25030-024), 100 µM non-essential amino acids (Gibco; 11140-035), 100 µM β-mercaptoethanol (Gibco; 21985-023), 50 U/ml penicillin/50 mg/ml streptomycin (Gibco; 15070-063), DMEM/F12 with GlutaMAX (Gibco; 10565-018)) and B27 (1X B27 with vitamin A (Gibco; 17504-044), 200 mM L-glutamine, 50 U/ml penicillin/50 mg/ml streptomycin, Neurobasal (Gibco; 21103-049)) supplemented with dorsomorphin (1 µM; Cambridge Biosciences; SM03-10) and SB431542 (10 µM; Cambridge Biosciences; SM33-10) inhibitors ('Neural Induction media (NIM)'). Cells were grown in NIM for 10 days with complete media changes daily before gentle passaging with 0.02% EDTA with manual disruption onto laminin-coated 12-well plates (1:50; Trevigen; 3400-010-02) at a 2:3 ratio in NB27 media. Half media changes for fresh NB27 were performed every 2-3 days. At 20 days post-induction cells were passaged again using 0.02% EDTA at 2:3 onto laminin-coated 12-well plates and half media changed every 2 days. For wells with a high number of non-neuronal cells two additional passages were performed by incubating cells with 10 µg/ml dispase (Gibco; 17105041) for 3 mins at 37°C and washing cell suspension 3 x 10 ml DPBS without centrifugation.

At 35 days post-induction cells were passaged with accutase (Gibco; A11105-01) at 37°C for 10 min, washed in DPBS and pelleted at 280 x g for 3 min. Cells were resuspended in 1 ml NB27 media, cell count measured using the Countess II FL Automated Cell Counter and seeded as required: 10,0000 cells/well into laminin coated (1:100) 96-well plates (Grenier Bio-One; 655090), 100,000 cells/well onto laminin-coated (1:50) 13 mm glass coverslips (Epredia; CBAD00130RA020MNZ#0) in a 24-well plate. Half media changes for fresh NB27 were performed every 2-3 days for up to 50 days post-induction. For cryopreservation of neural stem cells at 30 days post-induction, cells were passaged using accutase as described and cell pellet resuspended in NB27/10% DMSO. Cryovials were stored in a freezing container at -80°C for >6 hours and transferred to vapour phase nitrogen for long term storage.

2.8.10. Immunofluorescence

Cells were fixed with 3.7% formaldehyde in DPBS for 15 min at RT, washed 3 x 5 min DPBS and stored at 4°C until use. Prior to antibody staining cells were

permeabilised with 0.3% Triton X-100 in blocking buffer (3% bovine serum albumin (BSA; Sigma; 05479), 5% horse serum (Gibco; 16050122) in DPBS) for 5 min at RT. Wells were rinsed with DPBS before incubating with blocking buffer for 1.5 h at RT and incubation with primary antibodies ON at 4°C (Table 2) in antibody buffer (3% BSA, 1% horse serum, 0.1% Triton X-100 in DPBS). The following day wells were washed 3 x 5 min DPBS before incubation with fluorophore-conjugated secondary antibodies (1:500) for 1 h at RT in antibody buffer protected from light (Invitrogen; Table 3). Antibodies were aspirated and nuclei stained with DAPI (1:5000; Merck; D9542) for 15 min at RT before washing again 3 x 5 min DPBS. Coverslips were mounted onto microscope slides (Dixon Science; N/A143) with fluorescence mounting medium (Agilent; S3023) and left to dry ON before imaging. Images were acquired using a confocal microscope (Ziess; LSM 710) at 20 X and 63 X objective.

2.9. Prion transmission in *Stx6* knockout mice

2.9.1. Mice

2 x male and 2 x female *Stx6*$^{+/-}$ mice (C57BL/6NTac-Stx6$^{em1(IMPC)H}$/H) were obtained from MRC Harwell on a C57BL/6NTac genetic background. Briefly knockout was generated by MRC Harwell through CRISPR-mediated deletion of 1808 nt spanning critical exons 6 and 7 forming a premature stop codon.

In-house mouse husbandry and dissections were performed by staff at the animal facility including Lucy Draper, Ami Woodcock and Thomas Horan when breeding and maintaining these lines. The breeding plan was designed and instructed by myself. Cross-breeding established a knockout *Stx6*$^{-/-}$ line and a wildtype *Stx6*$^{+/+}$ line from littermates. Hemizygous litters were obtained as required through cross-breeding of these two lines. Work was performed under approval and license granted by the UK Home Office (Animals (Scientific Procedures) Act 1986), which conformed to UCL institutional and Animal Research: Reporting of In Vivo Experiments (ARRIVE) guidelines.

2.9.2. Genotyping

DNA was extracted by Shyma Hamdan from ear biopsies of all mice. Genotypes were confirmed using 2 PCR assays by myself. For PCR assay 1, 2 µl DNA was added to 23 µl PCR mix (500 nM forward primer (5'-

CGATCTGTGAGACTCATCGGG; Sigma), 500 nM reverse primer (5'-GGGAGTCCTAACACCACCTTC; Sigma), 2 mM $MgCl_2$, 0.2 mM each dNTP, 0.025 mM GoTaq G2 Hot Start Polymerase (Promega; M7401), 1X reaction buffer) and amplified using Alpha Cycler 4 thermocycler (PCRmax) (2 min 94°C; 30 cycles x 30 secs 94°C, 30 secs 61°C, 2.5 min 72°C; 5 min 72°C). PCR reactions were electrophoresed on a 1.5% agarose gel with 1 kb DNA molecular weight marker (Bioline; BIO-33053) at 70 V for 2 h. For PCR assay 2, 1 µl DNA was added to 24 µl PCR mix (500 nM forward primer (5'-CCTGACTCTCTGATAGCCAC; Sigma), 500 nM reverse primer (5'-ACAAAACCAAAGCCTGCAC; Sigma), other components as previous) and amplified as previous (2 min 94°C; 28 cycles x 30 secs 94°C, 30 secs 54°C, 45 secs 72°C; 5 min 72°C). PCR reactions were run on 2% agarose gel with 100 bp DNA molecular weight marker (Bioline; BIO-33056) at 70 V for 1.5 h. Bands were detected using RedSafe Nucleic Acid Staining Solution (1:20,000, iNtRON Biotechnology; 21141) on Universal Hood II Gel Doc System (Bio-Rad).

2.9.3. Immunoblot of mouse brain homogenate for syntaxin-6

Mice were culled at 61-65 days, brains removed, dissected on the sagittal plane and flash frozen. Samples were thawed on ice, weighed and ribolysed with ceramic homogenisation beads (Bertin Technologies; KT03961-1-009.2) at max speed for 105 secs as 20% homogenates in DPBS. 10 and 20% homogenates were stored at -80°C until use. Protein concentration was measured using a Bradford assay (see section 2.4.4) and 35 µg used for immunoblot analysis as previously described (see section 2.4.5). Syntaxin-6 was detected using two different monoclonal antibodies (clone C34B2, 1:500; clone 3D10, 1:500; Table 2).

2.9.4. ELISA for PrP^C expression

Brain homogenates were prepared for analysis by myself; ELISA was performed by Michael Wiggins De Oliveira. Brain homogenates were prepared and protein concentration assayed as previously described (see section 2.9.3). Samples were diluted to 3.5 mg/ml total protein in PBS in 40 µl volume. To correspond to standard protocols (i.e. where PK-resistant PrP is measured), 2 µl AEBSF (stock 100 µM) and 5 µl 20% w/v SDS was added to each sample and boiled at 100°C for 10 min. 8 µl sample aliquots were prepared and stored at -80°C until use. A

high-binding 96-well flat bottom plate was pre-coated with 100 µl of 2.5 µg/ml anti-PrP antibody (ICSM18; D-Gen Ltd) in 0.05 M carbonate coating buffer (0.035 M $NaHCO_3$, 0.015 M Na_2CO_3, pH 9.6) and incubated at 4°C overnight. The following morning plates were washed with 3 x 1% PBST. 240 µl pre-heated capture buffer (37°C, 30X, pH 8.4; 2% N-Lauroylsarcosyl, 2% BSA, 2% Triton X-100, 50 mM Tris base pH 8.0) was added to each 8 µl sample aliquot fresh, 50 µl sample added to each well in triplicate and incubated at 37°C for 1 h. Sample was washed with 3 x 1% PBST prior to detection with 1 µg/ml biotinylated anti-PrP antibody (ICSM35; D-Gen Ltd) diluted in 1% PBST at 37°C for 15 min and washed as previous. For detection 100 µl streptavidin-HRP (horse radish peroxidase; Thermo Scientific; PIER21126) diluted 1:10,000 in PBST was added to each well and incubated at 37°C for 15 min prior to development with QuantaBlu Fluorogenic Peroxidase Substrate Kit (Thermo Scientific; 15169) as per manufacturer's instructions. Plates were imaged using a plate reader (Tecan Infinite M200) with 313 nm and 398 nm excitation and emission wavelengths respectively.

2.9.5. Inoculation study

Experimental design, preparation of inocula, project management and oversight was performed by myself. Inoculation, subsequent monitoring and dissections were performed by staff at the animal facility including Nick Kaye, Craig Fitzhugh and Gavin Graham. Anaesthetised mice were inoculated intracerebrally in the right parietal lobe with 30 µl 1% C57BL/6J mouse-adapted RML or ME7 prion-infected brain homogenate (inocula codes I16183 and I16179 respectively) as previously described (O'Shea et al., 2008). Power calculations were used to propose group sizes of 20 mice per experimental condition, sufficient to identify a 5% difference in incubation time whilst allowing for loss due to incurrent illness. Mice were monitored daily and culled following diagnosis with scrapie sickness according to established criteria or identification of distinct health concerns (O'Shea et al., 2008). Brains were removed, one hemisphere flash frozen and stored at -80°C and the other fixed in 10% formal buffered saline for histopathological analysis.

2.9.6. Behavioral and physiological phenotyping

Behavioural studies were designed and analysed by myself along with Michael Farmer and Thomas Coysh. Experiments were performed by Michael Farmer and Thomas Coysh on PBS-inoculated control mice (4-5 mice per group) aged 52-60 weeks.

Mice were lone housed for these analyses with sufficient rest time between tests, and not tested within 24 h of cages being cleaned. Nesting analysis was performed according to (Deacon, 2006a). Briefly, animals were lone housed with nestlets (LBS Biotechnology; 1039029) in the afternoon and nestlets scored from 0-5 the following morning based on a standard quality scale. Burrowing was performed as per (Deacon, 2006b) and mice were habituated with cylinders for 24 h prior to testing. Burrowing cylinders were filled with 200 g food pellets the afternoon and added to lone housed mice for 18 h. Remaining pellets were then weighed the following morning and difference calculated. Two rounds were performed to allow for practice and reduced variability; the second round only used in the analysis. Similarly, diet consumed overnight was measured as the difference in weights between food pellets added to the hopper (standard apparatus in mouse cage) (~200 g) and remaining food measured after 18 h. Motor coordination was measured as the time spent on the rotarod apparatus at an acceleration of 4 rpm and max speed 40 rpm, with a practice run followed by three replicates per animal, according to standard procedure (Deacon, 2013). Finally combined hind and forelimb grip strength was measured using a standard grip strength apparatus with three replicates per animal, normalised to mouse weight at the time of measurement. Behavioural tests were performed by Michael Farmer and Thomas Coysh.

At time of culling (aged 56-61 weeks), PBS-inoculated mice were weighed and nasoanal length measured, prior to dissection to remove both brains (as per section 2.8.7) and peripheral tissues. Subcutaneous perigonadal white adipose tissue (WAT) was removed and weighed and proportion relative to total body weight measured.

2.9.7. Survival analysis

Incubation time was defined as the number of days from inoculation until definite scrapie diagnosis (O'Shea et al., 2008). Disease-free incubation time was defined as the number of days from inoculation to presentation of the first scrapie-associated neurological symptom. Kaplein-Mayar survival curves and analyses were generated using RStudio packages “survival” and “survminer” and differences in survival between genotypes for each inocula was analysed using a log-rank test. For analysis of incubation time to scrapie diagnosis, animals culled due to other reasons were censored, however for analysis of incubation time to onset of first symptoms animals culled due to wet genital region were not censored.

2.9.8. Immunohistochemistry for prion-related neuropathology

Immunohistochemistry for prion-related neuropathology was performed by Tamsin Nazari, Florin Pintilli and Jackie Linehan and analysed by Sebastian Brandner as previously described with modifications (Wadsworth et al., 2021). Project management and design was performed by myself with Jackie Linehan. Transgenic mouse brains were fixed in 10% buffered formal-saline, processed and paraffin wax embedded. Serial sections of 5 µm nominal thickness were taken. Deparaffinised sections were investigated for abnormal human PrP, microglial, and astrocyte deposition on a Ventana Discovery XT automated IHC staining machine (Roche Tissue Diagnostics) using protocols developed on a Ventana Benchmark staining machine. Anti-PrP monoclonal antibody ICSM35 (1:1000; D-Gen Ltd) was used in conjunction with biotinylated polyclonal rabbit anti-mouse immunoglobulin secondary antibodies (Dako; Agilent) and Ventana proprietary detection reagents utilizing 3,3′-diaminobenzidine tetrahydrochloride as the chromogen (DAB Map Detection Kit; Roche Tissue Diagnostics). Sections were treated with cell conditioning solution (Discovery CC1; Roche Tissue Diagnostics) at 95°C for 60 minutes followed by treatment with a low concentration of protease (Protease 3; Roche Tissue Diagnostics) for 12 minutes prior to staining. Anti-iba1 microglial antibody (1:250; AlphaLaboratories; 019-19741) or anti-GFAP antibody (1:1000; Agilent; Z0334) were used in conjunction with biotinylated polyclonal goat anti-rabbit immunoglobulin secondary antibodies (Dako; Agilent) and Ventana proprietary detection reagents utilizing 3,3′-

diaminobenzidine tetrahydrochloride as the chromogen (DAB Map Detection Kit; Roche Tissue Diagnostics). Sections were treated with cell conditioning solution (Discovery CC1; Roche Tissue Diagnostics) at 95°C for 60 minutes or a medium concentration of protease (Protease 1; Roche Tissue Diagnostics) for 4 minutes 0respectively prior to staining. Conventional methods on a Gemini AS Automated Slide Stainer (Thermo Fisher Scientific) were used for hematoxylin and eosin (H&E) staining. Positive controls for the staining technique were used throughout. All slides were digitally scanned on a Hamamatsu NanoZoomer 360 instrument, and images were captured from the NDP.serve3 software (NanoZoomer Digital Pathology) and composed with Adobe Photoshop.

2.9.9. Immunohistochemistry quantification and statistical analysis

Immunostaining of GFAP and Iba1 in whole brain sections were quantified using QuPath (v0.3.0) software on 4-5 mice from PBS-inoculated groups (1-3) and 7-10 mice from prion-inoculated groups. Colour deconvolution was performed to distinguish DAB staining from H&E background and pixel classification used to select tissue for analysis (whole brain). Pixel classification was applied further to select regions positive for DAB staining (classifier trained on 10% of total images). Area positive for DAB staining was calculated for each image and % area stained calculated relative to total tissue area analysed. Statistical differences genotypes within each group were determined using a one-way ANOVA (after confirmation of normal distribution and equal variances for use of a parametric test) and Tukey's post-hoc test using RStudio (v1.1.463) software.

2.10. Expression analysis in human samples

2.10.1. Immunohistochemistry of frontal cortex and cerebellum

Immunohistochemistry performed by Tamsin Nazari, Helena Costa and Jackie Linehan and analysed by Sebastian Brandner. Immunostaining was performed on 19 sCJD cases obtained from the Division of Neuropathology, University College London Hospitals NHS Foundation Trust and 15 non-prion control cases obtained from Queen Square Brain Bank as frozen material which was formalin fixed by immersion, formic acid treated and processed as standard into a Formalin Fixed Paraffin Embedded (FFPE) sample. Frontal cortex and

cerebellum (including the dentate nucleus) were stained with anti-syntaxin-6 antibody (1:100, Atlas Antibodies; HPA038558) for 8 h at RT.

2.10.2. RT-qPCR analysis of human cerebellum

RNA extraction and RT performed by Penny Norsworthy and myself. RNA was extracted from 50 – 100 mg post-mortem cerebellum of 10 sCJD cases and 10 neurologically normal controls using the Directzol DNA/RNA miniprep kit (Zymo; R2080) according to manufacturer's instructions. Following an additional DNase I digestion and purification using RNA Clean and Concentrator-5 (Zymo; R1013) samples were analysed using TapeStation 2200 (Agilent) for integrity (RNA integrity number (RIN) > 4) and concentration. RT-qPCR was then performed as previously described (section 2.4.3) using the following primer assays: *CYC1*: Hs_CYC1_1_SG, *RPL13*: Hs_RPL13_1_SG, *UBE2D2*: Hs_UBE2D2_1_SG, *BMERB1*: Hs_C16orf45_2_SG, *STX6*: Hs_STX6_2_SG, *PDIA4*: Hs_PDIA4_1_SG, *GAL3ST1*: Hs_GAL3ST1_1_SG, *PRNP*: Hs_PRNP_1_SG.

2.11. Statistical analysis

Statistical analysis was performed using RStudio (v1.1.463) software. Where feasible populations were tested for normal distribution using Shapiro-Wilk test and equal variances using Levene's test and transformed as appropriate. Group differences were analysed using Student's t-test or One-Way ANOVA with Tukey's *post-hoc* test. *n* number indicates independent biological replicates. Plots were generated using RStudio package "ggplot2".

3. Genome-wide association study for sCJD

3.1. Introduction

3.1.1. Genome-wide association studies

The advent of lower-cost and higher-quality methods to obtain “genome-wide” information has allowed collation of increasing sample numbers for human genetics studies, allowing researchers to overcome previous limitations of power due to vast human genetic diversity in whole-genome comparisons. This has led to increasing GWAS being performed for a vast number of complex traits and diseases over the last two decades. The “completion” of the first human genome sequence in 2003 and the since development of a reference sequence, has led to accumulating knowledge of common variation in the human population and identification of SNPs, as well as description of regularly inherited regions or haplotypes with patterns of LD separated by recombination hotspots (International HapMap Consortium, 2005; International Human Genome Sequencing Consortium, 2004). It is this understanding of “block-like” inheritance and consequent redundant SNPs which increased feasibility of GWAS, allowing for “genome-wide” information to be obtained from the genotype of just a subset of variants.

Generally GWAS are performed by comparing the allele frequency of SNPs (but can also be used to look at other variation such as copy number variants) between different groups of individuals, to identify genetic regions associated with a particular phenotype (Figure 8) (GWAS methodology comprehensively reviewed recently in (Uffelmann et al., 2021)). After collation of DNA and relevant phenotype information, genotypes are currently most commonly obtained through commercially available microarrays, now available with probes for over two million SNPs. Due to the aforementioned haplotypes and LD structures, additional SNPs can then be imputed from reference genomes to obtain near whole-genome information. Of note, data obtained from whole-genome sequencing (WGS) still provides more accurate genetic information such the presence of rare variants, which is likely to be increasingly used for GWAS with reducing costs of these technologies.

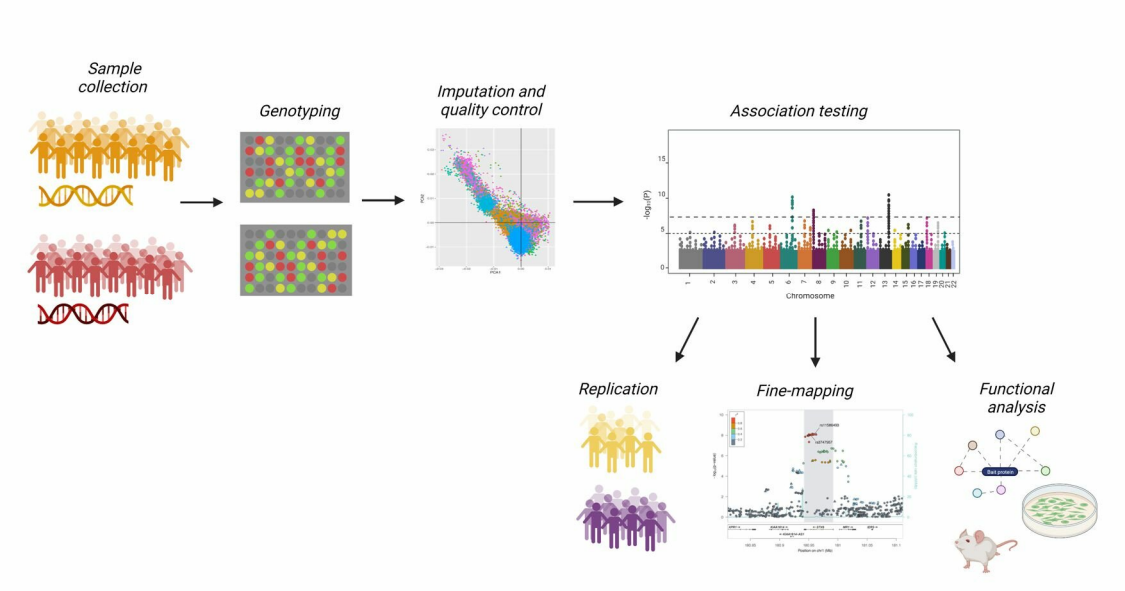

Figure 8: Outline of case-control genome-wide association studies (GWAS).
Outline of a typical case-control GWAS. Samples are collected from individuals with the phenotype of interest (e.g. disease) and relevant matched controls and genotyped i.e. using a microarray. Following imputation of additional variants (if required) data is processed through quality control parameters such as genotyping quality, low allele frequencies and detection of population stratification (depicted). Allele frequencies between the two populations can then be compared in an association test, typically a logistic regression test. Significant variants can then be replicated in an independent cohort to secure association, fine-mapped to highlight putative causal variants and analysed using various functional data sets and wet-lab testing to define underlying biological mechanisms. Figure adapted from (Uffelmann et al., 2021) and generated with biorender.com.

After sufficient quality control measures are implemented, for example to identify inaccurate genotype calls or to ensure that all samples are of similar ancestry to avoid false-positive associations, allele frequencies can be compared in a statistical association test. Typically this a logistic regression test for case-control GWAS (or linear regression if looking at continuous traits) with inclusion of covariates which may confound results such as age, sex and ancestry. Importantly, careful consideration must be given to thresholds for identifying significant variants, due to the vast number of simultaneous tests performed; a Bonferroni-corrected threshold of $P < 5 \times 10^{-8}$ is generally applied to account for an estimated one million independent genomic signals ($P = 0.05/10^6$) (International HapMap Consortium, 2005). To most accurately account for false-discovery rates, allele frequencies should be replicated in an independent cohort.

3.1.2. Post-GWAS analysis

Although the presence of LD blocks is highly useful for obtaining genome-wide information at low cost, this also generates one of the most prominent limitations with GWAS studies; genome-wide significant variants do not immediately amount to mechanisms of association due to the concurrent identification of multiple variants. These can often encompass multiple genes, or more frequently no genes at all, making identification of which genes or variants are driving this causal association difficult. Therefore, to limit the number of variants and genes required for follow-up analysis, statistical and functional tools are implemented in a process termed “fine-mapping” (Schaid, Chen, & Larson, 2018; Spain & Barrett, 2015).

Fine-mapping can be performed solely using statistical modelling (Schaid et al., 2018). Firstly this can be performed using a stepwise conditional analysis, using the lead variant as a covariate in the association analysis and including subsequent significant SNPs until no tests are significant. This can be used to identify independent signals from the lead SNP. However there are limitations to this simple method, including the aforementioned issues with performing multiple statistical tests in tandem, as well as limited power to detect additional SNPs with low effect sizes. Therefore, alternative fine-mapping strategies have been developed, primarily using Bayesian frameworks. In these methods, Bayes factors (the likelihood of the data given that each variant is causal) are calculated using the evidence of association at each variant, allowing for input of additional evidence such as LD structure and sample size, to calculate the posterior probabilities for causality for each variant. The possibility of multiple causal variants can also be included to generate the prior model. Typically these tools output a 95% credible set for each locus, containing the minimum variants summing to a total of 95% posterior probability. In the current study, CAVIAR (‘Causal Variants Identification in Associated Regions’) was implemented which uses this Bayesian model allowing for up to six causal SNPs at a locus to output a causal posterior probability (Hormozdiari et al., 2014).

In silico fine-mapping can be useful for increasing the resolution at a locus and highlighting putative independent causal SNPs, however these are only ever indications and cannot provide robust evidence for causality and is especially

limited in regions of high LD. Integration of functional datasets with GWAS data can be very powerful in both highlighting causal variants and genes, as well as indicating the underlying mechanisms which might be driving the association (Spain & Barrett, 2015). A plethora of publically available tools and datasets have now been developed. These include annotations of the functional consequences of variants (e.g. ANNOVAR, variant effect predictor (VEP) (McLaren et al., 2010; K. Wang et al., 2010)) and deleterious effects (e.g. CADD (Kircher et al., 2014)), non-coding regulatory elements including methylation sites, transcription factor binding sites, promoters and enhancers (e.g. the Encyclopaedia of DNA Elements (ENCODE) project, Functional Annotation of the Mammalian Genome (FANTOM) and the NIH Roadmap Epigenomics Consortium (Encode Project Consortium, 2012; Fantom Consortium and the RIKEN PMI and CLST et al., 2014; Roadmap Epigenomics Consortium et al., 2015)) as well as variants which modify gene expression called expression quantitative trait loci (eQTL; e.g. the Genotype-Tissue Expression (GTEx) project (GTEx Consortium, 2015)). The spatial nature of these datasets can indicate tissues in which variants are most likely to have a functional effect, and the advent of single-cell experiments can even highlight the most relevant cell types. After all, the ability to translate genomic loci into biological mechanisms underpins the motivation for performing GWAS in the first place. For example, in this chapter, eCAVIAR (an extension of the tool previously described) is used to identify overlap in causal variants from the GTEx eQTL analysis (Hormozdiari et al., 2016).

3.1.3. Benefits and limitations of GWAS methodology

It is no doubt that GWAS have been successful at furthering our understanding of the genetic architecture of complex traits and disease (Tam, Patel, Turcotte, & Boss, 2019). At the time of writing the NHGRI-EBI GWAS catalogue lists 5273 different publications identifying over 275,000 associations, demonstrating the huge value of this method (Buniello et al., 2019; NHGRI-EBI, 2021). The number of variants identified however is reliant on the sample size used; along with the decreasing cost, the increasing appreciation of multi-study meta-analyses and cultivation of cross-laboratory consortiums is facilitating larger scale studies, now reaching over one million participants (J. J. Lee et al., 2018). This has not only allowed realisation of biological mechanisms contributing to a number of

diseases, but is aiding our understanding of complex traits through identification of loci contributing to the 'missing heritability' not attributed from family studies, as well as furthering knowledge of the ethnic variation seen in both quantitative traits and disease risk (Tam et al., 2019). Furthermore, the expanse of genetic data that GWAS have amassed has widespread applications beyond genotype-phenotype testing, such as population studies, analysis of LD structure, generating polygenic risk scores, forensic analysis and ancestry testing.

GWAS, as with all methodologies, does come with limitations which should be considered (reviewed in (Tam et al., 2019)). As previously mentioned, fundamentally identification of regions of association does not equal pinpointing of causal genes or variants due to LD linking neighbouring genes and trans-acting regulatory regions. Furthermore, over 90% of disease-associated variants identified by GWAS are in non-coding regions of the genome of which relatively little is understood (Maurano et al., 2012). Although our understanding of these regions is increasing, for example through mapping of regulatory and epigenetic elements, there are a substantial number of associated loci for which the biological mechanism is unknown. The methodology behind GWAS also poses challenges with separating true-positives from noise due to multiple testing and population stratification; the implementation of stringent significance thresholds limits false-positive associations but is also likely resulting in substantial data loss. Furthermore there is debate about the translational nature of these studies both to a clinical setting (i.e. whether large numbers of variants with small effects sizes pose as feasible drug targets) as well as to other populations – as of 2019 over 80% of GWAS were performed solely on individuals of European descent, the findings of which are often not applicable to other populations (M. C. Mills & Rahal, 2019).

3.1.4. GWAS for human prion diseases

For diseases such as sCJD for which little is understood about susceptibility, GWAS could provide key insight into novel underlying mechanisms and even therapeutic targets. Although *PRNP* is clearly a key genetic determinant for all human prion diseases (previously discussed in section 1.4), it is not yet known whether targeting this will prove an effective and viable treatment in the clinic (Jones & Mead, 2020). It is therefore still of interest to identify additional disease

modifiers for both mechanistic and therapeutic applications. Furthermore there is increasing evidence that related neurodegenerative diseases share common mechanisms with prion diseases such as the templated conversion into pathogenic aggregates (see section 1.6.1)), and so modifiers of prion disease risk have the potential to translate to the spread of other 'prion-like' proteins (Jaunmuktane & Brandner, 2020).

The requirement of large sample sizes for sufficient power to detect associations has posed issues for prion disease research to date. A number of GWAS have been performed for a variety of disease types, all supporting *PRNP* codon 129 as a strong risk factor for all prion diseases, but the number of variants identified at genome-wide significance outside of the *PRNP* locus is minimal. In one of the largest studies totalling 2000 human prion disease cases, combining individuals from all disease subtypes to increase sample size, no non-*PRNP* SNPs were significantly associated with prion disease risk (although the *ZBTB38–RASA2* locus was suggestive) (Mead et al., 2012). The heterogeneity between diseases may not permit such analysis for identification of variants with weaker effect sizes. Studies focusing primarily on vCJD described evidence for an association with *RARB-THRB* in a single stage study (n = 119) (Mead, Poulter, et al., 2009) and *MTMR7* and variants nearby *NPAS2* in a meta-analysis of two cohorts (n = 135) (Sanchez-Juan et al., 2012), however these studies are both limited by a lack of replication evidence increasing likelihood of false-positive associations. There is some evidence for common genetic influences between diseases however, with *RARB-THRB* and *STMN2* also associated with iCJD and kuru risk respectively (Mead, Poulter, et al., 2009).

The sample sizes for these acquired prion diseases are limited due to reducing case numbers from public health intervention, but for sCJD sample resources are constantly growing, especially with international collaboration. Previous to the current study, the largest published GWAS to date for sCJD risk comprised a total of 1,543 cases (Sanchez-Juan et al., 2014). The discovery phase constituting only 434 of these however did not identify any non-*PRNP* genome-wide significant hits, but replication of top SNPs in the remaining samples and subsequent meta-analysis proposed association of one non-*PRNP* intronic SNP

in *GRM8*; subsequent fine-mapping of this locus suggested perturbations in miRNA binding.

Beyond risk, GWAS for prion diseases have also investigated genetic association with related clinical parameters. Poleggi and colleagues recently provided some evidence for SNPs tagging *CYP4X1* modifying age of onset for E200K-related IPD and sCJD by approximately 16 and 13 years respectively, however the discovery cohort in this study was highly limited with only 19 individuals (Poleggi et al., 2018). More modest effects have also been suggested for the *STMN2* locus for sCJD (five years for homozygous genotypes) as well as *ZBTB38–RASA2* SNPs however this targeted analysis of non-significantly-associated variants is likely subject to bias (Mead, Poulter, et al., 2009; Mead et al., 2012). Thompson et al additionally investigated genetic association for behavioural disturbance and psychiatric symptoms in human prion diseases, however no genome-wide significant loci were identified (Thompson et al., 2015).

3.1.5. Chapter summary

The discovery stage of this GWAS was performed by others (see Methods section 2.1) prior to the initiation of this thesis; all subsequent work described in this chapter, as well as all visualisation and analysis described, was original work performed by myself.

This study describes the first GWAS powered to detect variants with moderate effect sizes associated with sCJD risk with the aim to identify additional non-*PRNP* genetic associations and pathways associated with the disease. Statistical tools and publicly-available functional datasets were employed to predict the most likely causal genes and variants at associated sites, to minimise those required for time-consuming and costly functional follow-up, highlighting *STX6* and *GAL3ST1* as novel sCJD risk genes.

3.2. Results

3.2.1. Genome-wide discovery of risk-associated variants

Note that the work described in the current sub-section (3.2.1) was previously performed by others in the Mead lab, however has been included for completeness of the study described in this chapter.

Large sample sizes are essential for GWAS analysis to overcome the substantial multiple testing burden associated with comparing large numbers of variants in a single statistical test. Over the last decade, due to the rarity of sCJD making sample ascertainment difficult, an international collaboration of most prion disease research and surveillance centres in countries with populations of predominantly European ancestries was established, allowing collation of a total of 5,208 DNA samples from patients diagnosed with probable or definite sCJD for this study (Figure 9). These samples were divided across a two-stage study design with an initial genome-wide discovery phase followed by targeted replication of significant variants.

In the discovery study previously performed in the group, case genotypes were obtained using Illumina's BeadChip microarrays and additional variants imputed using the Michigan server. Following quality control (QC; see Methods section 2.1.2) genetic information for 6,314,525 SNPs was compared between 4,110 sCJD cases and 13,569 population-matched controls obtained from publically available databases (Figure 9) (Jones et al., 2020). A frequentist association test with an additive model performed using SNPTEST with population covariates did not demonstrate substantial genomic inflation ($\lambda = 1.026$) indicating a lack of systemic bias in the analysis.

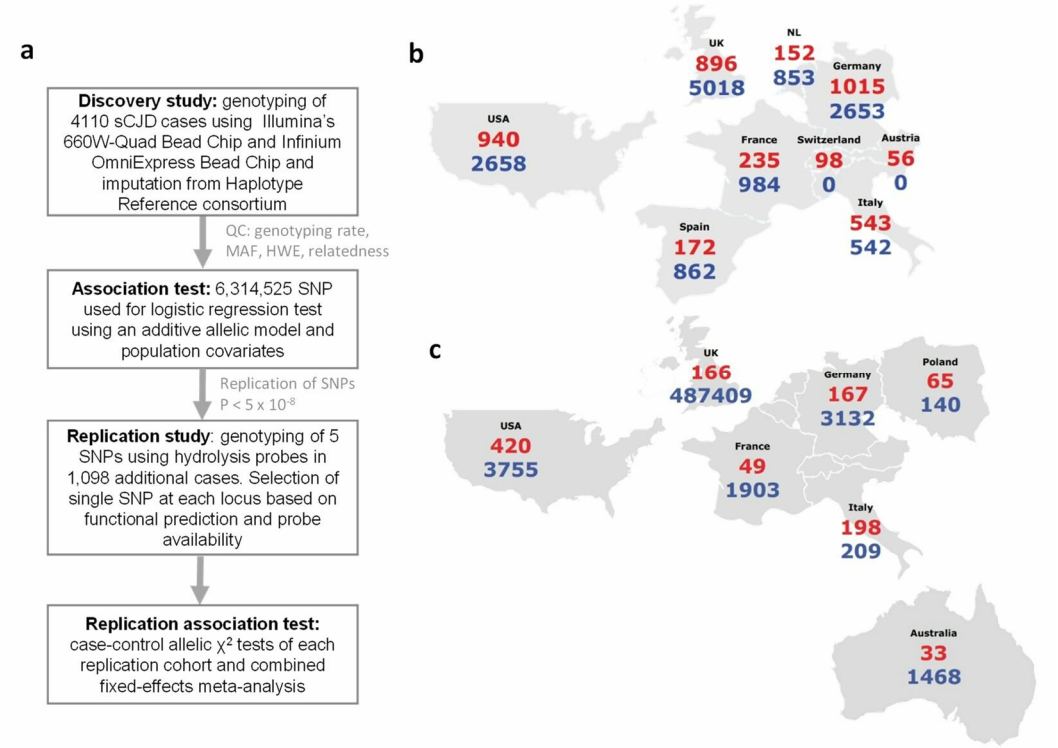

Figure 9: Study design for sCJD GWAS discovery and replication relied on worldwide collaboration.
(**a**) Flowchart of the GWAS two-stage study design including genotyping, imputation and quality control (QC) prior to association testing using SNPTEST. A single SNP at each genome-wide significant locus was then genotyped and to control for population differences independent association tests were combined in a meta-analysis. (**b**, **c**) Country of origin of all samples; (**b**) the discovery stage utilised a total of 4110 sCJD cases (red) and 13569 matched publicly available controls (blue) and (**c**) the replication phase an additional 1,098 cases and 498,016 further independent control samples matched for population. Note that the discovery study was performed previous to the original work described in this thesis; the replication study was performed by myself.

In this first phase a number of variants surpassed the significance threshold at $P < 5 \times 10^{-8}$ as shown in Figure 10. Alongside the known genetic risk at the *PRNP* gene (20p13, rs1799990; OR 1.23 [1.17 – 1.30], $P = 2.68 \times 10^{-15}$; Figure 11d), SNPs at two novel loci reached genome-wide significance, in and around the genes *STX6* (1q25.3, rs3747957; OR 1.16 [1.10 – 1.22], $P = 9.74 \times 10^{-9}$; Figure 11a) and *GAL3ST1* (22q12.2, rs2267161; OR 1.18 [1.12 –1.25], $P = 8.60 \times 10^{-10}$; Figure 11e). Two further sites were also suggestive of association around the genes *PDIA4* (7q36.1, rs9065; OR 1.17 [1.09 – 1.24], $P = 1.66 \times 10^{-6}$; Figure 11b) and *BMERB1* (16p13.11, rs6498552; OR 1.11 [9.96 – 1.29], $P = 6.45 \times 10^{-8}$;

Figure 11c); gene-based testing using VEGAS2 supported the association of these genes with sCJD risk (data not shown).

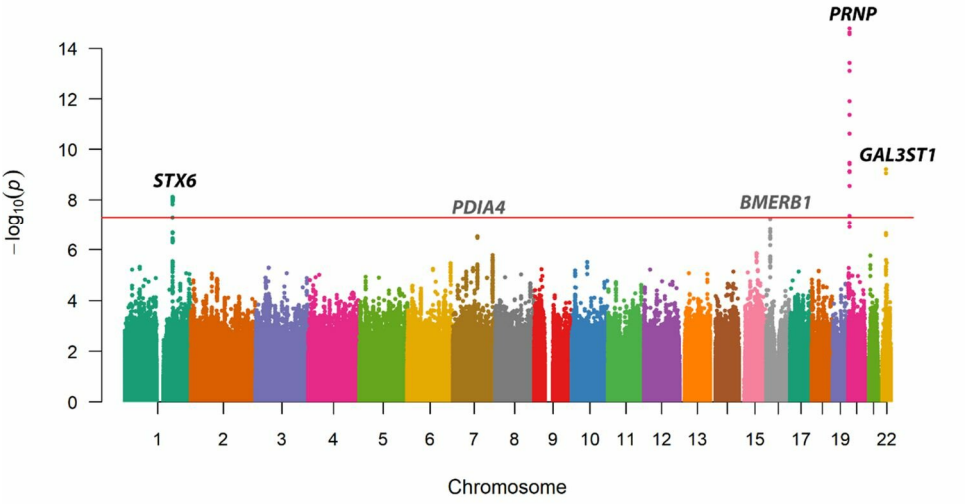

Figure 10: Manhattan plot highlighting *PRNP* and 2 novel non-*PRNP* sCJD loci, in or near to *STX6* and *GAL3ST1*, with associations that reached genome wide significance ($P < 5 \times 10^{-8}$) in the discovery GWAS.
Plot of $-\log_{10}$ of the P-values from an allelic logistic regression test of 4110 sCJD cases vs 13569 controls, with genome-wide significance threshold ($P = 5 \times 10^{-8}$) depicted by the horizontal line and colours indicating chromosome number. Labelled loci were chosen for further validation and replication following quality control, with multiple associated SNPs at these sites. *PDIA4* and *BMERB1* in grey were not significant at the replication stage. The analysis depicted in this figure was performed by Holger Hummerich and James Uphill; visualisation generated by myself.

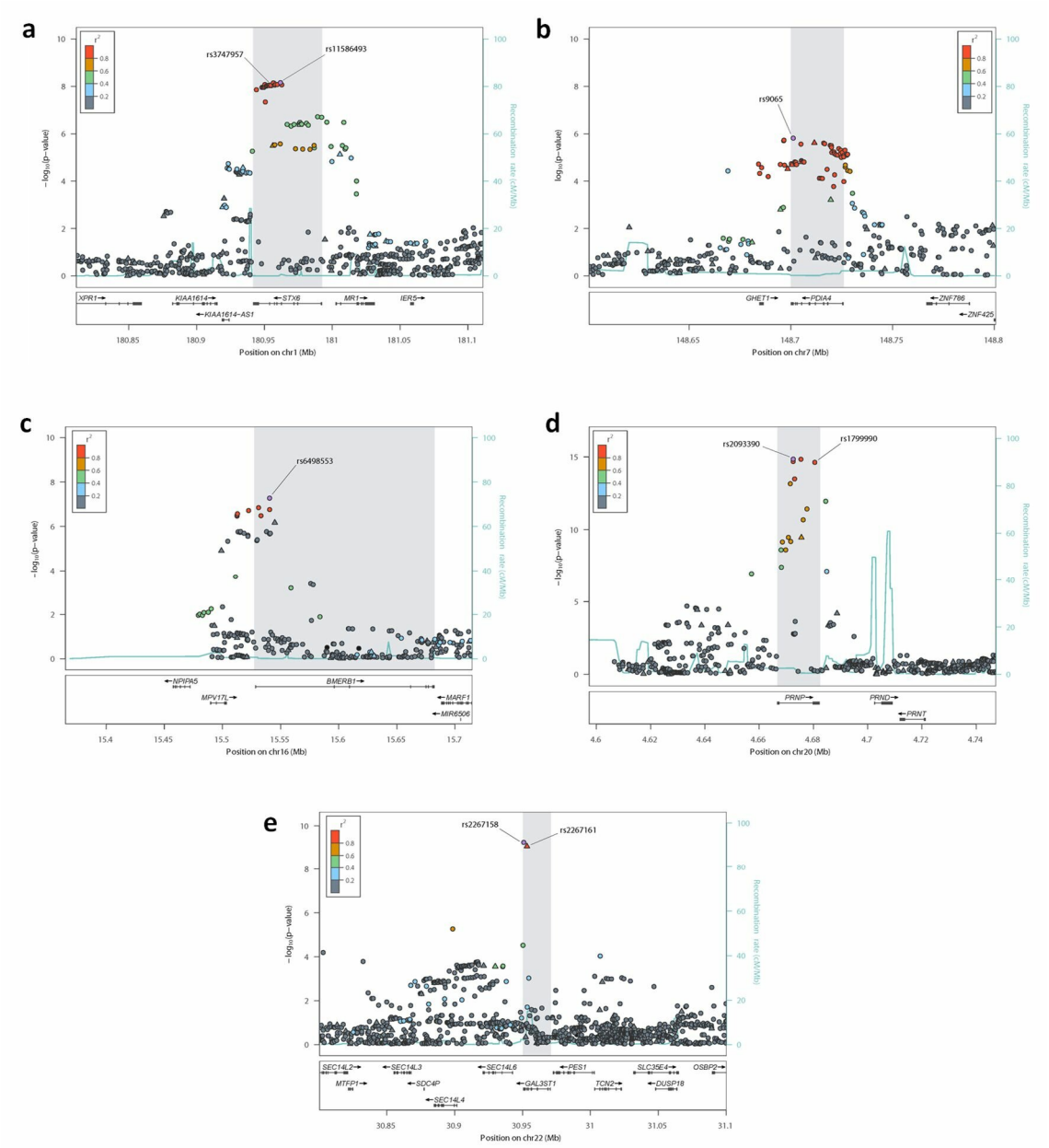

Figure 11: Regional plots for each of the significant loci shows expected linkage disequilibrium structure between top SNPs and neighbouring variants.
(**a**-**e**) Plot of $-\log_{10}$ of the P-values from the association analysis of SNP with highest significance at each locus. Colour indicates level of linkage disequilibrium (r^2) with top SNP estimated using the 1000 Genomes EUR dataset. The green line indicates recombination hotspots estimated from the HapMap project. SNPs directly genotyped are shown as a triangle symbols. (**a**) rs11586493 ± 150 kb, replication SNP rs3747957; (**b**) rs9065 ± 100 kb; (**c**) rs6498553 ± 175 kb; (**d**) rs2093390 ± 75 kb, replication SNP rs1799990; (**e**) rs2267158 ± 100 kb, replication SNP rs2267161. The analysis depicted in this figure was performed by Holger Hummerich and James Uphill; visualisation generated by myself.

3.2.2. Replication of genome-wide significant variants in an independent cohort

Replication of associations in an independent cohort is necessary in GWAS to prevent false-positive results due to the propensity for bias in this methodology. A SNP at each of the aforementioned loci which passed or approached the genome-wide significance threshold in the discovery stage were genotyped in the current study, using hydrolysis probes in an additional 1,098 cases and compared to 498,016 further controls (Figure 9). These variants were chosen from SNPs at each locus due to functional annotation or commercial availability of probes. Due to the lack of genome-wide data in the replication phase, association tests were performed independently for each case-control cohort matched for country of origin to avoid population stratification, and a meta-analysis was performed on the results.

Association of SNPs within *PRNP*, *STX6* and *GAL3ST1* was successfully replicated (P = 0.0049, P = 0.0034 and P = 0.042 respectively) in this new cohort, however *PDIA4* and *BMERB1* were not significant at this stage (P = 0.88 and P = 0.17 respectively) and reduced association in a meta-analysis with the discovery stage (Table 7); genotypes at multiple variants would be required to replicate the results of the gene-based test for these variants. As expected, the direction of effect was the same for both stages of the study (Figure 12a and b) with sufficient power (>80%) to detect an association for variants with genotype relative risk (approximate to odds ratio for diseases with low penetrance such as sCJD) of greater than 1.16 with an allele frequency over 0.2 in the discovery and replication phases (as is the case for the significant loci in this study) (Figure 12c and d). Due to the lower allele frequency of rs9065 and rs6498552, larger sample sizes maybe required to obtain sufficient power.

			rs1799990	rs3747957	rs2267161	rs9065	rs6498552
Nearest gene			***PRNP***	***STX6***	***GAL3ST1***	***PDIA4***	***BMERB1***
Location (GRCh37)			20:4680251	1:180953853	22:30953295	7:148700849	16:15539901
Type of mutation			Missense Intragenic	Synonymous Intragenic	Missense Intragenic	3' UTR	Intronic
Risk allele			A	A	C	T	T
Minor allele			G	A	T	T	T
Discovery stage	**Number of samples**	*Cases*	4110	4110	4110	4110	4110
		Controls	13569	13569	13569	13569	13569
	MAF	*Cases*	0.288	0.452	0.289	0.220	0.120
		Controls	0.340	0.410	0.322	0.191	0.102
	***P*-value**		2.68×10^{-15}	9.74×10^{-9}	8.60×10^{-10}	1.66×10^{-6}	5.75×10^{-8}
	Odds ratio (95% CI)		1.23 (1.17-1.30)	1.16 (1.10-1.22)	1.18 (1.12-1.25)	1.17 (1.09-1.24)	1.27 (1.16-1.38)
Replication stage	**Number of samples**	*Cases*	1,098	1,098	1,098	1,098	1,098
		Controls	498,016	498,016	498,016	498,016	498,016
	Average MAF*	*Cases*	0.294	0.450	0.302	0.203	0.105
		Controls	0.328	0.420	0.326	0.204	0.0972
	***P*-value; replication cohorts only**[†]		**0.0049**	**0.0034**	**0.042**	0.88	0.17
	Odds ratio (95% CI)		1.15 (1.04 – 1.28)	1.15 (1.05 – 1.26)	1.11 (1.00 – 1.23)	1.01 (0.90 – 1.13)	1.11 (0.96 – 1.29)
	***P*-value; with discovery cohort**[††]		9.61×10^{-17}	1.23×10^{-10}	1.97×10^{-10}	8.49×10^{-5}	6.45×10^{-8}

Table 7: *PRNP*, *STX6* and *GAL3ST1* SNPs were successfully replicated in an independent cohort (P < 0.05) to a similar effect as the discovery phase.
Summary of SNPs taken through from discovery to replication stages with P-value and odds ratios calculated from association tests listed. The replication P-values are given as [†]a meta-analysis of new case-control cohorts alone or [††]in combination with discovery summary statistics. *Replication minor allele frequencies (MAF) are estimated as a weighted mean of each cohort based on case sample number.

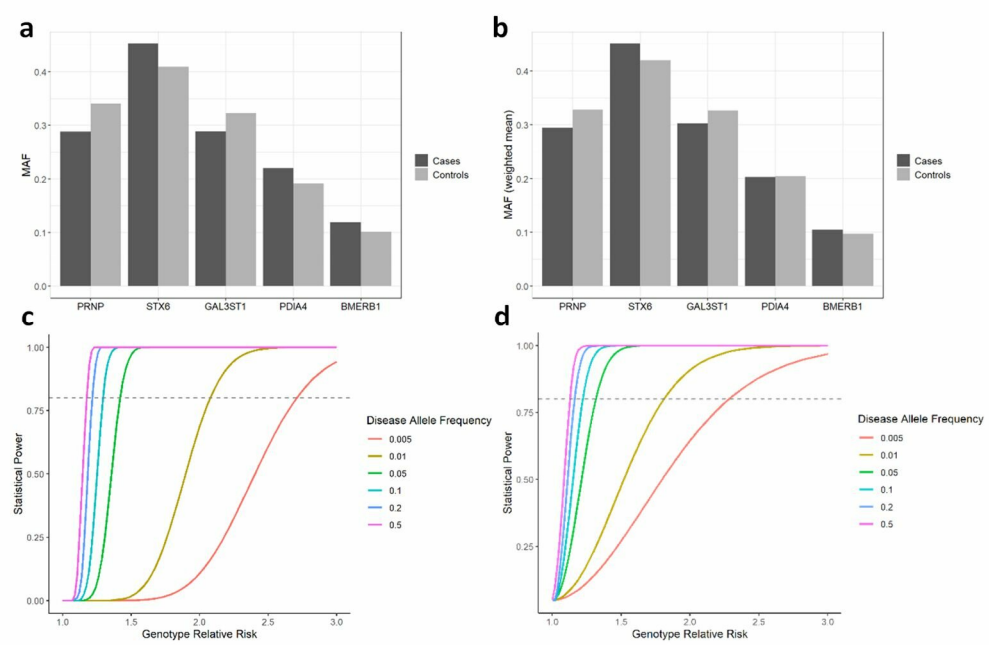

Figure 12: Case-control minor allele frequencies (MAF) support the replication of *PRNP*, *STX6* and *GAL3ST1* with >80% power to detect significant associations.
(**a**, **b**) MAF of replication SNPs in sCJD cases and controls for the (**a**) discovery and (**b**) replication stages. There is a clear distinction in allele frequency between the two groups for all 5 SNPs tested for the discovery, however in the replication phase the frequencies for *PDIA4* (rs9065) and *BMERB1* (rs6498552) are similar as reflected in the association test. Replication MAF calculated using a weighted mean of each cohort based on case sample number to better represent power allocation in the meta-analysis. (**c**, **d**) Statistical power to detect alleles with genotype relative risk stratified by disease allele frequency calculated using the Genetic Association Study (GAS) Power Calculator for the (**c**) discovery study ($P = 5 \times 10^{-8}$) and (**d**) replication study ($P = 0.05$) based on disease prevalence of 0.0002. Grey dotted line indicates statistical power of 0.8.

3.2.3. Fine-mapping of causal variants at risk-associated loci using linkage disequilibrium structure

Statistical fine-mapping was used initially to fine-map each locus and identify the most likely causal variants at each site. The CAVIAR ('Causal Variants Identification in Associated Regions') statistical framework was first utilised to identify a set with 95% probability of containing the causal SNP ('causal set') (Hormozdiari et al., 2014). This tool utilises a Bayesian framework to model the probability of each variant being causal, whilst allowing for the possibility of multiple causal variants at a single site. For *PRNP,* SNPs tagging rs1799990 were predominantly identified as expected, however a cluster of SNPs 5' to this in low LD were also putatively causal suggesting a potential additional signal at this locus (Figure 13a). In a secondary GWAS analysis utilising a heterozygous model more relevant to the known genetic effect of codon 129, conditioning for genotype at this site did not however support the association of this upstream signal (data not shown) (Jones et al., 2020).

At the *STX6* locus, the region of high LD surrounding rs3747957 increases the size of the causal set identified by the CAVIAR framework and makes identification of a single causal variant more challenging, however the variants with the highest causal posterior probability (CPP) fell within the *STX6* gene supporting this as a likely causal gene at this site (mean CPP of causal set; in *STX6* = 0.037 ± 0.0023 (SEM), outside *STX6* = 0.016 ± 0.0018) (Figure 13b). As the GWAS signal at the *GAL3ST1* locus is only associated with two SNPs in low LD with surrounding variants, these predominantly define the causal set as expected, but are statistically indistinguishable from each other using this method (Figure 13c).

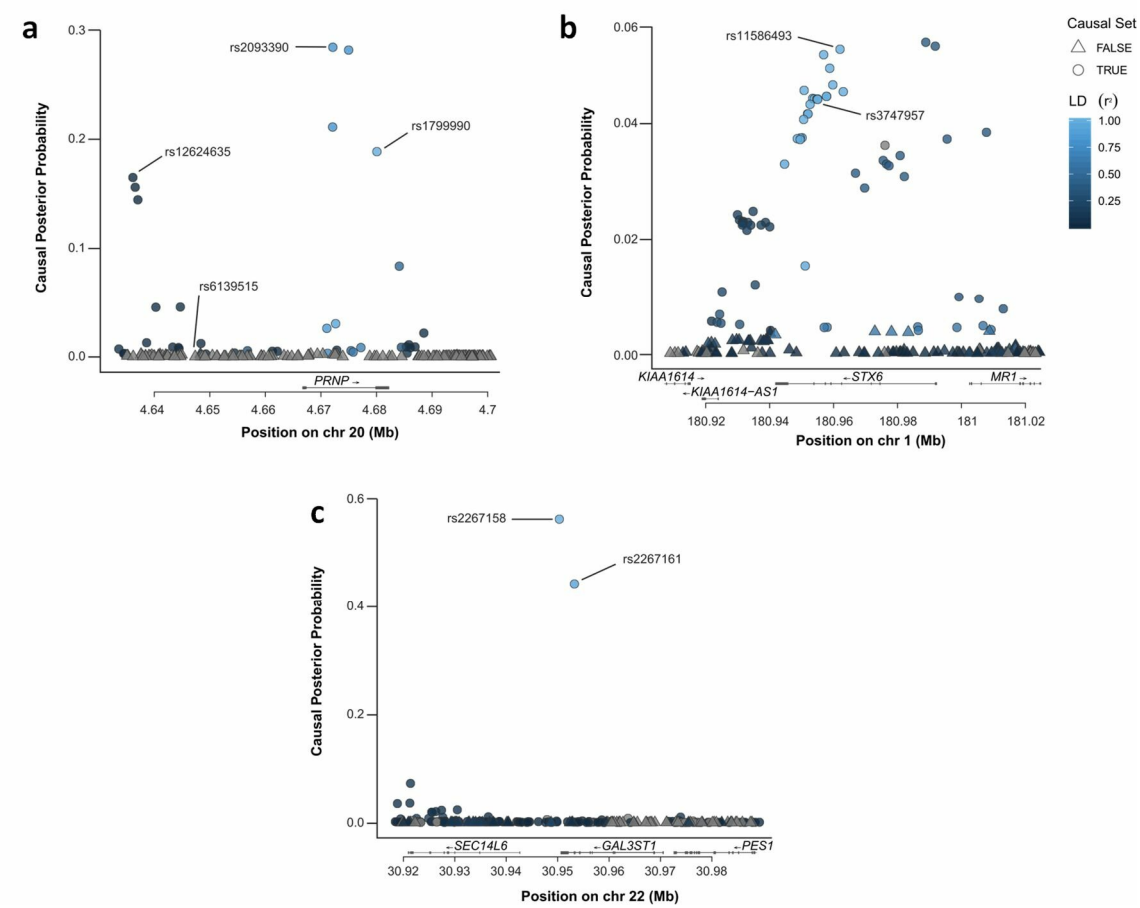

Figure 13: Statistical fine-mapping using CAVIAR identifies set of putative causal variants at each GWAS significant locus, suggesting potential additional signal in *PRNP* upstream of codon 129.

CAVIAR utilizes summary statistics and LD structure to predict the probability of each variant being causal, producing a 'causal set' with 95% probability of containing the causal SNP, whilst allowing for the possibility of multiple causal SNPs at each locus. Each locus was defined as 100 variants upstream and downstream of the top SNP. Plots show causal posterior probability of each variant at (**a**) *PRNP*, (**b**) *STX6* and (**c**) *GAL3ST1* coloured by LD with the top SNP. Circles indicate variants within the 95% causal set. LD calculated from 1000 genomes European population.

3.2.4. Integration of functional data with GWAS data at STX6 locus

Utilising LD structure to predict likely causal variants at a locus has utility for minimising the number of SNPs for functional follow up, however integrating additional functional datasets with GWAS results can be more powerful in both fine-mapping causal genes and variants, as well indicating potential biological mechanisms.

It was initially noted that, in the Genotype-Tissue Expression (GTEx) dataset, significant GWAS variants including rs3747957 were also significant eQTLs for the increased expression of *STX6* in the dorsal striatum (formed of the putamen and caudate) with the risk alleles, (putamen: rs3747957, $P = 2.3 \times 10^{-13}$, GTEx v7) (GTEx Consortium, 2015; Zerr et al., 2009); the log allelic fold change for rs7516739T ($r^2 > 0.99$ with rs3747957G; 1000 genomes EUR population) relative to the reference allele in the putamen is -0.231, corresponding to a 14.8% reduction in mRNA expression for the non-risk allele. The dorsal striatum is largely implicated in sCJD pathogenesis, clearly abnormal in patients in diagnostic magnetic resonance imaging (MRI) scans (Meissner et al., 2009).

Previous data have reported however that up to half of all risk-associated SNPs can act as an eQTL in at least one study (Gallagher & Chen-Plotkin, 2018). Therefore in order to investigate whether these eQTL and GWAS signals are driven by the same genetic mechanism, eCAVIAR (an extension of the CAVIAR software integrating eQTL causal variants) was utilised to analyse the degree of colocalisation of the sCJD GWAS risk variants with eQTLs in all 48 tissues present in the GTEx dataset, to elucidate the most relevant tissue and gene at this locus (Hormozdiari et al., 2016).

As the causal probability at this site is diluted across a region of high LD, the SNPs were first pruned against a variant inflation factor (VIF) threshold of five to extract independent signals (i.e. removing SNPs within high LD of $r^2 > 0.8$ with each other to generate a refined set of independent variants). A gene with expression significantly associated with any of the remaining variants ($P \leq 10^{-5}$) was defined as an eGene for that tissue and colocalisation posterior probability (CLPP) determined (Table 8). *STX6* expression in the caudate and putamen was most likely to be associated with the GWAS variants, along with this gene in the

hypothalamus and nearby *KIAA1614* expression in the tibial nerve. This is demonstrated by colocalisation of regional P-values from both studies as shown in Figure 14. Although eGenes are present for other variants, the low CLPP indicates a site distinct from the GWAS association signal is driving this, as demonstrated for *KIAA1614* eQTLs in the tibial artery (Figure 14e).

Gencode ID	Gene Symbol	Tissue	CLPP
ENSG00000135823	STX6	Brain - Caudate (basal ganglia)	0.918
ENSG00000135823	STX6	Brain - Putamen (basal ganglia)	0.916
ENSG00000135823	STX6	Brain - Hypothalamus	0.893
ENSG00000135835	KIAA1614	Nerve - Tibial	0.891
ENSG00000232586	KIAA1614-AS1	Whole Blood	0.120
ENSG00000135835	KIAA1614	Brain - Putamen (basal ganglia)	0.094
ENSG00000135823	STX6	Brain - Substantia nigra	0.063
ENSG00000232586	KIAA1614-AS1	Thyroid	0.005
ENSG00000230124	ACBD6	Cells- Transformed fibroblasts	0.003
ENSG00000243155	RP11-46A10.5	Small Intestine - Terminal Ileum	0.003
ENSG00000121454	LHX4	Cells - Transformed fibroblasts	0.003
ENSG00000135835	KIAA1614	Artery - Tibial	0.002

Table 8: Colocalisation of association statistics for sCJD GWAS and eQTLs in the GTEx dataset for SNPs at the *STX6* locus demonstrate highest colocalisation posterior probability (CLPP) with modified *STX6* expression in the dorsal striatum. 100 variants upstream and downstream of the top SNP at the *STX6* locus (rs11586493) were pruned for LD (variant inflation factor threshold = 5). The 48 tissues present in the GTEx dataset were tested and 'eGenes' were identified as having at least one variant with significant association ($P \leq 10^{-5}$) with expression of that gene in that tissue. CLPP of causal SNPs in both datasets for each eGene were calculated using eCAVIAR.

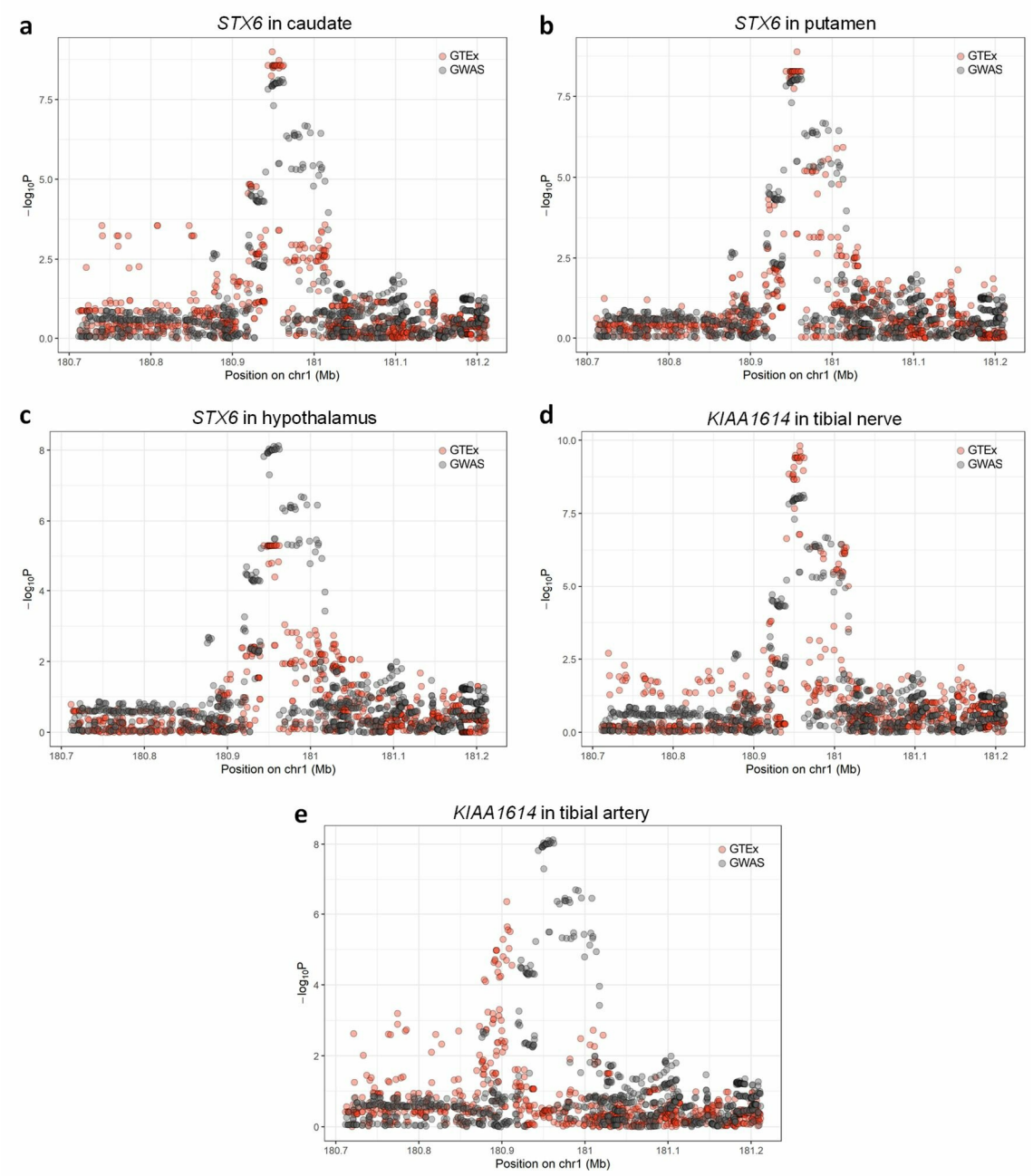

Figure 14: GWAS results for sCJD GWAS at *STX6* colocalise with eQTLs for *STX6* expression in the caudate, putamen and hypothalamus, and *KIAA1614* expression in the tibial nerve.

Plot of $-\log_{10}$ of P-values from the GWAS association analysis at the *STX6* locus (black) against the eQTL association analysis from the GTEx dataset (red) for: (**a**) *STX6* expression in the caudate, (**b**) *STX6* expression in the putamen, (**c**) *STX6* expression in the hypothalamus, (**d**) *KIAA1614* expression in the tibial nerve, (**e**) *KIAA1614* expression in the tibial artery. Peaks correspond to the CLPP in the eCAVIAR analysis with a higher degree of colocalisation with increasing CLPP.

To investigate further the putative causal variants at the *STX6* locus, the PAINTOR ('Probabilistic Annotation Integrator') framework was utilised to integrate epigenetic and gene regulatory data in brain and related tissues with the sCJD GWAS through an Empirical Bayes estimation, including the NIH Roadmap Epigenomics Mapping Consortium (Roadmap) (Roadmap Epigenomics Consortium et al., 2015) and FANTOM (Fantom Consortium and the RIKEN PMI and CLST et al., 2014) studies as well as independent datasets (Hnisz et al., 2013; Kichaev et al., 2014; Maurano et al., 2012). Variants with a CPP > 0.9 within the 99% credible causal set are listed in Table 9. This analysis identified three SNPs as putatively causal for the GWAS signal due to association with DNase hypersensitivity sites (rs12754041, rs6425657), histone modifications (rs12754041, rs10797664) and enhancer regions or chromatin states (rs12754041, rs10797664). As well as minimising causal variants for any functional follow up, the presence of significant variants in elements associated with gene regulation support the hypothesis that the GWAS signal at the *STX6* locus is driven by altered gene expression in relevant brain regions.

Rsid	A0	A1	GWAS Z-score	Post. prob.	Dataset	Annotation
rs12754041	T	G	-5.762	0.95	Maurano et al (Science 2012): DHS	fBrain-DS14815 fBrain-DS16302
rs6425657	A	G	-5.738	0.8	Maurano et al (Science 2012): DHS	fBrain-DS14803 fBrain-DS14815
rs12754041	T	G	-5.762	1.00	RoadMap: Assayed Narrow Peak (CHIP-seq)	H3K27ac_Brain_Hippocampus_Middle H3K4me1_Brain_Hippocampus_Middle H3K36me3_Brain_Substantia_Nigra H3K36me3_Brain_Angular_Gyrus H3K9ac_Brain_Angular_Gyrus H3K4me1_Fetal_Brain_Male H3K27ac_Brain_Cingulate_Gyrus H3K36me3_Brain_Cingulate_Gyrus H3K4me1_Fetal_Brain_Female H3K4me1_Brain_Cingulate_Gyrus H3K4me3_Fetal_Brain_Female
rs10797664	C	T	-5.192	0.99	RoadMap: Assayed Narrow Peak (CHIP-seq)	H3K4me1_Brain_Hippocampus_Middle H3K4me1_Brain_Inferior_Temporal_Lobe H3K4me1_Brain_Mid_Frontal_Lobe H3K27ac_Brain_Substantia_Nigra H3K4me1_Brain_Substantia_Nigra H3K4me1_Brain_Angular_Gyrus H3K4me1_Brain_Anterior_Caudate H3K4me1_Fetal_Brain_Female H3K4me1_Brain_Cingulate_Gyrus
rs12754041	T	G	-5.762	1.00	RoadMap: 15 State CHROME-HMM model	TxWk_Brain_Angular_Gyrus EnhG_Brain_Anterior_Caudate EnhG_Brain_Cingulate_Gyrus Tx_Brain_Germinal_Matrix EnhG_Brain_Hippocampus_Middle TxWk_Brain_Inferior_Temporal_Lobe EnhG_Brain_Mid_Frontal_Lobe EnhG_Brain_Substantia_Nigra Enh_Fetal_Brain_Male TssA_Fetal_Brain_Female
rs10797664	C	T	-5.192	1.00	RoadMap: 15 State CHROME-HMM model	Enh_Brain_Angular_Gyrus Enh_Brain_Anterior_Caudate Enh_Brain_Cingulate_Gyrus Enh_Brain_Germinal_Matrix Enh_Brain_Hippocampus_Middle Enh_Brain_Inferior_Temporal_Lobe Enh_Brain_Mid_Frontal_Lobe Enh_Brain_Substantia_Nigra TxWk_Fetal_Brain_Male Enh_Fetal_Brain_Female
rs12754041	T	G	-5.762	1.00	RoadMap: Enhancers	-
rs10797664	C	T	-5.192	1.00	RoadMap: Enhancers	regions_enh_Brain_Angular_Gyrus regions_enh_Brain_Anterior_Caudate regions_enh_Brain_Cingulate_Gyrus regions_enh_Brain_Hippocampus_Middle regions_enh_Fetal_Brain_Female regions_enh_Brain_Inferior_Temporal_Lobe regions_enh_Brain_Mid_Frontal_Lobe regions_enh_Brain_Substantia_Nigra

Table 9: Integration of gene regulatory datasets using PAINTOR identifies rs12754041, rs6425657 and rs10797664 with high confidence for causality at the *STX6* locus.

PAINTOR utilises GWAS summary statistics, LD structure and functional annotations to generate a posterior probability of causality through an Empirical Bayes estimation whilst allowing for multiple causal SNPs at a locus. 100 kb surrounding the top SNP at the *STX6* locus were integrated with regulatory datasets in brain and related tissues obtained from eight sources available through the PAINTOR tool. Variants for each dataset were filtered for a causal posterior probability (CPP) > 0.9 and overlapping annotations

extracted. fBrain = fetal brain, TxWk = weak transcription, EnhG = genic enhancers, TssA = active TSS, Enh = enhancers.

To combine both expression and regulation datasets a web-based tool was subsequently utilised, FUMA ('Functional Mapping and Annotation of Genome-Wide Association Studies'), which employs a number of different methods and datasets to perform substantial post-GWAS analysis (Watanabe et al., 2017). This includes classification of variants by enrichment of functional consequences and gene sets, as well as utilising numerous eQTL and regulatory datasets to highlight putative causal genes and variants.

In total the FUMA software identified five independent significant SNPs in the sCJD GWAS, comprising three at the *PRNP* locus and one at each other site, supporting the conclusions from the CAVIAR analysis. A Fisher's exact test on functional annotations from ANNOVAR (K. Wang et al., 2010) demonstrated significant enrichment of intronic variants (relative to the reference genome) with 83.3% of the sCJD GWAS variants intronic ($P = 3.3 \times 10^{-15}$). This reflects previous studies showing that the majority of variants identified through GWAS lie within non-coding regions of the genome (Maurano et al., 2012). Gene-set enrichment analysis using MAGMA (de Leeuw et al., 2015) identified only one significant association with the Ca^{2+}/Calmodulin-dependent Protein Kinase Activation pathway (BIOCARTA_CACAM_PATHWAY; $P_{bon} = 0.0313$) driven by nine different genes, not including any of the significant loci in the GWAS. No gene sets containing the *STX6* locus were significant following Bonferroni correction.

40 different SNPs mapped to the chromosome 1 locus (including 14 not included in the GWAS but identified from the 1000 genomes dataset with $r^2 > 0.6$) yet these were all driven by the same genetic signal with only one independently-significant SNP proposed. The following datasets were then mapped to these candidate SNPs to support identification of causal variants: predicted deleterious variants (CADD ('Combined Annotation Dependent Depletion')) (Kircher et al., 2014), predicted regulatory elements (RegulomeDB) (Boyle et al., 2012), eQTLs (various sources; see Methods section 2.2.4), functional annotations (ANNOVAR) (K. Wang et al., 2010), chromatin state (Roadmap) (Roadmap Epigenomics Consortium et al., 2015) and chromatin interactions (Giusti-Rodríguez et al., 2019).

The best way to interpret CADD scores is debated, however a threshold of >30 has been suggested to indicate a likely deleterious variant (Kircher et al., 2014). No variants in this analysis surpassed this threshold indicating none would be deleterious to gene function, however these scores can still indicate functional consequences and can thus be used to predict causality. An intronic variant within *STX6,* rs3789362, had the highest CADD score (19.4) followed by two exonic variants, in *STX6* (rs3747957; synonymous) and *AL162431.1* (rs6680541; non-coding RNA) (17.1 and 16.5 respectively) (Figure 15).

RegulomeDB annotates SNPs with regulatory elements obtained from multiple published datasets to predict variants in regulatory regions, with each receiving a rank from 1 to 7 to represent the quantity and quality of this evidence. In this analysis one SNP, rs3789364, was ranked as 3a indicating some evidence for a role (one of transcription factor binding, any binding motif, DNase peak(s)) with a probability score of 0.670 (scale 0-1, with 1 being most likely to be a regulatory element) (Figure 15). Further investigation indicated interaction of this SNP with 26 transcription factors (CHIP-seq) and its presence in DNase peaks and highly transcribed and enhancer chromatin states, including in two brain regions highlighted in the eCAVIAR analysis, the caudate and hippocampus. A number of SNPs in this region are also involved in intra-chromosomal chromatin interactions providing further potential mechanisms for regulating gene expression.

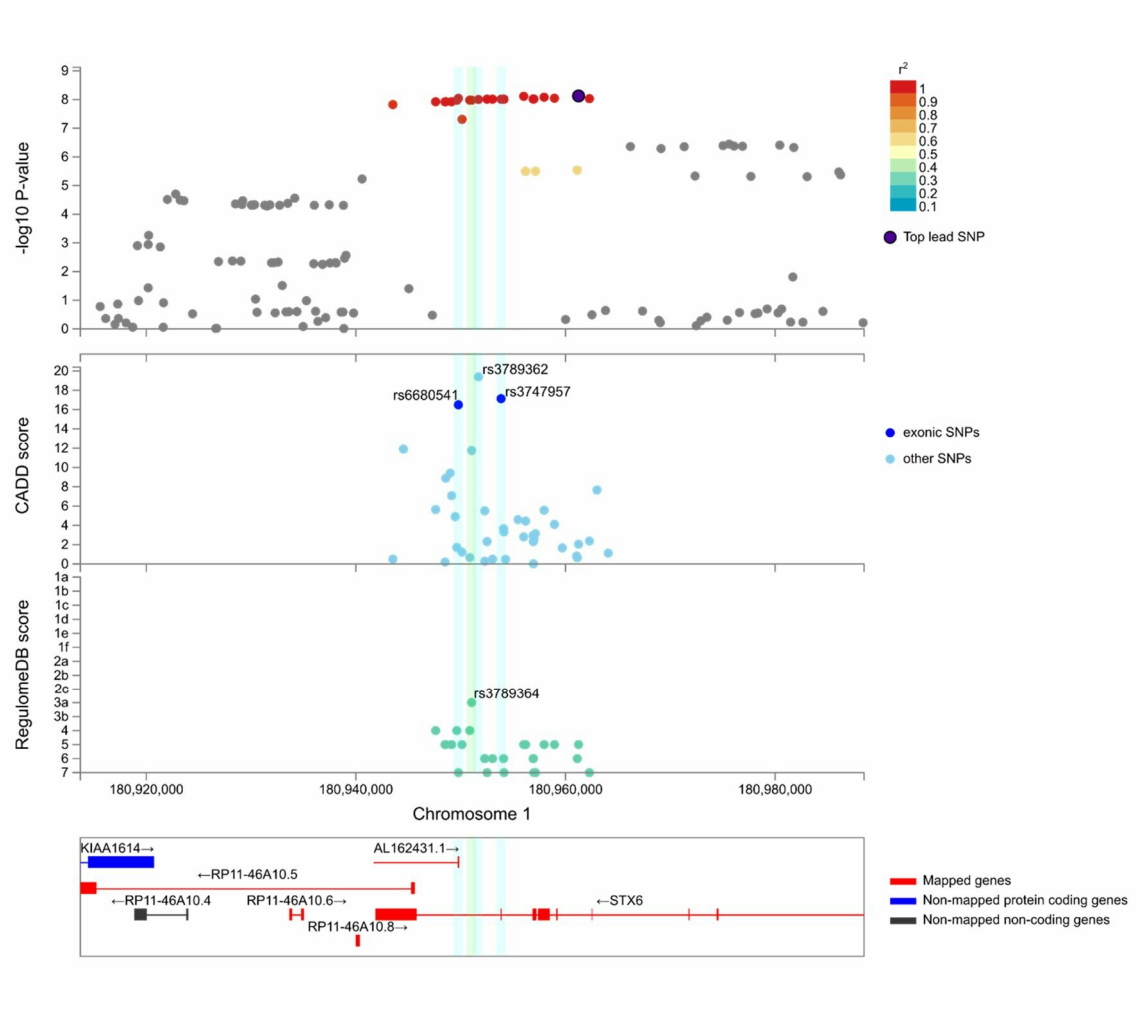

Figure 15: Overlay of regional association plot at *STX6* locus with CADD and RegulomeDB scores highlights putative deleterious and regulatory SNPs.
FUMA is a web-based application for numerous post-GWAS analyses including integration of functional datasets from CADD (middle segment) and RegulomeDB (bottom segment) with GWAS summary statistics (top segment) to assist prediction of potential causal variants. The top 3 SNPs by CADD score (rs3789362, intronic; rs3747957, synonymous in *STX6* exon; rs6680541, non-synonymous in non-coding RNA *AL162431.1* exon) are highlighted in blue, and the SNP with the highest RegulomeDB rank (rs6680541) is highlighted in green. LD is estimated from the 1000 Genomes EUR population and shown relative to the lead GWAS SNP (rs11586493). Plot generated with FUMA.

Finally, FUMA also provides the functionality to integrate further eQTL datasets. Mapping of SNPs to genes through eQTLs that are most likely to influence their expression mapped all 40 SNPs include in the analysis to *STX6,* including eQTLs in multiple brain tissues from the GTEx dataset (GTEx Consortium, 2015) as expected from the eCAVIAR analysis, as well as the white matter (BRAINEAC) (Ramasamy et al., 2014), prefrontal cortex (PsychENCODE) (D. Wang et al., 2018) and dorsolateral prefrontal cortex (BrainSeq; xQTLServer) (Jaffe et al., 2018; Ng et al., 2017) (Table 10). Of note, all SNPs were also mapped to expression of neighbouring *KIAA1614* through a subset of brain tissues from both GTEx and PsychENCODE, however causality of this gene is not supported by the eCAVIAR analysis in the GTEx dataset. Modified *STX6* expression in the dorsolateral prefrontal cortex (rs3747957, $P = 3.05 \times 10^{-16}$) and hippocampus (rs3747957, $P = 6.87 \times 10^{-13}$) is further supported by eQTLs in the Lieber Institute for Brain Development (LIBD) study (phase 2) (Collado-Torres et al., 2019). Additionally a GWAS of 19,629 individuals (obtained from the UK Biobank) identified SNPs in this region to be significantly associated with altered volume of the right pallidum (rs6667291, $P = 4.94 \times 10^{-10}$; r^2 with rs3747957 = 0.84 (1000G EUR)) and white matter (rs1044595, $P = 9.20 \times 10^{-13}$; r^2 with rs3747957 = 0.96) driving association of *STX6* with these phenotypes in gene-based tests, providing an additional putative biological mechanism (Zhao et al., 2019).

Source	Tissue	Ref
eQTL catalogue (BrainSeq)	Dorsolateral prefrontal cortex	(Jaffe et al., 2018)
eQTL catalogue (Fairfax 2014)	Monocytes (+ IFN-γ)	(Fairfax et al., 2014)
eQTL catalogue (Fairfax 2014)	Monocytes (+ LPS)	(Fairfax et al., 2014)
eQTL catalogue (Nedelec 2016)	Macrophages (+ Listeria)	(Nedelec et al., 2016)
eQTL catalogue (Nedelec 2016)	Macrophages (+ Salmonella)	(Nedelec et al., 2016)
eQTL catalogue (Quach 2016)	Monocytes (+ Influenza A)	(Quach et al., 2016)
eQTL catalogue (TwinsUK)	Lymphoblastoid cell lines	(Buil et al., 2015)
PsychENCODE eQTLs	Dorsolateral prefrontal cortex	(D. Wang et al., 2018)
eQTLGen cis eQTLs	Whole blood	(Võsa et al., 2018)
BIOSQTL (BIOS eQTL geneLevel)	Whole blood	(Zhernakova et al., 2017)
xQTLServer eQTLs	Dorsolateral prefrontal cortex	(Ng et al., 2017)
CommonMind Consortium	Dorsolateral prefrontal cortex	(Fromer et al., 2016)
BRAINEAC	White matter	(Ramasamy et al., 2014)
GTEx (v8)	Whole blood	(GTEx Consortium, 2015)
GTEx (v8)	Brain Amygdala	(GTEx Consortium, 2015)
GTEx (v8)	Brain Anterior cingulate cortex BA24	(GTEx Consortium, 2015)
GTEx (v8)	Brain Caudate basal ganglia	(GTEx Consortium, 2015)
GTEx (v8)	Brain Cortex	(GTEx Consortium, 2015)
GTEx (v8)	Brain Frontal Cortex BA9	(GTEx Consortium, 2015)
GTEx (v8)	Brain Hippocampus	(GTEx Consortium, 2015)
GTEx (v8)	Brain Hypothalamus	(GTEx Consortium, 2015)
GTEx (v8)	Brain Nucleus accumbens basal ganglia	(GTEx Consortium, 2015)
GTEx (v8)	Brain Putamen basal ganglia	(GTEx Consortium, 2015)
GTEx (v8)	Brain Substantia nigra	(GTEx Consortium, 2015)
GTEx (v7)	Brain Caudate basal ganglia	(GTEx Consortium, 2015)
GTEx (v7)	Brain Cortex	(GTEx Consortium, 2015)
GTEx (v7)	Brain Hypothalamus	(GTEx Consortium, 2015)
GTEx (v7)	Brain Nucleus accumbens basal ganglia	(GTEx Consortium, 2015)
GTEx (v7)	Brain Putamen basal ganglia	(GTEx Consortium, 2015)
GTEx (v7)	Brain Substantia nigra	(GTEx Consortium, 2015)
GTEx (v6)	Brain Caudate basal ganglia	(GTEx Consortium, 2015)

Table 10: Datasets and tissues identified through FUMA, mapping GWAS SNPs at the chromosome 1 locus to *STX6* through significant eQTLs including in multiple brain tissues.
Publicly available eQTL datasets were screened for significant eQTLs associated with any of the 40 candidate SNPs defined through the FUMA software (variants in LD with any significant GWAS SNPs with GWAS P < 0.05) in order to map variants to a gene. Listed are all datasets containing significant eQTLs associated with *STX6* expression which were used to map *STX6* to the GWAS chromosome 1 locus.

rsID	Description	Location (GRCh37)	R^2 (D')
rs11586493	Discovery (lead SNP)	1:180961245	1.0 (1.0)
rs3747957	Replication; FUMA (CADD, exonic)	1:180953853	1.0 (1.0)
rs12754041	PAINTOR	1:180957962	1.0 (1.0)
rs6425657	PAINTOR	1:180956905	1.0 (1.0)
rs10797664	PAINTOR	1:180988636	0.39 (0.99)
rs6680541	FUMA (CADD, exonic)	1:180949780	1.0 (1.0)
rs3789364	FUMA (RegulomeDB)	1:180951043	1.0 (1.0)

Table 11: Summary of variants at chromosome 1 locus highlighted in the sCJD GWAS and post-GWAS analysis.
LD (r^2 and D') is shown relative to rs3747957 and was estimated from the 1000 Genomes EUR population.

3.3. Discussion

This study has described the first replicated association of genome-wide significant variants outside of the *PRNP* gene as conferring risk for sCJD, with variants in and around the genes *STX6* on chromosome 1 (rs3747957) and *GAL3ST1* on chromosome 22 (rs2267161). Through replication of these variants in an independent cohort with an additional genotyping method, these were shown to be robustly associated with conferring risk for the disease.

Previous GWAS aiming to identify variants for sCJD risk have been primarily limited by inadequate sample sizes to obtain sufficient power to overcome the statistical multiple testing burden. A preceding study investigating sCJD risk variants performed by Sanchez-Juan et al included only 434 sCJD cases in the genome-wide discovery phase and consequently no non-*PRNP* loci surpassed their significance threshold (Sanchez-Juan et al., 2014). Replication of suggestive variants in an additional 1109 cases identified SNPs in an intronic region of *GRM8* (encoding mGluR8 metabotropic glutamate receptor) as significant at this stage, however these same variants were not associated with sCJD in the current GWAS study (rs6951643; P = 0.201) highlighting potential bias in the targeted replication of non-significant variants.

Another study performed by Mead et al included sCJD cases in the genome-wide discovery phase as part of a broader GWAS primarily investigating common risk genes for multiple human prion diseases (sCJD, vCJD, IPD, iCJD and kuru)

(Mead et al., 2012). This study included 1259 sCJD cases in the discovery phase of a total 2000 samples, however again no loci outside of *PRNP* were genome-wide significant. Suggestive association across the *ZBTB38-RASA2* locus for all CJD risk was upheld for UK sCJD cases alone, yet there was no replication evidence when investigating this locus in German sCJD cases suggesting these variants are either specific to the UK population or that this result indicates a false-positive association. Again these were not associated with sCJD risk in the current GWAS supporting the latter (rs295301; P = 0.105).

Further GWAS have been performed with other human prion diseases as the primary outcome, yet it is feasible risk variants may be shared between multiple prion diseases as the mechanisms as we understand them are highly related. This includes two studies aiming to identify loci conferring risk of vCJD. These are substantially limited by sample size as only 232 vCJD cases have been recorded to date worldwide, nonetheless one of these identified genome-wide significant variants located upstream of the gene *RARB* (but lacked independent replication) (Creutzfeldt-Jakob Disease International Surveillance Network, 2021; Mead, Poulter, et al., 2009). These studies and the current sCJD GWAS did not find an association of any suggestive vCJD risk variants with sCJD risk (sCJD GWAS: *RARB:* rs6794719, P = 0.280; *STMN2*: rs1460163, P = 0.614; *MTMR7*: rs4921542, P = 0.978 (nearby rs4921543); *NAPS2*: rs7565981, P = 0.142) (Mead, Poulter, et al., 2009; Sanchez-Juan et al., 2012). A secondary analysis by further imputation of a vCJD GWAS additionally identified variants in *PLCXD3* as significant for vCJD risk, also suggested to confer risk for sCJD using 109 cases, however in a much larger independent follow-up study with 2500 sCJD patients or the current study this was again not replicated (rs319013, P = 0.609) (Balendra et al., 2016; Bishop, Sanchez-Juan, & Knight, 2013). The lack of association of vCJD variants with sCJD risk may suggest that there are distinct mechanisms which drive disease susceptibility, however the lack of replication evidence across studies suggests it is perhaps more likely due to false-positive associations in underpowered studies. In-house genotype data for vCJD, iCJD and kuru (and resistance to kuru) were queried for *STX6* (rs3747957) and *GAL3ST1* (rs2267161) variants; no evidence of an association was found (P > 0.05) but power in these tests was again limited by small sample sizes.

Identification of disease modifiers through GWAS have potentially greater clinical benefit as these could provide therapeutic targets after the initial diagnosis has been made. This has been the focus of further previous GWAS for human prion diseases, including Thompson and colleagues who performed an initial study investigating variants which modify a number of behavioural and psychiatric phenotypes in prion diseases (including 114 sCJD cases) (Thompson et al., 2015). In this study no genome-wide significant variants were identified again likely due to limited samples available with such depth of phenotypic data, however some loci were suggestive of association including variants within *ANK3*. Similarly genetic modifiers of age-of-onset could provide potential drug targets for delaying progression, especially conceivable for treatment of IPDs. A study of 19 individuals with E200K IPD within the Italian Calarbrian cluster again lacked power to identify genome-wide significant variants, however targeted replication of suggestive variants in *CYP4X1* in 32 additional E200K IPD cases and 259 sCJD cases found association with age-of-onset in both diseases (Poleggi et al., 2018). None of these variants confer risk for sCJD in the current study (*ANK3*: rs10509125, P = 0.398 (nearby rs11814723); *CYP4X1:* rs9793471, P = 0.086) indicating potentially differing pathways for disease modifiers to risk variants, however further replication is required to secure these associations due to limiting power in these studies. In future, integrating phenotypic data with the current GWAS will allow more comprehensive comparison and provide important information about disease mechanisms and potential therapeutic targets.

Although evidence for shared genetic risk outside of *PRNP* for different human prion diseases is currently lacking, there are examples of genes such as *APOE* and *MAPT* which appear to play a role in multiple neurodegenerative diseases (Strang, Golde, & Giasson, 2019; Zhou, Fu, & Ip, 2021). With increasing evidence indicating that a number of these diseases share common underlying mechanisms with prion diseases, such as the self-templated conversion of proteopathic seeds and the potential for different ‘strains’ of pathogenic aggregates, genetic risk factors identified for prion diseases may shed light on other ‘prion-like’ diseases. Supporting this, a previous GWAS by Höglinger et al reproducibly identified the same variants in and around *STX6* from the current study as conferring risk for PSP, which was subsequently replicated in an

independent study of pathologically confirmed cases and an independent GWAS analysis (Table 12) (section 1.7.3.2) (J. A. Chen et al., 2018; Hoglinger et al., 2011; Sanchez-Contreras et al., 2018). More recently a proteome wide association study (PWAS) integrating AD GWAS data with dorsolateral prefrontal cortex proteomes (from the ROSMAP study) identified *STX6* protein expression in this region as associated with AD risk (Wingo et al., 2021). *STX6* is likely therefore to have pleiotropic effects on multiple related diseases potentially contributing to these common 'prion-like' mechanisms; whether this is all mediated by the prion protein, with evidence of a role of PrP^C in both tau and β-amyloid function, provides a fascinating route for further research (Corbett et al., 2020).

Disease	SNP	Position (GRCh37)	P-value	OR (95 CI)	MAF Cases	MAF Cont.	LD (r^2)	Ref
PSP	rs1411478	1:180962282	1.80×10^{-9}	1.37 (1.23-1.53)	0.50	0.42	1	(Hoglinger et al., 2011)
sCJD	rs1411478	1:180962282	9.34×10^{-9}	1.16 (1.10-1.22)	0.45	0.41	1	-
PSP	rs57113693	1:180952294	3.51×10^{-15}	1.35 (1.25-1.45)	-	-	0.99	(J. A. Chen et al., 2018)
PSP	rs11586493	1:180961245	4.65×10^{-15}	1.34 (1.25-1.45)	-	-	1	(J. A. Chen et al., 2018)
sCJD	rs11586493	1:180961245	7.51×10^{-9}	1.16 (1.10-1.22)	0.45	0.41	1	-
sCJD	rs3747957	1:180953853	9.74×10^{-9}	1.16 (1.10-1.22)	0.45	0.41	1	-

Table 12: Association statistics at *STX6* locus for PSP and sCJD.
Odds ratio (OR) shown relative to the major allele for each study. Linkage disequilibrium (LD) with rs3747957 derived from 1000 Genomes EUR population.

GWAS methodology has undoubtedly been revolutionary to identifying risk variants for a multitude of diseases, however the propensity for false positive associations in these studies requires important considerations to study design. As previously discussed, there is an extensive multiple testing burden associated with performing whole-genome analysis in tandem. The appropriate significance threshold required to account for resultant errors is debated due to the lack of certainty of how to calculate independent tests due to complex LD structures, which is also largely dependent on the population studied. The P-value threshold of 5×10^{-8} used in this study may therefore be excluding weaker associations, however this was upheld due to the propensity for type I error in this study. For

example here samples were collated from multiple different countries and populations; although these were limited to those of predominantly European ancestry and was controlled for during both the QC and included as covariates in the association analysis, this will increase the likelihood of population stratification and therefore spurious associations. Furthermore the controls used in both phases of this study were obtained from publicly available repositories and therefore genotyped at a different time to the case samples, with likely discrepancies in both methodology and experimental design. Ideally plate controls would have been included to account for this (i.e. including the same samples on both case and control genotyping arrays) unfortunately these were not obtainable. Nonetheless the additional replication phase with independent samples and an alternative genotyping method limits the likelihood of concluding false-positive associations in the current study.

In this study evidence was provided that *PRNP, STX6* and *GAL3ST1* define the causal gene at their respective sites. Homozygous genotypes at *PRNP* codon 129 have been robustly demonstrated to increase risk for sCJD (Palmer et al., 1991). Evidence in this study from the CAVIAR and FUMA fine-mapping analysis suggested potential variants outside of this as conferring independent risk supporting previous studies which have highlighted putative independent signals (Mead et al., 2001). As the key gene in prion pathogenesis it is not unlikely that additional variants may modify disease risk, for example any variants acting as eQTLs may feasibly act to alter susceptibility as the expression level of *PRNP* has been shown to modify disease incubation time in animal models (Beler et al., 1994). However no variants identified were significant eQTLs in a relevant tissue and were not significant after adjusting for homozygosity at codon 129 (rs1799990).

Mapping of the causal gene at the *GAL3ST1* locus was aided by the isolated significance of just two variants, including the rare occurrence of a non-synonymous variant. This variant encodes a valine to methionine substitution at codon 29 of the enzyme encoded by this gene, cerebroside sulfotransferase (CST), highly likely to be driving this association. CST is involved in a key step during the synthesis of sulfatide, a fundamental component of the myelin sheath and a pathway previously implicated in neurological disorders (i.e. metachromatic

leukodystrophy) (Shaimardanova et al., 2020); further research will be required to elucidate the direction of effect here.

This study has provided both statistical and functional genetic evidence that *STX6* is the most likely causal gene at the chromosome 1 locus. In order to do this a number of computational tools were implemented. Firstly statistical fine-mapping was performed using CAVIAR in order to minimise the number of causal variants at this and the other significant loci. As previously described (see section 3.1.2) this tool uses a Bayesian framework allowing for the possibility of multiple causal variants at each locus with improved statistical power to detect variants with low effect sizes. However statistical fine-mapping is only really useful to separate independent signals at a locus and suggest putative causal variants, but is not able to provide definitive conclusions due to the lack of biological information of functionality of each variant. Furthermore such analysis is not able to differentiate between variants in near-perfect LD of which numerous variants at this locus are, resulting in a large number of suggested causal variants not largely reduced from the number of variants surpassing the significance threshold. This analysis did confirm that the SNPs which fall within the *STX6* gene are most likely to be causal, however utility beyond this was minimal.

Applying functional annotations and biological information to the variants at this site was a more informative and powerful method to conclude the likely causal gene at this locus. Colocalisation analysis with eCAVIAR highlighted that eQTLs which modify *STX6* expression in the putamen and caudate in the striatum are driven by the same genetic mechanism as that which increases risk for sCJD. This was an important finding due to the vast number of eQTLs in the genome leading to the likelihood for mere overlap of risk SNPs with these variants due to overlapping LD structures, when they could be associated with two independent genetic signals. This provides both strong evidence for a putative causal gene, as well as highlighting a potential causal mechanism at this site; fascinatingly these two brain regions are the most commonly abnormal in diagnostic brain MRI for sCJD (Meissner et al., 2009). Furthermore interestingly a GWAS of UK biobank participants also demonstrated altered pallidum volume with these variants which forms part of the basal ganglia with the striatum and is highly functionally connected (Zhao et al., 2019). A smaller brain volume in this region

as well as the putamen has been reported in patients with PSP (Messina et al., 2011). The implication of *STX6* GWAS variants in brain tissues is further supported by a number of additional independent eQTL datasets and has additionally led to independent mapping of the gene to PSP risk variants (Ferrari et al., 2014). Repeated association of sCJD risk variants with *STX6* in multiple datasets secures this as the likely casual gene, as well as providing strong evidence for modified RNA expression of this gene in relevant brain regions as a likely biological mechanism.

Pinpointing the causal variants and subsequently the precise genetic mechanism leading to modified *STX6* expression in this study was attempted through integrating a number of regulatory and epigenetic annotations at this site. However this analysis was less conclusive with different tools suggesting distinct putative causal variants, likely due to divergent datasets. For example analysis using PAINTOR identified variants associated with DNase hypersensitivity sites (rs12754041, rs6425657), histone modifications (rs12754041, rs10797664) and enhancer regions or chromatin states (rs12754041, rs10797664), however regulomeDB instead proposed rs3789364 for similar association with DNase hypersensitivity sites as well as highlighting potential transcription factor binding alterations. Furthermore the presence of rs3747957 in an exon of *STX6* increases its likelihood to have an effect on gene function. Therefore in order to delineate the precise variant which is driving the association at this site requires further investigation and, due to the inconclusive and inconsistent nature of these statistical analysis, this will likely require practical determination through step-by-step analysis of gene expression with each variant in a biological system (such as CRISPR-mediated mutagenesis in a biological system). Nonetheless this analysis has limited the number of variants as a starting point for experimental validation, and the repeated association of putative causal variants with regulatory mechanisms supports altered RNA expression as a likely functional consequence of these variants. Importantly the lack of an exact causal variant does not prevent targeting of expression of *STX6* in future functional studies and therapeutic treatments.

It is important to consider the evidence supporting other genes as causal before investing in costly and time-consuming functional analysis. There is limited

evidence for neighbouring gene *KIAA1614* (encoding an uncharacterised protein) as causal as significant variants also act as eQTLs for this gene in a subset of brain tissues, but these are much more limited than those for *STX6,* do not reach the same levels of significance and do not appear to colocalise with the GWAS variants. Additionally a SNP at this locus is a variant in *AL162431.1* (encoding a long non-coding RNA) however there is no evidence for association of any other variants with this gene. Finally from Hi-C analysis in the context of PSP, Chen et al described *XPR1* as putatively causal for these SNPs but the evidence used to draw this conclusion is not clear and Hi-C data was only obtained from foetal tissue or cell culture, not directly relevant to sCJD (J. A. Chen et al., 2018).

Future work described in this thesis focusses on using cellular and animal models to delineate the biological mechanism through which increased *STX6* expression increases the risk of sCJD. Primarily this work focussed on modelling the protective effects reducing expression may have on prion disease progression. This was selected over increasing gene expression for a number of reasons: firstly, investigating whether disease can be slowed or inhibited has a more direct therapeutic application, a primary focus of the research performed in the Mead lab and wider Institute. Furthermore preliminary evidence (discussed later in section 2.5) indicated that overexpression of *STX6* leads to protein dimerisation rather than increased expression of the monomer form, unlikely to represent the primary physiological function of the protein. Nonetheless it will be important to support any findings related to reduced gene expression with either overexpression or rescue experiments to prevent false conclusions related to knockdown artefacts (i.e. due to off-target effects).

Robust identification of non-*PRNP* risk loci and security in the causal genes driving these associations has highlighted two new pathways for future prion research. Although further functional analysis will be required to elucidate the precise roles of these genes in prion diseases, having robust genetic evidence to support experimental work will undoubtedly accelerate research and prevent wasting both time and money on futile leads.

4. Investigating the role of *STX6* in prion diseases in vitro

4.1. Introduction

4.1.1. Cell lines as a model for prion infectivity

The use of cell lines in research has been fundamental to countless discoveries over the last half century, limiting the requirement for hard-to-source tissues and allowing in-depth analysis of biological mechanisms. This is inclusive of prion disease research, with cell models providing not only a way to study biology, but a reliable alternative to time-consuming mouse bioassays. In this gold-standard assay, animals are traditionally inoculated with serial dilutions of biomaterials and disease incubation time (interval format) or dilution for 50% disease onset (end-point format) is used to determine prion titre, taking over five months to produce an output (Prusiner, Cochran, et al., 1982). Immortalised cell lines provide a quick, easy to maintain and easy to manipulate source of material, making them appealing models for functional genetic investigations to complement biochemical methods in a biological system.

The first cell line shown to be permissive to prion replication in culture was isolated from a scrapie-infected mouse brain (termed ‘SMB’ cells) by Clarke and Haig in 1970 and later demonstrated to be of mesodermal origin (Clarke & Haig, 1970). However this and subsequent models were limited by a lack of sensitivity comparable to the mouse bioassay and it was not until the development of PK1 cells, a sub-clone of mouse neuroblastoma N2a cells, by Klöhn and colleagues over 30 years later when this was achieved and implemented in the form of the scrapie cell assay (SCA) (Klohn et al., 2003). In this assay PK1 cells are seeded in a 96-well plate format, exposed to RML-infected brain homogenate for three days and subjected to at least three passages to remove any material from the initial inoculum. The number of cells remaining infected following this final passage with proteinase K (PK) resistant PrP aggregates (as a surrogate for infectivity) are measured in an ELISA-based assay using an enzyme-linked immunospot (ELISPOT) plate. Using this method the authors demonstrated similar sensitivities to the end-point mouse bioassay, able to quantitatively detect PK-resistant PrP at up to ~10^{-7} dilution of infected brain homogenate. Importantly

these de novo aggregates have also been confirmed to be authentically infectious in a mouse bioassay (Butler et al., 1988). Subsequent inclusion of liquid handling robots in the automated SCA (ASCA) has led to routine use of this fast, simple and reliable assay as a tool to measure prion infectivity.

This landmark study revolutionised the field by providing a sensitive read-out of infectious prion titre within a couple of weeks, however limitations were already realised with apparent lack of susceptibility of PK1 cells to additional murine prions strains (ME7 and 22A tested) or those from other species (hamster 263K, BSE, vCJD) (Klohn et al., 2003). This has driven further studies to identify additional cell lines able to propagate alternative prion strains in culture, including additional neuronal-like cell lines such as PC12 and CAD5 cells, as well as peripheral cells such as the mouse fibroblast line L929 and rabbit kidney epithelial RK13 cells (prion propagation in cell culture recently reviewed in (Pineau & Sim, 2021)). Although the majority of lines have still only demonstrated susceptibility to murine prions, in some cases expression of species-relevant PrP has enabled propagation of additional strains including CWD and BSE prions, providing researchers with a plethora of experimental models in which to study this disease-associated mechanism.

Unfortunately no human mitotic cell lines have demonstrated sustained aggregation of prions in culture across passages, and none of the previously identified cell lines have been able to reliable propagate human prion strains, something which would be of great benefit to human functional genetics. A number of studies have however shown an increase in PK-resistant PrP following exposure of relevant post-mitotic neural cells to various human strains, including primary neuronal cultures derived from mice expressing human PrP and more recently human iPS-derived astrocytes and cerebral organoids, however the lack of serial passage limits their utility as a read-out for infectivity (Groveman et al., 2021; Hannaoui et al., 2014; Krejciova et al., 2017). The disease-relevance of the aggregates is also yet to be tested (discussed in detail later in chapter 5, section 5.1.2). Therefore, along with the added drawbacks of extended culture times and relative difficulties with genetic manipulation, these models are not yet sufficient to replace the use of immortalised cell lines and murine prions in functional genetics studies.

4.1.2. Cell lines as a tool to study prion biology

As well as providing a tool to easily measure infectivity, the ability to feasibly monitor prion propagation in culture has allowed exploration of the mechanisms of this process in real-time. This has included insightful studies into the role of the endolysosomal system in prion biology, including permitting experiments into the initial site of prion conversion. For example, in an elegant study, Goold and colleagues used the PK1 cell line expressing aggregation-permissive myc-tagged PrP^{C} (allowing discrimination of de novo aggregates) to provide evidence for the formation of PrP aggregates at the cell surface occurring within minutes after exposure to infectious prions (Goold et al., 2011). Of note however the site of prion conversion is contested with other studies in similar cell lines concluding differing compartments as the predominant site of conversion (prion biology previously discussed in section 1.5.4). These differ in their methods including time-resolution, prion strains and cell lines used, highlighting the necessity for multiple complementary techniques as well as the likely heterogeneity between cell lines and prion strains.

One of the more self-evident benefits of being able to utilise affordable, low maintenance and easily manipulated culture systems as a model for infectious prion replication, is its clear use in large-scale screening for therapeutics and genetic modulators in biological systems. Multiple research groups have exploited this, predominantly using cells chronically infected with murine prion strains and testing the results of treatment on PK-resistant PrP levels 3-5 days later (cell models in prion therapeutics recently reviewed in (Krance et al., 2020)). This has included multiple high-throughput screens of up to 50,000 compounds in various cell lines, as well as more targeted hypothesis-driven studies, leading to identification of numerous anti-prion compounds including well-studied quinacrine and polyanions such as pentosan polysulphate (PPS) (Caughey & Raymond, 1993; Doh-Ura, Iwaki, & Caughey, 2000). However, although there is evidence to support efficacy of some compounds in mouse models of prion disease, trials in patients have not succeeded in providing sufficient evidence for a clinical impact on disease progression (outside of observational reports of increased survival time for PPS) (Bone, Belton, Walker, & Darbyshire, 2008; Collinge et al., 2009). This lack of clinical efficacy emphasises the need for

caution in extrapolating conclusions drawn from cell culture systems to human disease. Nonetheless functional genetics studies in these cell lines have been somewhat successful, for example a screen performed Brown et al of 14 putative disease associated genes (previously identified in various human and mouse studies) in PK1 cells supported a role for 7 of these in prion infection and/or propagation in the ASCA, indicating some overlap between this mechanism in cell lines and patients (C. A. Brown et al., 2014).

Although none of the immortalised human cell lines tested appear susceptible to sustained prion aggregation, they still provide the added appeal of more accurately representing the genetic background (and thus potentially biology) of human diseases whilst retaining the ease-of-use and low cost benefits (Pineau & Sim, 2021). Therefore numerous human lines have been used in prion research, predominantly for explorations of PrP^C function. For example the neuroblastoma SH-SY5Y cell line has often been utilised due to its human neuronal origin, as well as its lack of PrP^C expression permitting transfection of mutant and epitope-tagged PrP without interference from endogenous protein (however increasing propensity for overexpression artefacts), such as for study of PrP^C receptors, glycosylation, shedding and regulation (Parkin et al., 2004; Pease et al., 2019; Walmsley, Zeng, & Hooper, 2001). Although their apparent resistance to prion infection cannot be overlooked, there are certainly benefits for studying human genetics in a species-matched system. The aforementioned recent demonstration of human prion propagation in iPS-derived neural cell lines may overcome this limitation (however this is yet to be fully characterised) permitting studies of prion function in a cell line with a relevant genetic background; iPS-derived neuronal cells have already been used for studies of PrP^C including its function as a receptor for other oligomeric amyloid species and exploration of the associated pathways (Corbett et al., 2020; Jarosz-Griffiths et al., 2019).

4.1.3. Cell lines as a model for related proteopathic aggregates

The increasing appreciation of the ability of different proteopathic aggregates to also induce the self-templated conversion of cellular proteins into pathogenic forms, has driven inevitable studies attempting to model this process in cell culture, similar to those described for the prion protein. As previously discussed,

these provide not only tools to investigate the seeding propensities of biomaterials (which may relate to disease aetiology), but as biological systems to study the mechanisms of these processes.

In the SCA, de novo prion aggregates are differentiated from initial material through serial passage and subsequent PK digestion. Due to the relative protease sensitivity of other protein aggregates and to limit the requirement for sustained aggregation, a number of cell lines have been engineered to express alternative reporters for protein aggregation (often termed ‘biosensors’). For example Marc Diamond’s group engineered a HEK293T cell line to stably express the tau repeat domain with the pathogenic P301S mutation fused to either YFP or CFP (Holmes et al., 2014). Upon protein aggregation, these RDs become sufficiently close for detectable fluorescence resonance energy transfer (FRET), which can be used to report the seeding capabilities of biosamples (Holmes et al., 2014). The same publication also described a similar biosensor for synucleinopathies via fusion of full-length α-synuclein with A53T mutation to the same fluorophores. These models were able to detect tau and α-synuclein aggregates in a highly sensitive (<300 pM) dose-dependent manor which preceded the onset of tau histopathology in mice. Similar studies have also been described for other related proteins including huntingtin, β-amyloid and superoxide dismutase 1 (SOD1), providing researchers with a plethora of tools for investigating propagation of related proteins in biological systems (Aoyagi et al., 2019; Munch, O'Brien, & Bertolotti, 2011; P. H. Ren et al., 2009). This is vital not only for mechanistic studies of this key pathogenic process but has potential applications for public health, with increasing uncertainty over the relevance of this mechanism to infectivity, and maybe even diagnostics if seeding can be detected in biofluids.

Although the development of cell culture systems able to reflect the seeded aggregation of disease associated proteins is undoubtedly going to be a great asset for elucidating this mechanism, the relevance of these models to the disease is yet to be fully established. Importantly whether aggregates formed in these cells are representative of those which may be causing pathogenic spread in the disease is unknown. This is partially driven by the lack of sustained propagation across multiple passages preventing accumulation of aggregates,

also hindering distinction of de novo aggregates from seeding material. This may be due to the reduced infectivity of these proteins compared to prions as suggested by the limited evidence of human-to-human transmission. Therefore further studies will be required to determine the relevance of these systems to disease aetiology and thus suitability of mechanistic and functional genetic studies.

4.1.4. Chapter summary

The work described in this chapter was assisted by Emmanuelle Viré where stated and ASCAs performed by Christian Schmidt, Parvin Ahmed and George Thirlway; all other work was performed by myself.

This study aimed to utilise genetic manipulation in cell models able to propagate relevant proteopathic seeds, in combination with biochemical protein-based methods, to investigate the role of *STX6* in both prion protein biology – as previously described, *STX6* has been established as a genetic risk factor for sCJD with a change in gene expression in brain tissues likely driving this association (see section 3.2.4) – as well as tau due to association of the same genetic signal with the tauopathy PSP (Hoglinger et al., 2011; Jones et al., 2020). Experiments in this study focus on prion infection and clearance, protein-protein interactions and intracellular transport due to the previously described roles of syntaxin-6 in endolysosomal protein transport (see section 1.7).

4.2. Results

4.2.1. Role of STX6 in prion infection

To begin to investigate the potential role of syntaxin-6 in prion disease biology, gene expression was manipulated in the N2a sub-clone, PK1 cells, as the most commonly used and well established cell line in prion research. Short-hairpin RNAs (shRNA) were utilised to generate stable cell lines with reduced *Stx6* expression to monitor infectivity with RML over multiple passages in the ASCA (as previously described in section 4.1.1).

Retroviruses were generated containing one of four shRNA sequences (STX6 A-D; Figure 16a) in a pRetroSuper vector, each targeting a different part of the *Stx6* mRNA coding sequence, and transduced cells selected using puromycin resistance. Knockdown efficiency in PK1 cells was measured by immunoblotting

relative to a scrambled non-silencing shRNA sequence ('Non-silencing_1) (Figure 16b and c). In this initial screen STX6_D demonstrated the highest level of protein knockdown, by 30% relative to this control.

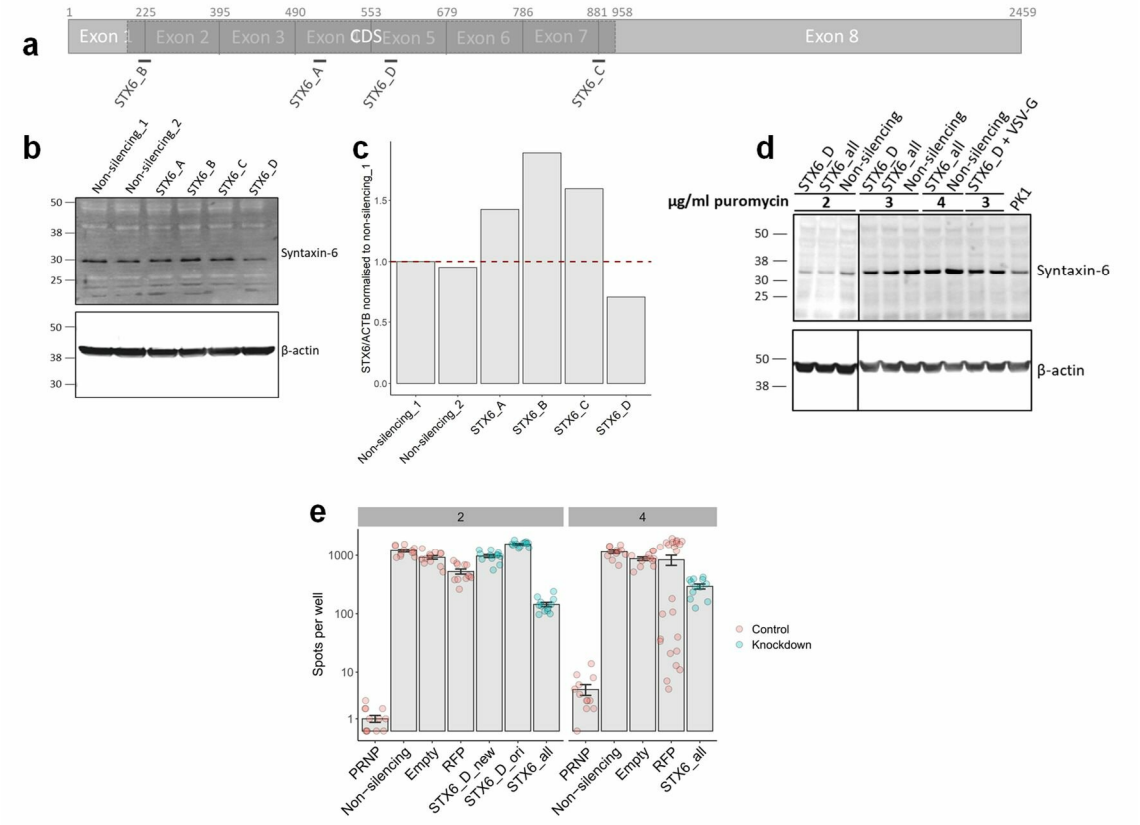

Figure 16: Optimisation of retroviral *Stx6* knockdown in PK1 cells and pilot study of influence of prion propagation in automated scrapie cell assay (ASCA).
(**a**) Binding sites of *Stx6* shRNAs (STX6_A; STX6_B; STX6_C; STX6_D) in mouse *Stx6* mRNA open reading frame spanning exons 2-7 within the coding sequence (CDS). (**b**, **c**) Screening of knockdown efficiency of 4 shRNA sequences in transduced PK1 cells relative to non-silencing sequence (Non-silencing_1, Non-silencing_2). (**b**) Immunoblot for syntaxin-6 and β-actin protein levels (**c**) quantified as intensity of syntaxin-6 staining as a proportion of β-actin, normalised to Non-silencing_1. (**d**) Optimisation of knockdown with STX6_D alone or combination of 4 shRNAs (STX6_all) with different puromycin concentrations (2-4 µg/ml) for selection or addition of VSV-G retroviral envelope protein (+ VSV-G). Immunoblot for syntaxin-6 and β-actin protein levels (solid line indicates distinct blots). (**e**) ASCA on cell lines with highest level of knockdown (STX6_D_new, STX6_D_all and Non-silencing as shown in panel D, STX6_D_ori as shown in panels B and C; puromycin concentration for selection (2-4 µg/ml) indicated in grey at top of plot) with additional control cell lines (*Prnp* knockdown (PRNP), empty pRS vector (Empty), shRNA targeting RFP (RFP)). Variable effect of knockdown on infected cell number (Spots per well; data show post-4th split, RML dilution 3 x 10^{-6}). Error bars: mean ± SEM (technical replicates); n = 1. ASCA performed by Christian Schmidt, Parvin Ahmed and George Thirlway.

Knockdown efficiency following retroviral transduction with *Stx6* shRNAs was optimised through manipulation of a number of parameters; concentration of puromycin used for selection of transduced cells (2-4 µg/ml), the combination of vectors (STX6_D alone, all 4 tested shRNAs in combination ('STX6_all')), the addition of retroviral envelope vector VSV-G) (Figure 16d). By immunoblot analysis, cells under selection at 2 and 4 µg/ml demonstrated the highest efficiency of syntaxin-6 protein knockdown. These were used for a pilot ASCA along with cell lines transduced with a *Prnp*-targeting shRNA which has previously been shown to inhibit prion propagation in this assay (positive control), and an shRNA targeting red fluorescent protein (RFP) as an additional negative control (Goold et al., 2011). As can be seen in Figure 16e, unlike PrP, knockdown of syntaxin-6 to this extent does not appear to reliably influence the ability of PK1 cells to propagate RML prions, however the efficiency of knockdown here is both limited and variable.

To therefore further increase the level of *Stx6* knockdown, a modified method was used in which shRNAs were directly transfected (bypassing the requirement for retroviruses), cells passaged to induce shRNA integration during mitosis, and single cell cloned to identify cells demonstrating the largest reduction in gene expression. Following direct transfection of PK1 cells with STX6_D shRNA, single cell populations were screened by RT-qPCR; clones 2, 5 and 6 demonstrated the largest reduction in *Stx6* mRNA expression (termed 'STX6_D 2', 'STX6_D 5' and 'STX6_D 6'; data not show). This was validated by further RT-qPCR (Figure 17a; STX6_D 6 vs Non-sil A, P = 0.049) and immunoblot in which clones STX6_D 5 and STX6_D 6 demonstrated a 70% (Figure 17b and c; P = 0.047 vs Non-sil B) and 80% (P = 0.036 vs Non-sil B) reduction in syntaxin-6 protein expression relative to control lines respectively, however in clone STX6_D 2 there was no difference (Figure 17b and c). *Prnp* knockdown was also confirmed by RT-qPCR (Figure 17d; P = 0.0073 vs Non-sil A, P = 0.015 vs Non-sil B, P = 0.00010 vs RFP) and immunoblot with anti-PrP antibody (Figure 17e and f: ~65%, P = 0.041 vs Non-sil B, P = 0.0085 vs Non-sil A). These data also demonstrate consistent PrP expression between other cell lines and which has been shown to influence prion propagation in the SCA (unpublished data). Similarly growth rate measured

across three passages (doubling time calculated as per Methods section 2.4.6) is consistent between all cell lines (Figure 17g).

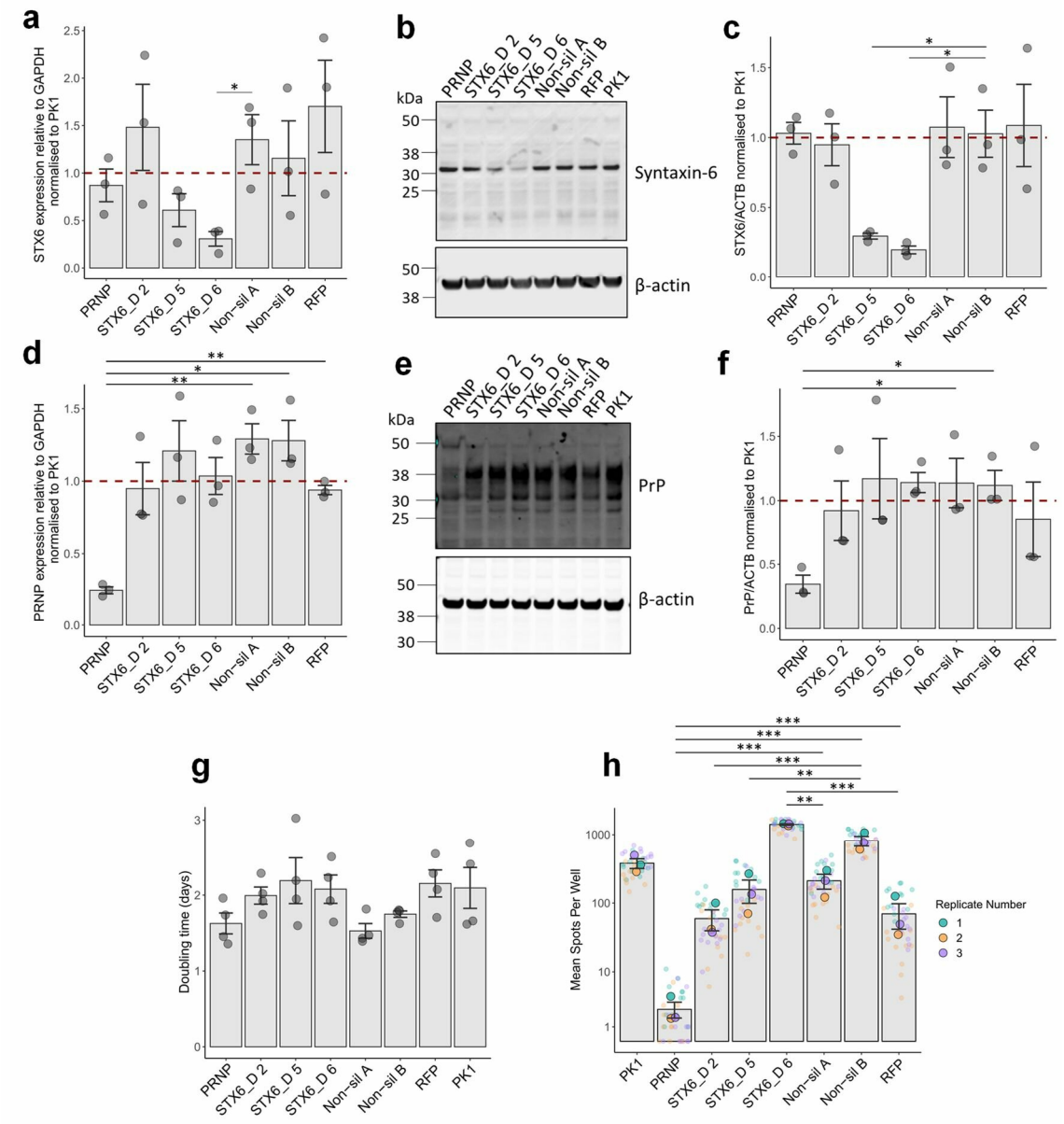

Figure 17: Knockdown of *Stx6* expression in PK1 cells by >70% does not have a consistent effect on prion propagation in the automated scrapie cell assay (ASCA). PK1 cells were transfected with shRNAs targeting *Stx6* or *Prnp*, or red fluorescent protein (RFP) or a scrambled sequence (Non-sil) for controls. Following transfection cells were split to integrate shRNA and transfected cells selected using puromycin. Clones were screened by RT-qPCR. (**a**-**c**) Knockdown in clones 2 (STX6_D 2), 5 (STX6_D 5) and 6 (STX6_D 6) were verified by (**a**) RT-qPCR relative to *Gapdh* housekeeping gene and (**b**) immunoblot with anti-syntaxin-6 anitibody with (**c**) band intensity measured relative to β-actin loading control. (**d**-**f**) *Prnp* expression measured by (**d**) RT-qPCR relative to *Gapdh* reference gene and (**e**) immunoblot with anti-PrP antibody (clone ICSM18) with (**f**) band intensity measured relative to β-actin loading control. (**g**) Growth rate measured as doubling time in days (all ns; one-way ANOVA with Tukey's post-hoc test). (**h**) Average

spot count of infected cell number post-4th split in ASCA with RML at 3 x 10^{-6} dilution (means cube-root transformed for normality). (Student's t-test; *P < 0.05, ** P < 0.01, *** P < 0.001). Error bars: mean ± SEM; n = 3. Initial screening with assistance from Emmanuelle Viré and ASCA performed by Christian Schmidt, Parvin Ahmed and George Thirlway.

As expected PrP knockdown greatly reduced prion propagation in the ASCA (Figure 17h; PRNP vs Non-sil A, P = 2.9 x 10^{-6}; vs Non-sil B, P = 2.3 x 10^{-7}; vs RFP, P = 4.9 x 10^{-5}). However, despite knockdown of syntaxin-6 to similar levels in the two clones tested, the effect on propagation was not consistent: clone STX6_D 5 had reduced spot count relative to controls (STX6_D 5 vs Non-sil B, P = 0.006) compared to STX6_D 6 for which this was increased (STX6_D 6 vs Non-sil A, P = 0.002; vs RFP, P = 1.6 x 10^{-5}). This difference is likely due to other biological factors arising from clonal selection influencing the ability of these cells to propagate prions. The knockdown of syntaxin-6 did not demonstrate an effect on prion infection or propagation above this inter-clonal variation.

In addition to N2a cells a number of other immortalised cell lines have been developed for modelling prion propagation in culture. These cell lines all differ substantially in their prion strain susceptibility, likely due to the presence or absence of different cofactors required for efficient propagation, for example caveolin-1 largely missing from N2a cells may contribute to prion uptake (Fehlinger et al., 2017; Show Ling Shyng et al., 1994). Therefore, to account for this and the potential absence of other key proteins which may relate to the role of syntaxin-6, an additional cell line to PK1 cells was utilised (Choudhury et al., 2006); CAD5 cells (subclone of Cath.a-differentiated (CAD) mouse catecholaminergic neuronal tumour cell line termed CAD-2A2D5) were selected due to their susceptibility to a wide range of prion strains and their routine use in the Unit (Mahal et al., 2007). The same protocol optimised for knockdown of *Stx6* and *Prnp* in PK1 cells was used (as used in Figure 17) however, unlike for the *Prnp*-targeting shRNA which demonstrated up to 97% reduction in mRNA expression, neither the pool of transfected cells or any of the 22 clones screened demonstrated any evidence of reduced *Stx6* expression greater than 31% difference compared to non-silencing controls (Figure 18a and b). An alternative method would therefore be required for manipulating *Stx6* expression in this line.

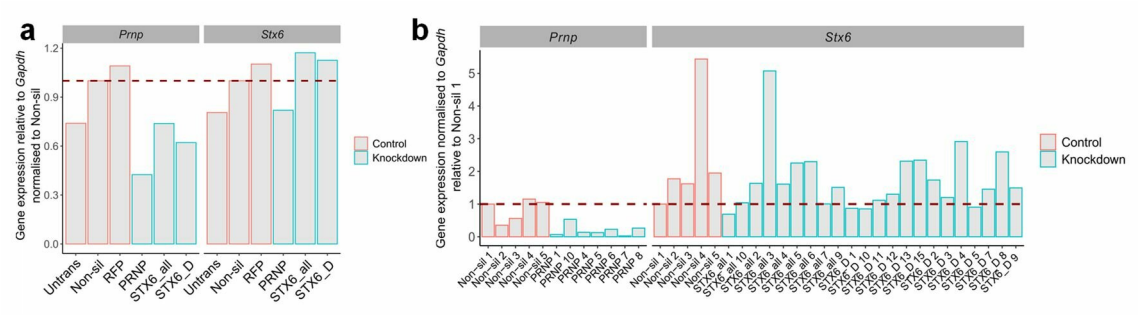

Figure 18: Optimised protocol for shRNA-mediated gene knockdown does not yield stable cell lines with reduced *Stx6* expression in CAD5 cells.
CAD5 cells were transfected with shRNA sequences targeting *Stx6* (STX6_D, STX6_all) or *Prnp* to generate knockdown cell lines (blue), or red fluorescent protein (RFP) or a scrambled sequence (Non-sil) for controls (red). Following transfection, cells were split to integrate shRNA sequence and selected using puromycin resistance. (**a**, **b**) RT-qPCR on (**a**) cell pools following selection and (**b**) following single cell cloning of 'Non-sil', 'PRNP', 'STX6_all' and 'STX6_D' cell lines, measuring *Prnp* and *Stx6* mRNA (shown in grey at top of plot) expression relative to *Gapdh* housekeeping gene (n = 1). No cell lines demonstrate knockdown of *Stx6* mRNA greater than 30% relative to non-silencing control.

4.2.2. Role of STX6 in prion clearance

To isolate prion propagation from infection, gene expression in PK1 cells chronically infected with RML prions (termed 'iPK1' cells) was modified and the level of 'curing' of PK-resistant PrP measured using a dot blot immunoassay (N. C. Ferreira et al., 2014). As the knockdown was not required long-term (and traditionally 'cell curing' is measured just 3-5 days post-treatment) initially transient knockdown of *Prnp* and *Stx6* expression was tested.

Transfection of the same shRNA plasmid constructs as previous was optimised (transfection reagent type and concentration, amount of DNA) by measuring GFP expression and % confluence in real-time over 72 hours (see Methods section 2.5.1). The final transfection conditions demonstrated a knockdown of both *Stx6* and *Prnp* mRNA expression by ~50% relative to controls at 72 h post-transfection (Figure 19a and b respectively). A dot blot immunoassay however showed variable and limited evidence of syntaxin-6 or PrP knockdown at the protein level (Figure 19c-f).

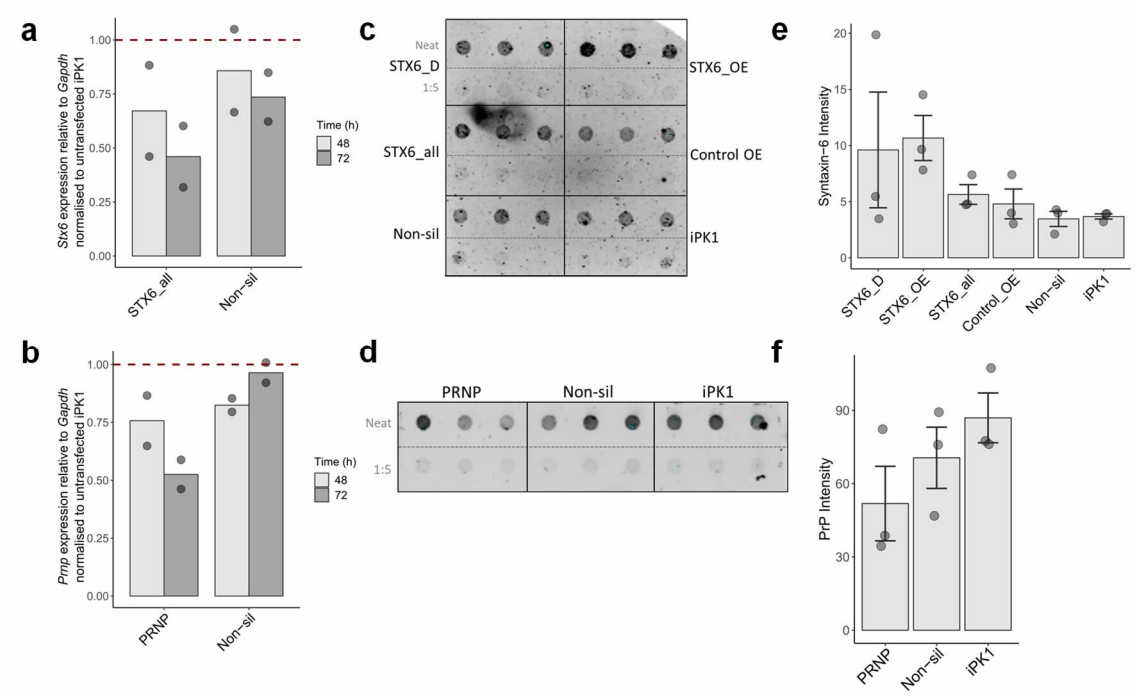

Figure 19: Transient knockdown of *Stx6* expression for use in cell curing assay is not sufficient
(**a**, **b**) Knockdown of mRNA expression at 48 and 72 h post-transfection using (**a**) *Stx6* or (**b**) *Prnp* targeting shRNAs determined by RT-qPCR relative to *Gapdh* expression shows ~50% knockdown after 72 h for both genes (n = 1). (**c**-**f**) Knockdown of (**c**) syntaxin-6 and (**d**) PrP^C protein levels determined using dot blot (as for cell curing assay) 72 h post-transfection normalising to cell counts prior to lysis. Dot intensity measured for (**e**) syntaxin-6 and (**f**) PrP^C shows high variability and inefficient knockdown. Error bars: mean ± SEM (technical replicates); n = 1.

To minimise variability and increase knockdown efficiency stable cell lines were generated as previous. iPK1 cells were transfected with *Stx6* ('STX6_D', 'STX6_all') or *Prnp* ('PRNP') targeting shRNAs or negative control vectors ('Non-sil', 'RFP'), as well as a vector encoding *Stx6* cDNA for gene overexpression ('STX6_OE') and related empty vector control ('Control_OE'). Immunoblot confirms knockdown with STX6_D (76%), STX6_all (90%) and PRNP (81%) shRNAs relative to Non-sil control to a sufficient level, so single cell cloning was not performed (Figure 20a and b). Overexpression of *Stx6* produces an additional immunoreactive band at approximately 60 kDa, likely due to dimerisation as a cellular response to remove excess protein from the functional pool.

PK-resistant PrP levels in these cell lines was measured by treatment of the nitrocellulose membrane with 5 µg/ml PK for 1 h after applying the lysates, prior

to antibody staining. This treatment is sufficient to digest the cellular prion protein on the membrane and leave only PK-resistant prion aggregates (as demonstrated by the lack of immunoreactivity in uninfected PK1 cells (Figure 20c; PK1). *Prnp* knockdown significantly reduced PK-resistant PrP levels in iPK1 cells as expected (Figure 20d; P = 0.033 vs Non-sil; P = 0.023 vs RFP) however there was no significant effect of *Stx6* knockdown or overexpression in any cell line tested, suggesting that syntaxin-6 does not play a role in prion propagation or clearance detectable with this assay.

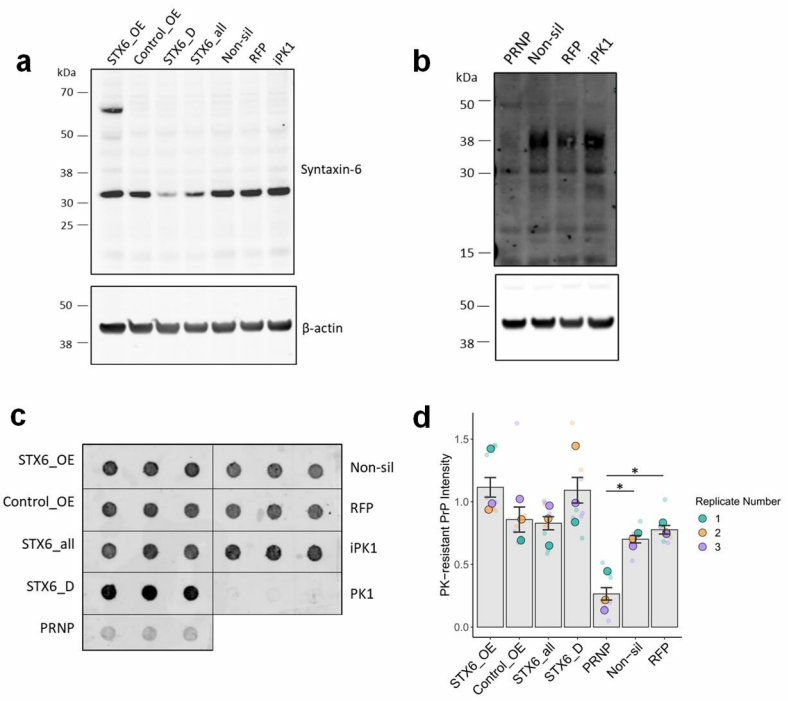

Figure 20: Knockdown or overexpression of *Stx6* in chronically infected iPK1 cells does not cure cells of PK-resistant PrP.
(**a**, **b**) Stable knockdown of syntaxin-6 following transfection with a single *Stx6* shRNA (STX6_D) or a combination of 4 (STX6_all). PRNP, scrambled non-silencing (Non-sil) and RFP shRNAs were used as controls. (**a**) Immunoblot using anti-syntaxin-6 antibody and anti-β actin as a loading control. (**b**) Immunoblot using anti-PrP antibody (clone ICSM18) and anti-β actin as a loading control (non-proteinase K (PK) treated). (**c**, **d**) PK-resistant PrP levels in stable knockdown cells measured in cell curing assay. (**c**) Immunoblot for PrP using anti-PrP antibody following 1 h incubation with 5 µg/ml PK. Uninfected PK1 cells used as control (PK1). (**d**) Intensity of PrP staining normalised to iPK1 to standardise between blots (Student's t-test; * P < 0.05). Error bars: mean ± SEM; n = 3.

4.2.3. Role of STX6 in prion protein interactions

A direct protein-protein interaction could enable syntaxin-6 to modify multiple prion protein functions, for example through altering the kinetics of protein misfolding or as a mechanism to modify the transport of either PrP^C or aggregated protein through the endolysosomal network.

To firstly explore the relationship between syntaxin-6 and PrP within cells at steady state, PK1 and chronically prion-infected iPK1 cells were fixed, permeabilised and co-immunostained for the two proteins. iPK1 cells were pre-treated with guanidine thiocyante, a well-established method to select for prion aggregates over the cellular prion protein as there is not currently an antibody available to differentiate between these two forms (Taraboulos, Serban, & Prusiner, 1990). As shown in Figure 21a and b, both PrP^c and PrP aggregates localise to the perinuclear region and the plasma membrane of these cells to differing extents. In the cytoplasm and particularly this perinuclear region, syntaxin-6 demonstrates a high degree of colocalisation with both PrP^C and PrP aggregates, although this is highly variable between cells. Quantification of this estimates that in PK1 cells, 59% of PrP^C is found within areas of syntaxin-6 staining and 79% of syntaxin-6 colocalises with PrP, indicating the majority of syntaxin-6 positive compartments contain PrP^C (Figure 21c). Similarly in iPK1 cells 72% of PrP aggregates (as guanidine treatment prevents immunodetection of PrP^C) in the cytoplasm are found within areas of syntaxin-6 staining, and 67% for the reverse, suggesting a slightly higher proportion PrP aggregates are in syntaxin-6-labelled compartments than PrP^C (Figure 21d). There is a significant positive correlation between the localisation of both PrP forms and syntaxin-6 in both cell lines (PK1: $R = 0.61$, $P < 2.2 \times 10^{-16}$; iPK1: $R = 0.54$, $P < 2.2 \times 10^{-16}$) (Figure 21e and f).

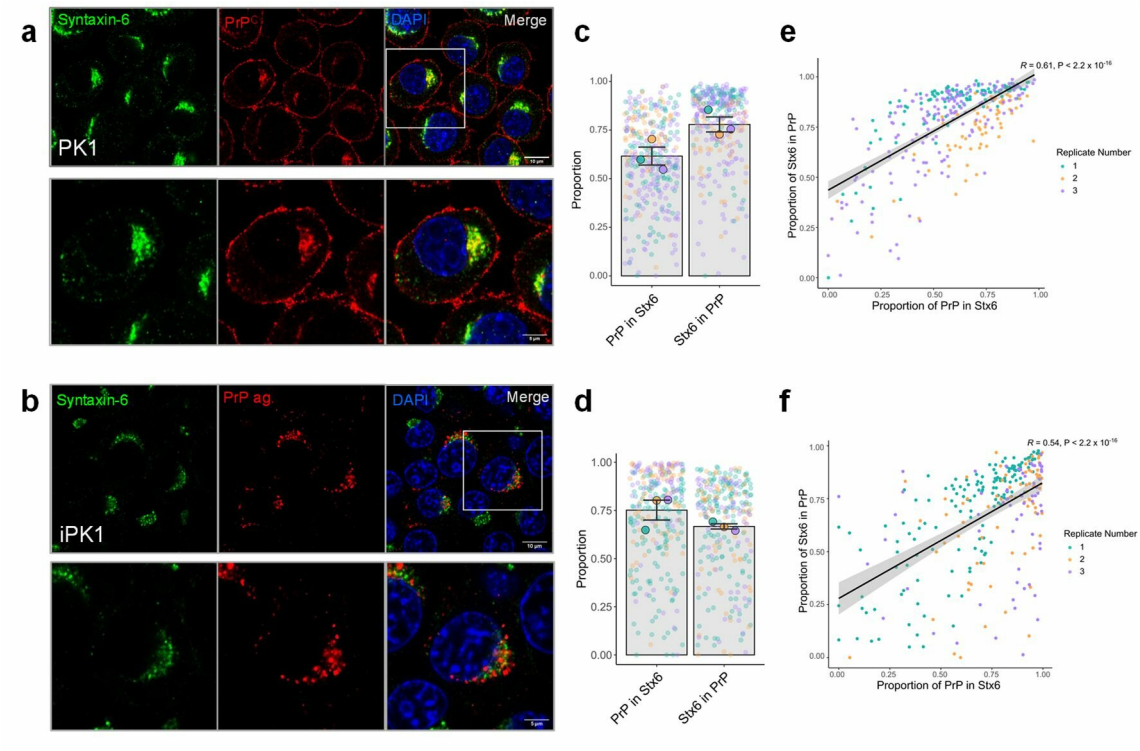

Figure 21: Syntaxin-6 shows a high degree of colocalisation with both PrP^C and PrP aggregates in the cytoplasm of PK1 cells.
Co-immunofluorescence for syntaxin-6 (green) and PrP (red) in permeabilised uninfected (PK1) and chronically infected (iPK1) cells. (**a**,**b**) Representative images of cells stained with anti-syntaxin-6 antibody and (**a**) anti-PrP antibody (clone 8H4) for PK1 cells or (**b**) anti-PrP antibody (clone 6D11) following treatment with 3.5 M guanidine thiocyanate to select for PrP aggregates in iPK1 cells. Images at 2x zoom shown below as indicated by white box. Nuclei stained with DAPI (blue). (**c**-**f**) Quantification of the proportion of PrP staining that colocalises with syntaxin-6 (Stx6) and vice versa in the cytoplasm of (**c**) PK1 cells and (**d**) iPK1 cells shows 59.4% of PrP^C and 72.2% of PrP aggregates colocalise with syntaxin-6 respectively, with (**e**,**f**) a significant positive correlation between the localisation of syntaxin-6 and PrP in both (**e**) PK1 and (**f**) iPK1 cells (Spearman's rank). Scale bar: 10 μm (top), 5 μm (bottom).

The high degree of colocalisation between syntaxin-6 and PrP within cells does indicate potential for a direct protein-protein interaction. To explore this, a protein-based ELISA-based assay was utilised as shown in the literature to be an effective method for investigating PrP^C interactors (Figure 22a; see Methods section 2.6) (Corbett et al., 2020). Although it would be preferable to investigate this interaction in cells or tissues to allow for a role of post-translational modifications or other intracellular components, as both PrP^C and syntaxin-6 are membrane proteins strong detergents would be required to release these

proteins from cell membranes which would be highly likely to disturb any non-covalent interactions.

To optimise conditions for detection of recombinant syntaxin-6 in this format, plates were coated with 10 or 100 µg/ml full length human syntaxin-6 (huStx6$^{1-255}$; 'Stx6') or buffer alone and two different anti-syntaxin-6 antibodies tested for their detection efficiency. Antibody clone C34B2 produced a good signal at both coating dilutions, however clone 3D10 did not produce a signal above the background from uncoated wells (Figure 22b). The anti-PrP antibody used also detected protein in wells coated with full length recombinant human PrP (huPrP$^{23-231}$; 'PrP'). Clone C34B2 was then titrated to optimise detection and a dilution of 1:200 was used going forward to give a strong signal whilst minimising antibody used (Figure 22c).

Having shown both syntaxin-6 and PrP can be detected in this assay format, a 3-fold serial dilution of syntaxin-6 ranging from 0.4 to 10 µg/ml was titrated onto wells coated with either 10 µg/ml PrP or blocking buffer alone. There was no change in the levels of syntaxin-6 detected between PrP-coated and uncoated wells under these conditions indicating syntaxin-6 is not binding to PrP, unlike syntaxin-6 or PrP coated wells alone which were efficiently detected (Figure 22d and e respectively).

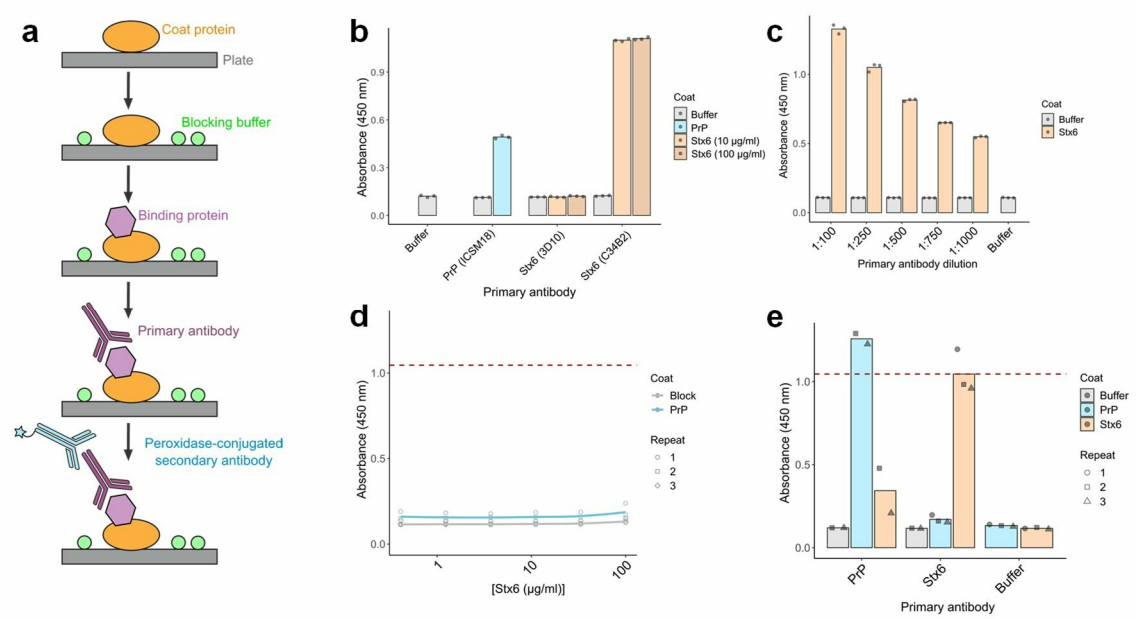

Figure 22: Recombinant syntaxin-6 does not interact with full length recombinant PrP^{C}.

(**a**) Schematic overview of protein-protein interaction ELISA. A 96-well plate is coated with 10 µg/ml protein before blocking to prevent non-specific binding, following addition of a secondary binding protein, washing and incubation with a relevant primary antibody. A peroxidase-conjugated secondary antibody generates a colorimetric signal quantified by absorbance at 450 nm. (**b**,**c**) Optimisation of ELISA assay for detection of full length huStx6$^{1-255}$ and huPrP$^{23-231}$. (**b**) PrP (10 µg/ml) was efficiently detected with anti-PrP antibody (clone ICSM18) and Stx6 (10 and 100 µg/ml) was detected with anti-Stx6 antibody clone C34B2 but not 3D10. (**c**) Titration of anti-Stx6 antibody (C34B2) shows increased detection with higher concentrations. (**d**) A 3-fold dilution series of Stx6 onto PrP-coated wells (blue line) does not increase detection with anti-Stx6 antibody relative to uncoated plates (grey line) indicating lack of interaction, (**e**) compared to Stx6-coated control wells (indicated by dashed horizontal line). PrP coating is detected with anti-PrP antibody (clone 6D11). Bars: mean of biological replicates, n = 3; shapes: mean of triplicate wells.

4.2.4. Role of STX6 in intracellular prion trafficking

As a protein involved in the intracellular trafficking of proteins and vesicles it is possible that syntaxin-6 functions in the localisation of PrP^C or aggregated forms of the protein within cells, independent from an effect on its seeded aggregation, clearance or interaction, whether it be through a differing mechanism or due to a lack of sensitivity in the assays used to test these phenotypes. This could provide multiple pathways for syntaxin-6 to influence disease including localisation of proteins to sub-cellular compartments with more aggregation-prone conditions, altering the rate of pathogenic protein degradation or promoting intercellular spread of seeding-competent proteins.

To investigate a role of syntaxin-6 in the steady-state localisation of the cellular prion protein, the stable PK1 clones previously generated with reduced syntaxin-6 expression were fixed, permeabilised and stained for PrP^C and syntaxin-6 (Figure 23a). In all clones (except *Prnp* knockdown control) PrP^C displayed the expected perinuclear and plasma membrane staining previously described, however the extent to which it localised to each compartment appeared variable. To quantify this, three different sub-cellular compartments were defined: nucleus, cytoplasm and membrane, and total PrP in each calculated (see Methods section 2.4.8; Figure 7). The localised proportions of PrP were highly variable between both cells and independent replicates, however this analysis demonstrated a moderate increase in the proportion of PrP^C on the plasma membrane in STX6_D 6 knockdown cells relative to the two non-silencing controls, which was significant in a two-proportions z-test of all cells (Figure 23b and c; Non-sil A vs STX6_D 6, $P = 0.013$; Non-sil B vs STX6_D 6, $P = 0.014$). This suggests a potential role of syntaxin-6 in trafficking of PrP^c to or from the plasma membrane, however this requires validation with additional methods and experiments due to the variability in this assay and between clones. A preliminary immunoblot for surface PrP, isolated through biotinylation and immunoprecipitation, does not support any gross increases in *Stx6* knockdown cell lines relative to non-silencing controls (Figure 23d). Measuring total protein by immunofluorescence supported a reduction in protein expression of both PrP^C and syntaxin-6 in all knockdown lines although modest for STX6_D 5 clone (Figure 23e and f).

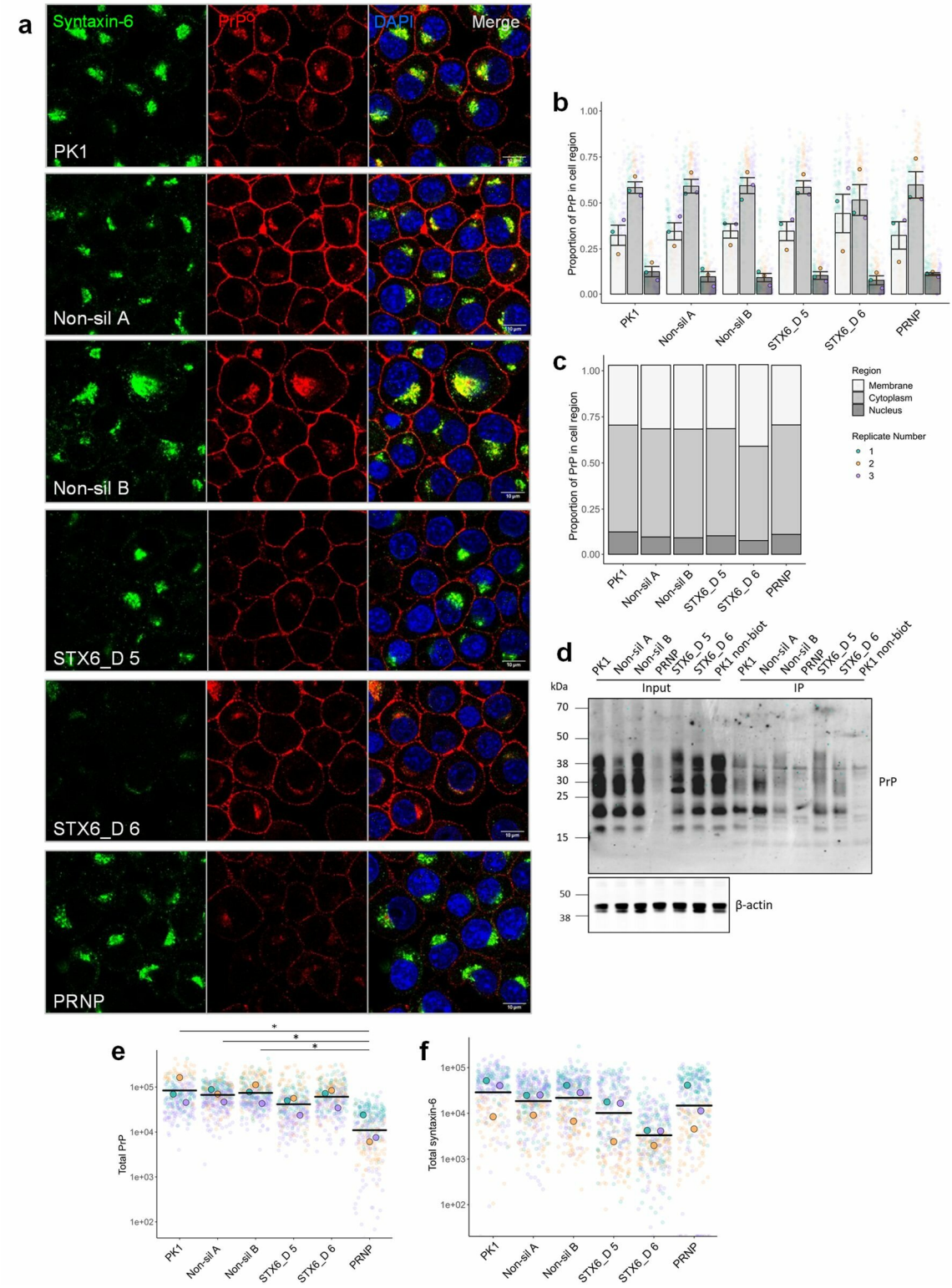

Figure 23: Knockdown of *Stx6* does not have a gross effect on the localisation of PrP^C in PK1 cells

Immunostaining for PrP^C and syntaxin-6 in stable PK1 cell lines previously shown to have reduced *Stx6* (STX6_D 5, STX6_D 6) or *Prnp* expression or non-silencing (Non-sil A, Non-sil B) or untransfected (PK1) controls. Cells were fixed and permeabilised before co-immunolabelling with anti-syntaxin-6 antibody (green) and anti-PrP antibody (clone

8H4) (red) (**a**) Representative images for each cell line. Nuclei are stained with DAPI (blue). (**b**,**c**) Quantification of the localisation of PrP to each cellular compartment (nuclei, cytoplasm, membrane) does not highlight a gross mis-localisation of PrP. Protein expression calculated as a function of area and mean pixel intensity, and proportions calculated relative to total protein per cell. Proportion per cell line shown (**b**) per independent replicate and (**c**) as a mean proportion only as stacked bars for clarity. (**d**) No gross change in surface PrP with syntaxin-6 knockdown measured by immunoblot following immunoprecipitation of surface biotinylated proteins using streptavidin-coated beads. β-actin used as loading control for diluted whole cell lysates used for immunoprecipitation. (**e**,**f**) Total expression of (**e**) PrP and (**f**) syntaxin-6 in each cell line supports gene knockdown (*P < 0.05; one-way ANOVA with Tukey's post-hoc test). Error bars: mean ± SEM; n = 3. Scale bar: 10 μm.

The stable iPK1 cell lines were additionally stained for PrP and syntaxin-6 following treatment with 3.5 M guanidine thiocynate, to study the localisation of PrP aggregates in cells with reduced syntaxin-6 expression. PrP again demonstrated the expected perinuclear staining with some aggregates present on the plasma membrane for all cell lines (except *Prnp* knockdown and uninfected PK1 cells) (Figure 24a). Definition of subcellular compartments as previous did not identify any significant alterations in the proportion of PrP staining on the membrane suggesting syntaxin-6 does not play a role in the trafficking of prion aggregates in iPK1 cells (Figure 24b and c). This analysis again demonstrated the expected reduction in both syntaxin-6 and PrP expression (Figure 24d and e).

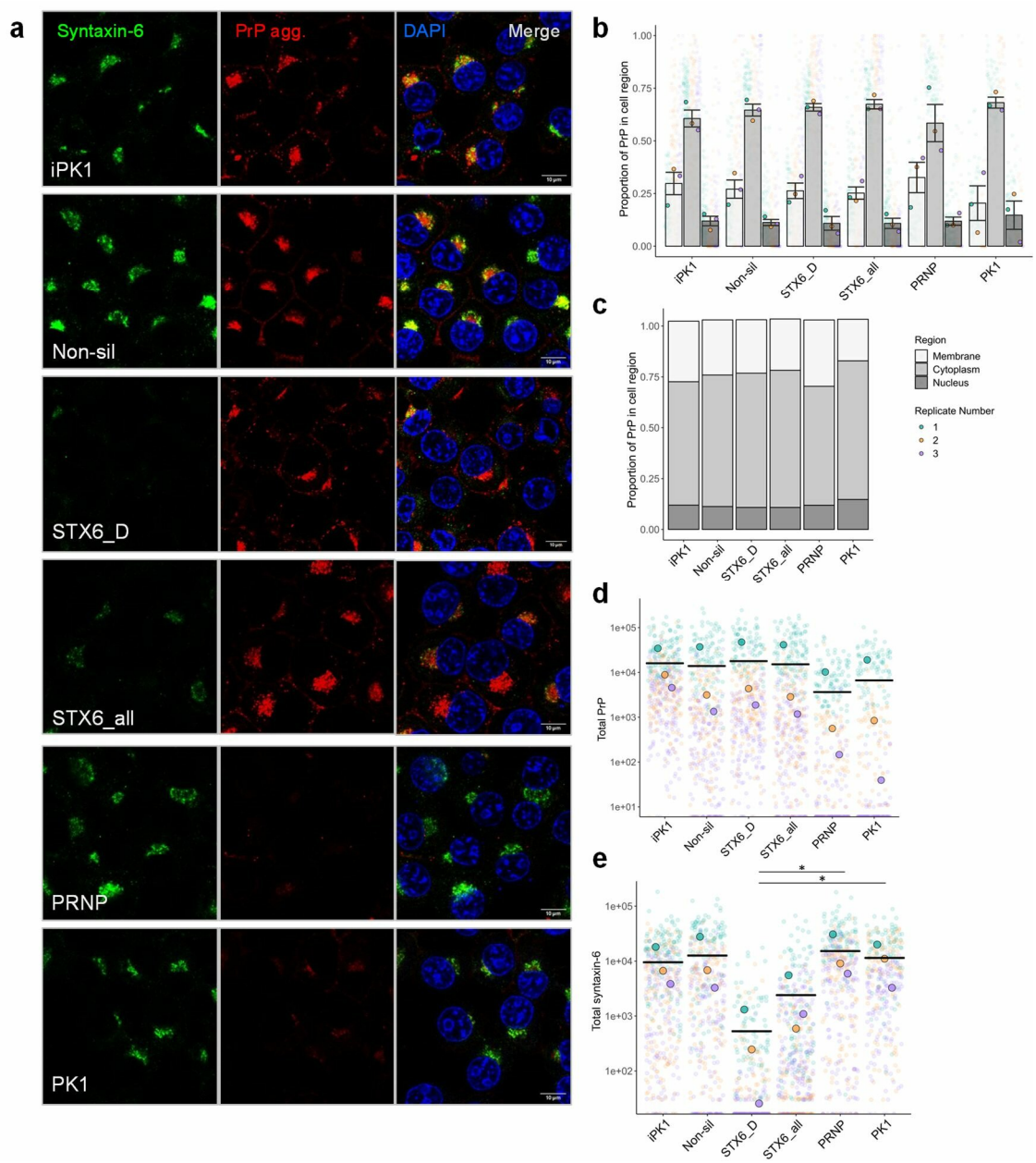

Figure 24: Knockdown of *Stx6* does not have a gross effect on the localisation of PrP aggregates in chronically infected iPK1 cells.
Immunostaining for PrP and syntaxin-6 in stable iPK1 cell lines with reduced *Stx6* (STX6_D, STX6_all) or *Prnp* expression or non-silencing (Non-sil), untransfected (iPK1) or uninfected (PK1) controls. Cells were fixed and permeabilised before treatment with 3.5 M guanidine thiocynate to select for PrP aggregates. Co-immunolabelling was performed with anti-syntaxin-6 antibody (green) and anti-PrP antibody (clone 6D11) (red). (**a**) Representative images for each cell line. Nuclei are stained with DAPI (blue). (**b**,**c**) Quantification of PrP localisation in each cellular compartment (nuclei, cytoplasm, membrane) does not show a gross mislocalisation of PrP aggregates. Protein expression calculated as a function of area and mean pixel intensity, and proportions calculated relative to total protein per cell. Proportion per cell line shown (**b**) per independent replicate and (**c**) as a mean proportion only as stacked bars for clarity. (**d**,**e**) Total expression of (**d**) PrP and (**e**) syntaxin-6 in each cell line supports gene knockdown (*P < 0.05; one-way ANOVA with Tukey's post-hoc test). Error bars: mean ± SEM; n = 3. Scale bar: 10 µm.

There is limited evidence in the literature to suggest a role of syntaxin-6 in the secretion of proteins from cells. For example, Lee and colleagues found a relationship between tau release into the media from HEK293T cells and syntaxin-6 expression (W. S. Lee et al., 2021). To therefore explore whether syntaxin-6 may contribute to the release of prions and thus potential spread of pathogenic proteins, a preliminary study was performed in which media was collected from the stable iPK1 cell lines after 18 hours in culture and the resultant infectivity measured in the ASCA. To allow for multiple replicates, media was either frozen at -80^{o}C prior to use or used fresh to infect PK1 cells.

As the level of prions released into the culture media would be affected by growth rate after plating, this was first analysed for each line (Figure 25a). There was no significant differences in doubling time but these results suggest a slower growth rate for STX6_D and so ASCA results were normalised to cell count. There was no gross consistent difference in the calculated tissue culture infectious units (TCIU) secreted into the culture media between *Stx6* knockdown cell lines (STX6_D, STX6_all) compared to controls (Non-sil, RFP, PK1) either post-2nd or post-3rd passage, indicating syntaxin-6 is not contributing to the release of prions from iPK1 cells in this preliminary assay (Figure 25b). Media from *Prnp* knockdown and uninfected cells showed the expected reduction in infectivity. Interestingly using frozen media consistently reduced the infectivity in the samples and, although this was fairly consistent between lines, is likely to affect the results and should not be used for comparison.

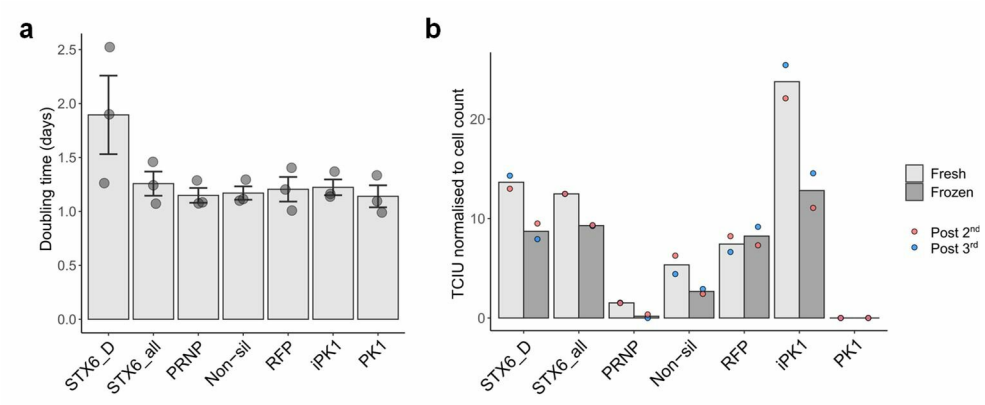

Figure 25: A preliminary study does not indicate a role of syntaxin-6 in prion release from iPK1 cells.
Stable knockdown of syntaxin-6 following transfection with a single STX6 shRNA (STX6_D) or a combination of 4 (STX6_all). PRNP, scrambled non-silencing (Non-sil) and RFP shRNAs were used as controls. (**a**) Growth rate of cell lines measured as doubling time in days (all ns; one-way ANOVA with Tukey's post-hoc test; mean ± SEM) (**b**) Automated scrapie cell assay (ASCA) to measure infectious prions in culture media at 5 x 10^{-1} dilution collected after 18 h in culture, used fresh or previously stored at -80°C, does not show any gross differences in infectivity with syntaxin-6 knockdown. Tissue culture infectious units (TCIU) calculated relative to a standard curve of RML-infected mouse brain homogenate post-2nd or post-3rd passage in the ASCA (n = 1).

4.2.5. Role of STX6 in tau aggregation

As *STX6* has also been associated with tauopathy PSP and more recently with AD, it is possible that syntaxin-6 plays a common role in these related neurodegenerative diseases, possibly contributing to the 'prion-like' spread of tau (Hoglinger et al., 2011; Wingo et al., 2021). To start to explore whether syntaxin-6 contributes to the seeded aggregation of tau in cell culture, gene expression was modified in the HEK293T 'tau biosensor' cell line previously generated by Marc Diamond's group (see section 4.1.3) (Holmes et al., 2014). In this line aggregation can be measured through the FRET signal generated (i.e. with flow cytometry) however aggregates also form distinct green puncta which can also be easily visualised under a fluorescent microscope (Figure 26a).

As the time-course of this experiment is short with aggregation reaching a plateau within three days post-seeding, transient knockdown of gene expression using short-interfering RNAs (siRNAs) was utilised. The ratio of siRNA to transfection reagent was first tested to optimise the efficiency of *STX6* mRNA knockdown

relative to a non-silencing siRNA control by RT-qPCR (Figure 26b; see Methods section 2.7.2). All conditions tested demonstrated reduced expression after 48 h, with condition ‘C’ (20 pmol siRNA/ml, 0.3 µl lipofectamine/ml) showing the highest perturbation. Knockdown of *STX6* mRNA under these conditions effectively reduced expression of syntaxin-6 protein as detected by immunoblot from 24 h post-transfection, sustained at up to 73% reduction for the 96 h tested (Figure 26c and d).

Having demonstrated siRNA transfection efficiently reduces syntaxin-6 protein expression over the time-course required for this assay, the effect on aggregate formation upon treatment with seeding-competent recombinant tau fibrils was measured. Cells were monitored in real-time and aggregate count quantified every 3 hours. Treatment of cells 24 hours post-siRNA transfection induced formation of visible aggregates in all samples (Figure 26e), however there was no effect of *STX6* knockdown on the rate of aggregate formation or maximum aggregate count compared to non-silencing or untreated controls, suggesting that syntaxin-6 does not contribute to the seeded aggregation of tau in this cell line (Figure 26f and g).

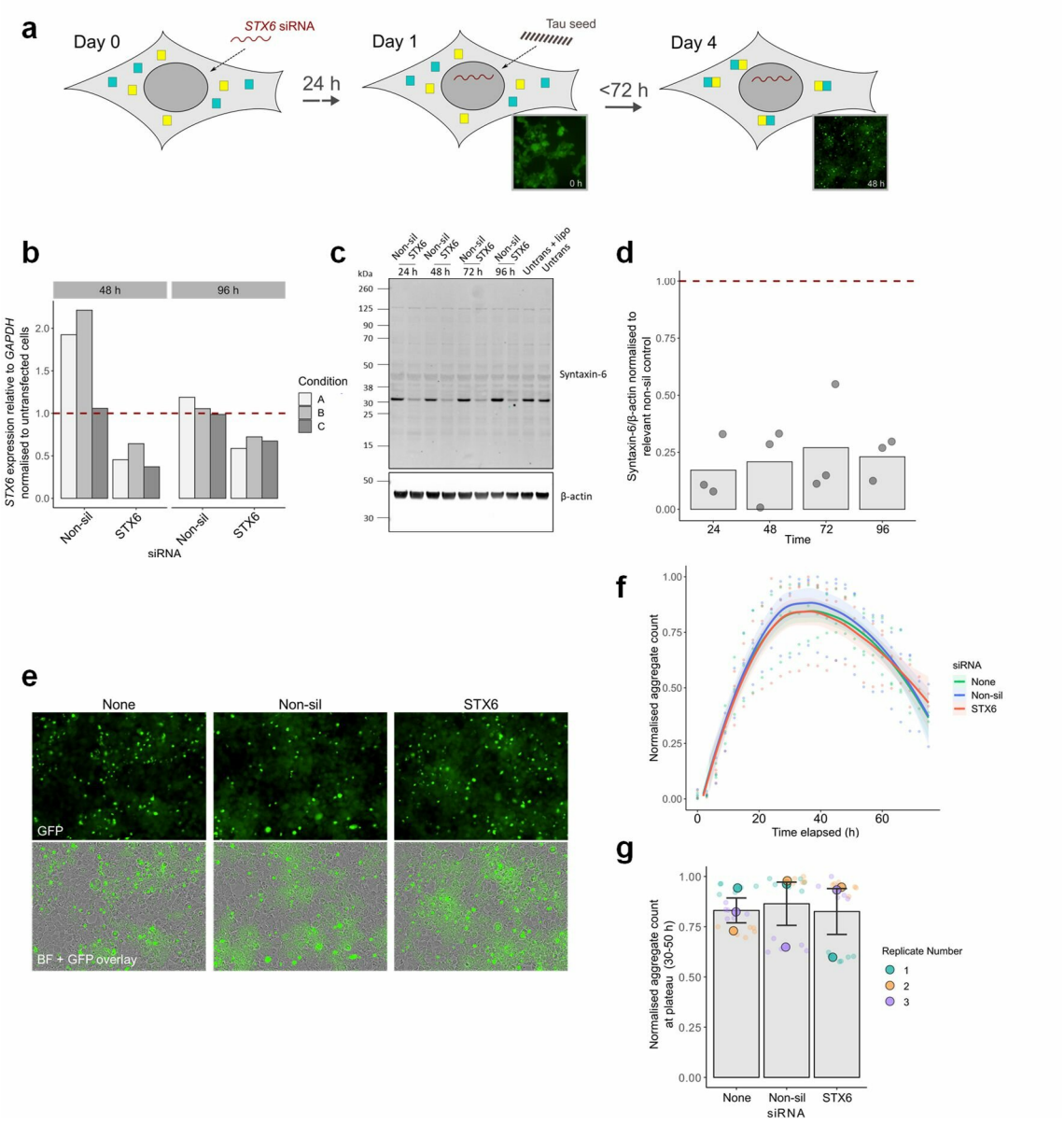

Figure 26: Knockdown of syntaxin-6 in HEK tau biosensors has no effect on seeded aggregation of tau.

(**a**) Schematic overview of seeding assay in HEK tau biosensor cells. HEK cells were transfected with siRNAs 24 h prior to treatment with seeding-competent tau and incubated for <72 hours in the Incucyte S3 Live-Cell Analysis System to monitor the appearance of fluorescent green puncta in real-time. (**b**-**d**) Validation of *STX6* knockdown using siRNAs. (**b**) Knockdown of *STX6* mRNA expression optimised for lipofectamine:siRNA ratio (conditions denoted A-C) by RT-qPCR relative to a scrambled non-silencing control (Non-sil) at 48 and 96 h post-transfection. Condition C demonstrated the highest efficiency of knockdown. Knockdown up to 82% was validated by (**c**) immunoblot using anti-syntaxin-6 antibody (**d**) quantified relative to anti-β-actin loading control normalised to non-silencing control at each time point (n = 3). (**e**-**g**) Tau aggregate formation in *STX6* knockdown cells compared to non-silencing and untreated (None) controls. (**e**) Representative images of tau aggregates at 48 h post-seeding. (**f**,**g**) Mean aggregate count from triplicate wells normalised to maximum count on plate and percentage confluence (n = 3). (**f**) Points: mean aggregate count per replicate; line: local

weighted regression ± SEM. (**g**) Aggregate count at peak (30-50 h) shows no significant difference between *STX6* knockdown cells and non-silencing control (Student's t-test). Error bars: mean ± SEM; n = 3.

4.3. Discussion

In this study the role of syntaxin-6 in the biology of two associated proteins, PrP and tau, was investigated using cell-based and protein-based assays. Multiple hypotheses were tested including a role in seeded aggregation and propagation of proteopathic aggregates, the localisation of proteins within cells as well as the possibility for direct protein-protein interactions. There was no evidence for a role of syntaxin-6 in any of the processes tested, except a potential modest reduction in surface PrP^{C} expression.

PK1 cells were predominantly utilised to investigate the role of syntaxin-6 in prion biology. N2a cells have been used most frequently in prion research and are routinely used in the ASCA to measure RML infectivity of biomaterials. Knockdown and overexpression of genes in this line has proved an effective way to model a number of previously identified genetic associations with human prion diseases (C. A. Brown et al., 2014). However in the current study generation of multiple PK1 cell lines with over 70% reduction in *Stx6* expression did not demonstrate a consistent effect on infectivity with RML prions in the ASCA or ability to maintain prion propagation relative to control lines in the cell curing assay, unlike the striking effect of *Prnp* knockdown in both of these. Of note, a high degree of variability was observed between both *Stx6* knockdown and control cell lines in the ASCA, highlighting the need for screening multiple clones.

Previous studies have shown substantial robustness of SNARE functions to gene knockdown including syntaxin-6; work by Bethani et al demonstrated up to 90% loss of *Stx6* expression in PC12 cells is still sufficient to form functional SNARE complexes (Bethani et al., 2009). This may prevent deleterious phenotypes in the cell lines generated in the current study, although deficits associated with *Stx6* knockdown have been demonstrated by other groups suggesting this is context specific (Choudhury et al., 2006; Ganley, Espinosa, & Pfeffer, 2008). Nonetheless the level of knockdown generated is far greater than the gene expression

changes driven by *STX6* risk associated variants in relevant brain tissues (~15% for rs3747957 in putamen (GTEx); see section 3.2.4) (GTEx Consortium, 2015).

PK1 cells and the ASCA were originally developed as a cell-based alternative to the time consuming mouse bioassay for measuring prion infectivity in biomaterials. This has been highly successful with sensitivities comparable to this gold-standard assay (Klohn et al., 2003). They were not however intended or selected for their ability to model the disease and are therefore far withdrawn from this. For example, the requirement for continuous passage to remove proteins from the inocula means a distinction from the predominantly post-mitotic neurons which are infected in the disease. Similarly the HEK tau biosensors developed by the Diamond lab provide a highly sensitive read-out of tau seeding activity able to report tau seeds before the onset of any related histopathology, yet the non-neuronal origin of this line limits the relevance to disease modelling (Holmes et al., 2014). A study by the same group found knockout of 22 AD associated genes identified through GWAS had no effect on tau uptake, seeding or aggregate propagation highlighting their limitations as a model for human disease (Kolay & Diamond, 2020). Similarly in the current study, knockdown of *STX6* expression did not impact the seeding capabilities of tau aggregates in this cell line.

N2a cells and other immortalised cell models able to propagate prions are further limited by their non-human origin: it is plausible the role of a gene associated with a human prion disease may be species-specific. As previously discussed (see section 3.3) there is currently no evidence for a shared genetic association outside of *PRNP* for different human prion diseases and therefore the role of syntaxin-6 may even be specific to sCJD prion strains, preventing observation of a phenotype in the current study focussing on the murine RML prion strain. Despite progress in modelling some non-rodent prion strains in culture, establishing a cell model able to propagate human prions has proven much more challenging (as previously discussed in section 4.1.1) (Bian et al., 2010; Courageot et al., 2008; Pineau & Sim, 2021; Vilette et al., 2001). Both a cell line able to propagate human prion strains and one of human origin would be pivotal to human functional genetics studies in the field.

Cell models for prion propagation are highly diverse in their species, origin and characteristics, exemplified by their distinct strain susceptibilities. To account for these differences, genetic manipulation of *Stx6* expression was tested in an additional cell line, CAD5. The reason behind the cell tropism in strain propagation is unclear; hypotheses include differential expression of a necessary cofactor or minor variations in PrP^C expression, however attempts to address this have been largely unsuccessful (Chasseigneaux et al., 2008). Nonetheless these clear differences, heightened by the substantial sub-cloning required to increase prion susceptibility, may mean that only a subset of cell lines will show a specific role of syntaxin-6 in prion propagation. For example previous research has highlighted a role of this protein in caveolae-mediated endocytosis and the transport of related proteins to the plasma membrane, a mechanism thought to contribute to the internalisation of some prion strains in culture, yet one of the key proteins in this pathway, Cav-1, is mostly lacking from N2a cells (Choudhury et al., 2006; Peters et al., 2003; Show Ling Shyng et al., 1994). CAD5 cells were utilised in the current study as an alternative to N2a cells due to their susceptibility to multiple prion strains, however the same protocol which robustly generated stable cell lines in PK1 cells was not successful. This may be due to a requirement of syntaxin-6 in normal cellular functions which is not reflected in PK1 cells, especially plausible with an established role of syntaxin-6 in both cell adherence and survival (Tiwari et al., 2011; Y. Zhang et al., 2008). Future studies should consider testing PrP-related parameters in transiently modified cells, or screening other prion-propagating cell lines. Further, the role of syntaxin-6 may be specific to prion propagation between cells of a solid tissue or in a live animal or patient, and not be evident in cell lines. This will be the subject of another chapter.

Immunofluorescence analysis of fixed cells in this study indicated a high-degree of colocalisation between PrP^C and syntaxin-6, yet in an ELISA-based assay with recombinant full-length human PrP and syntaxin-6 no direct protein-protein interaction was observed. This was used as an alternative to co-immunoprecipitation to study PrP interactors due to the membrane localisation leading to the requirement for strong detergents for extraction of both proteins, interfering with most protein-protein interactions. This assay provided no evidence for a direct interaction between PrP^C and syntaxin-6 unlike those seen

for other PrP-interactors including tau, β-amyloid and α-synuclein (Corbett et al., 2020). These data suggest that PrP and syntaxin-6 may be present on the same membrane or vesicular structures without direct contact, although further testing in situ is warranted due to the minimalist nature of this method.

Utilising recombinant proteins for this study has various limitations. Vitally this includes the lack of post-translational modifications potentially key to interactions, especially with the addition of a GPI-anchor to PrP for membrane insertion likely required to bring it in proximity with syntaxin-6, as well as the lack of other intracellular components raising the question of whether, just because two proteins might have the capability to interact, their localisation makes this feasible within a cell (e.g. the membrane barrier between extracellular PrP^C domains and cytosolic syntaxin-6 may prevent interaction). Additionally it would be important to differentiate between a functional, specific interaction and coincidental colocalisation i.e. due to trafficking of PrP^C through the biosynthetic pathway. Nonetheless no previous proteomics-based studies investigating PrP^C interactors in a variety of systems or evidence from the STRING protein interactions database highlight syntaxin-6 as a binding partner (recently reviewed in (Miranzadeh Mahabadi & Taghibiglou, 2020)). Of note, one study identified *PDIA4* (another suggestive sCJD risk gene) as a PrP-interactor in N2a cells however the evidence for this is variable (Torres et al., 2015; Watts et al., 2009).

A recent publication by Lee and colleagues did however provide some evidence supporting a direct interaction between syntaxin-6 and tau, a relationship that was not explored in the current study (W. S. Lee et al., 2021). Here they expressed tagged proteins in HEK293T cells and demonstrated co-purification of syntaxin-6 with both wild-type and pseudo-phosphorylated tau and co-localisation in primary neurons, however this interaction was not supported by proteomics analysis in the same study. The authors propose syntaxin-6 acts to facilitate tau uptake into vesicles and subsequent secretion, providing evidence for increased tau release with syntaxin-6 C-terminal expression, although the overexpression and mutant constructs used in this study may not reflect the physiological state. As tau is cytosolic, whereas both PrP^C and PrP aggregates are thought to localise predominantly to the plasma membrane and within membrane-bound compartments, it is hard to envisage a similar mechanism applicable in prion-

pathogenesis. This should be considered however, for example whether prions in the cytosol are more functional than previously thought (Godsave et al., 2008; Uchiyama et al., 2013). In the current study preliminary exploration of infectious prion release from RML-infected iPK1 cells does not support a similar role of syntaxin-6 in prion secretion, however further investigation is required to secure this conclusion.

A high degree of colocalisation between denaturation-resistant PrP aggregates and syntaxin-6 in iPK1 cells was also observed in the current study. Experimental investigation of interactors with disease-associated PrP is complicated by the need for purification to distinguish this from the cellular form, most commonly utilising protease digestion and thus removing any proteins external to the resistant core. This also fails to account for protease-sensitive PrP forms known to constitute a substantial proportion of disease-associated PrP, which may have distinct binding partners (Safar et al., 1998). Nonetheless, further investigations are required to determine if the colocalisation observed is due to a protein-protein interaction specific to this form of the protein.

As with all biochemical techniques, the tools used for phenotype analysis in this study fall to various limitations, important to consider when drawing conclusions from these data. The use of immunoblotting as the read-out in a number of assays in the current study is limited in its sensitivity and is not eminently quantitative in its nature, although the use of fluorescence-conjugated antibodies has somewhat increased the sensitivity and accuracy of differential protein expression measurements (Pillai-Kastoori, Schutz-Geschwender, & Harford, 2020). Visualisation of single colonies of cells with an ELISA-based assay in the ASCA has increased sensitivity over traditional immunoblotting to measure PK-resistant PrP. Additionally all assays are monitoring steady-state or end-point phenotypes. Traditionally, this is simpler, eliminating the requirement for more specialised equipment such as viable imaging chambers for live-cell confocal microscopy, and working with infectious material unfortunately limits the access to shared resources. However, especially due to the dynamic nature of the endolysosomal network in which syntaxin-6 functions, future work should importantly focus on investigating deficits in a time-resolved manor. Furthermore the need for stable genetic modification in the ASCA generates the possibility for compensation of

related genes likely to mask the effect of syntaxin-6 knockdown. In the current study no phenotype associated with syntaxin-6 knockdown was observed in cells at steady-state outside of a moderate but variable alteration in surface PrP in one line studied.

Limitations in cellular and biochemical systems along with cell line and temporal heterogeneity (e.g. cell cycle phases) have likely prevented elucidation of the mechanism driving the association of *STX6* with sCJD and tauopathies in this study, highlighting the requirement for a combinatorial approach to modelling genetic associations in biological systems, as well as careful consideration of the constraints in the models used. Although immortalised cell lines have great benefits with their low cost, ease of manipulation and quick results, more human disease relevant models as well as higher resolution in both time and magnification will be required to comprehensively test hypotheses of syntaxin-6 function in human prion diseases.

5. Development of a human cell model to investigate *STX6* function

5.1. Introduction

5.1.1. Development of iPS cells and iPS-derived neural cells

Since the first ground-breaking publication by Takahashi and Yamanaka in 2006 demonstrating the ability to reprogram mouse somatic cells to a state resembling embryonic stem (ES) cells, the application of induced pluripotent stem (iPS) cells has grown exponentially in an exciting period for disease modelling and regenerative medicine (Takahashi & Yamanaka, 2006). This technology revolutionised cell biology providing researchers with a way to generate almost any cell type desired with a human origin in an easily accessible and expandable manor, without the ethical limitations previously associated with stem cell research, especially instrumental for neurological disorders where relevant human cells are particularly inaccessible.

Initial generation of iPS cells from mouse and human fibroblasts was achieved by retroviral integration of four transcription factors, originally identified due to their functions in maintaining pluripotency in ES cells: *OCT4, SOX2, KLF4* or *MYC* and *NANOG* or *LIN28* (Takahashi et al., 2007; Takahashi & Yamanaka, 2006). Ectopic expression of these factors drove the generation of cell colonies indistinguishable from ES cells in their morphology, growth and gene expression. However the use of viruses has concerned researchers due to the propensity for unwanted integration and promotion of malignant transformation, especially with the application of these cell lines in regenerative medicine. This has therefore driven development of non-integrating methods for expression of these factors such as the now commonly used Sendei viral vectors, an RNA vector which replicates solely in the cytoplasm without entering the nucleus (Ban et al., 2011).

Differentiation of iPS and ES cells into a neural lineage was progressed from historically variable and inefficient methods (such as embryoid body differentiation) with work by Chambers and colleagues, who demonstrated that inhibition of signalling pathways involving two components of the TGF-β superfamily, bone morphogenic proteins (BMPs) and nodal, termed ‘dual SMAD inhibition’, drives efficient and homogenous neural conversion of ES cells

(Chambers et al., 2009). Down-regulation of BMP/SMAD protein signalling is required during neurogenesis in vivo for neural induction in the ectoderm, which is mimicked in dual-SMAD inhibition in vitro through the use of BMP inhibitors such as recombinant noggin (Liu & Niswander, 2005). The nodal/TGF-β/activin pathway appears to be required for maintenance of pluripotency in ES cells and so co-inhibition of this pathway (i.e. using inhibitor SB431542) is also required for neuroectoderm development with this method (James, Levine, Besser, & Hemmati-Brivanlou, 2005). Further improvements to the protocol such as the replacement of recombinant noggin with small molecule inhibitor dorsomorphin to limit variability and cost (originally by Morizane et al), and the addition of retinoic acid/vitamin A as required for cortical neurogenesis in vivo (Shi et al), allows robust generation (>95% efficiency) of neural stem and progenitor cells from all studied iPS cell lines (Morizane, Doi, Kikuchi, Nishimura, & Takahashi, 2011; Shi et al., 2012). This has led to dual-SMAD inhibition being the most frequently used method for generation of neural and glial cells from stem cells. Additionally, more recent advancements have progressed this to developing 3D cell-culture systems comprising multiple cell-types able to mimic to an extent physiological organ development, termed “organoids”.

5.1.2. iPS-derived cells in prion research

The generation of a cell line, especially of human origin, able to propagate human prions would be revolutionary to prion research (previously discussed in chapter 4, section 4.1.1). This would provide scientists with a tool to study the mechanism of human prion propagation in a physiologically-relevant biological system, for example allowing delineation between mechanisms driving infectivity over neurotoxicity (recently shown to be distinct pathways), as well as for screening potential modulators or therapeutics with ease and at a low cost (Benilova et al., 2020; Sandberg et al., 2011). It could be hypothesised that the more accurately one is able to simulate the disease-associated cell types in culture, the more likely they will be able to replicate this key disease-associated pathogenic mechanism. Therefore the advent of iPS cells has inevitably lead to testing different cell-type derivations for their ability to seed aggregation of human prion strains. The first successful demonstration came from Krejciova et al who showed an increase in PK-resistant PrP up to 28 days following exposure of iPS-derived astrocytes to

various vCJD and sCJD prion strains in a *PRNP* codon 129 and time dependent manor (Krejciova et al., 2017). More recent work led by Bradley Groveman similarly demonstrated an increase in PK-resistant PrP following exposure of a single iPS-derived cerebral organoid model to one sCJD prion strain (MV type 2 (Parchi)) up to 169 days later (Groveman et al., 2019). Importantly however there is only limited evidence for serial propagation of seeded aggregates (with both models predominantly post-mitotic) with neither testing the generation of authentically infectious prions, or including *PRNP* knockout controls to validate PrP templated seeding, required to conclude the utility of these models. Despite obvious further limitations with the cost and extended time course required to generate these, iPS-derived cell lines have successfully provided the first reproducible evidence for seeding of human prions in culture, in a cellular system relevant to the disease aetiology.

The ability to differentiate relevant cell types directly from patients granted by the advent of iPS cells was particularly beneficial to genetic disorders, allowing access to any cell type with the exact genetic background as the individual. In these studies, cells derived from individuals without the mutations were traditionally used as controls, however genetic variation introduces a high degree of discrepancy between lines and therefore often substantial noise into the phenotypes being investigated. This is especially problematic for sporadic diseases where the smaller genetic component, larger heterogeneity and later onset likely induces more moderate phenotypes in cellular models.

Patient-derived iPS cells have been used to model only a couple of IPDs. In 2018 Matamoros-Angles and colleagues first differentiated iPS cells obtained from an individual with a rare form of GSS caused by Y218N *PRNP* mutation into cortical neurons and “spheroids” (Matamoros-Angles et al., 2018): they were not able to demonstrate spontaneous generation of PK-resistant PrP (although this was only tested in relatively young cells at 45 days post-induction) or propagation of GSS or sCJD (MM1 (Parchi)) prions, however there was some evidence of increased reactive astrogliosis and hyper-phosphorylated tau in this small sample set related to the typical histopathological features in patients. Last year Cathryn Haigh’s group additionally utilised patient-derived cells from two individuals with a more common IPD, familial CJD with E200K *PRNP* mutation (Foliaki et al.,

2020). Cerebral organoids generated from either patient again lacked any PK-resistant or insoluble seeding-competent PrP aggregates up to 12 months in culture. Modelling of other common IPD mutations (such as D178N, P102L and ORIs) is yet to be published so further research is required to determine if patient-derived iPS cells could provide functional models for genetic prion diseases.

5.1.3. Gene editing and iPS cells

Advances in techniques for genetic manipulation have overcome some of the limitations associated with iPS cells, allowing generation of isogenic lines matched for genetic background outside of the region of interest. Demonstration that the CRISPR ('clustered regularly interspaced short palindromic repeat') mechanism used by prokaryotes to cleave foreign pathogenic DNA can be effectively modified for sequence-specific target recognition in mammalian cell culture opened up a new ream of genome editing possibilities, producing much higher efficiency and flexibility than the preceding technologies (recently reviewed in (Li et al., 2020)) (Cong et al., 2013; Jinek et al., 2012). Generation of isogenic controls reduces variability between cell lines improving not only familial disease modelling, but also highly beneficial when investigating genes associated with sporadic diseases for which the phenotypic effects may be reduced.

CRISPR sequences were first identified in *E.coli* as regular repeating motifs unusually dispersed by non-repeating sequences denoted 'spacers' (CRISPR comprehensively reviewed in (Doudna & Charpentier, 2014)). Increasing availability of whole genome information led to the unexpected mapping of these sequences to those from viruses and transposable elements, first indicating that this may mediate some kind of innate immunity in bacteria. Subsequent experiments by various groups quickly elucidated this, with the description of additional components including the conserved CRISPR-associated (Cas) genes upstream of the CRISPR region and protospacer adjacent motif (PAM) sequences critical for enzyme targeting (Figure 27). Cas9 was also crucially identified as a Cas protein with DNA endonuclease activity. This is driven by two short RNA sequences: CRISPR RNA (crRNA) for sequence recognition and trans-activating crRNA (tracrRNA) for protein scaffolding (later fused into a single guide RNA (sgRNA)).

Demonstration that these CRISPR regions are transferrable between organisms and can be programmed for directed target recognition led to the aforementioned application to gene editing in mammalian cells. Cas9/sgRNA complexes can be designed to specifically target a region of interest and, following generation of double-strand breaks, entopic DNA repair mechanisms are utilised to introduce desired modifications (Figure 27). Error-prone non-homologous end joining (NHEJ) is key for generating gene knockouts as introduction of insertions and deletions ('indels') into the break site can disrupt gene function. Alternatively, template sequences can be used to introduce more specific DNA modifications via homology directed repair (HDR). CRISPR utility has since been further expanded through various modifications, such as the use of nuclease-inactivated Cas enzymes to direct transcriptional repressors and activators to the region-of-interest, leading to CRISPR now being the tool of choice for increasing functional genetics studies (Gilbert et al., 2013; L. S. Qi et al., 2013).

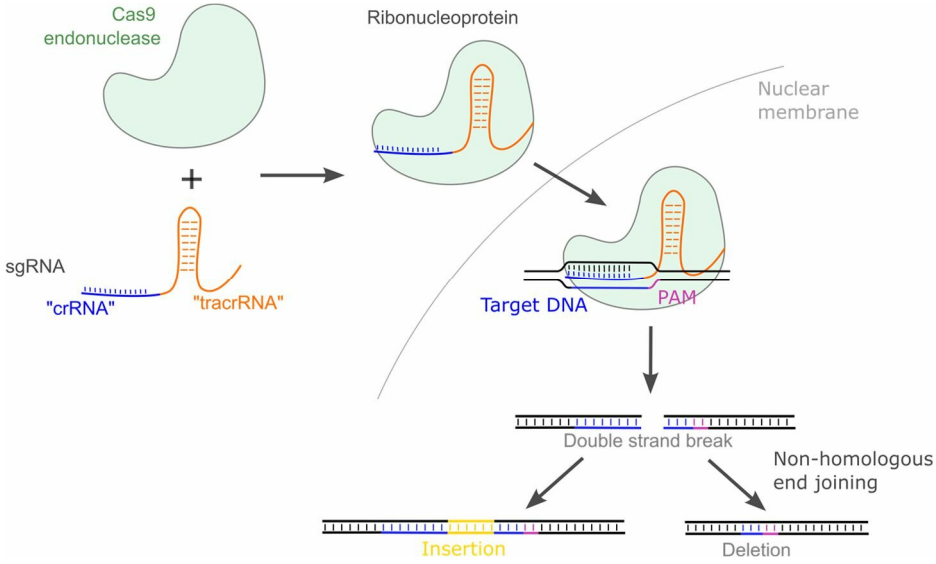

Figure 27: Gene knockout with CRISPR and Cas9 ribonucleoproteins.
Outside of the cell a synthetic single guide RNA (sgRNA) comprised of a gene-targeting segment (similar to the CRISPR RNA (crRNA) in prokaryotes) and a scaffolding segment (akin to the trans-activating CRISPR RNA (tracrRNA)) is complexed with recombinant Cas9 endonuclease to form a ribonucleoprotein (RNP). This complex is then transfected into cells and enters the nucleus, where it locates and binds its complementary target site upstream of a critical protospacer adjacent motif (PAM). DNA binding activates Cas9 endonuclease activity to induce a double strand break. This is repaired by the cells own DNA repair mechanisms, either through accurate homology directed repair (not shown) if a complementary sequence is present, or more commonly by error-prone non-homologous end joining (NHEJ). The latter is utilised for generating gene knockouts as NHEJ frequently introduces indels that can disrupt gene function.

Due to the reduced variability granted by this technology between isogenic cell lines and controls, genetic manipulation in iPS-derived neuronal cells has now been used to investigate genes associated with sporadic forms of neurodegenerative diseases. For example a variety of genetic risk factors for sporadic AD have been modelled including *APOE, TREM2* and *SORL1* utilising CRISPR technology to introduce either risk variants or knockouts (Cosker et al., 2021; Knupp et al., 2020; Lin et al., 2018). These studies were able to recapitulate a number of disease associated phenotypes in various iPS-derived cell types including accumulation of β-amyloid aggregates and hyper-phosphorylated tau, impaired microglial response and neuronal endosome enlargement. Although robust evidence for non-*PRNP* genetic risk factors for human prion diseases was previously lacking, iPS-derived neurons have been used in studies of PrP function including as a neurotoxic receptor for proteopathic oligomers and protease-mediated extracellular shredding (Corbett et al., 2020; Jarosz-Griffiths et al., 2019).

5.1.4. Chapter summary

In this study CRISPR is utilised to knockout the expression of *STX6* in iPS cells from a neurologically healthy individual with the aim to generate a human cell model for investigating the role of *STX6* in prion diseases. Here generation of cortical neurons from these cells through dual-SMAD inhibition demonstrates their ability to be successfully differentiated into a neural lineage for future experiments. As the effect size of the genetic association of *STX6* with sCJD is small it is likely any phenotype will be relatively subtle; gene knockout was performed to allow identification of gross perturbations which can provide direction for further studies modelling the more modest expression changes underlying the genetic risk.

5.2. Results

5.2.1. Characterisation of iPS cell lines

To obtain human iPS cell lines that would be multifaceted in their utility, two lines were imported matched for age, sex and disease status but with differing genotypes at the *STX6* haplotype associated with sCJD risk (i.e. rs3747957), providing the option to further investigate the impact of each genotype for example on gene expression if desired. Exomes of feeder-free cell lines from healthy male individuals (due to sex differences during differentiation), aged 60-69 (to match the typical sCJD age of onset) with MM genotype at *PRNP* codon 129 (iPS-derived astrocytes with MM previously demonstrated to be more susceptible to propagation of sCJD prions in culture (Krejciova et al., 2017)) listed in the Human Pluripotent Stem Cell Initiative (HipSci) database were screened and two cell lines were selected; HPSI0215i-oilg_3 ('OLIG3'; rs3747957 G/G) and HPSI1013i-pamv_1 ('PAMV1', rs3747957 A/A). These lines were generated using non-integrating Sendai vectors (Cytotune; Invitrogen) as previously described (see section 5.1.1).

OLIG3 and PAMV1 iPS cell lines were characterised to confirm the expected morphology and pluripotency. Immunofluorescence analysis of both cell lines detected expression of pluripotency markers Oct4 and Tra-1-60, with cells forming compact colonies with distinct borders and large nuclei as expected (Figure 28). There was no detectable difference between the two lines except OLIG3 demonstrated a growth rate and adherence in culture more closely reflecting previous used lines. This line only was used for future experiments due to experimental and cost limitations.

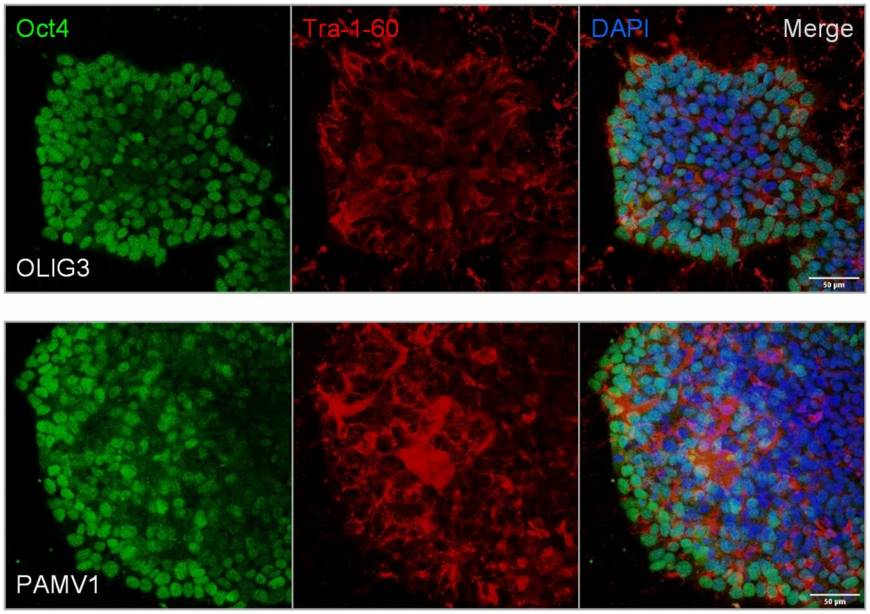

Figure 28: Both OLIG3 and PAMV1 iPS cell lines express pluripotency markers. Immunofluorescence for Oct4 (green) and Tra-1-60 (red) pluripotency markers in OLIG3 (top) and PAMV1 (bottom) iPS cell lines. Nuclei stained with DAPI (blue). Scale bar = 50 µm.

5.2.2. Optimisation of CRISPR-mediated gene knockout in iPS cells

In this study a commercially-available multi-guide strategy (Synthego) was utilised to knockout the expression of *STX6* in OLIG3 iPS cells with three sgRNAs targeting the gene obtained, as utilising multiple sgRNAs in tandem has been shown to increase the likelihood of obtaining functional knockouts through the introduction of larger indels (Jost et al., 2021).

The efficiency of successful CRISPR application in cell culture depends on a number of factors including desired output and required repair mechanism, sgRNA sequence and type of Cas endonuclease used, but will also be largely impacted by the efficiency of transfection of components into the cells, especially with hard-to-transfect cell lines such as iPS cells. In this study ribonucleoproteins (RNPs) comprising the synthetic sgRNA and recombinant Cas9 enzyme were utilised to minimise off-target effects, however both cutting and transfection efficiency for this system is likely to be reduced.

To first develop a protocol that could be used in-house for gene knockout in the OLIG3 iPS cell line, transfection of RNPs was tested at four different

lipofectamine:Cas9:sgRNA ratios (see Methods section 2.8.2, Table 6; ‘A’, ‘B1’, ‘B2’, ‘C’). Although nucleofection is used more routinely for transfection of iPS cells, a lipid-based reagent was used here due to availability of equipment. For optimisation, the same multi-guide strategy as described was used to target a gene previously shown commercially to produce functional knockout with viable cells, *TRAC*, as it was not yet known whether *STX6* knockout would be feasible.

Four days post-transfection with each condition, genomic DNA (gDNA) was isolated and the target region amplified by PCR. Agarose gel electrophoresis confirmed successful amplification of the target region in each sample, with evidence of an additional shorter band in three of the conditions compared to the unedited control (‘no RNP’) already indicating a potential deletion in some of these cells (Figure 29a). To compare knockout efficiency in these lines, amplicons were analysed by Sanger sequencing and a web-based application ‘Inference of CRISPR Edits’ (ICE; Synthego) was utilised to calculate editing efficiency and predict likely indels (Figure 29b-e). Prior to the first sgRNA binding site all sequences aligned well with the unedited control, however subsequent to this, traces in all samples started to become less coherent and demonstrated a higher level of relative discordance, indicating multiple DNA sequences are present in each sample (Figure 29b and c).

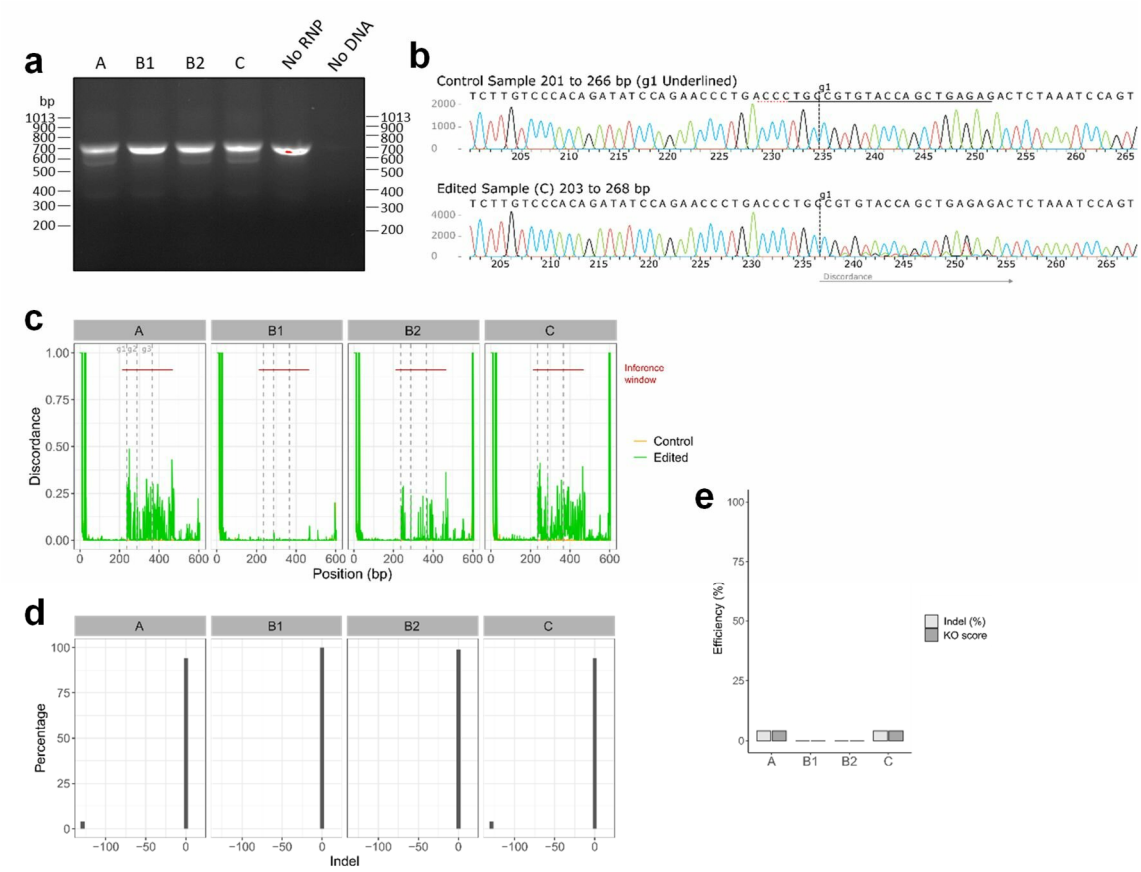

Figure 29: Optimisation of CRISPR-mediated gene knockout in OLIG3 iPS cell line. DNA extracted from OLIG3 iPS cells transfected with multi-guide ribonucleoproteins targeting *TRAC* positive control (Transfection Optimisation Kit; Synthego) at four different sgRNA:Cas9:Lipofectamine ratios (A, B1, B2, C). Edited region was amplified by PCR and products (**a**) run on an agarose gel to confirm amplification (WT = 667 bp) and (**b**-**e**) sequenced by Sanger sequencing. (**b**) Example sequencing traces with increased discordance between unedited control (top; 'No RNP') and edited sample (bottom) after sgRNA binding sequence (underlined) and cut site (dashed line). (**c**) Level of discordance at each position indicates well aligned sequences prior to sgRNA directed cut sites (dashed lines) used to infer (inference window) (**d**) indel percentage and (**e**) predicted functional knockout score ('KO score'; frameshift or indel > 21 bp). Conditions 'A' and 'C' showed evidence of gene KO (~4%, 129 bp deletion). Analysis performed using 'Inference of CRISPR Edits' (ICE; Synthego).

Through isolating these distinct signals, the tool bioinformatically identifies indels in the sample and predicts the percentage of cells in which these have occurred, with those indels which induce frameshifts or large-scale deletions (>21 bp) predicted to lead to functional KO (Figure 29d and e). Following transfection with conditions 'A' and 'C' an indel of 129 bp was identified in ~4% of the sample, demonstrating successful genetic modification using these methods in the OLIG3

iPS line. This large-scale deletion, although in-frame thus unlikely to generate a premature stop-codon, will remove a substantial section of mRNA and thus protein at the N-terminus which is likely to lead to non-sense mediated decay of the sequence. Condition ‘C’ was used going forward due to a moderate increase in the intensity of the shifted band on the agarose gel.

5.2.3. Knockout of STX6 in iPS cells

Having developed a protocol able to successfully induce genetic deletions in this iPS cell line, the same process was now repeated with sgRNAs targeting *STX6.* Alignment of the obtained sgRNAs shows binding of all three within the second exon of the primary protein-coding isoform (Stx6-201; Figure 30a). This targets the N-terminal of the protein sequence as this will most likely lead to functional knockout (over protein truncations for example). Of note there are a number of additional transcripts which do not contain this exon and may still be expressed.

Following transfection, cells were collected upon passage, gDNA extracted and the targeted region amplified by PCR. Products were analysed by agarose gel electrophoresis to confirm successful amplification (‘PCR 1’: Figure 30a and b); again, a faint band at a lower molecular weight was only present in the edited sample (‘STX6’) and not the no RNP control, indicating a potential deletion. Sanger sequencing across this region showed clear traces in both samples up to the first sgRNA binding site, after which the edited sample was noisier with evidence of multiple DNA sequences (Figure 30c). This is translated to a high level of discordance in the edited sample (Figure 30d). Isolation of distinct traces predicts a number of genetic modifications with the predominant being a 107-108 bp deletion in ~5% of the sample, with this large deletion predicted to cause functional gene knockout (Figure 30e and f).

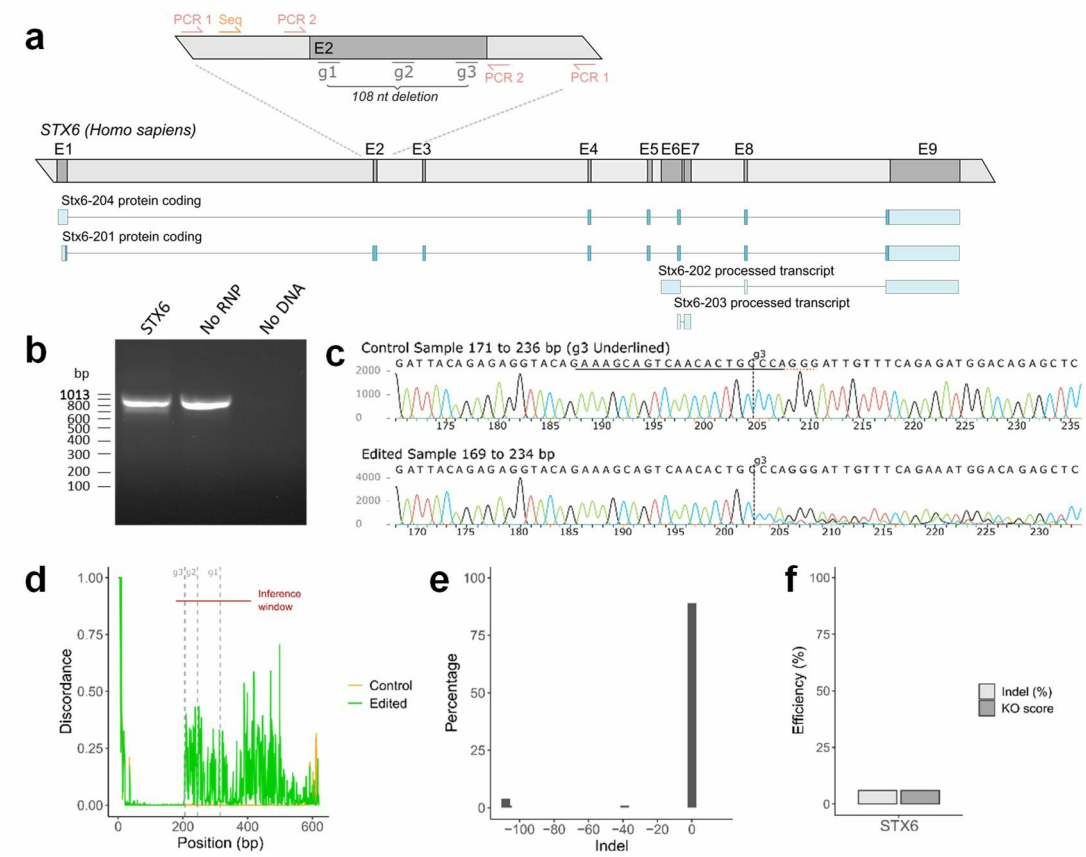

Figure 30: CRISPR-mediated knockout of *STX6* in iPS cell line pool using multi-guide strategy.

Three synthetic sgRNAs were obtained targeting exon 2 of the primary protein-coding transcript (Stx6-201) and transfected into OLIG3 iPS cells. (**a**) Diagram of human *STX6* gene and transcripts (darker blue = protein coding regions) with CRISPR target region and primer binding sites highlighted. (**b-f**) Edited region was amplified by PCR (PCR 1) and products (**b**) run on an agarose gel to confirm amplification (WT = 800 bp) and (**c-f**) sequenced by Sanger sequencing (primer: Seq). (**c**) Example sequencing traces with increased discordance between unedited control (No RNP, top) and edited sample (bottom) after sgRNA binding site (underlined) and cut site (dashed line). (**d**) Level of discordance at each position indicates well aligned sequences prior to sgRNA binding sites (dashed lines) used to infer ('inference window') (**e**) indel percentage and (**f**) predicted functional knockout score (KO score; frameshift or indel > 21 bp) (~4%, 108 bp deletion; ~1%, 107 bp deletion; ~1%, 39 bp deletion). Analysis performed using 'Inference of CRISPR Edits' (ICE; Synthego).

As a high proportion of the sample (~94%) does not contain any functional indels, the pool of cells was then single cell cloned to isolate homogenous populations to be screened for genetic deletion. Cells were passaged as single colonies into a 96-well plate and crude lysates generated from each well upon second passage. PCR amplification of these lysates using primers bordering the predicted indels produced distinct bands that could be visualised by agarose gel electrophoresis ('PCR 2': Figure 30a). In the 96 colonies screened there were a number of different length amplicons including a selection of samples with multiple bands, likely due to heterogeneous populations, as well as some with a single shorter amplicon at approximately the predicted 108 bp less than the positive unedited control (labelled 'KO 1-6'; Figure 31). The latter cells were expanded along with three clones without evidence of genetic modification as isogenic controls ('WT 1-3') for further validation.

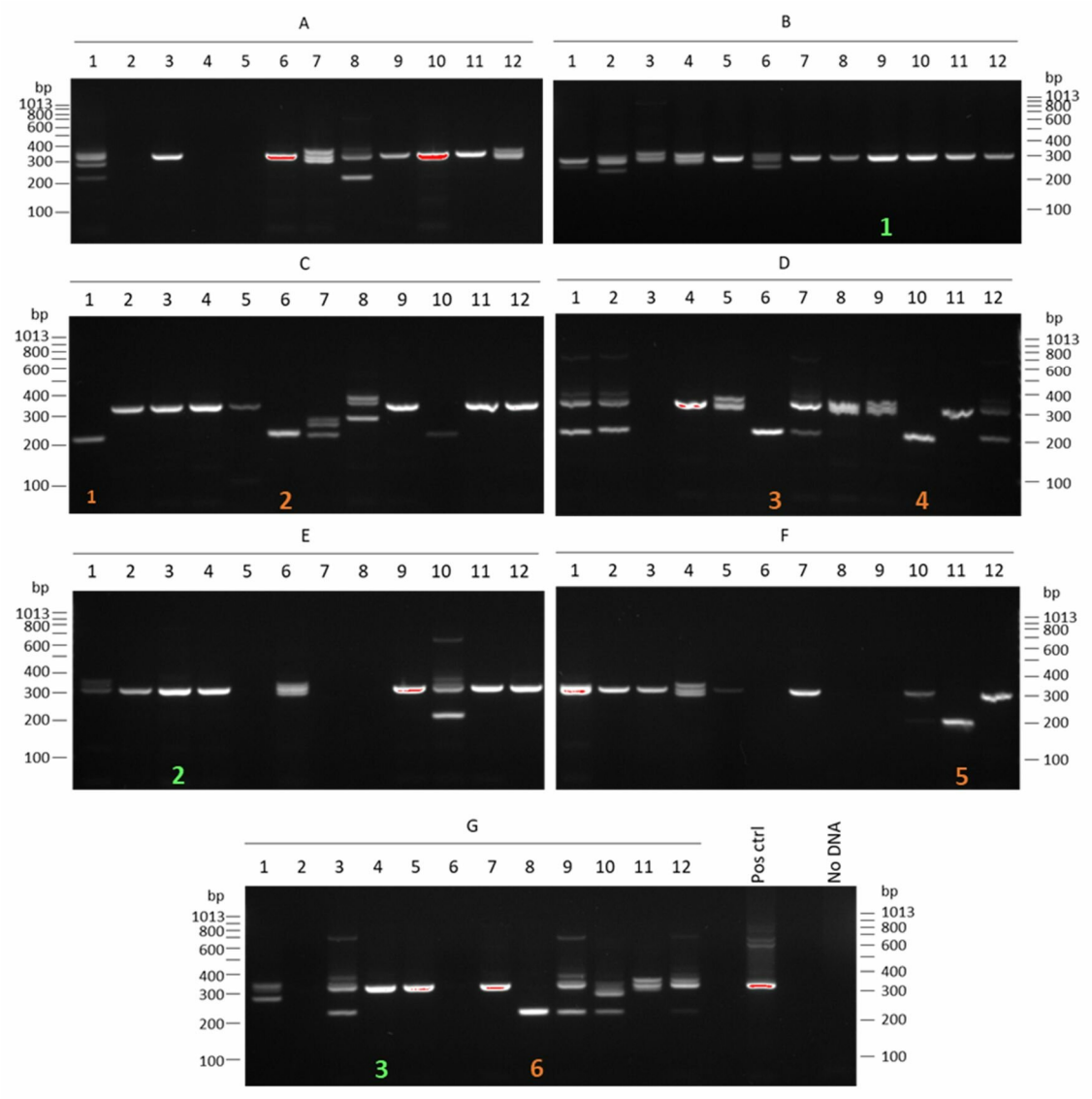

Figure 31: Single cell cloning of iPS cell pool isolates homogenous populations of predicted *STX6* knockout cells.
OLIG3 iPS cells transfected with *STX6*-targeting CRISPR ribonucleoproteins were single cell cloned to obtain homogeneous populations with deletions at the sgRNA target site. Target region was amplified by PCR and products analysed by agarose gel electrophoresis (WT = 319 bp) identifying multiple cell clones containing large deletions (red: C1 (KO 1), C6 (KO 2), D6 (KO 3), D10 (KO 4), F11 (KO 5), G8 (KO 6); band = ~211 bp) relative to positive control. Cell lines without evidence of genetic modification were used as negative controls (green: B9 (WT 1), E3 (WT 2), G4 (WT 3)).

5.2.4. Validation of STX6 knockout

Due to the possibility of protein truncations or modifications which do not lead to functional knockout it is important to validate any genetic modifications. To first determine whether the levels of *STX6* transcript were altered in the KO cell lines relative to the WT and unedited controls, RT-qPCR was performed on cDNA generated from each line, however there was no evidence of reduced expression relative to *GAPDH* (used as a 'housekeeping' gene) or *PRNP* (Figure 32a). This is perhaps not surprising as the sgRNA target sites lie in an exon distinct from the gene promoter or known transcriptional regulators.

To validate whether deletion occurred at the protein level, lysates were analysed by immunoblotting. This confirmed the expected immunoreactive band at 32 kDa was missing in the KO cell lines but not the WT controls, corresponding to the edited Stx6-201 isoform (Figure 32b). Of note there is a lower intensity band visible at approximately 17 kDa in all cell lines which likely represents the secondary protein-coding isoform Stx6-204 not targeted by this modification, however this appears to represent a substantially lower proportion of the total syntaxin-6 in these cells.

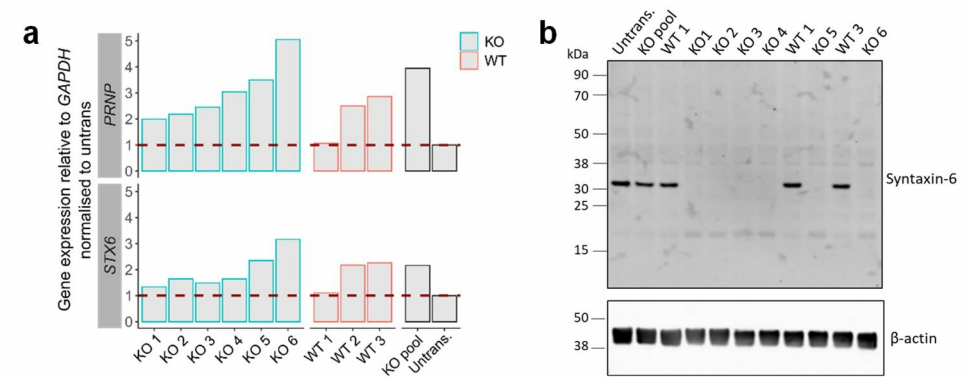

Figure 32: Validation of *STX6* gene knockout by RT-qPCR and immunoblot.
(**a**) RT-qPCR on cDNA generated from *STX6* KO (green) and WT controls (red) for *PRNP* (top) and *STX6* (bottom) expression does not show evidence of reduced *STX6* mRNA expression in KO cell lines relative to *GAPDH* housekeeping gene. (**b**) Immunoblot for syntaxin-6 (top) demonstrates loss of primary 32 kDa immunoreactive band in KO cell lines. β-actin (bottom) was used as a loading control.

5.2.5. Characterisation of isogenic STX6 knockout cell lines

When performing substantial genetic modifications such as gene knockouts, there are a number of potential unwanted consequences which should be considered, such as off-target cleavage by the Cas9 endonuclease and perturbations of cell function. These issues are further amplified when working with iPS cells due to increased genomic instability and propensity to spontaneously differentiate.

To therefore confirm clones have retained pluripotency through this process cells were fixed and again stained for pluripotency markers Oct4 and Tra-1-60 (Figure 33a). Both markers were present in all cell lines although with some variation in the level of detection between cells and between images. This may reflect differing levels of pluripotency but further testing is required to confirm this.

Karyotypic abnormalities are common in stem cells, with long term culture increasing genomic instability, especially problematic when trying to generate a model representative of whom the cells are derived. It has been shown that many abnormalities in iPS cells are recurrent with the same defects occurring in most instances, so a qPCR-based method was utilised to screen each cell line for the most common chromosomal alterations (Assou et al., 2020). In this screen no significant copy number alterations were identified, with two copies of each chromosomal region tested detected (except the X chromosome as these cells were derived from a male donor) (Figure 33b).

As previously mentioned, there is a possibility of off-target effects with CRISPR gene editing due to unwanted cleavage of Cas9 nuclease at additional sites. Identifying these off-target effects is however not trivial, for example to screen the whole genome would be time-consuming and costly. Large scale genetic alterations and clonal expansion have the potential to modify the growth rate of cells in culture so, to allow timely progressing with long-term differentiation, this was measured to gain an initial insight into any substantial differences in these modified cell lines. There was some variation between cell lines with KO lines 1, 2 and 6 having a longer doubling time relative to the untransfected parent line (Figure 33c). Due to the high cost of reagents and time commitments for the subsequent experiments, only KO lines 3, 4 and 5 were taken forward (Figure

32). Of note one of the WT control lines (WT 2) also demonstrated reduced growth rate, however all three WT controls were used going forward to obtain the same number of replicates for each condition.

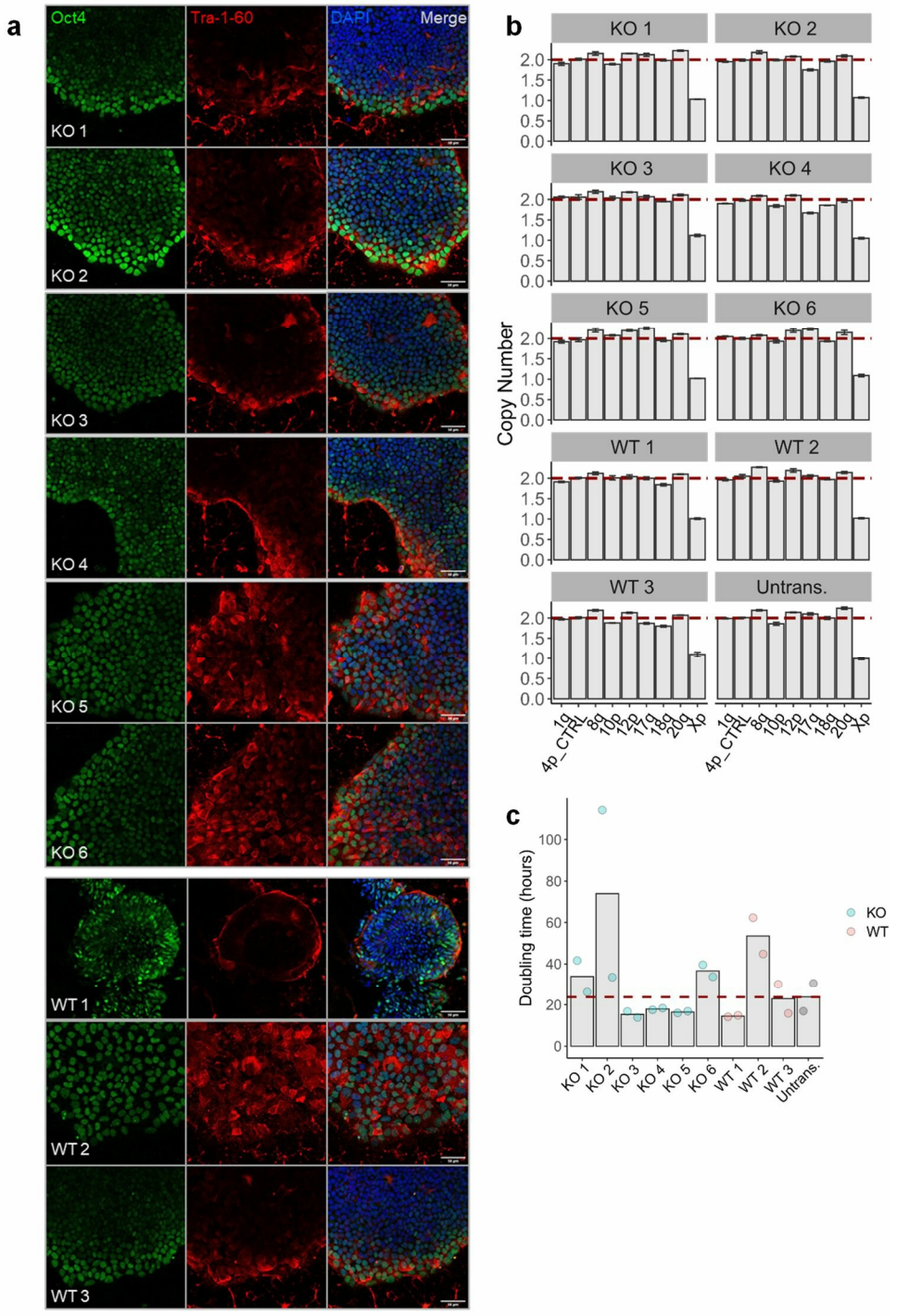

Figure 33: Characterisation of *STX6* knockout iPS clones.
(**a**) Immunofluorescence for Oct4 (green) and Tra-1-60 (red) in *STX6* KO (top) and WT controls (bottom) detects expression of pluripotency markers in all lines. Nuclei stained with DAPI (blue). Scale bars = 50 µm. (**b**) Karyotyping through detection of most common iPS copy number alterations by qPCR does not identify any significant abnormalities in

any cell line. (**c**) Measurement of growth rate as doubling time in days highlights multiple KO (blue) and WT (red) cell lines with slower growth relative to untransfected control (Untrans, dashed line). Bars: mean, n = 2

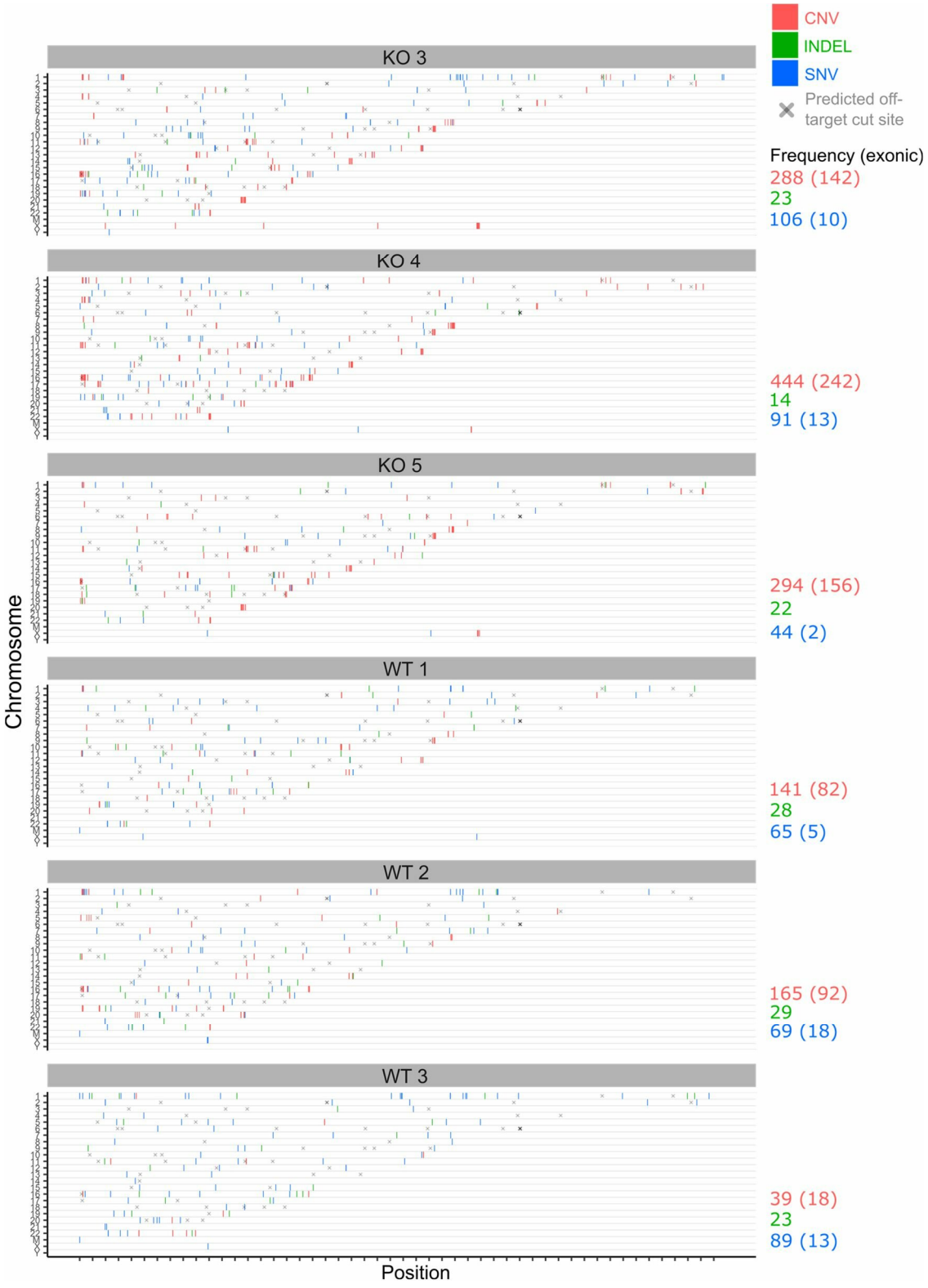

Figure 34: Varying frequency of indels, copy number variants (CNV) and single nucleotide variants (SNV) present in *STX6* knockout and control iPS cells identified by whole exome sequencing relative to unedited parent.

Whole exome sequencing of genomic DNA extracted from *STX6* knockout (KO 3-5) and wild-type control (WT 1-3) iPS cell clones. Plot of somatic CNVs (red), indels (green) and SNVs (blue) relative to untransfected parent line (OLIG3) by chromosome and genomic position. Most likely in silico predicted off-target effects indicated by cross shapes. Frequency of perturbation listed on right of plot with the number falling in exons indicated in brackets, demonstrates varying frequency of somatic alterations with the highest number of CNVs in the KO cell lines.

To more accurately screen for off-target perturbations following CRISPR, whole exome sequencing was subsequently performed on gDNA from the selected clones. Copy number variants (CNVs), indels and single nucleotide variants (SNVs) relative to the reference genome following QC were identified (see Methods section 2.8.8). These were compared to the unedited parent cell line to identify 'somatic' alterations following gene editing (Figure 34). Interestingly the highest proportion of differences, especially for CNVs, is present in the knockout cell lines. However, especially due to the added genomic instability of iPS cells, it is likely that numerous small differences in gene sequence will arise in these lines by chance. To therefore distinguish any changes due to off-target effects of Cas9 cleavage, in silico analysis was used to predict the most likely additional cut sites in the human genome with up to 4 sgRNA mismatches (Guide Verification Tool (Synthego) adapted from (Doench et al., 2016)). Screening for somatic changes 100 kb upstream and downstream of these predicted cut sites indicates some enrichment of CNVs surrounding one of these positions on chromosome 16 in multiple cell lines (KO 3, KO 4, WT 2) however these were all >15 kb distant from the cut site so are likely distinct from Cas9 activity (Table 13). There was no evidence of off-target mutagenesis within 15 kb of any predicted target site.

Cell line	Type	Chr	Position	Exonic?	sgRNA	Off-target site	Mis-matches	Cut site	PAM	Nearest gene	Distance (bp)
KO 3	CNV	16	690326	FALSE	UUGUUGCUGUGGAGGGGUCC	CGACCCCTCCACAGCCAGAA	3	709567	TGG	MSLN	19241
KO 3	CNV	16	690118	FALSE	UUGUUGCUGUGGAGGGGUCC	CGACCCCTCCACAGCCAGAA	3	709567	TGG	MSLN	19449
KO 3	CNV	16	688810.5	TRUE	UUGUUGCUGUGGAGGGGUCC	CGACCCCTCCACAGCCAGAA	3	709567	TGG	MSLN	20756.5
KO 3	CNV	16	687503	FALSE	UUGUUGCUGUGGAGGGGUCC	CGACCCCTCCACAGCCAGAA	3	709567	TGG	MSLN	22064
KO 3	CNV	16	687441	FALSE	UUGUUGCUGUGGAGGGGUCC	CGACCCCTCCACAGCCAGAA	3	709567	TGG	MSLN	22126
KO 3	CNV	16	656391.5	TRUE	UUGUUGCUGUGGAGGGGUCC	CGACCCCTCCACAGCCAGAA	3	709567	TGG	MSLN	53175.5
KO 4	CNV	16	650905	FALSE	UUGUUGCUGUGGAGGGGUCC	CGACCCCTCCACAGCCAGAA	3	709567	TGG	MSLN	58662
KO 4	CNV	16	649324	TRUE	UUGUUGCUGUGGAGGGGUCC	CGACCCCTCCACAGCCAGAA	3	709567	TGG	MSLN	60243
KO 4	CNV	16	647743	FALSE	UUGUUGCUGUGGAGGGGUCC	CGACCCCTCCACAGCCAGAA	3	709567	TGG	MSLN	61824
KO 4	CNV	16	774327	FALSE	UUGUUGCUGUGGAGGGGUCC	CGACCCCTCCACAGCCAGAA	3	709567	TGG	MSLN	64760
KO 4	CNV	16	777359	FALSE	UUGUUGCUGUGGAGGGGUCC	CGACCCCTCCACAGCCAGAA	3	709567	TGG	MSLN	67792
KO 4	CNV	16	780391	FALSE	UUGUUGCUGUGGAGGGGUCC	CGACCCCTCCACAGCCAGAA	3	709567	TGG	MSLN	70824
WT 2	CNV	16	634066	FALSE	UUGUUGCUGUGGAGGGGUCC	CGACCCCTCCACAGCCAGAA	3	709567	TGG	MSLN	75501
WT 2	CNV	16	632664	TRUE	UUGUUGCUGUGGAGGGGUCC	CGACCCCTCCACAGCCAGAA	3	709567	TGG	MSLN	76903
WT 2	CNV	16	631262	TRUE	UUGUUGCUGUGGAGGGGUCC	CGACCCCTCCACAGCCAGAA	3	709567	TGG	MSLN	78305
KO 3	CNV	16	625342	FALSE	UUGUUGCUGUGGAGGGGUCC	CGACCCCTCCACAGCCAGAA	3	709567	TGG	MSLN	84225
KO 3	CNV	16	625179	FALSE	UUGUUGCUGUGGAGGGGUCC	CGACCCCTCCACAGCCAGAA	3	709567	TGG	MSLN	84388
KO 3	INDEL	3	56282678	FALSE	UUGUUGCUGUGGAGGGGUCC	GGACACCTCCACTGCAACAG	3	56378826	AGG	ERC2	96148

Table 13: Somatic copy number variants (CNVs), single nucleotide variants (SNVs) and indels identified by whole exome sequencing within 100 kb surrounding in silico predicted off-target CRISPR cut sites.

Most likely off-target cleavage sites with *STX6*-targeting sgRNAs and Cas9 predicted by in silico analysis (Guide Verification Tool; Synthego) up to 4 target/sgRNA mismatches. Somatic alterations identified by whole exome sequencing relative to the untransfected parent line listed within 100 kb upstream and downstream of all predicted cut sites. Distance listed in bp between somatic site and predicted off-target cut site shows no off-target effects within 15 kb. Coordinates obtained from GRCh38.

5.2.6. Differentiation of STX6 KO iPS cells into cortical neurons

Through supplementing the growth media with different combinations of compounds and growth factors, iPS cells have been successfully differentiated into most neuronal subtypes. Widespread neuronal loss is a key pathology in patients with prion disease however the mechanism of this is not well understood, and so neurons have often formed the basis for investigating the cell biology of the prion protein and its related neurotoxicity (Benilova et al., 2020).

STX6 KO iPS cells and WT controls were differentiated into cortical neurons using the well-established dual SMAD inhibition as previously described (Shi et al., 2012). After 12 days in culture post-induction with neuronal differentiation media (see Methods section 2.8.9) all cell lines began to develop the expected neuronal rosette structures with expression of Pax6 transcription factor, a marker for neuronal stem/progenitor cells (Figure 35). This was accompanied by loss of expression of Oct4 pluripotency gene indicating a shift from iPS cell state.

After 25 days post-induction, visible neuronal processes began to appear in each well expanding radially from the neuronal rosettes as anticipated, confirmed by expression of neuron-specific β-III tubulin (Tuj1; Figure 35). At this stage there were a small number of mitotic cells stained by Ki67 highlighting possible intermediate progenitor cells, however it appears a high proportion of these cells are already post-mitotic at this stage.

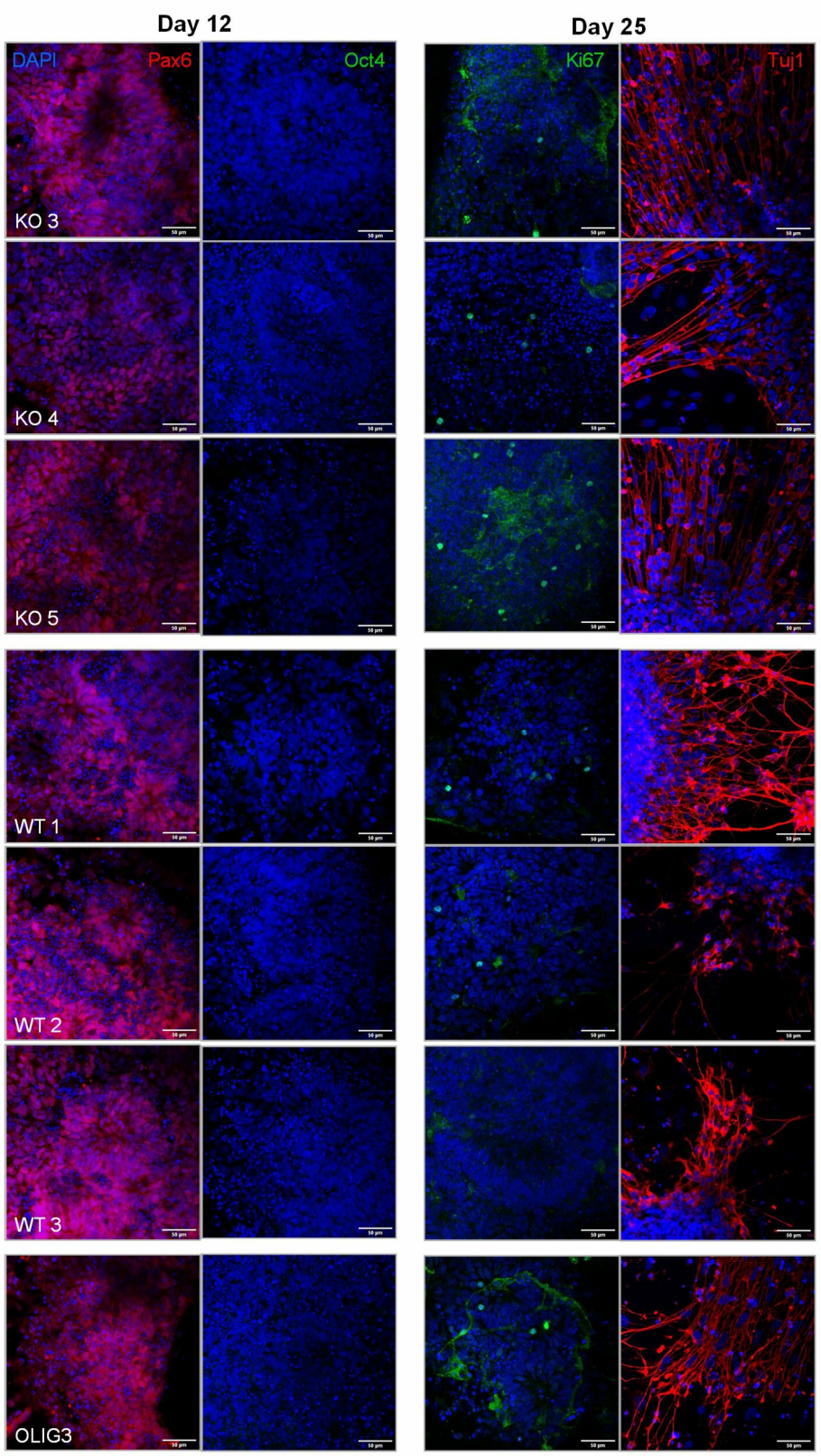

Figure 35: Characterisation of neural stem/progenitor cells derived from *STX6* KO and WT iPS cell lines at days 12 and 25 post-induction.
Dual SMAD inhibition was used to induce cortical differentiation in three *STX6* KO (KO 3, KO 4, KO 5) and three WT control (WT 1, WT 2, WT 3) cell lines, as well as the unedited parent line (OLIG3). Cells fixed at (**a**) day 12 post-induction expressed Pax6

(red; cortical transcription factor) but lacked Oct4 (green; pluripotency marker). (**b**) At day 25 post-induction a proportion of cells were positive for Ki67 (green; proliferation marker) and processes positive for Tuj1 (red; neuron specific tubulin).

Following the final passage performed at 35 days post-induction there was unfortunately a high degree of cell death in most of the cell lines used, with viable cells only visible in one of the KO cell lines (KO 5) and two of the WT cell lines (WT 1 and WT 2) to varying degrees. There are multiple potential reasons for loss of the other clones including too harsh passaging of fragile neurons, changes in pH due to recorded fluctuations in CO_2 levels in incubator, too low density of viable cells or biological differences between cell clones inducing programmed cell death. Unfortunately, due to time constraints the differentiation could not be repeated and so further investigations would be required to determine what lead to this cell loss, although it doesn't seem to be dependent on knockout status.

With this method it is expected that after 35 days post-induction early-born deep-layer neurons expressing Tbr1 and/or Ctip2 begin to become the major population (Shi et al., 2012). Staining of cell lines at day 50 showed clear expression of these markers in only one line (WT 2) with much lower detection in the other clones (WT 1 and KO 5) (Figure 36a). This is potentially due to higher levels of cell loss in these lines leading to low density of viable neurons and thus limiting the number of connections between cells, which would likely be required to promote neuronal maturation through the formation of functional synapses. In all cell lines however Map2-positive dendrites were detected indicating that knockout of *STX6* does not prevent differentiation of iPS cells into mature cortical neurons (Figure 36a). Immunoblotting confirmed that expression of the main syntaxin-6 isoform is still absent from the KO neurons with no evidence for compensation through increased expression of other isoforms at this stage (Figure 36b). Interestingly an additional immunoreactive band between 125 – 160 kDa is present in the WT 2 line only, potentially reflecting a reserve pool of homotypic syntaxin-6 SNARE complexes in more mature neurons.

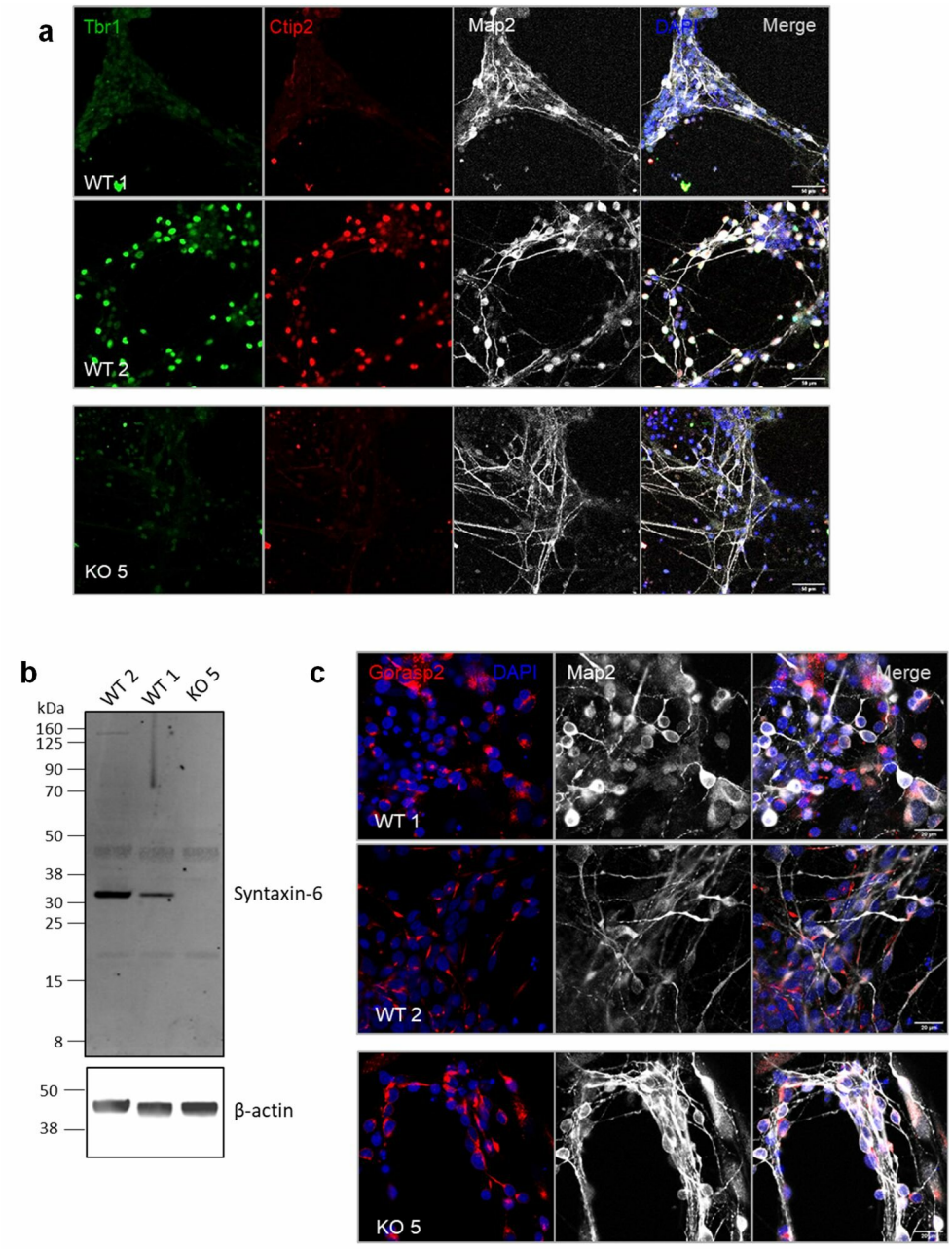

Figure 36: Characterisation of cortical neurons derived from *STX6* KO and WT iPS cell lines at day 50 post-induction.

Cortical neurons differentiated from *STX6* KO (KO 5) and WT control (WT 1, WT 2) iPS cells at 50 days post-induction of differentiation by dual SMAD inhibition. (**a**) Immunofluorescence shows varying expression of Tbr1 (green) and Ctip2 (red) (deep-layer cortical neuron markers) with Map2 (grey; dendrites/mature neurons) positive neurons for each line. Scale bar = 50 µm. (**b**) Immunoblot for syntaxin-6 (top) demonstrates sustained loss of 32 kDa band with similar immunoreactivity of other bands relative to β-actin loading control (bottom). (**c**) Immunofluorescence for Goraps2 (red; mid-/trans-golgi marker) and Map2 shows expected localisation in all lines. Scale bar = 20 µm.

Previous work has highlighted a requirement for syntaxin-6 and its cognate SNARE partners in maintaining the ribbon structure of the Golgi, with knockdown of any component in HeLa cells inducing a dispersion of the Golgi markers from a concentrated juxta-nuclear localisation to distinct Golgi fragments, highlighting a requirement for retrograde transport in maintaining organelle structure (Shitara et al., 2013). Therefore to begin to investigate whether there is any gross phenotype in the *STX6* KO iPS-derived neurons compared to the WT controls, cells fixed at day 50 post-induction were stained for Goraps2, a marker of the trans- and medial-Golgi, however in all cell lines the distinct asymmetrical perinuclear localisation was visible with no evidence of Golgi fragmentation (Figure 36c). This may be due to differing functions of syntaxin-6 in different cell lines, or differing mechanisms used for genetic manipulation, however in this preliminary investigation there was no evidence of a gross Golgi defect in these cells.

5.3. Discussion

In this study the feasibility of CRISPR-mediated gene knockout in an iPS cell line derived from a healthy individual was explored and subsequent isogenic lines lacking expression of the primary *STX6* isoform generated. Dual-SMAD inhibition was utilised to differentiate excitatory glutamatergic cortical neurons up to 50 days in vitro where mature neuronal processes were formed. Characterisation of knockout iPS cells, neuronal progenitor cells and mature neurons displays the expected morphology suggesting that knockout of *STX6* expression does not impact pluripotency or prevent differentiation of cells with neural lineage from these lines. This enables future studies of *STX6* function with indefinite availability of disease-relevant cell types of human origin, vital for investigating gene function associated with human neurodegenerative diseases.

Due to the small effect sizes of *STX6* risk variants in sCJD, with presence of associated alleles only increasing the odds of disease by a small amount (rs3747957: OR = 1.16 (95CI 1.10-1.22) (section 3.2.2, Table 7)), it was hypothesised that any relevant phenotypes associated with this gene are likely to be subtle and subject to variability. Therefore CRISPR-mediated knockout in human cells was utilised here to increase the likelihood of identifying phenotypes

related to gene function. This gross perturbation however is unlikely to be representative of the disease, with only a modest difference in gene expression between the two alleles in relevant brain regions (~15% in the putamen calculated from eQTLs in the GTEx study, discussed previously in chapter 3, section 3.2.4). Therefore the applicability of conclusions drawn from this and any future studies using these cell lines will rely on more modest changes in *STX6* function. For example, here two iPS cell lines were obtained with differing haplotypes at the *STX6* locus which could be used for comparison, however the genetic variation between lines may confound this.

Feasibility of differentiation of cells lacking *STX6* expression into neural lineages was explored here utilising a protocol previously demonstrated to efficiently generate excitatory glutamatergic neurons (Shi et al., 2012). Mature dendritic processes stained by Map2, with modest expression of deep-layer neuronal markers Ctip2 and Tbr1, indicate that knockout of *STX6* is conducive to generation of neural cells and therefore the iPS lines generated here can likely be used to produce additional neural subtypes for future studies. Unfortunately, further characterisation of neuronal properties or prion-related phenotypes in these cells was prohibited by vast cell loss unrelated to the gene knockout, likely also preventing full maturation due to low density cultures. Although preliminary investigations on Golgi structure as an indication of syntaxin-6 function in retrograde transport did not suggest a gross perturbation, more substantial analysis of other endolysosomal transport markers is required as disruption of TGN morphology is not always evident in previous studies with syntaxin-6 perturbation.

Cortical neurons were selected for this initial investigation due both to their relative ease of differentiation – as one of the first fully-differentiated cell types to populate from the neuroectoderm these are also one of the earliest neural sub-types to appear in culture – as well as their disease relevance (Hong & Do, 2019). Wide-spread neuronal loss is a hallmark of prion diseases however the mechanisms leading to this cytotoxicity are not well described (Benilova et al., 2020; Budka et al., 1995). The neuronal cell lines generated in the current study could therefore provide a tool to investigate the role of syntaxin-6 in prion-induced neurotoxicity. However other neural cell types are certainly of interest for disease

modelling (and likely *STX6* function) especially with evidence that iPS-derived astrocytes and cerebral organoids are able to propagate aggregated sCJD prions as previously described (Groveman et al., 2019; Krejciova et al., 2017). The impact of *STX6* knockout in these models will be an important follow-up experiment, particularly as previous explorations of syntaxin-6 function in the propagation of mouse prions in immortalised cells were not forthcoming (as discussed in chapter 4). Experiments in these human cell lines with human prion strains will therefore help elucidate whether syntaxin-6 function is sCJD or cell-type specific, as well as provide opportunities for functional investigations in more disease-relevant cell types.

A commercially available system was utilised to generate the CRISPR-mediated gene knockouts in this study, in which sgRNA sequences were pre-designed. This led to efficient gene editing of both a control gene (*TRAC*) and the gene of interest, *STX6*, through induction of large fragment deletions over 100 bp, supporting previous conclusions that using multiple sgRNAs in tandem is an effective method for generating sufficient indels for gene knockout (Jost et al., 2021). Although this was highly successful in preventing translation of the targeted transcripts, one limitation of utilising off-the-shelf products is that sequence details are not imminently revealed. Consequently, the sgRNA design failed to consider an additional *STX6* protein-coding transcript which lacks the targeted exon. This secondary transcript (denoted Stx6-204) is lacking exons 2 and 3 (as depicted in Figure 30), leading to translation of a shorter protein isoform without the N-terminal residues 1-101 of the primary full-length 255 amino acid protein, although the remaining sequence is conserved.

A specific exploration of the differing functions of the two protein-coding isoforms is absent from the literature, however a number of studies have elucidated specific functions of this N-terminal region. Generation of crystal structures of residues 1-113 described an anti-parallel three-helical bundle (Habc: a (4–32), b (38–60), c (92–109); syntaxin-6 structure and functions previously discussed in section 1.7; Figure 6) which would be absent in this secondary isoform (Misura et al., 2002). In this initial characterisation the expected regulatory function of this region in binding to the SNARE domain was not found (a common mechanism for SNARE protein inactivation), however subsequent experiments have revealed

the importance of this region in syntaxin-6 functions, including driving localisation to the TGN for retrograde protein transport, and in mediating interactions with multiple regulatory proteins (including α-SNAP NSF adaptor, GARP (Golgi) and EARP (endosomal) multi-subunit tethering complexes and related SHIP164, as well as separate EEA1 endosomal tether) (Bock et al., 1996; Koike & Jahn, 2019; Otto et al., 2010; Perez-Victoria et al., 2010). Furthermore, analysis of isoform expression from RNAseq data (obtained from the GTEx v7 database (GTEx Consortium, 2015)) indicates that this secondary isoform only comprises a small proportion of transcripts in all human brain regions; for example just 3% of transcript read counts in the cerebellum and 5% in the putamen are attributed to Stx6-204 (compared to 68% and 90% respectively for Stx6-201). Therefore it is unlikely that expression of Stx6-204 alone would be sufficient for syntaxin-6 to retain its usual function in cells, especially as the sCJD-risk associated alleles are thought to cause much more modest alterations in gene expression (~15%; section 3.2.4), and so this is unlikely to prevent phenotypic changes in these lines. However, targeting this secondary isoform should be considered if future work indicates the remaining syntaxin-6 is still functional. Of note in this study a modest increase in band intensity at ~17 kDa was detected by immunoblot of the knockout cell lines relative to the controls (corresponding to the predicted molecular weight of Stx6-204; Figure 32b), indicating some compensation may have occurred, potentially reflected in the RT-qPCR analysis with no evidence of non-sense mediated decay at this level.

Undoubtedly CRISPR has proven an invaluable tool for functional genetics providing researchers with unmet gene editing flexibility and efficiency. In iPS cells this has tackled one of the key limitations of sourcing appropriately matched controls. Like all techniques however this does not come without its issues. One of the dominant discussions surrounding this technology is the impact of off-target effects of Cas9 cleavage, with growing evidence to indicate that, even without sgRNA mismatches, off-target mutagenesis can occur at high rates in human cells (Fu et al., 2013); gene knockout or mutations in unwanted regions could easily lead to confounding phenotypes which may be wrongly associated with the intended target. In the current study multiple sgRNAs were used in tandem, further increasing the likelihood of off-target cleavage. Transfection of RNPs was

utilised to minimise the time endonucleases are present in the cell in an attempt to minimise this, and sgRNAs are designed to limit additional complementary sequences, however it is still important to control for these possibilities.

Screening for off-target effects is not trivial and the best practice is unclear. Here due to limited time, growth rate was initially measured to identify any gross perturbations in cell proliferation which may indicate unintended gene editing (or other clonal abnormalities) to allow prompt progression with differentiation. However, the utility of this is clearly limited with possible off-target effects which do not impact growth or a growth-related phenotype induced by the knockout itself. Therefore, subsequent exome sequencing was performed on the selected cell lines. This methodology was used in order to permit comprehensive identification the most likely functional off-target perturbations whilst minimising cost and computational burden (i.e. with whole genome sequencing). This analysis did not provide any evidence for off-target cleavage of Cas9 endonuclease at any in silico predicted sites, however there was some evidence for higher somatic alterations in the *STX6* knockout cell lines relative to the wild-type controls. Nonetheless selection of multiple clones for future experiments will allow for these differences and limit potential false appointment of deleterious off-target effects to *STX6* function.

iPS-derived cells pose clear advantages for investigating human neurodegenerative diseases, especially with the particularly limited access to other relevant human cell types, however as with all models there are clearly some limitations that should be considered. In the current study iPS cells derived from a “normal” healthy individual without sCJD were utilised due to the ease of obtaining these cells from publicly-available repositories; unfortunately no cell lines derived from sCJD patients were available at the time these experiments were performed. As previously discussed, the aim of this study was to perform large perturbations of gene function (i.e. knockout of *STX6*) in order to increase the likelihood of identifying a relevant phenotype, which is not representative of the modest effect size seen in patients. Therefore, due to limited time constraints which would not allow for obtaining the relevant cells from sCJD patients and set up reprogramming of patient-derived iPS cells in house, it was decided control iPS cells would still be beneficial for modelling gene function in a relevant species

and cell type. However it is likely that there are additional biological mechanisms occurring in sCJD patient cells which may be relevant to *STX6* function which would be missing from these cell lines, such as additional genetic risk factors (especially likely due to the limited power to identify low effect size variants in all GWAS performed to date for this disease). Therefore future studies should work to obtain sCJD patient-derived iPS cell lines in order to increase the relevance of this cell model to the disease being studied.

One of the primary concerns often evoked by using iPS cells is their foetal-like embryonic state induced by the reprogramming back to pluripotency (Studer, Vera, & Cornacchia, 2015). This is especially concerning when modelling late-onset diseases such as sCJD for which age is a significant risk factor. This is not yet an issue which has been clearly solved, with debate over whether attempts to recapitulate aging phenotypes with cellular stressors or inducing age-related gene expression for example are representative of natural cellular maturation, however there is evidence to suggest that iPS cells retain some epigenetic marks present in the somatic parent cell which may increase their relevance over ES cells (K. Kim et al., 2010).

Unlike in vivo models, iPS cells have most frequently been used for study of a single cell type in isolation which is clearly not representative of the systems in which human diseases occur, particularly in the brain for which over 75 unique cell types in over 100 distinct regions have been described (Glasser et al., 2016; Hodge et al., 2019). However, in recent years, progress has been made with incorporating cell-type interactions in experiments with the development of organoid technologies (iPS-derived self-organising three-dimensional culture systems comprising multiple cell types reflective of human organs). This includes modelling human brain development.

Organoids mimicking various brain structures have been developed including the cerebellum (cerebral organoids), as well as the midbrain, hypothalamus and hippocampus (recently reviewed in (Shou, Liang, Xu, & Li, 2020)). With only relatively short-term culture numerous cell types are generated in these organoids, including neurons, astrocytes and neural progenitor cells, and further developments have achieved oligodendrocyte development and vascularisation

to increase the relevance of these models to the human brain. As previously discussed these systems have successfully recapitulated some disease-associated phenotypes in both prion diseases and related neurodegenerative diseases, as well as proven therapeutic utility in the application of anti-prion compounds (Groveman et al., 2021). Although studies on *STX6* function in the brain have generally focused on its role in neuronal development and neurotransmitter signalling, due to the complex interplay between cell types in neurodegeneration future studies should focus on utilising organoid systems for modelling the disease. As the genetic effect of *STX6* risk variants on gene expression appears to be region specific (as discussed in chapter 3, section 3.2.4), generation of relevant organoids such as for the hippocampus may even be more fruitful for phenotypic studies.

Development of isogenic iPS cell lines with modified expression of *STX6* provides an important tool for future experiments investigating the role of this gene, not only in sCJD and human prion diseases, but for the multiple related neurodegenerative diseases such as PSP and AD for which syntaxin-6 function has been implicated. The opportunity for indefinite differentiation of any disease-relevant cell type, including those able to seed the aggregation of human prion strains, will grant accurate modelling of disease pathogenesis and therefore hopefully allow us to uncover the mechanisms through which syntaxin-6 drives risk of sCJD and neurodegeneration.

6. Investigating the role of *STX6* in prion diseases in vivo

6.1. Introduction

6.1.1. Overview of in vivo models for prion disease

Although reductionist models of disease (such as in silico, in vitro and tissue culture models) have their utility for developing a thorough understanding of specific aspects of pathogenesis, these are all limited by their relative lack of biological context. Applying discoveries in these models to in vivo whole systems is required to determine their relevance to disease biology, especially for neurological diseases where our understanding of complex brain functions is still relatively limited.

Using human tissues when researching human diseases has clear benefits for relevance and applicability. For example neuropathological examination of patient tissues is still required for post-mortem diagnosis of most human neurodegenerative diseases, and the examination of the distinct pathological hallmarks for different prion diseases has aided our definition of prion strains (Fraser & Dickinson, 1973). However human tissues are limited in their temporal resolution, with the availability of relevant samples prior to end-point rare due to difficulties with ascertainment (with the exception of circulating fluids), and understanding these initial stages before clinical onset will undoubtedly be fundamental to successful therapeutic treatments. Additionally, this lack of availability limits the statistical power that can be achieved especially for rarer diseases such as prion diseases.

Since the earliest experimental studies of prion diseases, animal models have been fundamental to our understanding. Although the cellular models previously discussed (chapters 4 and 5) certainly allow researchers to feasibly study a subset of biological mechanisms, these do not encompass the complex cell and tissue interactions or the relevant environments key to both physiology and pathology. Notably the experimental transmission of scrapie into healthy sheep and goats and later transmission of kuru and CJD into primates underpins our fundamental understanding of the infectious nature of prion diseases (see section 1.1) (Cuillé & Chelle, 1936; Gajdusek et al., 1966; Gibbs et al., 1968). Small

ruminants and primates, as well as cattle and cervids, are still used in prion research, albeit less frequently due to various limitations including their large size, time required for generation and study, difficult accessibility and genetic manipulation, increased ethical issues and cost of maintenance (see review (Brandner & Jaunmuktane, 2017)). Nonetheless these animal models are still contributing to our understanding, for example studies in primates were initially used to support the common originating strain of vCJD and BSE (Lasmezas et al., 1996).

In more recent years small rodents have been most commonly used as experimental models in the prion field. Wild-type Syrian golden hamsters were frequently used in earlier studies, for example for investigating the spread of prions in the CNS, and bank voles are sometimes utilised due to their apparent susceptibility to a wide range of prion strains (Kimberlin & Walker, 1986; Nonno et al., 2006). However mice are currently the most widely used animal model, primarily due to the wealth of tools for study and manipulation of these animals, as well as their low cost of upkeep, short time scales and small size making handling and maintenance manageable (see recent review (Marin-Moreno, Espinosa, & Torres, 2020)). Importantly, mice (as with the other species mentioned) are naturally susceptible to prion diseases and therefore faithfully recapitulate key pathogenic features, including differing susceptibility and transmissibility (i.e. to distinct prion strains) and distinct neuropathological features (i.e. PrP deposition, spongiosis and astrocyte proliferation).

As genetic engineering technologies have advanced, the tools available to researchers for modelling disease in vivo have developed. Genetically modified animals can generally be described as transgenic, knock-in or knock-out. Firstly, transgenic animals are generated through the microinjection of a DNA construct encoding a specific transgene into fertilised embryos, leading to random integration of the transgene into the genome (Marin-Moreno et al., 2020). This can disrupt other genes and often causes overexpression as the copy number is not controlled. Although this does not reflect natural physiology, this can be advantageous, for example increased PrP expression can reduce disease incubation for clinical onset within the life-span of the animal. Alternatively knock-in animals are generated by replacing the host gene (e.g. mouse PrP) with the

gene of interest (e.g. human PrP) thus expressed at normal levels and under endogenous regulation. Numerous genetic engineering tools have been developed, including the same programmable endonuclease-based methods as previously discussed for cell models (e.g. CRISPR, see chapter 5, section 5.1.3, Figure 27) which can be used for both knock-in and knockout, as well as more sophisticated tissue-specific and conditional modifications. In mice, gene editing components are usually microinjected into fertilised embryos, which are transplanted into pseudo-pregnant animals and off-spring positive for edits at the target site (F0) are bred with wildtype mice to confirm germline transmission (F1).

Prnp knockout mice have been fundamental to the prion field, securing the protein-only hypothesis by demonstrating that PrP is absolutely required for infection (Bueler et al., 1993). This model has also been used to try to delineate the molecular function of PrP^{C} as previously discussed (see section 1.3.3), however a peripheral demyelinating neuropathy is the only phenotype robustly associated with these animals (Bremer et al., 2010). As vitally though, the availability of *Prnp* null animals has allowed for ectopic expression of alternate PrP sequences (e.g. species-specific) without the interference of endogenous proteins. This has led to numerous important studies including of transmission and/or species barriers, strain characteristics, infectivity titres, cellular pathways, toxicity and therapeutic discovery and validation (discussed in the next section).

Although the use of animals to model prion diseases, especially those which affect humans, has clear utility, there are still limitations that should be considered. Firstly, even though mice and humans are somewhat evolutionarily conserved with similar genetic and physiological mechanisms, these animals are still distinct from humans, which is likely to result in differences in pathogenic mechanism. The *PRNP* sequence in primates (specifically cynomolgus Macaques) is most similar to humans with the same critical polymorphism at codon 129 that confers genetic susceptibility to human prion diseases, however, as previously mentioned, the use of these animals is usually impractical and should be constrained to absolutely vital purposes for ethical reasons (Brandner & Jaunmuktane, 2017). Additionally genetic manipulation in animals is not always reliable or straight-forward. For example, the attribution of cerebellar degeneration with a late-onset ataxia phenotype to the knockout of *Prnp* in

multiple mouse lines was later refuted, shown to be instead caused by ectopic expression of related gene *Prnd* due to deletion of a splice acceptor in a *Prnp* intron (Weissmann & Aguzzi, 1999). Nonetheless, with appropriate considerations of the limitations and controls, animal models are undoubtedly currently essential for disease research.

6.1.2. Mouse models of acquired prion disease

Nearly all animal models in prion research have been restricted to acquired diseases due to the lack of spontaneous prion generation over the time-courses studied (with the exception of some IPD mutations discussed in the next section). Nonetheless this has fuelled our understanding of multiple aspects of disease pathogenesis including strains, transmission barriers and genetic susceptibility to disease (Marin-Moreno et al., 2020). The natural susceptibility of mice to prion infection has allowed studies of these properties in wildtype animals, with a typical study performing intraperitoneal or intracerebral inoculation of infectious material and monitoring onset of either characteristic clinical symptoms such as ataxia, generalised tremor, loss of righting reflex and limb paralysis (O'Shea et al., 2008), or neuropathological hallmarks including abnormal PrP deposition, reporting both time from inoculation (termed “incubation time”) and number of animals affected (termed “attack rate”).

Understanding the molecular basis of intra- and inter-species transmission of prions is clearly important from both a mechanistic and public health point of view. It has long been understood that there is a “transmission barrier” driven both by primary sequence (also referred to as a “species barrier” between animals with a different PrP sequence) and conformation (discussed previously in section 1.5.3) (Collinge & Clarke, 2007). For example, an early study in 1994 by Bruce and colleagues described a transmission barrier upon primary passage of scrapie and BSE isolates to mice with low attack rates and long incubation times, which was overcome upon secondary passage into further animals with high efficiency transmission, providing the first indication of strain adaptation (Bruce et al., 1994). Of note, similar mouse-adapted prion strains are now commonly used in prion research due to their high infectivity in wild-type mice. RML and ME7 used in the current study are both mouse-adapted scrapie prion strains from different origins: RML was originally derived from scrapie-infected sheep (SSBP/1) brain

homogenate passaged in goats and transmitted to CD1 mice, and ME7 from scrapie-infected sheep spleen tissue and passaged directly into RIII and C57BL/6 mice (Kimberlin, Walker, & Fraser, 1989; Zlotnik & Rennie, 1963). The reliability of ME7 inoculation into mice has even led to its use by non-prion researchers as a general model for chronic neurodegeneration (Chouhan, Fowler, Webster, & Teeling, 2017).

The generation of transgenic and knock-in animals expressing alternative species-specific PrP isoforms has fuelled further detailed studies of cross-species prion transmission. Numerous transgenic mouse models have now been developed to model naturally observed prion transmission, as well as animals in which natural disease has not been described for both scientific and public health reasons (Marin-Moreno et al., 2020).

Generation of transgenic mice expressing human PrP has been especially important for modelling the zoonotic potential of prion strains, and over 45 humanised mice lines have now been developed (Brandner & Jaunmuktane, 2017). For example, extensive transmission studies have been performed for BSE and vCJD prion strains, to investigate the molecular mechanisms and extent of risk these diseases pose to public health. Genotype at codon 129 is strongly associated with susceptibility in humans with nearly all vCJD cases homozygous for methionine at this site (see section 1.2.2.3); this is reflected in transgenic mice, with high attack rates upon transmission of both BSE and vCJD prions when expressing human PrP 129M (albeit often sub-clinical infection due to the long incubation times for clinical disease in this model) and faithful replication of strain type (denoted type 4 PrP^{Sc}) (Asante et al., 2002), whereas inoculation of BSE into mice expressing 129V leads to diffuse PrP deposition without detectable PrP^{Sc}, which cannot seed pathology upon serial passage (Hill et al., 1997; Wadsworth et al., 2004). Similarly, transmission of vCJD into human 129V mice has much lower attack rates with similar weak diffuse PrP deposits, interestingly with a distinct PrP strain type (denoted type 5 PrP^{Sc}) which shows minimal transmissibility on secondary passage, reflecting the lack of vCJD in valine homozygous individuals (Hill et al., 1997; Wadsworth et al., 2004). Interestingly when these mouse lines were crossed to generate a “heterozygous” line, a subset of animals propagated the expected prion strain upon inoculation with vCJD (type

4) but with a distinct neuropathology, suggesting the disease may be distinct in heterozygous individuals and should be monitored accordingly (Asante et al., 2006). Also of current importance, humanised mice have been used to model the zoonotic potential CWD strains to determine whether the increasing spread of this disease poses a risk to public health; to date there has been no evidence of transmission following intracerebral inoculation of these mice (or cynomolgus Macaques), however the results of important secondary passages to identify undetected infection are yet to be published (Kong et al., 2005; Race et al., 2009; Wadsworth et al., 2021).

6.1.3. Mouse models of prion disease genetics

The ability to express species-specific *PRNP* sequences in a practical model system such as mice, while seemingly recapitulating the function of the normal gene (at least in pathobiology), allows researchers to model the genetic susceptibility associated with this. This has included polymorphisms associated with disease risk such as codon 129 in human prion diseases as discussed, as well as scrapie-associated variation at codons 136, 154 and 171 in ovine PrP (Cordier et al., 2006) and the kuru-protective 127V allele which, in either the heterozygous or homozygous state, also drives resistance of transgenic mice to multiple human prion strains including kuru and sCJD (Asante et al., 2015).

Inherited prion diseases account for 10-15% of all human prion diseases (Ladogana et al., 2005). Currently the molecular mechanisms which drive aggregation of mutant PrP proteins is not understood. Unfortunately however, expressing these in humanised mice has, in the most part, not recapitulated disease, with no detectable abnormal PrP or relevant neuropathology with any mutation except the GSS mutation A117V, for which homozygous transgenic mice develop stochastic and limited PrP plaques which can be efficiently transmitted (Asante et al., 2020). It is not known whether the limited success of this is due to the restricted life-span of mice, or differences in physiology between species. Other IPD mutations that have induced neuropathology have been on a chimeric background, for example with mouse and bank vole PrP, which appear more prone to spontaneous misfolding and aggregation than human PrP (or have the required cofactors present in mice) (Marin-Moreno et al., 2020). However, these studies have had variable success with contrasting phenotypes, and

evidence suggests these mice are not faithfully propagating the same strain types (Watts et al., 2016).

Although *Prnp* is clearly a key player in prion diseases, we know that other genes and pathways must be involved in pathogenesis, for example primary PrP sequence does not perfectly correlate with disease susceptibility (Collinge & Clarke, 2007). Due to the natural susceptibility of mice to prion disease, and the relatively high degree of homology between genes present in humans and mice, these animals have been used for discovery studies to this effect (Mead et al., 2019). The varying incubation times between inbred mouse strains led to classification of two *Prnp* genotypes (denoted $Prnp^a$ and $Prnp^b$) associated with short and long incubation times, driven by genotypes at codons 108 and 189, but QTL studies have also eluded to non-*Prnp* genetic modifiers of this phenotype (previously discussed in section 1.4.3) (Lloyd et al., 2010; Lloyd et al., 2009; Westaway et al., 1987). At least in the case of *Hectd2*, this genetic association also appears relevant to human disease in a targeted analysis, supporting the use of mice in discovery studies (Lloyd et al., 2009). Additionally heat shock protein *Hspa13* has been associated instead through exploring differentially expressed genes in mice with distinct incubation times (Grizenkova et al., 2012). Mouse models also allow for important temporal resolution that is difficult to obtain in human samples; this has generated a wealth of data associating various genes and pathways, however causality is difficult to define here (Mead et al., 2019).

Finally, the ease of genetic manipulation in mice permits feasible studies of candidate genes in whole biological systems. Most commonly in the prion field, researchers have used knockout animals to explore gene function, generally comparing attack rate and disease incubation time following inoculation of well characterised prions strains (often RML) in the presence and absence of a candidate gene, although overexpression and more sophisticated methods to perturb gene function have also been utilised. Study of multiple genes involved in the cytokine and chemokine response in this way has been used to support a causal role of this pathway in prion diseases, which is robustly upregulated during scrapie infection; knockout of chemokine receptor *Cx3cr1* reduced disease incubation time following prion inoculation (at least in one study), and knockout

of *Cxcr3* and chemokine *Mcp1* extended survival times, although interestingly with evidence of a more rapid and substantial increase in prion titre (Felton et al., 2005; Grizenkova, Akhtar, Brandner, Collinge, & Lloyd, 2014; Riemer et al., 2008). Similarly knockout of interleukin receptor *Il1r1* prolonged disease in RML-inoculated mice, however knockout of interleukin *Il10* shortened incubation times and other common interleukins and subunits (e.g. *Il12b*, *Il4*, *Il13*) had no effect, likely reflecting the complexity of cytokine signalling (Tamgney et al., 2008; Thackray, McKenzie, Klein, Lauder, & Bujdoso, 2004; Tribouillard-Tanvier et al., 2012). Other pathways for which knockout mice have provided supportive evidence for causality include the heat shock response protein family (*Hsp70* null and *Hspa13* overexpressing mice both have reduced incubation times compared to wildtype animals) (Grizenkova et al., 2012; Mays et al., 2019), proteins involved in neuronal death and clearance (e.g. PAR2, MFGE8/lactadherin and IKKα kinase (in non-canonical NF-κB pathway)) (Julius et al., 2008; Kranich et al., 2010; Matej, Olejar, Janouskova, & Holada, 2012), as well as proteins involved in normal PrP^{C} function such as gangliosidase synthase (for synthesis of lipid rafts) and LRP endocytic receptor (Kobayashi et al., 2019; Pflanz et al., 2009). Lastly, exploration of genes associated with related neurodegenerative diseases has implicated superoxide dismutase 1 (*Sod1*, ALS) and amyloid precursor protein (*App,* AD) in prion diseases (but not PD-related α-synuclein (*Scna*)) highlighting a potential overlap in pathogenic mechanisms (Akhtar et al., 2013; Bistaffa et al., 2019; Tamgney et al., 2008).

Although inoculation studies in knockout mice have clearly been important for exploring the role of putative genes and pathways in prion pathogenesis, the use of such gross genetic perturbations must be interpreted cautiously due to the possibility for compensatory mechanisms or off-target effects, as well as the aforementioned species differences. Additionally, divergence in neuropathology or end-point prion deposition have rarely been described in these studies, and the magnitude of these effects is usually minimal with infrequent difference in incubation time of over 20% (unlike the absolute effects of *Prnp* knockout) so it is likely the role of these genes in prion diseases forms part of a complex regulatory mechanism.

6.1.4. Chapter summary

The experiments described in this chapter were designed, set up, managed and analysed by myself including genotyping, biochemistry, breeding management, inocula preparation, quantification and statistical analysis. The following practical work was performed by others: *STX6* hemizygous knockout mice generated by MRC Harwell; animal husbandry, care and dissection performed by staff at the animal facility (including Lucy Draper, Ami Woodcock, Thomas Horan, Nick Kaye, Craig Fitzhugh and Gavin Graham); histology performed by core facility (including Jackie Linehan, Tamsin Nazari and Sebastian Brandner).

This chapter describes exploration of the role of *Stx6* in prion diseases in vivo, including the generation of *Stx6* knockout and hemizygous mice and analysis of prion and non-prion related phenotypes. Inoculation of this model with two prion strains supports a pathological role for expression of this gene in prion diseases, with knockout extending the incubation time with both RML and ME7 prions. Immunohistochemical characterisation of neuronal loss, spongiform vacuolation, astrocyte proliferation and PrP deposition shows the expected neuropathology with no differences observed between lines. Exploration of behavioural and physiological phenotypes in these mice highlights a metabolic defect with *Stx6* knockout, with increased fat storage in subcutaneous adipose tissues, alterations in circulating metabolites and associated activity deficits.

6.2. Results

6.2.1. Generation of Stx6 knockout mice

C57BL/6 mice hemizygous for *Stx6* ('Hem'; *Stx6*$^{+/-}$) were generated externally via CRISPR-mediated deletion of 1808 nucleotides spanning two critical exons with an 8 nt insertion (exons 6 and 7 as depicted in Figure 37a, present within all protein coding isoforms), generating a premature stop codon (CRISPR described previously in section 5.1.3). Mice were then imported for the current study and cross-bred to generate lines homozygous for both the null *Stx6* allele ('KO'; *Stx6*$^{-/-}$) and wildtype allele ('WT'; *Stx6*$^{+/+}$). Genotypes were obtained via two PCR assays either spanning the deleted region ('PCR1') amplifying both the WT and KO alleles or binding within the deleted region ('PCR 2') amplifying the WT allele

only (Figure 37a); example electrophoresis gels for each primer pair are shown in Figure 37b and c respectively.

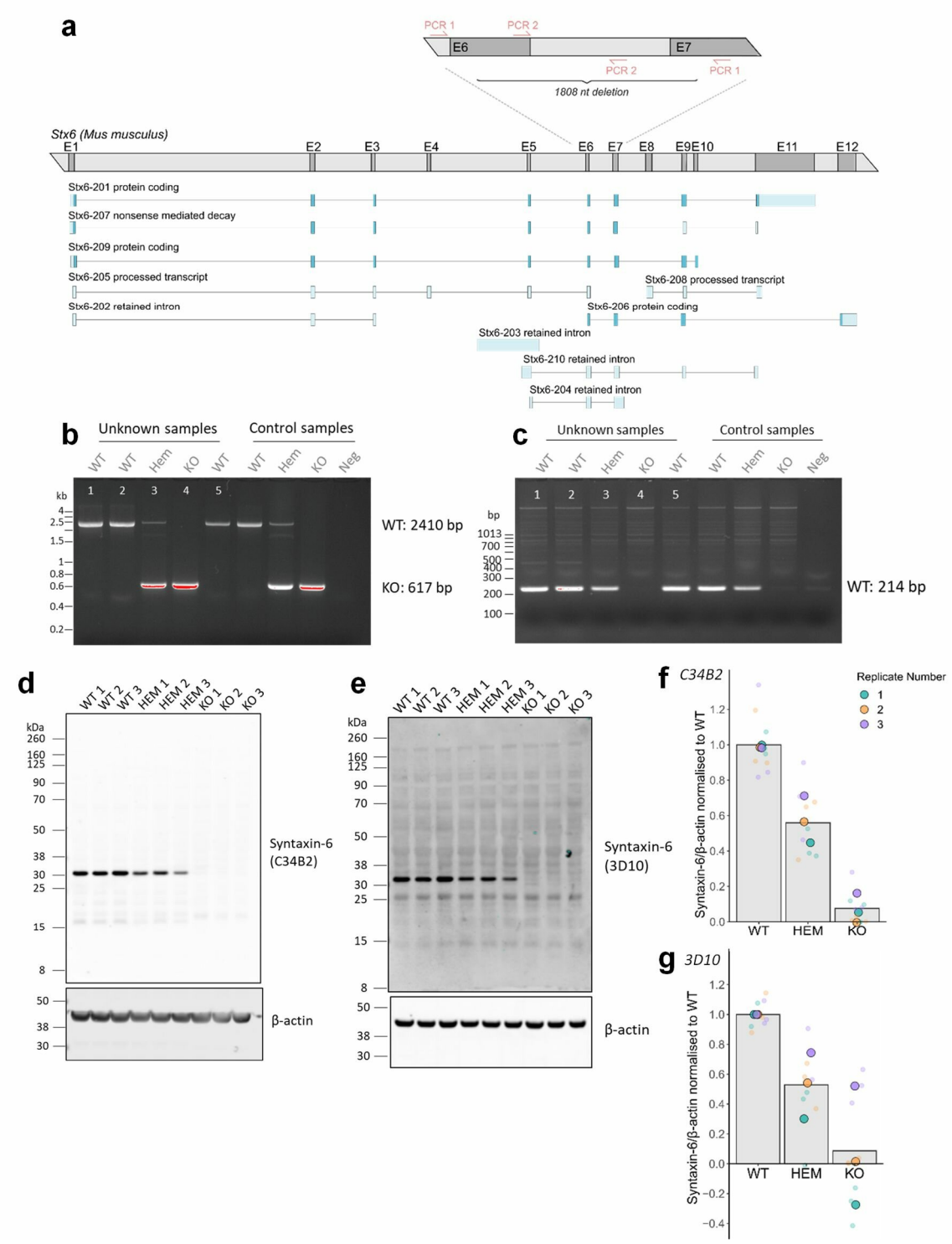

Figure 37: Generation of *Stx6*$^{-/-}$ and *Stx6*$^{+/-}$ C57BL/6N mice.
C57BL/6NTac mice hemizygous for a CRISPR-mediated deletion of critical exons (*Stx6*$^{+/-}$; HEM) were imported from MRC Harwell and bred to homozygosity to generate *Stx6*$^{-/-}$ (KO) mice and wildtype (*Stx6*$^{+/+}$; WT) littermate controls. (**a**) Diagram of C57BL/6 mus musculus *Stx6* gene indicating all transcripts (protein coding regions in dark blue) with 1808 nt deletion in exons 6 and 7 as depicted, with primer binding sites used for

genotyping indicated. (**b**,**c**) Example electrophoresis gels for PCR genotyping (**b**) across the deleted region (PCR 1) with a band at 2410 bp for the wildtype allele ('WT') and 617 bp for the knockout ('KO'), and (**c**) within the deletion (PCR 2) producing a band at 214 bp for the wildtype allele only. (**d**-**g**) Immunoblot of brain homogenate from three mice for each mouse line using anti-syntaxin-6 antibodies (**d**,**f**) clone C34B2 and (**e**,**g**) clone 3D10. β-actin used as loading control. Densitometry of syntaxin-6 immunostaining relative to β-actin used to quantify syntaxin-6 protein expression. Both antibodies confirm loss of primary ~32 kDa transcript in *Stx6*$^{-/-}$ (KO) mice with ~50% expression (55.9% and 52.9% respectively) in *Stx6*$^{+/-}$ (HEM) mice. Error bars: mean ± SEM (n = 3).

Protein knockout was validated by immunoblot using two antibodies targeting either the middle region (clone C34B2: an unspecified region surrounding residue 140) or an epitope at the N-terminus (clone 3D10: residues 1-25) of the 255 amino acid protein (Figure 37d and e respectively). Both antibodies support loss of the primary protein isoform detectable at ~32 kDa (likely representing Stx6-201 and/or Stx6-209 isoforms with predicted molecular weight of 29 kDa) and quantification of this band shows a ~50% reduction in protein expression relative to β-actin loading control in hemizygous mice with both antibodies (C34B2: 55.9%, Figure 37f; 3D10: 52.9%, Figure 37g). Other bands present at a lower intensity do not correspond to the predicted molecular weight of any full-length or truncated protein product, with the exception of a potential band at 17 kDa visible in Figure 37d, although this can also be detected in the wildtype mice so is unlikely to represent a truncated protein (Table 14).

Name	Transcript ID	bp	Protein	kDa	kDa before deletion
Stx6-201	ENSMUST00000027743.12	4589	255aa	29	17
Stx6-206	ENSMUST00000192690.1	1289	91aa	10	0.1
Stx6-209	ENSMUST00000195302.5	955	255aa	29	17
Stx6-207	*ENSMUST00000193059.5*	*934*	*199aa*	*23*	*17*

Table 14: *Stx6* protein-coding transcripts and putative truncated gene products
List of predicted protein-coding transcripts of *Stx6* in C57BL/6 mice with the calculated molecular weight of the wildtype isoform in kDa, as well as the molecular weight of any protein sequence prior to the CRISPR-mediated 1808 nucleotide deletion in the *Stx6* null allele to highlight any possible truncated gene products.

6.2.2. Inoculation of Stx6 knockout mice with mouse-adapted scrapie prions

To determine the effect of *Stx6* expression on survival and incubation time of prion disease in mice, *Stx6*$^{-/-}$ ('KO'), *Stx6*$^{+/-}$ ('HEM') and *Stx6*$^{+/+}$ ('WT') mice were inoculated intracerebrally with two mouse-adapted scrapie prion strains, RML and ME7 (see Methods section 2.9.5), or PBS as a mock-infected negative control. 20 mice per group were used, providing statistical power to detect a 5% difference in incubation time after allowing for loss due to incurrent illness and increased variation as the first experiment with this genetic modification.

The null hypotheses tested were that manipulation of *Stx6* expression has no effect on incubation time or pathological appearances in RML and ME7 mouse prion diseases. A log-rank test of the association of disease incubation time (measured as time from inoculation until mice were culled due to confirmation of scrapie symptoms) with *Stx6* genotype showed a significant relationship in both RML ($P = 0.0049$, Figure 38a) and ME7 ($P < 0.0001$, Figure 38b) inoculated animals, demonstrating *Stx6* genotype modulates survival time of prion disease with both prion strains (Table 15).

To quantify these effects, define associations with specific genotypes, and test the robustness of the results, secondary analyses were performed by looking at differences in effects between hemizygous and full knock-out animals, and by using different definitions of prion disease onset. Knockout of *Stx6* extended median incubation time following inoculation with both RML and ME7 prions by 12 days relative to wildtype mice (RML: WT = 147 days [144 – 161] vs KO = 159 days [156 – 160], Figure 38a; ME7: WT = 162 days [161 – 168]) vs KO = 174 days [174 – NA], Figure 38b). A post-hoc pairwise log-rank test was significant only for ME7-inoculated knockout animals (RML: $P = 0.17$ (KO vs WT); ME7: $P = 0.00075$ (KO vs WT)) (Table 15). However, supporting a role of *Stx6* expression on disease incubation time with RML prions, incubation time in *Stx6*$^{+/-}$ animals was extended by the same amount as in *Stx6*$^{-/-}$ animals relative to wildtype controls (RML: HEM = 159 days [154 – 168], Figure 38a) which was significant in the pairwise analysis ($P = 0.0047$ (HEM vs WT)) (Table 15). Of note there was no significant difference in survival between *Stx6*$^{+/-}$ and *Stx6*$^{-/-}$ mice inoculated with RML prions ($P = 0.14$, (not shown)). Interestingly however, following

inoculation with ME7 prions, survival time in *Stx6*$^{+/-}$ mice was instead moderately but significantly reduced by 4 days relative to wildtype animals (ME7: HEM = 158 days [155 – 160], P = 0.00040, Figure 38b) (Table 15). Whether this reflects a strain tropism or a chance occurrence within the variability of the experiment would require further replication. Importantly there was no difference in brain PrP^C expression between lines (Figure 38c).

		P*	Group	N start	N events	Median (days)	Lower 95% CI	Upper 95% CI	Diff. (vs WT) (days)	P (vs WT)**
Scrapie sickness	**RML**	P = 0.0049	***WT***	*20*	*19*	*147*	*144*	*161*		
			HEM	19	18	159	154	168	**+12**	0.0047
			KO	20	16	159	156	160	**+12**	0.17
	ME7	P < 0.0001	***WT***	*20*	*16*	*162*	*161*	*168*		
			HEM	20	19	158	155	160	**-4**	0.00040
			KO	20	7	174	174	NA	**+12**	0.00075
First scrapie symptom	**RML**	P = 0.14	***WT***	*19*	*19*	*133*	*127*	*139*		
			HEM	19	19	132	129	141	**-1**	0.86
			KO	20	20	138	133	141	**+5**	0.16
	ME7	P < 0.0001	***WT***	*20*	*18*	*147*	*146*	*150*		
			HEM	20	19	146	140	151	**-1**	0.29
			KO	17	14	154	153	160	**+7**	1.20×10^{-7}

Table 15: Summary of analysis for association of *Stx6* genotype with disease incubation time following inoculation with RML and ME7 prions.
Summary statistics for incubation times measured as time until animals were culled due to scrapie sickness (top) or onset of first scrapie-associated symptom (bottom) following intracerebral inoculation with 1% RML or ME7 infected C57BL/6 brain homogenate by *Stx6* genotype (KO: -/-; WT: +/+; HEM: +/-). Median incubation time in days listed with corresponding 95% confidence intervals. *P-value from overall log-rank test of *Stx6* genotype with disease incubation time. **P-value from a pairwise log-rank test for association of each group with relative WT controls.

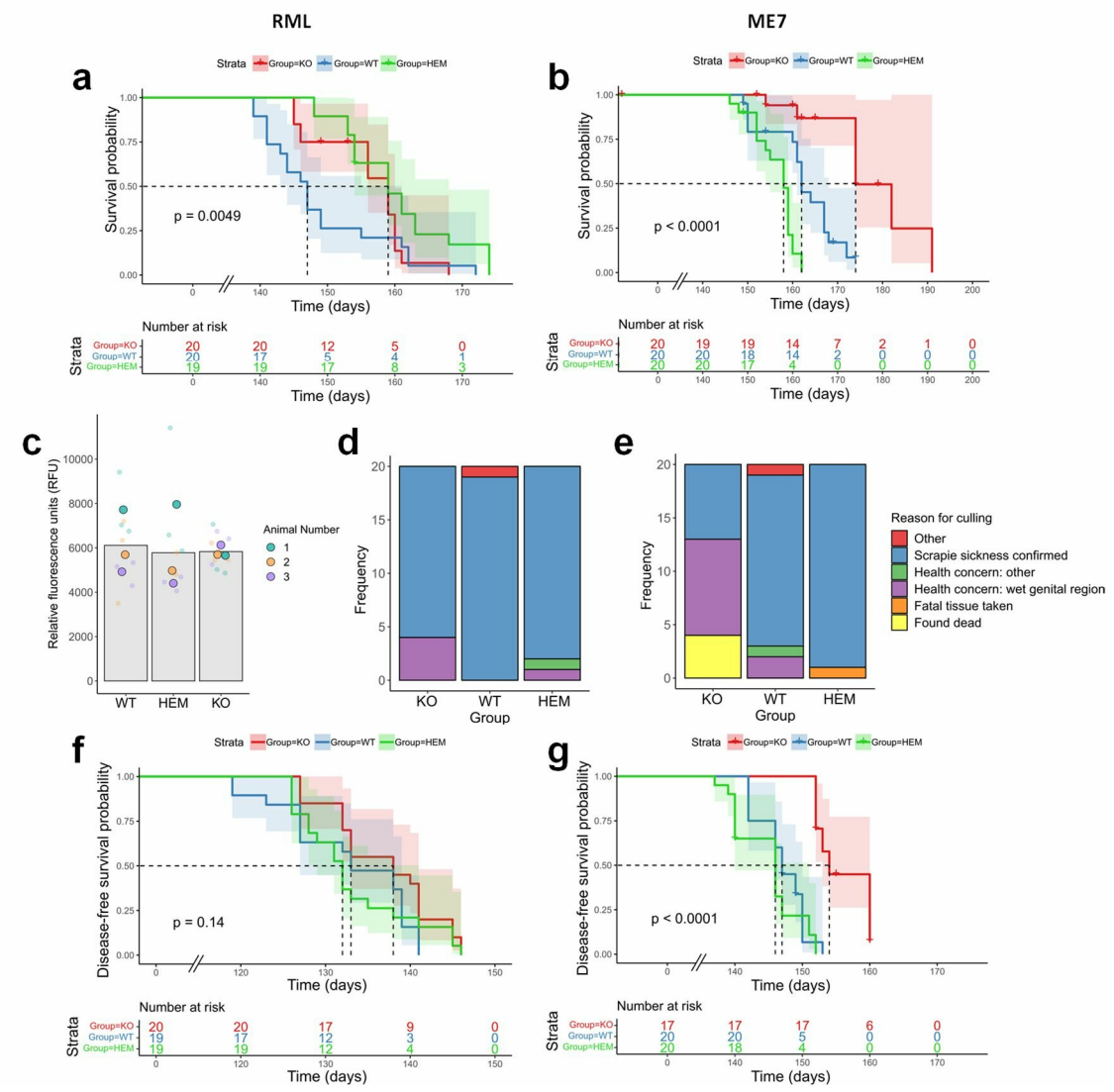

Figure 38: Extended survival times in *Stx6*$^{-/-}$ mice following intracerebral inoculation with RML and ME7 mouse-adapted scrapie prions.
Intracerebral inoculation in the right parietal lobe of *Stx6*$^{-/-}$ (KO; red), *Stx6*$^{+/-}$ (HEM; green) and *Stx6*$^{+/+}$ (WT; blue) C57BL/6 mice (n = 20 per group) with 1% brain homogenate from (**a**,**d**,**f**) RML and (**b**,**e**,**g**) ME7 infected C57BL/6 mice. (**a**,**b**) Survival probability until animals culled due to scrapie sickness shows 12 day increase in median incubation time for (**a**) both *Stx6*$^{-/-}$ and *Stx6*$^{+/-}$ mice following RML inoculation and (**b**) for *Stx6*$^{-/-}$ mice only following ME7 inoculation (with a 4 day decrease for *Stx6*$^{+/-}$) relative to *Stx6*$^{+/+}$ mice. (**c**) No difference in PrP^{C} expression in whole brain homogenates from *Stx6*$^{-/-}$, *Stx6*$^{+/-}$ and *Stx6*$^{+/+}$ early adult mice (9 weeks) measured by ELISA (one-way ANOVA on square root transformed data). (**d**,**e**) Reason for culling mice in (**d**) RML-inoculated and (**e**) ME7-inoculated groups demonstrates a large proportion of *Stx6*$^{-/-}$ mice were not diagnosed with scrapie sickness (blue) with ME7. (**f**,**g**) Disease-free survival probability (time until onset of first scrapie symptom) (**f**) does not show a significant association with *Stx6* genotype following RML-inoculation with only a nominal 5 day increase in median incubation time in *Stx6*$^{-/-}$ mice relative to controls, but (**g**) a 7 day increase in *Stx6*$^{-/-}$ mice inoculated with ME7. P-values shown from an overall log-rank test of association of all groups with incubation time. Crosses indicate censored animals. Inoculation and animal management performed by staff at the animal facility.

Prion disease in mice typically begins to present with general neurological symptoms such as hunching, lack of grooming or piloerection, however confirmatory onset of prion disease is well-defined by characteristic symptoms including ataxia, generalised tremor, loss of righting reflex and limb paralysis (O'Shea et al., 2008). It is the identification of these latter symptoms which leads to diagnosis of scrapie sickness and subsequent culling of animals, however under important animal welfare guidance, when animals present with uncharacterised symptoms which may indicate signs of distress or harm, animals are also terminated to prevent prolonged suffering. It is for this reason in the current study a large proportion of animals, particularly when inoculated with ME7, were culled prior to definite scrapie diagnosis and thus censored from the previously described analysis (Figure 38d and e, Table 15). As shown in Figure 38e, 45% of *Stx6*$^{-/-}$ mice inoculated with ME7 were culled due to an unusual “wet genital region” indicating incontinence; analysis of prior experiments performed in the Unit found mice culled due to this symptom had the same level of neuropathology and deposition of PrP^{Sc} as mice with confirmed prion disease, indicating this may be an unrecognised disease symptom (unpublished data).

To increase statistical power, time until the onset of the first neurological symptom was also analysed, with animals culled due to wet genital region included in the analysis as clinically-affected by prion disease. This has previously been used in the literature as an alternative measure of disease incubation time (Carlson et al., 1986). In an overall log-rank test of the association of this parameter with *Stx6* genotype, a significant relationship was again found for ME7 inoculated animals ($P < 0.0001$, Figure 38g), however there was no significant association of disease-free incubation time with *Stx6* genotype in RML-inoculated animals ($P = 0.14$, Figure 38f). Reassuringly though, incubation time measured in this way did indicate a prolonged disease progression in *Stx6*$^{-/-}$ mice albeit more modest than for survival time, with median time extended by 5 days in RML-inoculated mice (RML: WT = 133 days [127 – 139] vs KO = 138 days [133 – 141], Figure 38f) and 7 days in ME7-inoculated mice (ME7: WT = 147 days [146 – 150] vs KO = 154 days [153 – 160], Figure 38g) relative to wildtype controls. As expected however, this was only significant for ME7-inoculated animals in the post-hoc pairwise log-

rank test (RML: P = 0.16; ME7: P = 1.20 x 10^{-7}) (Table 15). Hemizygous *Stx6* expression however, unlike for survival time, did not impact the time until symptom onset for either prion strain compared to wildtype animals in this analysis (RML: HEM = 132 days [129 – 141], P = 0.86, Figure 38f; ME7: HEM = 146 days [140 – 151], P = 0.29, Figure 38g) (Table 15). Identification of the first neurological symptom is typically a more variable assessment (discussed later) which likely underpins the differences between these two analyses, however the repeated description of extended incubation time in *Stx6* knockout animals supports a pathological role of expression for this gene in prion disease progression.

6.2.3. Histological analysis of prion disease in Stx6 knockout mice

Prion disease is typically characterised by a triad of impairments including spongiform vacuolation, neuronal loss and astrocyte proliferation, which can be identified upon post-mortem histopathological analysis of the brain in both patients and animals with the disease.

To determine whether there were any distinctions in the prion-related neuropathology with differing *Stx6* expression, brains were removed following onset of terminal prion disease from RML and ME7 inoculated *Stx6*$^{-/-}$, *Stx6*$^{+/-}$ and *Stx6*$^{+/+}$ mice and processed for histological analysis (see Methods section 2.9.8). Samples were first stained with haematoxylin and eosin (H&E) to identify morphological changes in the tissue, including the neuronal loss and spongiosis associated with prion diseases (haematoxylin stains DNA to identify nuclei shown in blue, and eosin stains proteins in the cytoplasm and extracellular matrix in pink). As shown in Figure 39, H&E reveals the presence of distinct small, round vacuoles within the neuropil in multiple brain regions including the striatum, cortex and midbrain in all animals, reflecting the expected spongiform change in these tissues. This analysis also showed the typical neuronal loss within the hippocampus following ME7 inoculation. Unfortunately the process of generating tissue sections for histological analysis and subsequent H&E staining can introduce inconsistencies in staining independent from spongiform change (such as tears in the tissue from sectioning or water droplets) making quantification of spongiform change unreliable, however all groups showed the expected

distribution and level of spongiosis and neuronal loss characteristic of inoculated strain type.

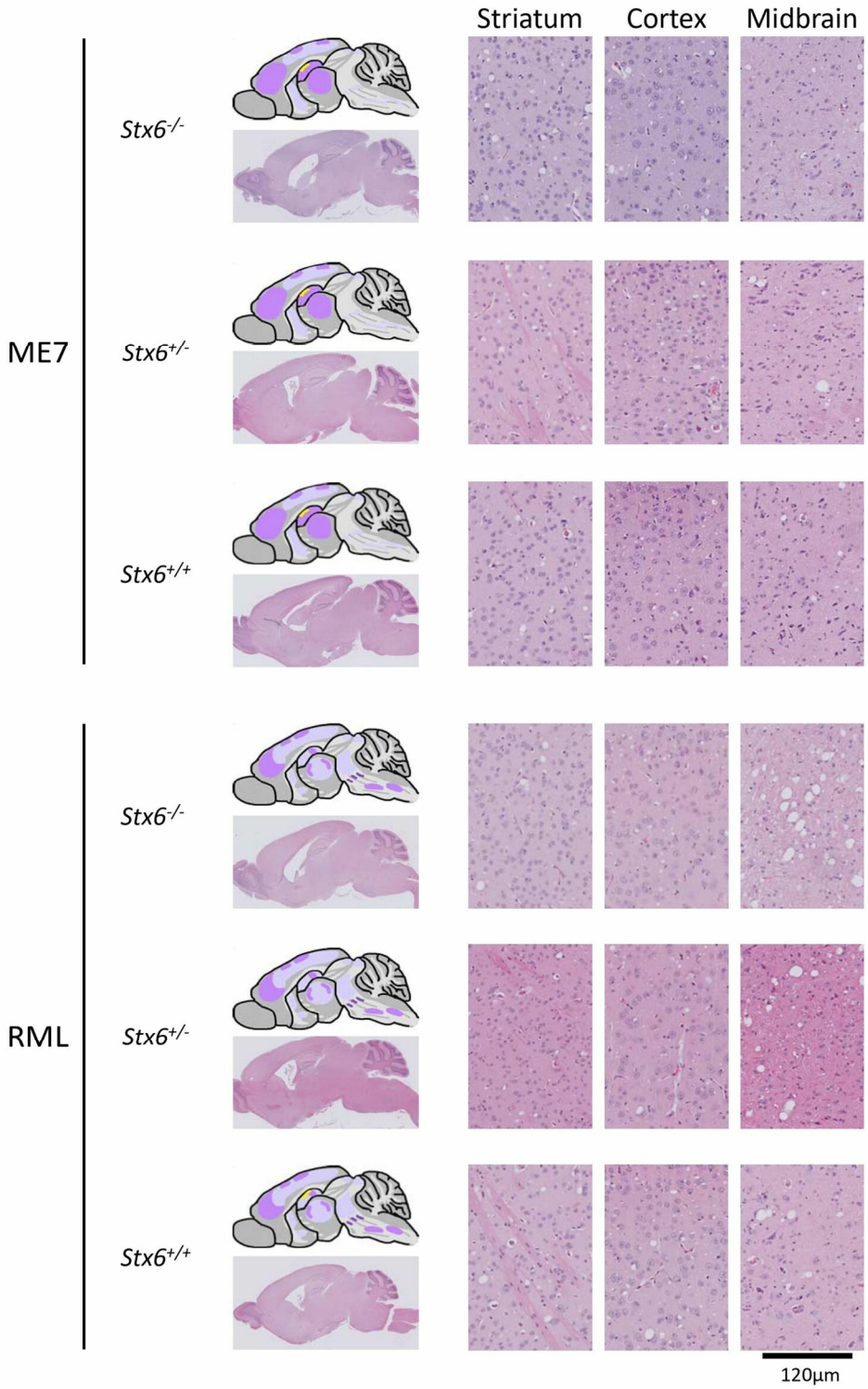

Figure 39: No difference in neuronal loss or spongiform change in prion disease with knockout of *Stx6*.
Hematoxylin and eosin (H&E) staining of whole brain (left) with schematic depiction of spongiosis (light purple shading: widely dispersed spongiosis; darker purple shading: intense focal spongiosis; yellow shading: neuronal loss) and representative images from striatum, cortex and midbrain (right) from *Stx6*$^{-/-}$, *Stx6*$^{+/-}$ and *Stx6*$^{+/+}$ mice inoculated with ME7 (top) and RML (bottom) mouse-adapted scrapie prions shows expected spongiform

pathology in all samples at end-point, including hippocampal neuronal loss with ME7, with no gross difference evident between genotypes. Brains from 7-10 mice diagnosed with scrapie sickness were compared for neuropathology analysis. Images generated by Jackie Linehan and Sebastian Brandner. Histology performed by core facility.

Reactive astrogliosis and microglia activation was also measured in these samples as a hallmark of prion diseases. Immunohistochemical staining with an anti-GFAP antibody for reactive astrocytes demonstrated the expected widespread astrocyte proliferation in all samples, with particular intensity in the thalamus and hippocampus as previously described in prion disease (Figure 40) (Makarava, Chang, Kushwaha, & Baskakov, 2019). Quantification of mean percentage area immunostained with GFAP confirms this wide-spread proliferation, with astrocytes present in >70% of the brain tissue by area under all conditions (ME7: KO = 82.3% ± 0.820, HEM = 71.7% ± 0.870, WT = 70.7% ± 2.15; RML: KO = 79.2% ± 1.06, HEM = 82.6% ± 1.20, WT = 78.6% ± 1.06) (Figure 40). This analysis highlighted a ~10% increase in astrocyte area in *Stx6*$^{-/-}$ mice inoculated with ME7 relative to both *Stx6*$^{+/-}$ ($P = 2.82 \times 10^{-4}$) and *Stx6*$^{+/+}$ animals ($P = 9.24 \times 10^{-5}$). Whether this is a cause of or result from the increased survival time of these animals requires further investigation, however highlights a potential protective mechanism for reduced *Stx6* expression in prion diseases if astrocytes are acting to maintain neuronal function. Immunostaining with anti-Iba1 antibody to detect microglia demonstrates the expected visible microglia activation following inoculation with both RML and ME7 prions, occupying 25-30% of whole brain area in all conditions (ME7: KO = 25.3% ± 1.20, HEM = 28.1% ± 0.972, WT = 24.8% ± 1.26; RML: KO = 23.7% ± 1.03, HEM = 29.9% ± 1.06, WT = 24.5% ± 0.899) (Figure 41). Interestingly with both prion strains *Stx6*$^{+/-}$ mice demonstrated a modestly higher proportion of microglia relative to both *Stx6*$^{+/+}$ and *Stx6*$^{-/-}$ mice, which was significant in RML inoculated animals ($P = 2.25 \times 10^{-3}$ and $P = 4.68 \times 10^{-4}$ respectively). Whether this is a dose-dependent result of *Stx6* expression in microglia function or a spurious effect requires further investigation, for example confirmation of Iba1 expression by immunoblotting.

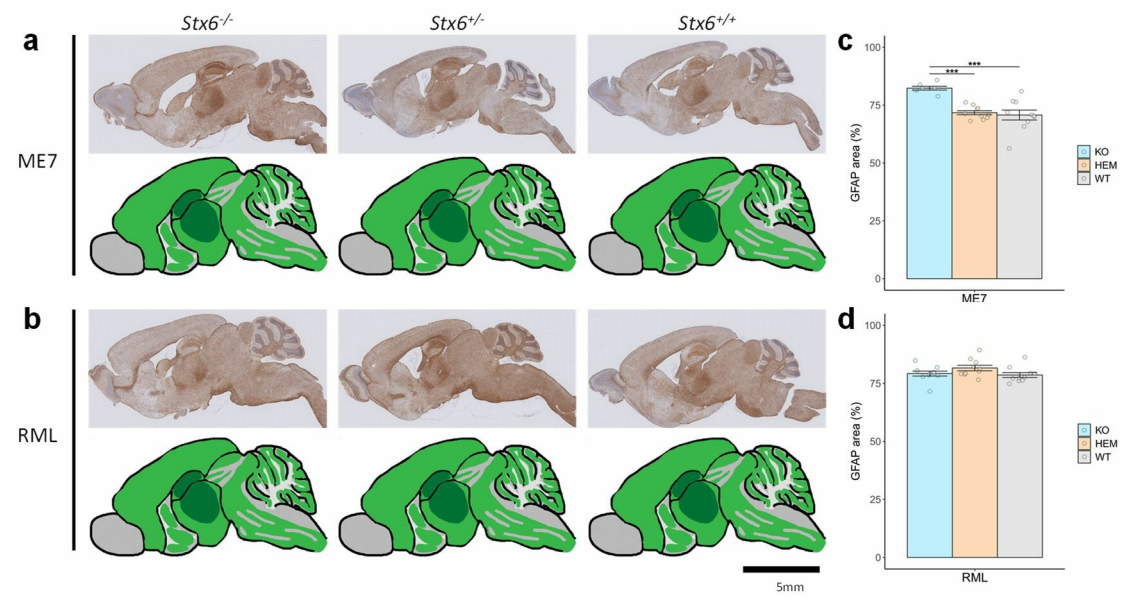

Figure 40: Modest increase in reactive astrogliosis in prion disease with knockout of *Stx6* following ME7 inoculation.
Reactive astrogliosis measured at end-point though immunohistochemistry with anti-GFAP antibody in whole brain, with (**a**,**b**) example images and schematic deposition of staining intensity (light green: moderate astrogliosis; dark green: intense astrogliosis) from *Stx6*$^{-/-}$, *Stx6*$^{+/-}$ and *Stx6*$^{+/+}$ mice inoculated with (**a**) ME7 and (**b**) RML mouse-adapted scrapie prions, shows expected intense GFAP staining including in the hippocampus and thalamus. (**c**,**d**) Quantification of % area stained with anti-GFAP antibody in whole brain demonstrates a (**c**) ~10% increase in astrocyte number in *Stx6*$^{-/--}$ relative to *Stx6*$^{+/-}$ and *Stx6*$^{+/+}$ animals when inoculated with ME7 however (**d**) no difference between genotypes following RML inoculation (***P < 0.001; one-way ANOVA with Tukey's post-hoc test). Brains from 7-10 mice diagnosed with scrapie sickness were compared for neuropathology analysis. Images generated by Jackie Linehan and Sebastian Brandner. Histology performed by core facility.

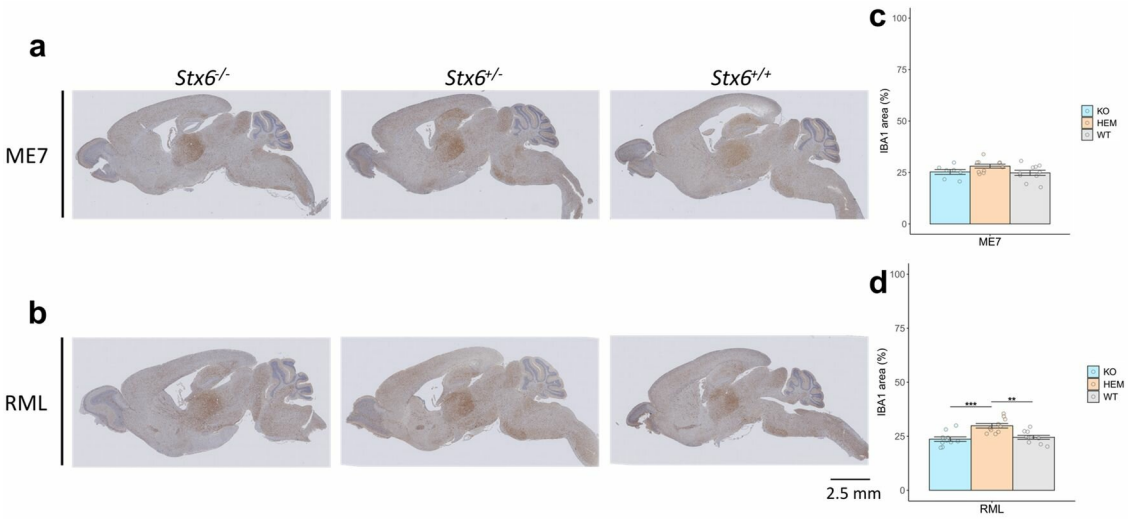

Figure 41: Variable effect of *Stx6* genotype on Iba1-positive microglia count in prion disease.
Microglia count measured at end-point though immunohistochemistry with anti-Iba1 antibody in whole brain, with (**a**,**b**) example images from *Stx6*$^{-/-}$, *Stx6*$^{+/-}$ and *Stx6*$^{+/+}$ mice inoculated with (**a**) ME7 and (**b**) RML mouse-adapted scrapie prions, shows expected intense GFAP staining including in the thalamus. (**c**,**d**) Quantification of % area stained with anti-Iba1 antibody in whole brain demonstrates a (**c**) no difference in microglia number between *Stx6* genotypes following ME7 inoculation however (**d**) an ~5% increase in *Stx6*$^{+/-}$ mice relative to both *Stx6*$^{+/+}$ and *Stx6*$^{-/-}$ animals following RML inoculation (**P < 0.01, ***P < 0.001; one-way ANOVA with Tukey's post-hoc test). Histology performed by core facility.

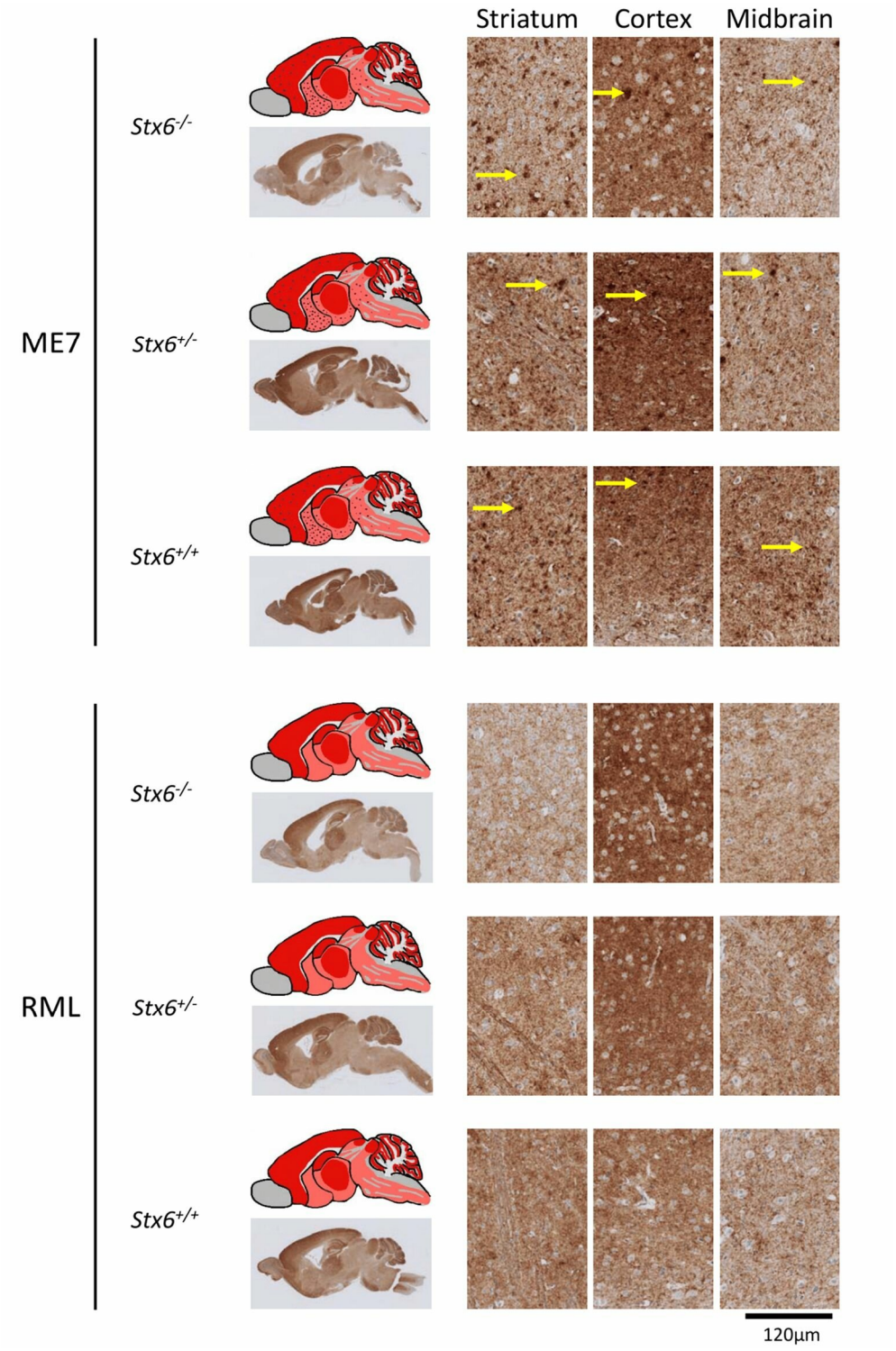

Figure 42: No difference in PrP deposition in prion disease with knockout of *Stx6*. Immunohistochemistry using anti-PrP antibody ICSM35 in whole brain (left) with schematic depiction of PrP deposition (pink shading: moderate PrP deposition; red shading: intense PrP deposition; red dots: PrP micro-plaques) or representative images from striatum, cortex and midbrain (right) from *Stx6*$^{-/-}$, *Stx6*$^{+/-}$ and *Stx6*$^{+/+}$ mice inoculated with ME7 (top) and RML (bottom) mouse-adapted scrapie prions, shows expected PrP deposition in all samples at end-point, with widespread diffuse staining for both strains and additional presence of micro-plaques with ME7 (yellow arrows). There is no gross difference evident between genotypes. Brains from 7-10 mice diagnosed with scrapie

sickness were compared for neuropathology analysis. Images generated by Jackie Linehan and Sebastian Brandner. Histology performed by core facility.

Along with the physiological changes in prion diseases, deposition of PrP aggregates in the brain is associated with disease pathology for most human and animal prion diseases, although the appearance and localisation of these aggregates varies. To determine whether *Stx6* expression alters the deposition, appearance or localisation of PrP aggregates following intracerebral inoculation with RML and ME7 prions, after processing to select for disease-associated PrP, samples were immunohistochemically stained with anti-PrP antibody ICSM35. As shown in Figure 42, PrP deposits can be identified in all samples at this end-stage of the disease; with both strains, disease-associated PrP can be detected diffusely with additional widespread deposition in micro-plaques with ME7 as previously described (Wenborn et al., 2015). The lack of an antibody specific to disease-associated or aggregated PrP immunohistochemistry for PrP aggregates generates high levels of background staining as a result of coincident detection of PrP^{C}; furthermore, as displayed in Figure 42, these aggregates are often diffuse and highly variable between strains. Therefore unfortunately meaningful quantification of these images was not feasible, however at this resolution and time-point there was no difference evident between the appearance, extent or localisation of disease-associated PrP with *Stx6* genotype.

6.2.4. Phenotypic characterisation of Stx6 knockout mice

As this was a newly generated mouse line with no other reports of *Stx6* null mice evident in the literature, additional characterisation of these lines was performed, for example to identify any pathological impairments in these animals which could undermine its use as a therapeutic target for neurodegeneration.

First, histological analysis for the typical neuropathological changes associated with prion disease was performed on mock-inoculated mice (as in section 6.2.3). H&E staining for gross morphological changes did not highlight any vacuoles indicative of spongiform change or neuronal loss as was seen with the inoculated animals, or any other gross neurological abnormalities (Figure 43). Furthermore, *Stx6* knockout or hemizygous expression did not induce spontaneous abnormal PrP deposition (Figure 43), reactive astrogliosis (Figure 44a and c) or microgliosis (Figure 44b and d) above baseline levels (anti-GFAP: KO = 42.4% ± 1.04, HEM = 44.3% ± 0.630, WT = 43.7% ± 0.478; anti-Iba1: KO = 7.37% ±1.33, HEM = 8.77% ± 0.525, WT = 7.09% ± 0.700). The absence of *Stx6* expression therefore is not detrimental to gross neurological physiology or development, and does not induce any evident independent pathological phenotypes.

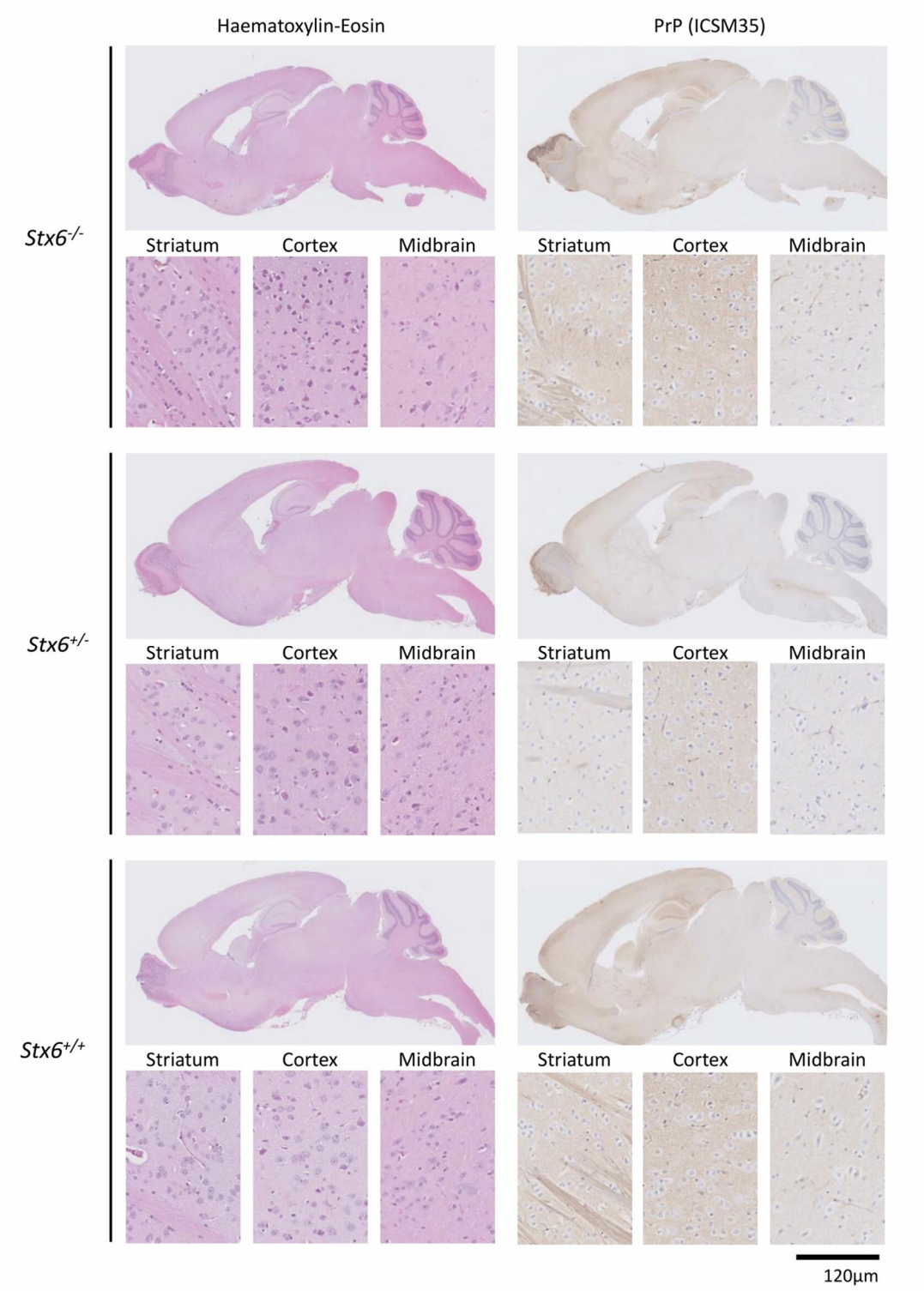

Figure 43: No evidence of neuropathology with knockout of *Stx6*.
Hematoxylin and eosin (H&E) staining (left) and anti-PrP immunohistochemistry (ICSM35; right) in *Stx6*$^{-/-}$, *Stx6*$^{+/-}$ and *Stx6*$^{+/+}$ mice mock-inoculated with PBS show no evidence of neuronal loss, spongiosis or abnormal PrP deposition with no gross difference evident between genotypes. Representative images of whole brain and striatum, cortex and midbrain. Brains from 4-5 mice aged between 52-60 weeks were compared for neuropathology analysis. Images generated by Jackie Linehan and Sebastian Brandner. Histology performed by core facility.

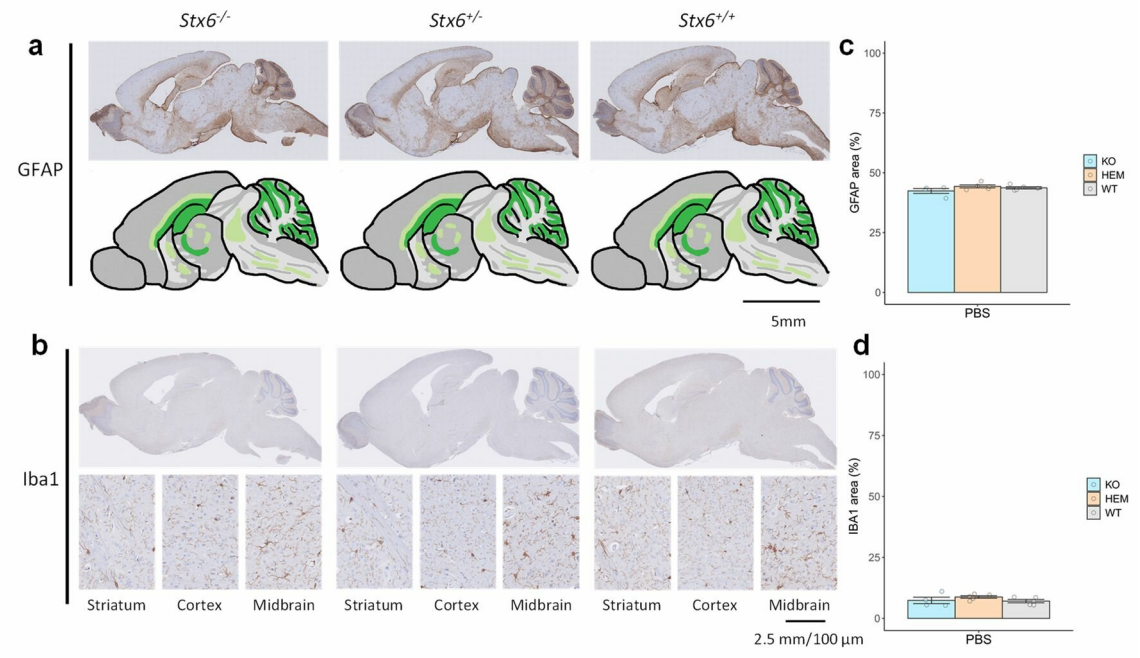

Figure 44: No evidence of widespread reactive astrogliosis or microgliosis with knockout of *Stx6*.
(**a**,**b**) Representative images of immunohistochemistry in *Stx6*$^{-/-}$, *Stx6*$^{+/-}$ and *Stx6*$^{+/+}$ mice mock-inoculated with PBS for (**a**) reactive astrogliosis measured though immunohistochemistry with anti-GFAP antibody in whole brain, with schematic deposition of staining intensity (light green: moderate astrogliosis; dark green: intense astrogliosis) and (**b**) microglia stained with anti-Iba1 antibody in whole brain and with straitum, cortex and midbrain shown at higher magnification. (**c**,**d**) Quantification of % area stained with (**c**) anti-GFAP and (**d**) anti-Iba1 antibodies in whole brain demonstrates no gross difference evident between genotypes or evidence of abnormal inflammatory response. Brains from 2-5 mice aged between 52-60 weeks were compared for neuropathology analysis. Images generated by Jackie Linehan and Sebastian Brandner. Histology performed by core facility.

To explore whether *Stx6* expression contributes to other physiological processes in these animals, a number of additional biological parameters were measured. Observational reports by colleagues during the handling of these animals described the *Stx6* knockout mice as larger and heavier than *Stx6*$^{+/-}$ and *Stx6*$^{+/+}$ animals in adulthood. To quantify this, at time of culling (mice aged 56-61 weeks), control PBS mock-inoculated mice were weighed. This supported a significant 27% increase in mean body weight in *Stx6*$^{-/-}$ mice relative to wildtype controls (WT = 34.7 g ± 2.06, KO = 44.1 g ± 2.45; P = 0.014) and a 44% increase relative to hemizygous animals (HEM = 30.6 g ± 1.14; P = 0.0012) (Figure 45a). To start

to investigate the underlying biological cause of this increase, both subcutaneous relative adipose mass and length of mice were measured. The proportion of abdominal subcutaneous white adipose tissue (WAT) (animals culled, total mass weighed and perigonadal WAT dissected and weighed immediately after) was significantly increased from 5.13% ± 0.197 of total body weight in *Stx6*$^{+/+}$ mice, to 6.57% ± 0.258 in *Stx6*$^{-/-}$ mice (P = 0.0049) (Figure 45b). Interestingly however in *Stx6*$^{+/-}$ mice, the proportion of adipose tissue was significantly reduced compared to *Stx6*$^{+/+}$ animals, to 3.66% ± 0.272 of total body weight (P = 0.0026) (Figure 45b). There was little difference between the overall size of these animals as measured by nasoanal length, with only a modest but significant reduction in *Stx6*$^{+/-}$ mice relative to *Stx6*$^{-/-}$ mice, but no difference of either line relative to wildtype controls (WT = 9.50 cm ± 0.158; KO = 9.63 cm ± 0.239 vs HEM = 9.00 cm ± 0.00, P = 0.040) (Figure 45c). The measurement of subcutaneous WAT weight by dissection is a somewhat approximate way of measuring fat storage due to the propensity for technical variation (i.e. this depends on the amount of tissue the researcher is able to remove) and does not reflect storage in other adipose tissues, however these results indicate a metabolic fat-storage defect associated with *Stx6* expression. Analysis of multiple biochemical parameters in blood performed by MRC Harwell, made publicly available as part of the International Mice Phenotyping Consortium (IMPC: an international collaborative effort to routinely phenotype all knockout mice), also described various significant differences associated with metabolism and/or homeostasis in *Stx6*$^{-/-}$ mice relative to controls. This includes increased circulating alkaline phosphatase, blood urea nitrogen and cholesterol levels as well as impaired glucose response (increased time to return to fasting blood glucose levels following administration), supporting a robust metabolic defect in these animals (Table 16). These significant results were not consistent between life stages measured however, and so whether this reflects developmentally-modulated phenotypes or lack of reproducibility requires further investigation.

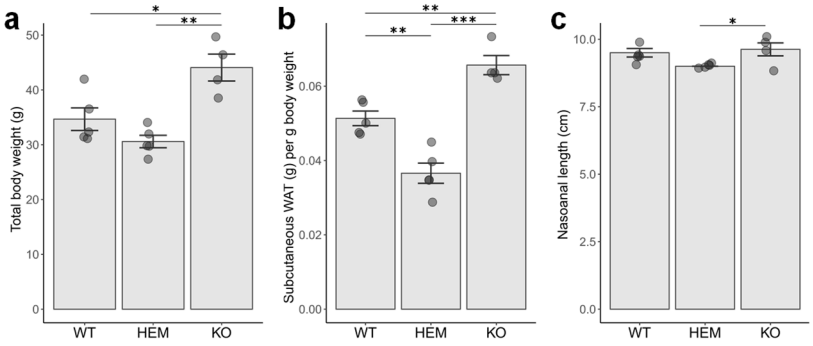

Figure 45: Physiological characterisation of *Stx6*$^{-/-}$ and *Stx6*$^{+/-}$ mice shows increased mass of subcutaneous inguinal white adipose tissue (iWAT) with knockout of *Stx6*.

(**a**) Increased total body weight of *Stx6*$^{-/-}$ (KO) mice compared to *Stx6*$^{+/-}$ (HEM) and *Stx6*$^{+/+}$ mice (PBS mock-inoculated mice at 56-61 weeks) corresponds to (**b**) increased adipose mass measured as weight of abdominal subcutaneous WAT per g of body weight (**c**) with no difference in nasonanal length compared to *Stx6*$^{+/+}$ indicating no change in overall size. Error bars: mean ± SEM. Significance determined from one-way ANOVA on normally distributed data (*P < 0.05, ** P < 0.01, *** P < 0.001). Dissections performed by Nick Kaye.

Associated phenotype	Procedure	Parameter	P-value	Significant life stage	Significant sex	P-value in other life stage
Increased circulating alkaline phosphatase	Clinical Chemistry	Alkaline phosphatase	1.58×10^{10}	Early adult	Both	0.094
Increased blood urea nitrogen	Clinical Chemistry	Urea (Blood Urea Nitrogen - BUN)	2.89×10^{5}	Early adult	Female	0.017
Increased circulating cholesterol	Clinical Chemistry	Total cholesterol	3.93×10^{5}	Late adult	Male	0.544
Decreased circulating glucose	Clinical Chemistry	Glucose	4.04×10^{5}	Late adult	Male	0.308
Abnormal vibrissae morphology	Combined SHIRPA and Dysmorphology	Vibrissae - appearance	7.40×10^{5}	Early adult	Male	0.251
Abnormal gait	Combined SHIRPA and Dysmorphology	Gait	7.43×10^{5}	Early adult	Both	0.562
Prolonged RR interval	Electrocardiogram (ECG)	RR	3.45×10^{5}	Early adult	Both	NA
Impaired glucose tolerance	Intraperitoneal glucose tolerance test (IPGTT)	Area under glucose response curve	3.14×10^{5}	Early adult	Male	NA
Hyperactivity	Open Field	Whole arena resting time	9.69×10^{6}	Early adult	Both	0.157
Hyperactivity	Open Field	Periphery resting time	3.77×10^{5}	Early adult	Both	0.010
Decreased anxiety related response	Open Field	Percentage centre movement time	4.46×10^{5}	Early adult	Both	0.009

Table 16: Significant phenotypes associated with *Stx6* knockout in the International Mouse Phenotyping Consortium (IMPC). Phenotyping tests performed by MRC Harwell as part of the IMPC including morphological, physiological and behavioural measurements measured at early adult (week 9-16) and late adult (week 52-59) life stages. Differences between *Stx6*$^{-/-}$ mice (Stx6$^{em1(IMPC)H}$) and wildtype C57BL6/N mice from the same facility analysed using a linear mixed model (continuous data) or Fisher's exact test (categorical data) and significant associations mapped to a Mammalian Phenotype (MP). Listed are all associated phenotypes below the $P < 10^{-4}$ threshold, as well as the P-value for the same test if performed at a different life stage (early or late adult). Data and analyses downloaded from www.mousephenotype.org.

Alongside physiological measurements, changes in animal behaviour can also indicate a pathological change, such as a neurological defect not detectable by histological analysis. Therefore, in order to determine if there was any gross behavioural phenotype associated with *Stx6* expression, a few preliminary tests were performed on the control PBS mock-inoculated mice during late adulthood. Firstly, diet consumed overnight (~18 hours) was measured to determine any differences in feeding behaviour, as well as to confirm whether the increase in body weight and fat storage observed in *Stx6*$^{-/-}$ mice was due to a higher intake of food (i.e. hyperphagia) or metabolic defect. Due to the propensity for extraneous food to be released from the feeding device there was substantial variability in this analysis, however there was no difference observed between the feeding behaviours in these animals with the expected consumption in all groups supporting the latter conclusion (Figure 46a).

Motor coordination and neuromuscular behaviours were also analysed using two tests: grip strength and time spent on a spinning rod (i.e. rotarod). This analysis highlights a reduced grip in *Stx6*$^{-/-}$ mice compared to both *Stx6*$^{+/+}$ (KO = 2.63 g.cm^{-1}.g^{-1} ± 0.09, WT = 3.92 g.cm^{-1}.g^{-1} ± 0.20; P = 0.0051) and *Stx6*$^{+/-}$ (HEM = 3.66 g.cm^{-1}.g^{-1} ± 0.29; P = 0.020) mice relative to body weight, suggesting a possible neuromuscular defect (Figure 46b). Similarly, a reduced time spent on the rotarod apparatus in *Stx6*$^{-/-}$ mice (KO = 49.4 s ± 4.1 vs WT = 101.1 s ± 17.2, P = 0.00030; vs HEM = 127.7 s ± 21.4, P = 8 x 10^{-7}) indicates a putative motor coordination defect (Figure 46c). However, both body weight and general activity associated with increased fat storage are also likely to confound these results.

Finally, analysis of burrowing and nesting as innate behaviours was performed to determine the general well-being of mice with varying *Stx6* expression; these are sensitive measures of overall health and motivation driven by the will to create safe and comfortable habitats. Defects in these behaviours have been associated with neurological dysfunction including sensitive early indicators of prion disease (Cunningham et al., 2005). Analysis of burrowing behaviour (measured as the amount of pellets displaced from a tube container overnight after habituation) showed a reduced motivation in *Stx6*$^{-/-}$ mice relative to wildtype animals (WT = 146.2 g ± 23.6, KO = 58.8 g ± 7.8; P = 0.0195), as well as a nominal reduction for *Stx6*$^{+/-}$ mice (HEM = 85.6 g ± 16.4) (Figure 46d) however there was no

significant change in nesting behaviours (measured as a score of nest quality) between genotypes (Figure 46e). Again, these analyses of broad behavioural phenotypes may highlight putative motivation-based neurological defects associated with *Stx6* knockout, however, like motor functions, these will also be influenced by the general activity of the animals. Unfortunately, due to time constraints and logistical limitations with access to facilities, these were the only feasible experimental set-ups available to provide an initial indication of behavioural defects in these animals, however in order to discern whether there is a neurological deficit independent from reduced activity further testing such as memory-specific tests would be required.

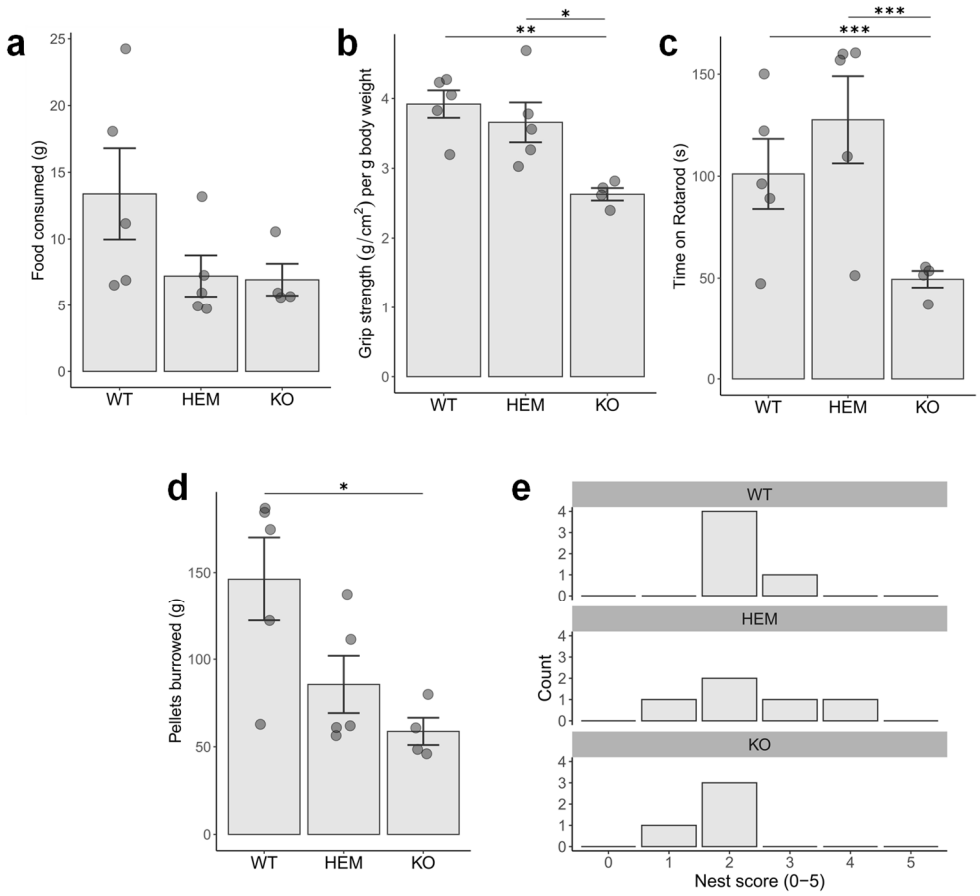

Figure 46: Behavioural characterisation of *Stx6*$^{-/-}$ and *Stx6*$^{+/-}$ mice indicates reduced motivation and motor ability with knockout of *Stx6*.
Preliminary behavioural analysis performed on control PBS-inoculated *Stx6*$^{-/-}$ (KO), *Stx6*$^{+/-}$ (HEM) and *Stx6*$^{+/+}$ (WT) adult mice (52-60 weeks; n = 4-5). (**a**) No difference in diet measured by food consumed overnight between genotypes. (**b**) Reduced grip strength in *Stx6*$^{-/-}$ mice normalised to total body weight, compared to both *Stx6*$^{+/+}$ and *Stx6*$^{+/-}$ mice. (**c**) Time spent on rotarod indicates reduced motor abilities in *Stx6*$^{-/-}$ mice compared to both *Stx6*$^{+/+}$ and *Stx6*$^{+/-}$ mice. (**d**) Pellets burrowed after ~18 h indicates reduced motivation in *Stx6*$^{-/-}$ mice compared to *Stx6*$^{+/+}$. Error bars: mean ± SEM.

Significance differences in continuous data measured with one-way ANOVA on normally distributed data (a,d: log-transformed, c: cube-root transformed) (*P < 0.05, ** P < 0.01, *** P < 0.001). (**e**) No significant association of genotype with quality of nests built after ~18 h suggesting no gross well-being deficits (scored from 0-5 with 0 indicating no nest built) (Fisher's exact test). Behavioural tests performed by Michael Farmer and Thomas Coysh.

6.2.5. Expression of STX6 in human brain

Because *STX6* is a genetic modifier of sCJD, as identified through GWAS and subsequent mapping analysis to link this gene to the associated region (e.g. through regulating brain gene expression, see chapter 3, section 3.2.4), the functional differences of this gene are implicitly causal for disease aetiology. The resultant working hypothesis is that increased *STX6* expression is driving this risk. To determine therefore whether there are any obvious distinctions between gene expression and/or localisation of syntaxin-6 in patients with sCJD, post-mortem brain tissues from 19 sCJD cases and 15 neurologically normal controls were first analysed through immunohistochemical staining (Figure 47). This revealed the expected predominantly neuronal staining of syntaxin-6 in both the frontal cortex and cerebellum of all individuals, restricted to the cell body cytoplasm without extending into the processes, indicative of the expected staining within the Golgi apparatus (see section 1.7.1). In the frontal cortex, other cell types, likely astrocytes or oligodendrocytes, were also less consistently stained. All cerebellar layers were positive for syntaxin-6 reactivity with immunostaining observed within Purkinje cells and large neurons of the dentate nucleus. A finer granular staining was also seen in the molecular layer. There was no difference detected in either staining intensity or distribution between sCJD cases and controls.

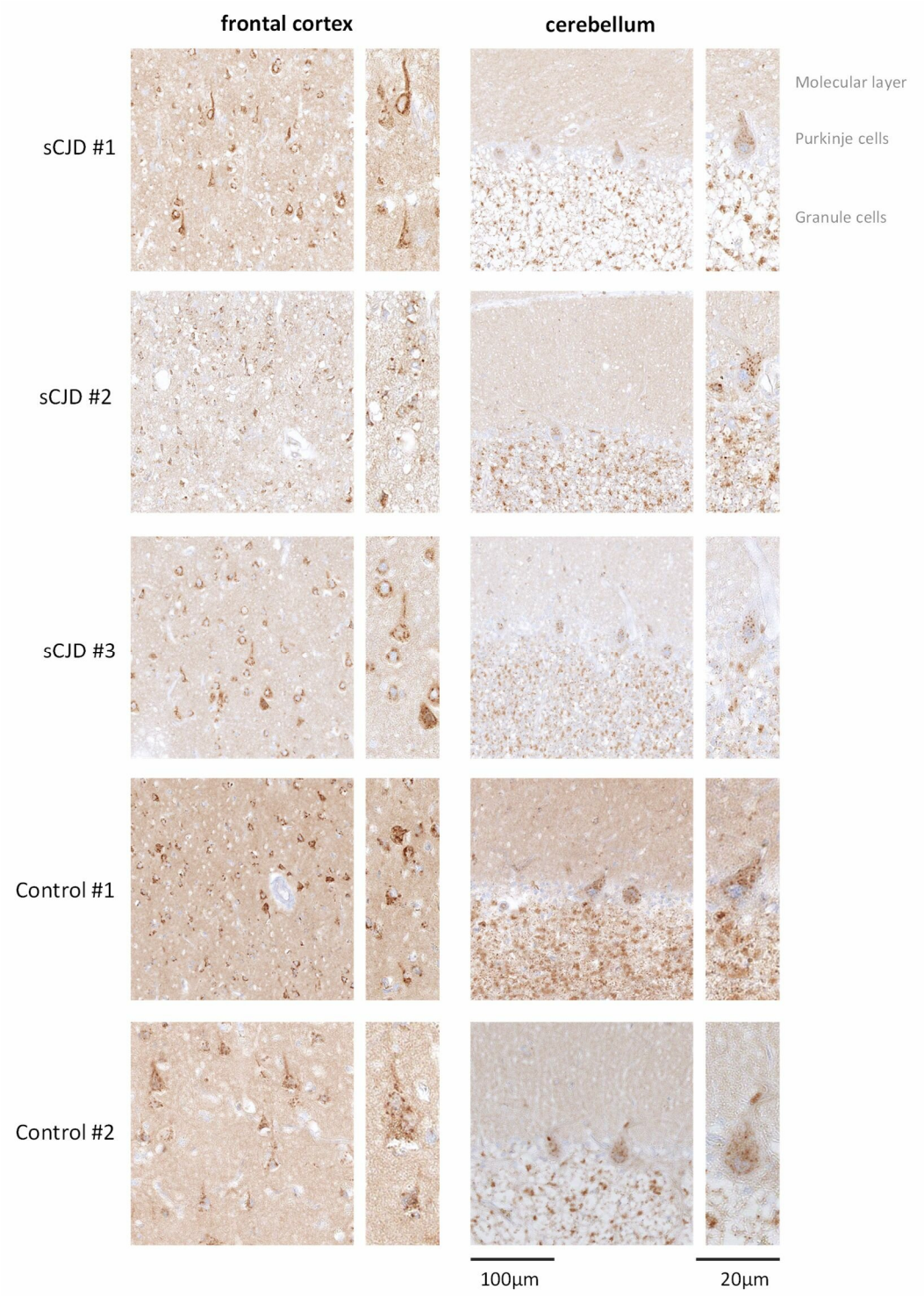

Figure 47: No difference in histological analysis of syntaxin-6 expression and distribution in frontal cortex and cerebellum between sCJD cases and controls. Immunohistochemistry with anti-syntaxin 6 antibody in formalin fixed paraffin embedded (FFPE) sections treated with formic acid from 3 sCJD patients ('sCJD #1', 'sCJD #2', 'sCJD #3') compared to non-prion controls ('Control #1' pre-frozen; 'Control #2' standard FFPE) (non-formic acid treated). Expected fine granular staining within the cytoplasm of neurons compatible with the Golgi. Staining indicative of neurons in frontal cortex. In the cerebellum, staining found in Purkinje cells, dentate nucleus and the molecular layer. No qualitative difference in staining intensity or distribution between sCJD cases and

controls. Images generated by Jackie Linehan and Sebastian Brandner. Histology performed by core facility.

To determine whether there was any difference in *STX6* expression at the mRNA level, as to provide a more sensitive and global read-out, cDNA was obtained from frozen cerebellum samples of 10 sCJD cases and 10 neurologically normal controls (see Methods section 2.10.2). Expression of *STX6* and other sCJD risk-associated genes identified in the sCJD GWAS (*PRNP* and *GAL3ST1*, as well as *PDIA4* and *BMERB1* which were significant in gene-based testing) (see chapter 3, section 3.2.1), were measured by RT-qPCR. Unfortunately in this analysis there was substantial variation in the expression of all housekeeper genes tested between cases and controls (i.e. *CYC1*, *RPL13* and *UBE2D2*), which were previously suggested to be stably expressed in the cerebellum in related neurodegenerative diseases (Figure 48) (Rydbirk et al., 2016). Nonetheless there was no difference evident between the expression of *STX6* or any other gene tested between sCJD patients and controls above this global variation.

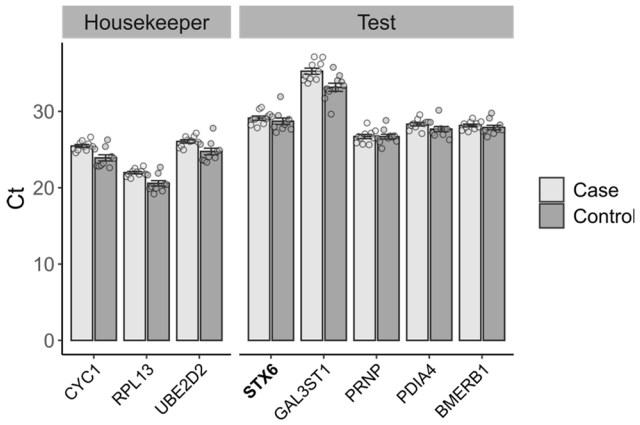

Figure 48: No change in *STX6* mRNA expression relative to housekeeping genes in sCJD patients compared to neurologically normal controls.
Cycle threshold (Ct) values from RT-qPCR analysis of mRNA extracted from cerebellum of 10 sCJD patients (case) and 10 neurologically normal controls for three recommended housekeeper reference genes and each of the genes implicated in sCJD risk in the GWAS analysis (Test). Due to variation in the housekeeper genes between populations these data were not normalised for relative expression, however Ct values do not indicate a difference in gene expression between cases and controls for any of the test genes above this variation.

6.3. Discussion

This study has described the investigation of syntaxin-6 function in both acquired prion disease in mice and post-mortem sCJD brain tissues. Knockout of *Stx6* in C57BL/6 mice prolonged incubation time by 12 days following inoculation of two mouse-adapted scrapie prion strains, RML and ME7, equating to 8% and 7% increase in survival time respectively relative to wildtype animals. Reduction of syntaxin-6 protein expression by 50% in hemizygous animals was also sufficient to nominally extend disease incubation time by 8% (measured as survival) following RML inoculation, however the effect was not withheld with ME7 in these animals (with a modest 2% reduction relative to wildtype). Interestingly an ~10% increase in astrocyte count was associated with the absence of *Stx6* specifically following ME7 inoculation, and a ~5% increase in microglia count seen only with hemizygous expression of the gene following RML inoculation. As these effects are not consistent between strains or levels of *Stx6* expression and do not correlate with survival time, how this may reflect a role of *Stx6* in the function of these non-neuronal cells is unclear and requires further investigation such as validation of astrocytic and microglial marker expression by an alternative method (i.e. Western blotting). Nonetheless this highlights a potential role of this gene in these cell types, potentially providing a supportive role to neuronal function. Characterisation of general physiology and well-being of *Stx6* knockout mice indicates a potential metabolic defect with increased fat storage in subcutaneous WAT and alterations in the level of related components in circulating blood in late adults (e.g. glucose, cholesterol), likely reflected in a reduced overall activity. There was no evidence of a neurological deficit in these animals. Analysis of syntaxin-6 in sCJD human brain tissues did not highlight any evident differences in either expression or localisation at the end-stage of disease.

Deletion of *Stx6* in mice was achieved externally through microinjection of CRISPR endonuclease components into zygotes (i.e. Cas9 mRNA and gRNA(s) – usually two gRNAs are used but exact sequences not provided) flanking critical exons 6 and 7 present in all protein-coding *Stx6* transcripts (as shown in Figure 37). Sequencing of the target site in F1 heterozygotes demonstrated a 1808 nt deletion at the target site with an 8 nt insertion, inducing a frame-shift mutation and thus a likely premature stop codon and null allele, which were crossed in-

house to generate mice homozygous for the null allele as well as wildtype littermates for controls. Immunoblotting of brain homogenate from these animals confirmed loss of the primary protein-coding transcript detected at ~32 kDa in *Stx6*$^{-/-}$ animals, as well as an approximate (due to the limited accuracy when quantifying immunoblots) 50% protein expression in hemizygous mice relative to the wildtype controls, indicating bi-allelic expression of *Stx6* under endogenous conditions. Of note, although it is debated whether off-target cleavage is a substantial problem in mouse genome editing due to colony variation during breeding increasing background mutagenesis and segregating small off-target effects, and algorithms employed during gRNA design to minimise non-specific binding sites, there was no evidence of off-target screening by the suppliers (Aryal, Wasylishen, & Lozano, 2018; Ayabe, Nakashima, & Yoshiki, 2019).

Although the presence of a premature stop codon will likely lead to nonsense-mediated decay and prevent protein expression in its entirety, it's important to consider potential for alternate truncated protein products. The primary structure of the main syntaxin-6 isoform is highly conserved between mouse and human, with 95% identity in sequence, the same predicted domain structure (i.e. predominantly cytoplasmic (residues 1-234) with a predicted SNARE domain (166-225) and a C-terminal transmembrane domain (235-255)) (Figure 6 (section 1.7.1.2) and Figure 49), however a crystal structure for this protein has not been published. Nonetheless structural prediction by the AlphaFold software (v2.0) indicates the same 3-helical coiled-coil N-terminus and an additional C-terminal helix (Jumper et al., 2021). Mice however also express two other protein-coding isoforms of syntaxin-6 which, unlike the alternate isoform in humans which is lacking the N-terminal region (see section 5.3), includes an additional full-length isoform (Stx6-209) differing only at residues 231-255 in the transmembrane C-terminal domain (interestingly with less hydrophobic residues not predicted to sit in the membrane by Phobius transmembrane topology software (EMBL) (Madeira et al., 2019)), as well as a shorter 91 amino acid isoform made up mostly by the SNARE domain (Stx6-206, corresponding to residues 147-230 of the full length protein) (Figure 49). The function of these isoforms has not been directly explored, however they are likely to be functionally distinct if they are not associated with the membrane. Nonetheless the 1808 nt deleted region

corresponds to residues 148-196, removing 50% of the SNARE domain in all isoforms, therefore even if a truncated gene product is remaining (as possibly indicated by a ~17 kDa immunoreactive band with one anti-syntaxin-6 antibody shown in Figure 37d), it is unlikely to be functional.

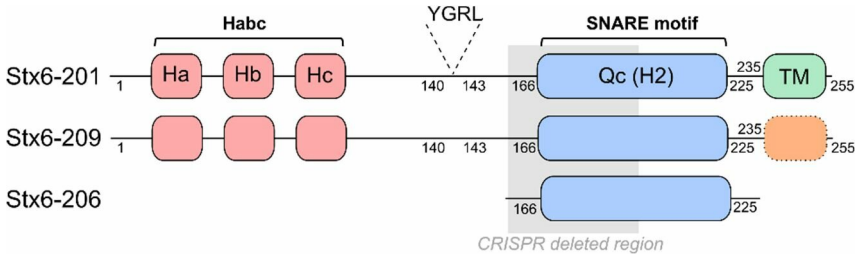

Figure 49: Protein coding isoforms of murine syntaxin-6 and deleted region in *Stx6* knockout mice.
Syntaxin-6 is a 255 amino acid protein comprised of two coiled-coil regions, one within the N-terminus constituting three independent helices (Ha-c; red) termed the Habc domain, and another within the SNARE motif (also called H2, classified as Qc due to a conserved glutamine residue; blue). A hydrophobic region at the C-terminal acts as a transmembrane anchor (TM; green) and a YGRL motif in the middle region is thought to be functionally important for localisation. In mice, Stx6-201 is thought to be the primary protein-coding isoform. Stx6-209 differs at residues 231-255 within the TM domain, and Stx6-206 comprises residues 147-230 of the full length protein only. The CRISPR deleted region spans residues 148-196 removing ~50% of the SNARE domain (grey box).

The current study explored the role of syntaxin-6 in acquired prion diseases in mice through inoculation of *Stx6*$^{+/+}$, *Stx6*$^{+/-}$ and *Stx6*$^{-/-}$ littermates with RML and ME7 prions. In this analysis prion incubation time was measured using two commonly used parameters: time until culling due to clinical prion disease diagnosis, and length of the disease-free period until onset of the first neurological symptom. In the former analysis, a log-rank test highlighted a significant association of genotype with both prion strains. Post-hoc exploration demonstrated a common 12 day increase in survival time with both strains in knockout animals relative to wildtype controls (albeit not significant for RML in knockout animals alone), and with RML in hemizygous animals. However with large numbers of censored animals in this study, who were culled prior to definitive scrapie diagnosis due to putative unclassified prion-related symptoms, the statistical power was reduced. Therefore a secondary analysis was performed of disease-free survival time and, although this did increase the statistical

significance of the association of *Stx6* knockout with incubation time following ME7 inoculation due to increased data points, there was no significant association with genotype and incubation time in RML-inoculated animals in this analysis. The clinical diagnosis of scrapie in mice is now very well-established and, after the aforementioned first signs of neurological dysfunction have been noted, mice are monitored very closely to guarantee that surviving mice adhere to important animal welfare guidelines with high levels of training to ensure suffering is not prolonged unnecessarily. However, the identification of these first more subtle signs of prion disease is somewhat more subjective and less closely monitored. Therefore, using the onset of the first neurological sign as an experimental end-point is often subject to more variability and bias, likely leading to the differences observed in these analyses for RML inoculated animals. Nonetheless the common at least nominal increase in median prion incubation time in knockout mice measured by both parameters, replicated in two independent studies with distinct prion strains, supports a common role of syntaxin-6 in prion disease.

The differential result of hemizygous *Stx6* expression on the two different prion strains tested, with a significant increase in prion incubation time (measured as survival time) following inoculation with RML but a modest reduction in ME7-inoculated animals, could be due to a stochastic relationship of hemizygous gene expression with prion incubation time driven by experimental variation or through remaining uncertainty in statistical analyses, however this may also highlight a potential strain tropism in this relationship. Prion strains are highly diverse in their biochemical, neuropathological and epidemiological properties (strains discussed previously in section 1.5.3). Although both RML and ME7 originate from scrapie prions and are highly efficient in inducing prion disease in mice, differential sub-passaging has resulted in strain adaptation and two clearly different strains, as evidenced by the distinct neuropathology (for example shown in Figure 39) and incubation times (Figure 38) as well as their diverse glycoform ratios and biochemical properties (Thackray, Hopkins, Klein, & Bujdoso, 2007). Therefore it is likely these strains are differentially processed within cells and tissues, such as through varying interactions of these strains with components of trafficking machinery. For example, investigation of the routes of endocytic prion uptake and

infection was recently shown to be differentially exploited by two different prion strains (RML and 22L) in mouse fibroblast cells (Fehlinger et al., 2017). Furthermore different strains display differential tissue tropism, for example substantial neuronal loss is observed in the hippocampus with ME7 but not RML, which may be due to the differential expression of cellular components within distinct brain regions and cell types. Therefore it is possible that RML is more reliant on syntaxin-6 function for efficient infection or disease than ME7, due to modest differences in the cellular processing of these strains. To confirm that the differential relationship of each strain with *Stx6* genotype is legitimate, these experiments in hemizygous animals would need to be replicated.

Generation of knockout animals is routinely used to explore gene function in both health and disease. As previously described (see section 6.1.3) knockout mice have been used to explore the role of many genes in prion diseases, routinely employing the same experimental design as the current study (i.e. measuring differences in incubation time following inoculation with mouse-adapted prion strains). Typically in these studies, the difference in incubation time recorded ranges from 5-25%. Although the effects observed in the current study are towards the more modest end of this range (7-8%), this is not unexpected due to the low effect size of this gene in the sCJD GWAS, with presence of associated alleles only increasing the odds of disease by ~16% (see chapter 3, section 3.2.2, Table 7). Robust evidence associates these *STX6* risk alleles with increased gene expression in multiple relevant brain regions (see section 3.2.4) lending itself to the hypothesis that reduced *Stx6* expression would be protective against the disease; the extended incubation time in knockout mice supports this direction of effect, as well as indicating the same mechanism is present in acquired prion disease in mice and sCJD in humans. In this report no difference in syntaxin-6 expression was found in patients with sCJD relative to controls across a range of *STX6* (rs3747957) and *PRNP* (codon 129, rs1799990) genotypes, suggesting a unilateral direction of effect with *STX6* expression not routinely modified as a result of disease, however this warrants further exploration due to technical difficulties with sourcing appropriate reference genes (especially difficult at the end-stage of the disease due to widespread neuropathology and resultant gene expression alterations) and the lack of sensitivity of immunohistology for

measuring protein expression. Importantly, however, disease does not appear to perturb syntaxin-6 localisation in the brain.

The evidence described here for a protective effect of reduced *Stx6* expression lends support to its putative use as a therapeutic target in prion diseases; although a direct comparison to human disease cannot be made from the current study, and it is not known when disease is initiated in humans, an 8% prolonged incubation time would likely be significant for patients. To this effect it was of interest to investigate whether perturbing gene function would be detrimental to general animal health. Histological analysis of brain tissue morphology and inflammation did not highlight any gross neurological defects associated with *Stx6* knockout, nor did this alone lead to abnormal PrP deposition. Preliminary assessment of general wellbeing behaviours in these animals highlighted some deficiencies relative to wildtype controls, however the repeated shortcomings of these animals more likely reflects a difference in general activity than a neurological defect, especially as *Stx6* null mice had an increased body weight compared to both hemizygous and wildtype animals

The increase in body mass in *Stx6* knockout mice was shown to be associated with a larger proportion of subcutaneous WAT. Publications by other researchers from cell culture experiments has robustly associated syntaxin-6 function with GLUT4 transport to the plasma membrane in both adipocytes and muscle cells (Foley & Klip, 2014; Hatakeyama & Kanzaki, 2011; Kumudu et al., 2003; Minami, Yokota, & Kawahara, 2020; Watson et al., 2008). In these experiments, knockdown or functional inhibition of syntaxin-6 results in an increase in surface GLUT4 expression at basal levels, but a reduction in the insulin-responsive translocation and uptake response into cells (Foley & Klip, 2014; Kumudu et al., 2003). It is possible therefore that the increased adipose mass in *Stx6* knockout mice is the result of a long-term increase in glucose uptake, leading to increased fat storage in adipocytes. This may also explain the observed decrease in circulating glucose yet impaired insulin-responsive glucose uptake. Peripheral tissues including adipose, liver and muscle tissue were sampled during the current experiment and future histological examination of these tissues i.e. for hypertrophy and/or hyperplasia will shed more light on the extent of fat storage defects in these animals. A putative role of syntaxin-6 in insulin synthesis in

pancreatic β-cells may also contribute to this perturbation but this is less well established (Kuliawat et al., 2004). Syntaxin-6 has also been shown to modify the transport of cholesterol between subcellular compartments in various cell lines, however how this would result in differential uptake from the bloodstream is unclear (Choudhury et al., 2006; Rogers et al., 2020; Urano et al., 2008). Nonetheless this may have led to the increased circulating cholesterol observed in these mice. Interestingly similar impaired glucose response and increased fat storage in adipose and liver tissue has been described in *Prnp* null mice potentially highlighting a common mechanism (de Brito et al., 2017). Regardless, however, knockout of syntaxin-6 does not appear detrimental to animal survival as all animals were fertile and viable (at least until late adulthood). Additionally, no physiological abnormalities were described in hemizygous animals suggesting this perturbation is specific to complete gene knockout, unlikely to reflect therapeutic inhibition of this protein. Future studies should now focus on investigating whether inhibiting syntaxin-6 function at a later stage of the disease, for example through generation of conditional *Stx6* knockout mice, is sufficient to prolong disease incubation time to better represent therapeutic treatment.

Demonstration that modified *Stx6* expression alters prion disease progression in an animal model supports this gene as causal not only for sCJD put potentially other prion diseases including acquired forms, as well as provides a putative therapeutic target, pathway and model for future research. Measuring an effect of gross perturbation of syntaxin-6 function in vivo provides direction for more restricted investigations in vitro, in cell culture models and in human tissues, required to elucidate the precise molecular mechanism of syntaxin-6 function in prion diseases.

7. Conclusions and future directions

7.1. Conclusions

The current thesis has described the replicated identification of two novel non-*PRNP* genes associated with sCJD risk, *STX6* and *GAL3ST1*, and subsequent exploration of the role of *STX6* in prion diseases in vitro and in vivo.

Acquisition of the largest collection of sCJD patient DNA to date through a vast international collaboration allowed for the first GWAS sufficiently powered to detect genetic risk factors for the disease with lower effect sizes than *PRNP*. This thesis described the follow up of this discovery study, with critical replication of putative loci in an independent cohort of sCJD patients, securing these variants as associated with disease risk. Computational fine-mapping and integration of functional datasets showed that *STX6* and *GAL3ST1* are the most likely causal genes driving this association, highlighting a robust increase in *STX6* expression in multiple relevant brain regions including the putamen and caudate as a functional consequence of the risk-associated haplotype, providing a likely causal mechanism driving the association of this gene.

In order to try to understand the molecular basis underlying the increased risk of sCJD with higher expression of *STX6*, as well as to secure this as the causal gene and mechanism in biological systems, both in vitro and in vivo models of gene function were developed. Firstly, cultured cells were utilised to model the role of syntaxin-6 in prion diseases. Primarily a sub-clone of the immortalised murine neuroblastoma line N2a, termed PK1, able to reliably propagate mouse-adapted prion strains with a high efficiency was explored. Knockdown of *STX6* expression in this line however did not reliably modify their ability to be infected or propagate prions in culture, or demonstrate any capacity to “cure” these cells of infection. Furthermore, despite the well-established function of syntaxin-6 in intracellular protein trafficking, there was no gross effect of gene knockdown on the steady-state localisation of either PrP^C or prion aggregates in this line. Although investigation in this model was not able to elucidate a functional mechanism of syntaxin-6 in prion disease, there are clear limitations to performing human functional genetics studies in immortalised mouse cell lines

and simplified uniform cultures, which may equate to absence of relevant cellular processes.

Because the role of *STX6* was identified in a human study and the lack of an effect of knockdown in murine cell lines, work then turned to developing a more relevant cell model for the disease. Propagation of human prions in culture has not proved an easy task, however recent publications have demonstrated that iPS-derived cell lines may be able to seed aggregation of human prion strains, including sCJD (Groveman et al., 2019; Krejciova et al., 2017). Therefore, in order to determine the function of syntaxin-6 in the propagation of human prions, as well as to utilise a more physiologically relevant cell type to the disease, CRISPR was applied to generate isogenic iPS cell lines for *STX6* knockout. Differentiation of these lines into cortical neurons confirmed the feasibility of generating relevant neuronal cell types, enabling future mechanistic studies in this line and hopefully providing researchers with a tool to clarify the cellular relationship between syntaxin-6 and human prions (discussed in the next section).

Although in vitro and tissue culture systems have certain advantages including their accessibility, feasibility of manipulation, relative low cost and short time-scales, these systems are mostly lacking the complex interactions and environments found in whole tissues. Therefore to support the cell culture studies, *Stx6* null mice were obtained to investigate the effect of modified gene expression in a whole biological system. Inoculation of these mice with two mouse-adapted prion strains as a general prion disease model showed a modest but robust extension in incubation time with the absence of *Stx6* expression relative to controls, supporting the pathological role of increased gene expression in sCJD. Importantly these mice were viable and neurologically normal, with only a likely metabolic defect associated with aberrant fat storage, encouraging its viable use as a therapeutic target. Whether this phenotype is relevant to the role of syntaxin-6 in prion disease is yet to be determined.

Finally, shared genetic association of *STX6* with tauopathies PSP and AD indicates a potential common biological mechanism in these related diseases. Although preliminary investigation of the effect of *STX6* expression on the “prion-like” seeding activity of tau in a cell culture model did not support a role of

syntaxin-6 in this process, again this restricted system may not accurately reflect pathobiology. Nonetheless, it will be fascinating to determine whether syntaxin-6 plays a common role in these related neurodegenerative diseases and whether this reflects the same cellular mechanism.

The identification of additional genetic modifiers for sCJD has highlighted putative new causal pathways that were not previously appreciated. Without an understanding of the biological mechanism however, the applicability of these discoveries is limited, especially due to complexities with pinpointing causal genes in GWAS studies. Demonstration that the same hypothesised effect in humans is reflected in a model system of the disease reassures that the correct causal gene was delineated and, through applying relevant model systems of gene function, will hopefully expand our understanding of the missing aetiological mechanisms in sCJD, prion diseases and other neurodegenerative diseases, moving us one step closer to a cure for these invariably fatal disorders.

7.2. Future directions

Work in this thesis was unable to delineate a mechanistic role of syntaxin-6 in prion diseases however, especially due to the promiscuity of functions of this SNARE protein described in cells (see section 1.7.2), there are many more feasible hypotheses one could propose for how this gene increases risk of sCJD. Importantly, although the propagation and seeded aggregation of the prion protein was primarily explored in this work and is certainly a key mechanism for disease progression, there are many other independent processes driving disease in humans including a distinct neurotoxic pathway, as well as a likely independent process which leads to formation of the first infectious prion in sporadic disease. A list of potential disease processes affected by syntaxin-6 function, a proposed biological mechanism for this and how these could be experimentally tested are listed in the following table (Table 17). Of note, due to the complexities of the network that comprises intracellular protein transport as well as protein aggregation, the specific consequence of increased syntaxin-6 expression is not immediately evident; this may not simply increase activity of a pathway, for example the hypothetical increase in vesicle recruitment to the TGN by retrograde transport with higher concentrations of syntaxin-6, may also act to

perturb endolysosomal transport due to the highly intertwined nature of these transport pathways. Furthermore SNARE protein function is often controlled post-translationally. For this reason speculation of the specific direction of effect increased expression may have on these functions was omitted.

As discussed frequently in this thesis, the choice of model applied to these experiments is as important as the experimental design itself. In personal opinion, increasing physiological relevance of models in human functional genetics studies is key to accurately delineating function, and so focussing future studies on human iPS-derived neural cells will provide both species and biological relevance, as well as the ability to study propagation of the specific prion disease the gene was discovered in. Additionally, the ability to differentiate into a plethora of cell types such as in organoids, will allow some progress towards modelling the complex interactions that occur in a brain, which can be supported by studies in whole systems such as mice to confirm the biological relevance in clinical disease.

Genetics has provided clues to important new pathways, and with careful consideration of experimental design, models and analysis, I have no doubt we will soon be that next step closer to a treatment for this fateful disease.

Disease process*	Potential biological mechanisms	Supporting evidence from syntaxin-6 function	Examples of experimental work	Strength of evidence (1-3)**
Formation of an initial prion *Unfortunately there are no models able to replicate spontaneous sCJD prion formation so this must be inferred*	Trafficking of PrP species to aggregation-prone compartments such as acidic environments or with correct lipid composition (section 1.5.4)	Regulates trafficking to acidic LE and lysosomes and to the plasma membrane (sections 1.7.2.1 and 1.7.2.4) Regulates removal of proteins from acidic EE via recycling to the TGN (section 1.7.1)	Employing methods to monitor PrP^C trafficking in real-time with transient *STX6* gene manipulation, such as fluorescently tagged proteins or pH-sensitive dyes, with markers for intracellular compartments Sensitive analysis (e.g. proteomics) to monitor surface (and total) protein expression with perturbation of *STX6* (would be interesting to look at global changes)	3
	Direct protein-protein interaction modifying kinetics of protein misfolding (section 1.5.1)	Present within the same intracellular vesicle membranes as PrP^C (albeit on predominantly different sides) (sections 1.3.2 and 1.7.1) Interaction with other neurodegeneration-associated proteins including tau and LRRK2 (section 1.7.3.2)	Co-IP of PrP^C and syntaxin-6 (likely of tagged constructs due to difficulties of PrP IP) from cell culture (e.g. HeLa) and subsequent deletion constructs FRET of fluorescently labelled proteins within living cells and higher resolution microscopy Pull-down using tagged PrP (e.g. glutathione-S-transferase) with wildtype and *Stx6* null brain homogenate (and vice versa) Addition of syntaxin-6 to in vitro aggregation assays	2
	Modulation of microenvironments such as lipid rafts to promote prion conversion (sections 1.5.4.1 and 1.3.2.1)	Modulates trafficking of lipid raft components and cholesterol to the PM, the composition of which alters prion aggregation (section 1.7.2.1)	Monitoring perturbations in PrP^C trafficking with varying cholesterol expression (e.g. BODIPY-cholesterol analogue) and localisation (e.g. small molecule U18666A) and effect of *Stx6* expression Lipidomics of DRMs in the presence and absence of *Stx6* expression	1

Intracellular propagation of infectious human prions *In general other models for prion propagation (such as iPS-derived cells with human prions) will help determine if Stx6 has any role in intracellular propagation*	Increase co-localisation and interaction of PrP^C and infectious prions on the cell surface (section 1.5.4.1)	Regulates trafficking of other GPI-anchored proteins to the plasma membrane (section 1.7.2.1)	Same techniques applicable as previously described with PrP^C alone, with exogenous application of PrP aggregates tagged with a different fluorophore to distinguish prions (including real-time trafficking, FRET) Kinetics of real-time generation of de novo prions on surface using tagged PrP^C (as per (Goold et al., 2011))	2
	Increase co-localisation of PrP^C and infectious prions in aggregation-prone intracellular compartments for conversion (e.g. multivesicular body, recycling endosomes) (section 1.5.4.1)	Regulates trafficking to acidic late endosomes and lysosomes and to the plasma membrane (sections 1.7.2.4 and 1.7.2.2) Regulates removal of proteins from acidic EE via recycling to the TGN (section 1.7.1)	As above with added manipulation of regulators of each pathway (e.g. Rabs, small molecules) to determine if same pathway shared with syntaxin-6 inhibition, and monitoring consequences on infectious prion load	3
	Modify uptake of infectious prions into cells via caveolae, clathrin or other raft-dependent routes (section 1.5.4.2)	Modification of caveolae-mediated endocytosis through transport of components to PM (section 1.7.2.2)	Microscopy and labelling of exogenous prions such as with pH-sensitive dyes to measure endocytosis, in the presence and absence of Cav-1 and syntaxin-6 Electron microscopy for transport of antibody-labelled PrP species into endosomes with *Stx6* perturbation (for direct visualisation coated vs uncoated structures)	2
Cell-to-cell spread of infectious prions	Exosomal release of prions (section 1.5.4.2)	Some evidence to suggest regulates exosomal release in cell lines e.g. pancreatic cancer (section 1.7.2.3)	Selective isolation of exosomes from culture media with varying *Stx6* expression and from circulating fluids in mice Determine resultant infectivity (e.g. in SCA)	1
	Constitutive secretion of prions (section 1.5.4.2)	Evidence to suggest modifies the release of tau into cell culture media (section 1.7.2.3)	Infectivity in general culture media with perturbation of *Stx6*	2

		Regulation of recycling pathway may regulate surface PrP^C for conversion or release of infectious material e.g. through increased shedding (section 1.7.2.2)	Intercellular transfer of infectivity between separated cells (e.g. through processes of neurons in microfluidics devices) Study of sheddase function (e.g. ADAM10) with *Stx6* inhibition (e.g. localisation, total and surface PrP^C expression, immunodetection of shed PrP)	
Modifying prion degradation	Trafficking of misfolded species to lysosomes (section 1.5.4.2)	Regulates lysosomal degradation of multiple cargo (section 1.7.2.4) Interaction with ubiquitin ligases (section 1.7.2.4)	Trafficking of PrP species to lysosomal vesicles (e.g. LAMP1 postive or pH sensitive dyes) with inhibition of syntaxin-6 Effect of modifying *Stx6* expression in lysosome inhibited cells (e.g. does increasing syntaxin-6 activity increase lysosomal degradation of PrP)	3
	Trafficking of misfolded species to autophagosomes (section 1.5.4.2)	Implicated in recruitment of autophagic vesicles during xenophagy (section 1.7.2.4) Putative interaction with components of autophagy machinery (section 1.7.2.4)	As above with components of autophagy pathway Note: the role of syntaxin-6 in autophagy under normal physiological conditions needs validating	1
Driving neurotoxicity	Trafficking, degradation or secretion of unidentified toxic species (section 1.5.1)	As previously listed, regulates multiple intracellular transport pathways (section 1.7.2)	This would require identification of the toxic species – in progress within the Unit	2
	Modifying synaptic signalling (section 1.3.3)	Presence in synaptosomes with putative role in recycling of synaptic vesicles (section 1.7.3.1)	Determine whether reduced *Stx6* expression in a cell system developed for assaying prion-induced neuritotoxicity (i.e. dendrite number, neurite length (Benilova et al., 2020), calcium signalling) is protective Effect of increasing syntaxin-6 expression on synaptic signalling defects in *Prnp* null cultures	1

	Role in neurite outgrowth modulated by NGF (also found to regulate PrP expression (Mobley, Neve, Prusiner, & McKinley, 1988))	Some evidence of requirement in NGF-induced outgrowth of cells in culture (section 1.7.3.1) Regulates trafficking of integrins mediating neurite outgrowth (sections 1.7.2.2 and 1.7.2.5) Regulates trafficking of IGF-1R (section 1.7.3.1)	Real-time analysis of neurite outgrowth in developing neurons in presence and absence of syntaxin-6 (e.g. primary cultures, iPS-derived neurons)	2
	General role in cell survival, adhesion and apoptosis which maybe applicable to neural cells	Perturbing syntaxin-6 function induces apoptosis and/or release in multiple cell lines (section 1.7.2.5)	As above with PrP toxicity to monitor general cell survival with application of toxic prions Effect of transient knockdown of syntaxin-6 on apoptosis in multiple neural cell lines	2
	Inducing insulin resistance-related cognitive decline in concordance with PrP function (e.g. insulin resistance in knockout mice) (section 6.3)	Regulates insulin-responsive transport of GLUT4 (and IRAP) to the PM (section 1.7.2.2) Putative evidence for a role in insulin synthesis in pancreatic β-cells (section 6.3)	Further investigation of insulin resistance in *Stx6* null mice and consequent cognitive deficits Measuring metabolic parameters (e.g. insulin, circulating glucose, glucose response) in prion-infected *Stx6* null mice relative to wildtype	1

Table 17: Proposed biological mechanisms of syntaxin-6 in prion diseases and future experimental work.
*Prion could also be substituted for other disease-associated proteopathic seeds such as tau. **3 = strongest evidence from literature, 1 = weakest.

Acknowledgements

Whenever I told people I was going to do a PhD they usually recoiled in horror and so I was certainly expecting the worst, however now looking back I can say with confidence I have (in the most part) thoroughly enjoyed this experience, and I know that I have the people who were supporting me along the way to thank for that.

Firstly I would like to thank my primary supervisor, Simon Mead, for imparting his endless knowledge and enthusiasm in our meetings and in feedback for this thesis, as well as generating the environment to allow me to develop my confidence, pursue my ideas and grow as a scientist. I am also grateful for all of the opportunities he's provided to establish myself within the scientific community. I would also like to thank my secondary supervisor, Emmanuelle Viré, not only for her thorough training and guidance, but for her support as a friend and mentor over the course of my PhD, and for reminding me there's more to life than failing experiments. And to the rest of the Human Genetics team past and present; Holger Hummerich, Tracy Campbell, Penny Norsworthy, Thanos Dimitriadis, Lee Darwent, Will Taylor, James Uphill, Fernando Guntoroi, Liam Quinn, Chiara Giordani, Helen Speedy, Elizabeth Hill, Nour Majbour, Isabel Natho, who have always provided honest advice and been so unfalteringly helpful and generous with their time. This work would also not have been possible without the support of the Unit director, Professor John Collinge, and I am thankful for his belief in this project and providing guidance and encouragement along the way.

Much of the work in this thesis has relied on collaboration with many of the wonderful scientists within the MRC Prion Unit at UCL from whom I have learned so much. I would like to thank James Uphill and Holger Hummerich for the collaborative effort on the GWAS; Emma Quarterman, Nunu Arora and Parmjit Jat for their assistance with cell culture protocols and provision of cell lines; Christian Schmidt, George Thirlway and Parvin Ahmed for their work on the ASCA; Madeleine Reilly for her assistance with image quantification; Juan Ribes and Peter Khlön for their training in microscopy; Mark Batchelor for provision of recombinant protein preparations; Julia Ravey, Beena Mistry and Catherine Turnball for their assistance and training with tau and iPS cell work; Emmanuel

Asante, Shyma Hamdan and the rest of the Transgenics group for their continuous support with the generation and characterisation of the mouse lines used in this study; Malin Sandberg, Huda Al-Doujaily and Michael De Oliveira for their assistance with generating inocula and measuring PrP expression; all of the staff at the BSF for their endless care, expertise and work with the mice in this study, including Lucy Draper, Ami Woodcock and Thomas Horan for breeding and maintaining these lines, and Nick Kaye, Craig Fitzhugh and Gavin Graham for their careful work in the inoculation experiment; Thomas Coysh and Michael Farmer for their expertise in behavioural analysis; and finally, the first-class histology team of Jackie Linehan, Tamsin Nazari, Sebastian Brandner, Florin Pintilli and Helena Costa.

External collaborators have also driven and supported much of this work. Not in the least are the other 64 authors who co-authored the GWAS paper – this was undoubtedly a mass collaborative effort and without the provision of both samples and experimental guidance from these individuals this would not have been possible. Also, a special thanks to Selina Wray and Charlie Arber at the Institute of Neurology, who were always so unwavering with their support, guidance and world-leading knowledge on all things iPS cells and I am very grateful for all of their selfless help with my project.

A very important thanks goes out to all of the patients and their families for providing us with invaluable samples and allowing this work to happen, and for their support in all of the work that happens in the Unit.

Huge thanks goes to all of the other students and friends at the Unit who have kept me smiling along the way, shared my woes and provided necessary light relief on a lunch break and Friday pub trip: Madeleine Reilly, Julia Ravey, Thanos Dimitriadis, Fernando Guntoroi, Lee Darwent, Bernie Simone, Liam Quinn, Luke Dabin, Ines Whitworth, Hazim Halim, Chiara Giordani, Elizabeth Hill, Nour Majbour, Lauren Wooley, Mark Batchelor, Beena Mistry, Catherine Turnball, Kezia Jack, Isabella Sheikh. This experience wouldn’t have been so enjoyable without you all.

Finally I would like to thank my continued support network of friends and family who have led me to this point and kept me grounded along the way, I know I

wouldn’t have made it through without such wonderful people in my life. To my dearest friends: to Sean Polden, for listening to my cries and excitement with endless support and cheerleading, and for trying to invent new ways to stop me having to feed my cells on a Saturday morning; to Lindsey Millward, for listening to me rant over lunch and always being there to listen and laugh with; to my everlasting school friends whose unfaltering support and hysterical laughter could always bring me back down to earth; to my homies Chloé Deneuve and Aliena Archer for always being there at the end of the day to cheer me on and making my home such a joyous space; and to all my other friends in London and across the UK for always being there to catch me. Sue, Andy and Dave Jones, I couldn’t ask for a more loving or supportive family, you have taught me that I can achieve anything I put my mind to whilst reminding me that there is so much more to life, and I am eternally grateful for everything you have given me. I know I couldn’t have got here without you.

This work was funded by the UK Medical Research Council to the MRC Prion Unit at UCL.

References

Abascal-Palacios, G., Schindler, C., Rojas, A. L., Bonifacino, J. S., & Hierro, A. (2013). Structural basis for the interaction of the Golgi-Associated Retrograde Protein Complex with the t-SNARE Syntaxin 6. *Structure, 21*(9), 1698-1706. doi:10.1016/j.str.2013.06.025

Abdulrahman, B. A., Abdelaziz, D. H., & Schatzl, H. M. (2018). Autophagy regulates exosomal release of prions in neuronal cells. *Journal of Biological Chemistry, 293*(23), 8956--8968. doi:10.1074/jbc.RA117.000713

Abid, K., Morales, R., & Soto, C. (2010). Cellular factors implicated in prion replication. *FEBS Letters, 584*(11), 2409--2414. doi:10.1016/j.febslet.2010.04.040

Agliardi, C., Guerini, F. R., Zanzottera, M., Bianchi, A., Nemni, R., & Clerici, M. (2019). SNAP-25 in Serum Is Carried by Exosomes of Neuronal Origin and Is a Potential Biomarker of Alzheimer's Disease. *Mol Neurobiol, 56*(8), 5792-5798. doi:10.1007/s12035-019-1501-x

Akhtar, S., Grizenkova, J., Wenborn, A., Hummerich, H., Fernandez de Marco, M., Brandner, S., . . . Lloyd, S. E. (2013). Sod1 deficiency reduces incubation time in mouse models of prion disease. *PLoS ONE, 8*(1), e54454. doi:10.1371/journal.pone.0054454

Alper, T., Cramp, W. A., Haig, D. A., & Clarke, M. C. (1967). Does the agent of scrapie replicate without nucleic acid? *Nature, 214*(5090), 764-766. doi:10.1038/214764a0

Anderson, R. M., Donnelly, C. A., Ferguson, N. M., Woolhouse, M. E., Watt, C. J., Udy, H. J., . . . Wells, G. A. (1996). Transmission dynamics and epidemiology of BSE in British cattle. *Nature, 382*(6594), 779-788. doi:10.1038/382779a0

Aoyagi, A., Condello, C., Stohr, J., Yue, W., Rivera, B. M., Lee, J. C., . . . Prusiner, S. B. (2019). Abeta and tau prion-like activities decline with longevity in the Alzheimer's disease human brain. *Sci Transl Med, 11*(490). doi:10.1126/scitranslmed.aat8462

Arellano-Anaya, Z. E., Huor, A., Leblanc, P., Lehmann, S., Provansal, M., Raposo, G., . . . Vilette, D. (2015). Prion strains are differentially released through the exosomal pathway. *Cellular and Molecular Life Sciences, 72*(6), 1185--1196. doi:10.1007/s00018-014-1735-8

Arnold, J. E., Tipler, C., Laszlo, L., Hope, J., Landon, M., & Mayer, R. J. (1995). The abnormal isoform of the prion protein accumulates in late-endosome-like organelles in scrapie-infected mouse brain. *The Journal of Pathology, 176*(4), 403--411. doi:10.1002/path.1711760412

Aryal, N. K., Wasylishen, A. R., & Lozano, G. (2018). CRISPR/Cas9 can mediate high-efficiency off-target mutations in mice in vivo. *Cell Death Dis, 9*(11), 1099. doi:10.1038/s41419-018-1146-0

Asante, E. A., Linehan, J. M., Desbruslais, M., Joiner, S., Gowland, I., Wood, A. L., . . . Collinge, J. (2002). BSE prions propagate as either variant CJD-like or sporadic CJD-like prion strains in transgenic mice expressing human prion protein. *EMBO J, 21*(23), 6358-6366. doi:10.1093/emboj/cdf653

Asante, E. A., Linehan, J. M., Gowland, I., Joiner, S., Fox, K., Cooper, S., . . . Collinge, J. (2006). Dissociation of pathological and molecular phenotype of variant Creutzfeldt-Jakob disease in transgenic human prion protein 129 heterozygous mice. *Proc Natl Acad Sci U S A, 103*(28), 10759-10764. doi:10.1073/pnas.0604292103

Asante, E. A., Linehan, J. M., Tomlinson, A., Jakubcova, T., Hamdan, S., Grimshaw, A., . . . Collinge, J. (2020). Spontaneous generation of prions and transmissible PrP amyloid in a humanised transgenic mouse model of A117V GSS. *PLoS Biol, 18*(6), e3000725. doi:10.1371/journal.pbio.3000725

Asante, E. A., Smidak, M., Grimshaw, A., Houghton, R., Tomlinson, A., Jeelani, A., . . . Collinge, J. (2015). A naturally occurring variant of the human prion protein completely prevents prion disease. *Nature, 522*(7557), 478-481. doi:10.1038/nature14510

Assou, S., Girault, N., Plinet, M., Bouckenheimer, J., Sansac, C., Combe, M., . . . De Vos, J. (2020). Recurrent Genetic Abnormalities in Human Pluripotent Stem Cells: Definition and Routine Detection in Culture Supernatant by Targeted Droplet Digital PCR. *Stem Cell Reports, 14*(1), 1-8. doi:10.1016/j.stemcr.2019.12.004

Aulic, S., Masperone, L., Narkiewicz, J., Isopi, E., Bistaffa, E., Ambrosetti, E., . . . Legname, G. (2017). alpha-Synuclein Amyloids Hijack Prion Protein to Gain Cell Entry, Facilitate Cell-to-Cell Spreading and Block Prion Replication. *Sci Rep, 7*(1), 10050. doi:10.1038/s41598-017-10236-x

Ayabe, S., Nakashima, K., & Yoshiki, A. (2019). Off- and on-target effects of genome editing in mouse embryos. *J Reprod Dev, 65*(1), 1-5. doi:10.1262/jrd.2018-128

Babelhadj, B., Di Bari, M. A., Pirisinu, L., Chiappini, B., Gaouar, S. B. S., Riccardi, G., . . . Vaccari, G. (2018). Prion Disease in Dromedary Camels, Algeria. *Emerg Infect Dis, 24*(6), 1029-1036. doi:10.3201/eid2406.172007

Baker, M., Mackenzie, I. R., Pickering-Brown, S. M., Gass, J., Rademakers, R., Lindholm, C., . . . Hutton, M. (2006). Mutations in progranulin cause tau-negative frontotemporal dementia linked to chromosome 17. *Nature, 442*(7105), 916-919. doi:10.1038/nature05016

Balendra, R., Uphill, J., Collinson, C., Druyeh, R., Adamson, G., Hummerich, H., . . . Mead, S. (2016). Variants of PLCXD3 are not associated with variant or sporadic Creutzfeldt-Jakob disease in a large international study. *BMC Medical Genetics, 17*(1), 1--6. doi:10.1186/s12881-016-0278-2

Ballmer, B. A., Moos, R., Liberali, X. P., Pelkmans, L., Hornemann, S., & Aguzzi, X. A. (2017). Modifiers of prion protein biogenesis and recycling identified by a highly parallel endocytosis kinetics assay. *Journal of Biological Chemistry, 292*(20), 8356--8368. doi:10.1074/jbc.M116.773283

Ban, H., Nishishita, N., Fusaki, N., Tabata, T., Saeki, K., Shikamura, M., . . . Nishikawa, S. (2011). Efficient generation of transgene-free human induced pluripotent stem cells (iPSCs) by temperature-sensitive Sendai virus vectors. *Proc Natl Acad Sci U S A, 108*(34), 14234-14239. doi:10.1073/pnas.1103509108

Barthelson, K., Newman, M., & Lardelli, M. (2020). Sorting Out the Role of the Sortilin-Related Receptor 1 in Alzheimer's Disease. *J Alzheimers Dis Rep, 4*(1), 123-140. doi:10.3233/ADR-200177

Bartoletti-Stella, A., Corrado, P., Mometto, N., Baiardi, S., Durrenberger, P. F., Arzberger, T., . . . Parchi, P. (2019). Analysis of RNA Expression Profiles Identifies Dysregulated Vesicle Trafficking Pathways in Creutzfeldt-Jakob Disease. *Molecular Neurobiology, 56*(7), 5009--5024. doi:10.1007/s12035-018-1421-1

Basler, K., Oesch, B., Scott, M., Westaway, D., Walchli, M., Groth, D. F., . . . Weissmann, C. (1986). Scrapie and cellular PrP isoforms are encoded by the same chromosomal gene. *Cell, 46*(3), 417-428. doi:10.1016/0092-8674(86)90662-8

Baylis, M., & Goldmann, W. (2004). The genetics of scrapie in sheep and goats. *Curr Mol Med, 4*(4), 385-396. doi:10.2174/1566524043360672

Beck, J., Collinge, J., & Mead, S. (2012). Prion protein gene M232R variation is probably an uncommon polymorphism rather than a pathogenic mutation. *Brain, 135*(2), e209--e209. doi:10.1093/brain/awr294

Beilina, A., Bonet-Ponce, L., Kumaran, R., Kordich, J. J., Ishida, M., Mamais, A., . . . Cookson, M. R. (2020). The Parkinson's Disease Protein LRRK2 Interacts with the GARP Complex to Promote Retrograde Transport to the trans-Golgi Network. *Cell Rep, 31*(5), 107614. doi:10.1016/j.celrep.2020.107614

Beland, M., & Roucou, X. (2012). The prion protein unstructured N-terminal region is a broad-spectrum molecular sensor with diverse and contrasting potential functions. *J Neurochem, 120*(6), 853-868. doi:10.1111/j.1471-4159.2011.07613.x

Beler, H., Raeber, A., Sailer, A., Fischer, M., Aguzzi, A., & Weissmann, C. (1994). High prion and PrPSc levels but delayed onset of disease in scrapie-inoculated mice heterozygous for a disrupted PrP gene. *Molecular medicine (Cambridge, Mass.), 1*(1), 19--30. doi:10.1007/bf03403528

Bellenguez, C., Küçükali, F., Jansen, I., Andrade, V., Moreno-Grau, S., Amin, N., . . . Lambert, J.-C. (2020). New insights on the genetic etiology of Alzheimer's and related dementia. *medRxiv*.

Benestad, S. L., Austbo, L., Tranulis, M. A., Espenes, A., & Olsaker, I. (2012). Healthy goats naturally devoid of prion protein. *Vet Res, 43*, 87. doi:10.1186/1297-9716-43-87

Benestad, S. L., Sarradin, P., Thu, B., Schonheit, J., Tranulis, M. A., & Bratberg, B. (2003). Cases of scrapie with unusual features in Norway and designation of a new type, Nor98. *Vet Rec, 153*(7), 202-208. doi:10.1136/vr.153.7.202

Benilova, I., Reilly, M., Terry, C., Wenborn, A., Schmidt, C., Marinho, A. T., . . . Collinge, J. (2020). Highly infectious prions are not directly neurotoxic. *Proc Natl Acad Sci U S A, 117*(38), 23815-23822. doi:10.1073/pnas.2007406117

Beraldo, F. H., Arantes, C. P., Santos, T. G., Machado, C. F., Roffe, M., Hajj, G. N., . . . Martins, V. R. (2011). Metabotropic glutamate receptors transduce signals for neurite outgrowth after binding of the prion protein to laminin gamma1 chain. *FASEB J, 25*(1), 265-279. doi:10.1096/fj.10-161653

Berman, H. M., Westbrook, J., Feng, Z., Gilliland, G., Bhat, T. N., Weissig, H., . . . Bourne, P. E. (2000). The Protein Data Bank. *Nucleic Acids Res, 28*(1), 235-242. doi:10.1093/nar/28.1.235

Bessen, R. A., Kocisko, D. A., Raymond, G. J., Nandan, S., Lansbury, P. T., & Caughey, B. (1995). Non-genetic propagation of strain-specific properties of scrapie prion protein. *Nature, 375*(6533), 698-700. doi:10.1038/375698a0

Bethani, I., Werner, A., Kadian, C., Geumann, U., Jahn, R., & Rizzoli, S. O. (2009). Endosomal Fusion upon SNARE Knockdown is Maintained by Residual SNARE Activity and Enhanced Docking. *Traffic, 10*(10), 1543--1559. doi:10.1111/j.1600-0854.2009.00959.x

Biacabe, A. G., Laplanche, J. L., Ryder, S., & Baron, T. (2004). Distinct molecular phenotypes in bovine prion diseases. *EMBO Rep, 5*(1), 110-115. doi:10.1038/sj.embor.7400054

Bian, J., Napier, D., Khaychuck, V., Angers, R., Graham, C., & Telling, G. (2010). Cell-based quantification of chronic wasting disease prions. *J Virol, 84*(16), 8322-8326. doi:10.1128/JVI.00633-10

Bishop, M. T., Sanchez-Juan, P., & Knight, R. S. G. (2013). Splice site SNPs of phospholipase PLCXD3 are significantly associated with variant and sporadic Creutzfeldt-Jakob disease. *BMC Medical Genetics, 14*(1). doi:10.1186/1471-2350-14-91

Bistaffa, E., Rossi, M., De Luca, C. M. G., Cazzaniga, F., Carletta, O., Campagnani, I., . . . Moda, F. (2019). Prion Efficiently Replicates in alpha-Synuclein Knockout Mice. *Mol Neurobiol, 56*(11), 7448-7457. doi:10.1007/s12035-019-1602-6

Block, M. R., Glick, B. S., Wilcox, C. A., Wieland, F. T., & Rothman, J. E. (1988). Purification of an N-ethylmaleimide-sensitive protein catalyzing vesicular transport. *Proc Natl Acad Sci U S A, 85*(21), 7852-7856. doi:10.1073/pnas.85.21.7852

Bock, J. B., Klumperman, J., Davanger, S., & Scheller, R. H. (1997). Syntaxin 6 functions in trans-Golgi network vesicle trafficking. *Molecular Biology of the Cell, 8*(7), 1261--1271.

Bock, J. B., Lin, R. C., & Scheller, R. H. (1996). A new syntaxin family member implicated in targeting of intracellular transport vesicles. *The Journal of Biological Chemistry, 271*(30), 17961--17965. doi:10.1074/JBC.271.30.17961

Bock, J. B., Matern, H. T., Peden, A. A., & Scheller, R. H. (2001). A genomic perspective on membrane compartment organization. *Nature, 409*(6822), 839-841. doi:10.1038/35057024

Bogan, J. S., Xu, Y., & Hao, M. (2012). Cholesterol Accumulation Increases Insulin Granule Size and Impairs Membrane Trafficking. *Traffic, 13*(11), 1466--1480. doi:10.1111/j.1600-0854.2012.01407.x

Bolton, D. C., McKinley, M. P., & Prusiner, S. B. (1982). Identification of a protein that purifies with the scrapie prion. *Science, 218*(4579), 1309-1311. doi:10.1126/science.6815801

Bone, I., Belton, L., Walker, A. S., & Darbyshire, J. (2008). Intraventricular pentosan polysulphate in human prion diseases: an observational study in the UK. *Eur J Neurol, 15*(5), 458-464. doi:10.1111/j.1468-1331.2008.02108.x

Borchelt, D. R., Taraboulos, A., & Prusiner, S. B. (1992). Evidence for synthesis of scrapie prion proteins in the endocytic pathway. *The Journal of Biological Chemistry, 267*(23), 16188--16199.

Boyle, A. P., Hong, E. L., Hariharan, M., Cheng, Y., Schaub, M. A., Kasowski, M., . . . Snyder, M. (2012). Annotation of functional variation in personal genomes using RegulomeDB. *Genome Res, 22*(9), 1790-1797. doi:10.1101/gr.137323.112

Brandhorst, D., Zwilling, D., Rizzoli, S. O., Lippert, U., Lang, T., & Jahn, R. (2006). Homotypic fusion of early endosomes: SNAREs do not determine fusion specificity. *Proceedings of the National Academy of Sciences*. doi:10.1073/pnas.0511138103

Brandner, S., & Jaunmuktane, Z. (2017). Prion disease: experimental models and reality. *Acta Neuropathol, 133*(2), 197-222. doi:10.1007/s00401-017-1670-5

Branger, F., & Mang. (2002). Stimulation of PrPC retrograde transport toward the endoplasmic reticulum increases accumulation of PrPSc in prion-infected cells. *Journal of Biological Chemistry, 277*(41), 38972--38977. doi:10.1074/jbc.M205110200

Bremer, J., Baumann, F., Tiberi, C., Wessig, C., Fischer, H., Schwarz, P., . . . Aguzzi, A. (2010). Axonal prion protein is required for peripheral myelin maintenance. *Nature Neuroscience, 13*(3), 310--318. doi:10.1038/nn.2483

Brown, C. A., Schmidt, C., Poulter, M., Hummerich, H., Klohn, P. C., Jat, P., . . . Lloyd, S. E. (2014). In vitro screen of prion disease susceptibility genes using the scrapie cell assay. *Hum Mol Genet, 23*(19), 5102-5108. doi:10.1093/hmg/ddu233

Brown, P., Brandel, J. P., Sato, T., Nakamura, Y., MacKenzie, J., Will, R. G., . . . Schonberger, L. B. (2012). Iatrogenic Creutzfeldt-Jakob disease, final assessment. *Emerg Infect Dis, 18*(6), 901-907. doi:10.3201/eid1806.120116

Bruce, M., Chree, A., McConnell, I., Foster, J., Pearson, G., & Fraser, H. (1994). Transmission of bovine spongiform encephalopathy and scrapie to mice: strain variation and the species

barrier. *Philos Trans R Soc Lond B Biol Sci, 343*(1306), 405-411. doi:10.1098/rstb.1994.0036

Budka, H., Aguzzi, A., Brown, P., Brucher, J. M., Bugiani, O., Gullotta, F., . . . et al. (1995). Neuropathological diagnostic criteria for Creutzfeldt-Jakob disease (CJD) and other human spongiform encephalopathies (prion diseases). *Brain Pathol, 5*(4), 459-466. doi:10.1111/j.1750-3639.1995.tb00625.x

Bueler, H., Aguzzi, A., Sailer, A., Greiner, R. A., Autenried, P., Aguet, M., & Weissmann, C. (1993). Mice devoid of PrP are resistant to scrapie. *Cell, 73*(7), 1339-1347. doi:10.1016/0092-8674(93)90360-3

Buil, A., Brown, A. A., Lappalainen, T., Viñuela, A., Davies, M. N., Zheng, H. F., . . . Dermitzakis, E. T. (2015). Gene-gene and gene-environment interactions detected by transcriptome sequence analysis in twins. *Nat Genet, 47*(1), 88-91. doi:10.1038/ng.3162

Buniello, A., MacArthur, J. A. L., Cerezo, M., Harris, L. W., Hayhurst, J., Malangone, C., . . . Parkinson, H. (2019). The NHGRI-EBI GWAS Catalog of published genome-wide association studies, targeted arrays and summary statistics 2019. *Nucleic Acids Res, 47*(D1), D1005-D1012. doi:10.1093/nar/gky1120

Burre, J., Sharma, M., & Sudhof, T. C. (2014). alpha-Synuclein assembles into higher-order multimers upon membrane binding to promote SNARE complex formation. *Proc Natl Acad Sci U S A, 111*(40), E4274-4283. doi:10.1073/pnas.1416598111

Burre, J., Sharma, M., Tsetsenis, T., Buchman, V., Etherton, M. R., & Sudhof, T. C. (2010). Alpha-synuclein promotes SNARE-complex assembly in vivo and in vitro. *Science, 329*(5999), 1663-1667. doi:10.1126/science.1195227

Butler, D. A., Scott, M. R., Bockman, J. M., Borchelt, D. R., Taraboulos, A., Hsiao, K. K., . . . Prusiner, S. B. (1988). Scrapie-infected murine neuroblastoma cells produce protease-resistant prion proteins. *J Virol, 62*(5), 1558-1564. doi:10.1128/JVI.62.5.1558-1564.1988

Caiati, M. D., Safiulina, V. F., Fattorini, G., Sivakumaran, S., Legname, G., & Cherubini, E. (2013). PrPC controls via protein kinase A the direction of synaptic plasticity in the immature hippocampus. *J Neurosci, 33*(7), 2973-2983. doi:10.1523/JNEUROSCI.4149-12.2013

Calero, O., Bullido, M. J., Clarimon, J., Frank-Garcia, A., Martinez-Martin, P., Lleo, A., . . . Calero, M. (2011). Genetic cross-interaction between APOE and PRNP in sporadic Alzheimer's and Creutzfeldt-Jakob diseases. *PLoS ONE, 6*(7), e22090. doi:10.1371/journal.pone.0022090

Calero, O., Bullido, M. J., Clarimon, J., Frank-Garcia, A., Martinez-Martin, P., Lleo, A., . . . Calero, M. (2012). A common BACE1 polymorphism is a risk factor for sporadic Creutzfeldt-Jakob disease. *PLoS ONE, 7*(8), e43926. doi:10.1371/journal.pone.0043926

Carlson, G. A., Kingsbury, D. T., Goodman, P. A., Coleman, S., Marshall, S. T., DeArmond, S., . . . Prusiner, S. B. (1986). Linkage of prion protein and scrapie incubation time genes. *Cell, 46*(4), 503-511. doi:10.1016/0092-8674(86)90875-5

Casalone, C., Zanusso, G., Acutis, P., Ferrari, S., Capucci, L., Tagliavini, F., . . . Caramelli, M. (2004). Identification of a second bovine amyloidotic spongiform encephalopathy: molecular similarities with sporadic Creutzfeldt-Jakob disease. *Proc Natl Acad Sci U S A, 101*(9), 3065-3070. doi:10.1073/pnas.0305777101

Castilla, J., Saa, P., Hetz, C., & Soto, C. (2005). In vitro generation of infectious scrapie prions. *Cell, 121*(2), 195-206. doi:10.1016/j.cell.2005.02.011

Cataldo, A. M., Peterhoff, C. M., Troncoso, J. C., Gomez-Isla, T., Hyman, B. T., & Nixon, R. A. (2000). Endocytic pathway abnormalities precede amyloid beta deposition in sporadic

Alzheimer's disease and Down syndrome: differential effects of APOE genotype and presenilin mutations. *Am J Pathol, 157*(1), 277-286. doi:10.1016/s0002-9440(10)64538-5

Caughey, B., Race, R. E., Ernst, D., Buchmeier, M. J., & Chesebro, B. (1989). Prion protein biosynthesis in scrapie-infected and uninfected neuroblastoma cells. *J Virol, 63*(1), 175-181. doi:10.1128/JVI.63.1.175-181.1989

Caughey, B., & Raymond, G. J. (1991). The scrapie-associated form of PrP is made from a cell surface precursor that is both protease- and phospholipase-sensitive. *J Biol Chem, 266*(27), 18217-18223.

Caughey, B., & Raymond, G. J. (1993). Sulfated polyanion inhibition of scrapie-associated PrP accumulation in cultured cells. *J Virol, 67*(2), 643-650. doi:10.1128/JVI.67.2.643-650.1993

Chambers, S. M., Fasano, C. A., Papapetrou, E. P., Tomishima, M., Sadelain, M., & Studer, L. (2009). Highly efficient neural conversion of human ES and iPS cells by dual inhibition of SMAD signaling. *Nat Biotechnol, 27*(3), 275-280. doi:10.1038/nbt.1529

Chao, D. S., Hay, J. C., Winnick, S., Prekeris, R., Klumperman, J., & Scheller, R. H. (1999). SNARE membrane trafficking dynamics in vivo. *J Cell Biol, 144*(5), 869-881. doi:10.1083/jcb.144.5.869

Chasseigneaux, S., Pastore, M., Britton-Davidian, J., Manie, E., Stern, M. H., Callebert, J., . . . Lehmann, S. (2008). Genetic heterogeneity versus molecular analysis of prion susceptibility in neuroblasma N2a sublines. *Arch Virol, 153*(9), 1693-1702. doi:10.1007/s00705-008-0177-8

Chen, C., & Dong, X. P. (2016). Epidemiological characteristics of human prion diseases. *Infect Dis Poverty, 5*(1), 47. doi:10.1186/s40249-016-0143-8

Chen, J. A., Chen, Z., Won, H., Huang, A. Y., Lowe, J. K., Wojta, K., . . . Coppola, G. (2018). Joint genome-wide association study of progressive supranuclear palsy identifies novel susceptibility loci and genetic correlation to neurodegenerative diseases. *Mol Neurodegener, 13*(1), 41. doi:10.1186/s13024-018-0270-8

Chen, S. G., Teplow, D. B., Parchi, P., Teller, J. K., Gambetti, P., & Autilio-Gambetti, L. (1995). Truncated forms of the human prion protein in normal brain and in prion diseases. *J Biol Chem, 270*(32), 19173-19180. doi:10.1074/jbc.270.32.19173

Cheng, J., Cebotaru, V., Cebotaru, L., & Guggino, W. B. (2010). Syntaxin 6 and CAL mediate the degradation of the cystic fibrosis transmembrane conductance regulator. *Molecular Biology of the Cell, 21*(7), 1178--1187. doi:10.1091/mbc.e09-03-0229

Cheng, J., & Guggino, W. (2013). Ubiquitination and Degradation of CFTR by the E3 Ubiquitin Ligase MARCH2 through Its Association with Adaptor Proteins CAL and STX6. *PLoS ONE*. doi:10.1371/journal.pone.0068001

Cheng, L., Zhao, W., & Hill, A. F. (2018). Exosomes and their role in the intercellular trafficking of normal and disease associated prion proteins. *Molecular Aspects of Medicine, 60*, 62--68. doi:10.1016/J.MAM.2017.11.011

Chesebro, B., Race, R., Wehrly, K., Nishio, J., Bloom, M., Lechner, D., . . . et al. (1985). Identification of scrapie prion protein-specific mRNA in scrapie-infected and uninfected brain. *Nature, 315*(6017), 331-333. doi:10.1038/315331a0

Choi, B. K., Choi, M. G., Kim, J. Y., Yang, Y., Lai, Y., Kweon, D. H., . . . Shin, Y. K. (2013). Large alpha-synuclein oligomers inhibit neuronal SNARE-mediated vesicle docking. *Proc Natl Acad Sci U S A, 110*(10), 4087-4092. doi:10.1073/pnas.1218424110

Choudhury, A., Marks, D. L., Proctor, K. M., Gould, G. W., & Pagano, R. E. (2006). Regulation of caveolar endocytosis by syntaxin 6-dependent delivery of membrane components to the cell surface. *Nature Cell Biology, 8*(4), 317--328. doi:10.1038/ncb1380

Chouhan, J. K., Fowler, S. B., Webster, C. I., & Teeling, J. L. (2017). The ME7 prion model of neurodegeneration as a tool to understand and target neuroinflammation in Alzheimer's disease. *Drug Discovery Today: Disease Models, 25-26*, 45-52. doi:10.1016/j.ddmod.2018.10.004

Clarke, M. C., & Haig, D. A. (1970). Multiplication of scrapie agent in cell culture. *Res Vet Sci, 11*(5), 500-501.

Clary, D. O., Griff, I. C., & Rothman, J. E. (1990). SNAPs, a family of NSF attachment proteins involved in intracellular membrane fusion in animals and yeast. *Cell, 61*(4), 709-721. doi:10.1016/0092-8674(90)90482-t

Collado-Torres, L., Burke, E. E., Peterson, A., Shin, J., Straub, R. E., Rajpurohit, A., . . . Jaffe, A. E. (2019). Regional Heterogeneity in Gene Expression, Regulation, and Coherence in the Frontal Cortex and Hippocampus across Development and Schizophrenia. *Neuron, 103*(2), 203-216 e208. doi:10.1016/j.neuron.2019.05.013

Collinge, J., & Clarke, A. R. (2007). A general model of prion strains and their pathogenicity. *Science, 318*(5852), 930-936. doi:10.1126/science.1138718

Collinge, J., Gorham, M., Hudson, F., Kennedy, A., Keogh, G., Pal, S., . . . Darbyshire, J. (2009). Safety and efficacy of quinacrine in human prion disease (PRION-1 study): a patient-preference trial. *Lancet Neurol, 8*(4), 334-344. doi:10.1016/S1474-4422(09)70049-3

Collinge, J., Palmer, M. S., & Dryden, A. J. (1991). Genetic predisposition to iatrogenic Creutzfeldt-Jakob disease. *Lancet (London, England), 337*(8755), 1441--1442. doi:10.1016/0140-6736(91)93128-v

Collinge, J., Whitfield, J., McKintosh, E., Beck, J., Mead, S., Thomas, D. J., & Alpers, M. P. (2006). Kuru in the 21st century--an acquired human prion disease with very long incubation periods. *Lancet, 367*(9528), 2068-2074. doi:10.1016/S0140-6736(06)68930-7

Collinge, J., Whittington, M. A., Sidle, K. C., Smith, C. J., Palmer, M. S., Clarke, A. R., & Jefferys, J. G. (1994). Prion protein is necessary for normal synaptic function. *Nature, 370*(6487), 295-297. doi:10.1038/370295a0

Collins, S. J., Sanchez-Juan, P., Masters, C. L., Klug, G. M., van Duijn, C., Poleggi, A., . . . Will, R. G. (2006). Determinants of diagnostic investigation sensitivities across the clinical spectrum of sporadic Creutzfeldt-Jakob disease. *Brain, 129*(Pt 9), 2278-2287. doi:10.1093/brain/awl159

Cong, L., Ran, F. A., Cox, D., Lin, S., Barretto, R., Habib, N., . . . Zhang, F. (2013). Multiplex genome engineering using CRISPR/Cas systems. *Science, 339*(6121), 819-823. doi:10.1126/science.1231143

Conibear, E., Cleck, J. N., & Stevens, T. H. (2003). Vps51p mediates the association of the GARP (Vps52/53/54) complex with the late Golgi t-SNARE Tlg1p. *Mol Biol Cell, 14*(4), 1610-1623. doi:10.1091/mbc.e02-10-0654

Conibear, E., & Stevens, T. H. (2000). Vps52p, Vps53p, and Vps54p form a novel multisubunit complex required for protein sorting at the yeast late Golgi. *Mol Biol Cell, 11*(1), 305-323. doi:10.1091/mbc.11.1.305

Corbett, G. T., Wang, Z., Hong, W., Colom-Cadena, M., Rose, J., Liao, M., . . . Walsh, D. M. (2020). PrP is a central player in toxicity mediated by soluble aggregates of

neurodegeneration-causing proteins. *Acta Neuropathol, 139*(3), 503-526. doi:10.1007/s00401-019-02114-9

Cordier, C., Bencsik, A., Philippe, S., Betemps, D., Ronzon, F., Calavas, D., . . . Baron, T. (2006). Transmission and characterization of bovine spongiform encephalopathy sources in two ovine transgenic mouse lines (TgOvPrP4 and TgOvPrP59). *J Gen Virol, 87*(Pt 12), 3763-3771. doi:10.1099/vir.0.82062-0

Cosker, K., Mallach, A., Limaye, J., Piers, T. M., Staddon, J., Neame, S. J., . . . Pocock, J. M. (2021). Microglial signalling pathway deficits associated with the patient derived R47H TREM2 variants linked to AD indicate inability to activate inflammasome. *Sci Rep, 11*(1), 13316. doi:10.1038/s41598-021-91207-1

Courageot, M. P., Daude, N., Nonno, R., Paquet, S., Di Bari, M. A., Le Dur, A., . . . Vilette, D. (2008). A cell line infectible by prion strains from different species. *J Gen Virol, 89*(Pt 1), 341-347. doi:10.1099/vir.0.83344-0

Creutzfeldt-Jakob Disease International Surveillance Network. (2019). CJD Surveillance Data 1993-2018. Retrieved from https://www.eurocjd.ed.ac.uk/surveillance%20data%201.html

Creutzfeldt-Jakob Disease International Surveillance Network. (2021). vCJD Cases Worldwide. Retrieved from https://www.eurocjd.ed.ac.uk/data_tables

Creutzfeldt, H. G. (1920). Über eine eigenartige herdförmige Erkrankung des Zentralnervensystems (vorläufige Mitteilung). *Zeitschrift für die gesamte Neurologie und Psychiatrie, 57*(1), 1-18.

Cuillé, J., & Chelle, P. (1936). La maladie dite “tremblante du mouton” est-elle inoculable? *CR Seances Acad Sci, 203*, 1552-1554.

Cunningham, C., Deacon, R. M., Chan, K., Boche, D., Rawlins, J. N., & Perry, V. H. (2005). Neuropathologically distinct prion strains give rise to similar temporal profiles of behavioral deficits. *Neurobiol Dis, 18*(2), 258-269. doi:10.1016/j.nbd.2004.08.015

de Brito, G., Lupinacci, F. C., Beraldo, F. H., Santos, T. G., Roffe, M., Lopes, M. H., . . . Hajj, G. N. (2017). Loss of prion protein is associated with the development of insulin resistance and obesity. *Biochemical Journal, 474*, 2981-2991. doi:10.1042/Bcj20170137

De Cecco, E., Celauro, L., Vanni, S., Grandolfo, M., Bistaffa, E., Moda, F., . . . Legname, G. (2020). The uptake of tau amyloid fibrils is facilitated by the cellular prion protein and hampers prion propagation in cultured cells. *J Neurochem, 155*(5), 577-591. doi:10.1111/jnc.15040

de Leeuw, C. A., Mooij, J. M., Heskes, T., & Posthuma, D. (2015). MAGMA: generalized gene-set analysis of GWAS data. *PLoS Comput Biol, 11*(4), e1004219. doi:10.1371/journal.pcbi.1004219

Deacon, R. M. (2006a). Assessing nest building in mice. *Nat Protoc, 1*(3), 1117-1119. doi:10.1038/nprot.2006.170

Deacon, R. M. (2006b). Burrowing in rodents: a sensitive method for detecting behavioral dysfunction. *Nat Protoc, 1*(1), 118-121. doi:10.1038/nprot.2006.19

Deacon, R. M. (2013). Measuring motor coordination in mice. *J Vis Exp*(75), e2609. doi:10.3791/2609

Dickinson, A. G., Meikle, V. M., & Fraser, H. (1968). Identification of a gene which controls the incubation period of some strains of scrapie agent in mice. *J Comp Pathol, 78*(3), 293-299. doi:10.1016/0021-9975(68)90005-4

Doench, J. G., Fusi, N., Sullender, M., Hegde, M., Vaimberg, E. W., Donovan, K. F., . . . Root, D. E. (2016). Optimized sgRNA design to maximize activity and minimize off-target effects of CRISPR-Cas9. *Nat Biotechnol, 34*(2), 184-191. doi:10.1038/nbt.3437

Doh-Ura, K., Iwaki, T., & Caughey, B. (2000). Lysosomotropic agents and cysteine protease inhibitors inhibit scrapie-associated prion protein accumulation. *J Virol, 74*(10), 4894-4897. doi:10.1128/jvi.74.10.4894-4897.2000

Doudna, J. A., & Charpentier, E. (2014). Genome editing. The new frontier of genome engineering with CRISPR-Cas9. *Science, 346*(6213), 1258096. doi:10.1126/science.1258096

Du, J., Liu, X., Wu, Y., Zhu, J., & Tang, Y. (2016). Essential role of STX6 in esophageal squamous cell carcinoma growth and migration. *Biochemical and Biophysical Research Communications, 472*(1), 60--67. doi:10.1016/j.bbrc.2016.02.061

Du, Y., Shen, J., Hsu, J. L., Han, Z., Hsu, M. C., Yang, C. C., . . . Hung, M. C. (2014). Syntaxin 6-mediated Golgi translocation plays an important role in nuclear functions of EGFR through microtubule-dependent trafficking. *Oncogene, 33*(6), 756--770. doi:10.1038/onc.2013.1

Duffy, P., Wolf, J., Collins, G., DeVoe, A. G., Streeten, B., & Cowen, D. (1974). Letter: Possible person-to-person transmission of Creutzfeldt-Jakob disease. *N Engl J Med, 290*(12), 692-693.

Edvardson, S., Cinnamon, Y., Ta-Shma, A., Shaag, A., Yim, Y. I., Zenvirt, S., . . . Elpeleg, O. (2012). A deleterious mutation in DNAJC6 encoding the neuronal-specific clathrin-uncoating co-chaperone auxilin, is associated with juvenile parkinsonism. *PLoS ONE, 7*(5), e36458. doi:10.1371/journal.pone.0036458

Encalada, S. E., Szpankowski, L., Xia, C. H., & Goldstein, L. S. B. (2011). Stable kinesin and dynein assemblies drive the axonal transport of mammalian prion protein vesicles. *Cell, 144*(4), 551--565. doi:10.1016/j.cell.2011.01.021

Encode Project Consortium. (2012). An integrated encyclopedia of DNA elements in the human genome. *Nature, 489*(7414), 57-74. doi:10.1038/nature11247

Fairfax, B. P., Humburg, P., Makino, S., Naranbhai, V., Wong, D., Lau, E., . . . Knight, J. C. (2014). Innate immune activity conditions the effect of regulatory variants upon monocyte gene expression. *Science, 343*(6175), 1246949. doi:10.1126/science.1246949

Falcon, B., Zhang, W., Murzin, A. G., Murshudov, G., Garringer, H. J., Vidal, R., . . . Goedert, M. (2018). Structures of filaments from Pick's disease reveal a novel tau protein fold. *Nature, 561*(7721), 137-140. doi:10.1038/s41586-018-0454-y

Falcon, B., Zivanov, J., Zhang, W., Murzin, A. G., Garringer, H. J., Vidal, R., . . . Scheres, S. H. W. (2019). Novel tau filament fold in chronic traumatic encephalopathy encloses hydrophobic molecules. *Nature, 568*(7752), 420-423. doi:10.1038/s41586-019-1026-5

Fantom Consortium and the RIKEN PMI and CLST, Forrest, A. R., Kawaji, H., Rehli, M., Baillie, J. K., de Hoon, M. J., . . . Hayashizaki, Y. (2014). A promoter-level mammalian expression atlas. *Nature, 507*(7493), 462-470. doi:10.1038/nature13182

Faris, R., Moore, R. A., Ward, A., Race, B., Dorward, D. W., Hollister, J. R., . . . Priola, S. A. (2017). Cellular prion protein is present in mitochondria of healthy mice. *Sci Rep, 7*, 41556. doi:10.1038/srep41556

Fasshauer, D., Sutton, R. B., Brunger, A. T., & Jahn, R. (1998). Conserved structural features of the synaptic fusion complex: SNARE proteins reclassified as Q- and R-SNAREs. *Proc Natl Acad Sci U S A, 95*(26), 15781-15786. doi:10.1073/pnas.95.26.15781

Fehlinger, A., Wolf, H., Hossinger, A., Duernberger, Y., Pleschka, C., Riemschoss, K., . . . Vorberg, I. M. (2017). Prion strains depend on different endocytic routes for productive infection. *Scientific Reports, 7*(1), 6923. doi:10.1038/s41598-017-07260-2

Feldmann, A., Winterstein, C., White, R., Trotter, J., & Kramer-Albers, E. M. (2009). Comprehensive analysis of expression, subcellular localization, and cognate pairing of SNARE proteins in oligodendrocytes. *J Neurosci Res, 87*(8), 1760-1772. doi:10.1002/jnr.22020

Felton, L. M., Cunningham, C., Rankine, E. L., Waters, S., Boche, D., & Perry, V. H. (2005). MCP-1 and murine prion disease: Separation of early behavioural dysfunction from overt clinical disease. *Neurobiology of Disease, 20*(2), 283--295. doi:10.1016/j.nbd.2005.03.008

Ferrari, R., Ryten, M., Simone, R., Trabzuni, D., Nicolaou, N., Hondhamuni, G., . . . de Silva, R. (2014). Assessment of common variability and expression quantitative trait loci for genome-wide associations for progressive supranuclear palsy. *Neurobiol Aging, 35*(6), 1514 e1511-1512. doi:10.1016/j.neurobiolaging.2014.01.010

Ferreira, D. G., Temido-Ferreira, M., Vicente Miranda, H., Batalha, V. L., Coelho, J. E., Szego, E. M., . . . Outeiro, T. F. (2017). alpha-synuclein interacts with PrP(C) to induce cognitive impairment through mGluR5 and NMDAR2B. *Nat Neurosci, 20*(11), 1569-1579. doi:10.1038/nn.4648

Ferreira, N. C., Marques, I. A., Conceio, W. A., Macedo, B., Machado, C. S., Mascarello, A., . . . Cordeiro, Y. (2014). Anti-Prion Activity of a Panel of Aromatic Chemical Compounds: In Vitro and In Silico Approaches. *PLoS ONE, 9*(1), e84531. doi:10.1371/journal.pone.0084531

Ferrer, I., Rivera, R., Blanco, R., & Mart. (1999). Expression of proteins linked to exocytosis and neurotransmission in patients with Creutzfeldt-Jakob disease. *Neurobiology of Disease, 6*(2), 92--100. doi:10.1006/nbdi.1998.0226

Fevrier, B., Vilette, D., Archer, F., Loew, D., Faigle, W., Vidal, M., . . . Raposo, G. (2004). Cells release prions in association with exosomes. *Proceedings of the National Academy of Sciences of the United States of America, 101*(26), 9683--9688. doi:10.1073/pnas.0308413101

Fitzpatrick, A. W. P., Falcon, B., He, S., Murzin, A. G., Murshudov, G., Garringer, H. J., . . . Scheres, S. H. W. (2017). Cryo-EM structures of tau filaments from Alzheimer's disease. *Nature, 547*(7662), 185-190. doi:10.1038/nature23002

Fluharty, B. R., Biasini, E., Stravalaci, M., Sclip, A., Diomede, L., Balducci, C., . . . Harris, D. A. (2013). An N-terminal fragment of the prion protein binds to amyloid-beta oligomers and inhibits their neurotoxicity in vivo. *J Biol Chem, 288*(11), 7857-7866. doi:10.1074/jbc.M112.423954

Foley, K. P., & Klip, A. (2014). Dynamic GLUT4 sorting through a syntaxin-6 compartment in muscle cells is derailed by insulin resistance-causing ceramide. *Biology Open, 3*(5), 314--325. doi:10.1242/bio.20147898

Foliaki, S. T., Groveman, B. R., Yuan, J., Walters, R., Zhang, S., Tesar, P., . . . Haigh, C. L. (2020). Pathogenic Prion Protein Isoforms Are Not Present in Cerebral Organoids Generated from Asymptomatic Donors Carrying the E200K Mutation Associated with Familial Prion Disease. *Pathogens, 9*(6). doi:10.3390/pathogens9060482

Ford, M. J., Burton, L. J., Morris, R. J., & Hall, S. M. (2002). Selective expression of prion protein in peripheral tissues of the adult mouse. *Neuroscience, 113*(1), 177-192. doi:10.1016/s0306-4522(02)00155-0

Fraser, H., & Dickinson, A. G. (1973). Scrapie in mice. Agent-strain differences in the distribution and intensity of grey matter vacuolation. *J Comp Pathol, 83*(1), 29-40. doi:10.1016/0021-9975(73)90024-8

Fraser, H., Pearson, G. R., McConnell, I., Bruce, M. E., Wyatt, J. M., & Gruffydd-Jones, T. J. (1994). Transmission of feline spongiform encephalopathy to mice. *Vet Rec, 134*(17), 449. doi:10.1136/vr.134.17.449

Freir, D. B., Nicoll, A. J., Klyubin, I., Panico, S., Mc Donald, J. M., Risse, E., . . . Collinge, J. (2011). Interaction between prion protein and toxic amyloid beta assemblies can be therapeutically targeted at multiple sites. *Nat Commun, 2*(May), 336. doi:10.1038/ncomms1341

Frigg, R., Klein, M. A., Hegyi, I., Zinkernagel, R. M., & Aguzzi, A. (1999). Scrapie pathogenesis in subclinically infected B-cell-deficient mice. *Journal of Virology, 73*(11), 9584--9588.

Fromer, M., Roussos, P., Sieberts, S. K., Johnson, J. S., Kavanagh, D. H., Perumal, T. M., . . . Sklar, P. (2016). Gene expression elucidates functional impact of polygenic risk for schizophrenia. *Nat Neurosci, 19*(11), 1442-1453. doi:10.1038/nn.4399

Fu, Y., Foden, J. A., Khayter, C., Maeder, M. L., Reyon, D., Joung, J. K., & Sander, J. D. (2013). High-frequency off-target mutagenesis induced by CRISPR-Cas nucleases in human cells. *Nat Biotechnol, 31*(9), 822-826. doi:10.1038/nbt.2623

Fukuda, H., Nakamura, N., & Hirose, S. (2006). MARCH-III is a novel component of endosomes with properties similar to those of MARCH-II. *Journal of Biochemistry, 139*(1), 137--145. doi:10.1093/jb/mvj012

Fusco, G., Pape, T., Stephens, A. D., Mahou, P., Costa, A. R., Kaminski, C. F., . . . De Simone, A. (2016). Structural basis of synaptic vesicle assembly promoted by alpha-synuclein. *Nat Commun, 7*, 12563. doi:10.1038/ncomms12563

Gajdusek, D. C., Gibbs, C. J., & Alpers, M. (1966). Experimental transmission of a Kuru-like syndrome to chimpanzees. *Nature, 209*(5025), 794-796. doi:10.1038/209794a0

Gajdusek, D. C., & Zigas, V. (1959). Kuru; clinical, pathological and epidemiological study of an acute progressive degenerative disease of the central nervous system among natives of the Eastern Highlands of New Guinea. *Am J Med, 26*(3), 442-469. doi:10.1016/0002-9343(59)90251-7

Gallagher, M. D., & Chen-Plotkin, A. S. (2018). The Post-GWAS Era: From Association to Function. In (Vol. 102, pp. 717--730).

Galvan, C., Camoletto, P. G., Dotti, C. G., Aguzzi, A., & Ledesma, M. D. (2005). Proper axonal distribution of PrP(C) depends on cholesterol-sphingomyelin-enriched membrane domains and is developmentally regulated in hippocampal neurons. *Mol Cell Neurosci, 30*(3), 304-315. doi:10.1016/j.mcn.2005.07.003

Gambetti, P., Dong, Z., Yuan, J., Xiao, X., Zheng, M., Alshekhlee, A., . . . Zou, W. Q. (2008). A novel human disease with abnormal prion protein sensitive to protease. *Ann Neurol, 63*(6), 697-708. doi:10.1002/ana.21420

Ganley, I. G., Espinosa, E., & Pfeffer, S. R. (2008). A syntaxin 10-SNARE complex distinguishes two distinct transport routes from endosomes to the trans-Golgi in human cells. *J Cell Biol, 180*(1), 159-172. doi:10.1083/jcb.200707136

Garca-Melero, A., Reverter, M., Hoque, M., Meneses-Salas, E., Koese, M., Conway, J. R. W., . . . Rentero, C. (2016). Annexin A6 and late endosomal cholesterol modulate integrin recycling and cell migration. *Journal of Biological Chemistry, 291*(3), 1320--1335. doi:10.1074/jbc.M115.683557

Gasperini, L., Meneghetti, E., Pastore, B., Benetti, F., & Legname, G. (2015). Prion protein and copper cooperatively protect neurons by modulating NMDA receptor through S-nitrosylation. *Antioxid Redox Signal, 22*(9), 772-784. doi:10.1089/ars.2014.6032

Gerstenecker, A., Roberson, E. D., Schellenberg, G. D., Standaert, D. G., Shprecher, D. R., Kluger, B. M., & Litvan, I. (2017). Genetic influences on cognition in progressive supranuclear palsy. *Movement Disorders, 32*(12), 1764--1771. doi:10.1002/mds.27196

Ghetti, B., Tagliavini, F., Takao, M., Bugiani, O., & Piccardo, P. (2003). Hereditary prion protein amyloidoses. *Clin Lab Med, 23*(1), 65-85, viii. doi:10.1016/s0272-2712(02)00064-1

Gibbs, C. J., Jr., Gajdusek, D. C., Asher, D. M., Alpers, M. P., Beck, E., Daniel, P. M., & Matthews, W. B. (1968). Creutzfeldt-Jakob disease (spongiform encephalopathy): transmission to the chimpanzee. *Science, 161*(3839), 388-389. doi:10.1126/science.161.3839.388

Gilbert, L. A., Larson, M. H., Morsut, L., Liu, Z., Brar, G. A., Torres, S. E., . . . Qi, L. S. (2013). CRISPR-mediated modular RNA-guided regulation of transcription in eukaryotes. *Cell, 154*(2), 442-451. doi:10.1016/j.cell.2013.06.044

Gilch, S., Kehler, C., & Schatzl, H. M. (2006). The prion protein requires cholesterol for cell surface localization. *Mol Cell Neurosci, 31*(2), 346-353. doi:10.1016/j.mcn.2005.10.008

Gill, O. N., Spencer, Y., Richard-Loendt, A., Kelly, C., Brown, D., Sinka, K., . . . Brandner, S. (2020). Prevalence in Britain of abnormal prion protein in human appendices before and after exposure to the cattle BSE epizootic. *Acta Neuropathol, 139*(6), 965-976. doi:10.1007/s00401-020-02153-7

Gimbel, D. A., Nygaard, H. B., Coffey, E. E., Gunther, E. C., Lauren, J., Gimbel, Z. A., & Strittmatter, S. M. (2010). Memory impairment in transgenic Alzheimer mice requires cellular prion protein. *J Neurosci, 30*(18), 6367-6374. doi:10.1523/JNEUROSCI.0395-10.2010

Giusti-Rodríguez, P., Lu, L., Yang, Y., Crowley, C. A., Liu, X., Juric, I., . . . Sullivan, P. F. (2019). Using three-dimensional regulatory chromatin interactions from adult and fetal cortex to interpret genetic results for psychiatric disorders and cognitive traits. *bioRxiv*.

Glasser, M. F., Coalson, T. S., Robinson, E. C., Hacker, C. D., Harwell, J., Yacoub, E., . . . Van Essen, D. C. (2016). A multi-modal parcellation of human cerebral cortex. *Nature, 536*(7615), 171-178. doi:10.1038/nature18933

Godsave, S. F., Wille, H., Kujala, P., Latawiec, D., DeArmond, S. J., Serban, A., . . . Peters, P. J. (2008). Cryo-immunogold electron microscopy for prions: Toward identification of a conversion site. *Journal of Neuroscience, 28*(47), 12489--12499. doi:10.1523/JNEUROSCI.4474-08.2008

Goold, R., McKinnon, C., Rabbanian, S., Collinge, J., Schiavo, G., & Tabrizi, S. J. (2013). Alternative fates of newly formed PrPSc upon prion conversion on the plasma membrane. *Journal of Cell Science, 126*(16), 3552--3562. doi:10.1242/jcs.120477

Goold, R., Rabbanian, S., Sutton, L., Andre, R., Arora, P., Moonga, J., . . . Tabrizi, S. J. (2011). Rapid cell-surface prion protein conversion revealed using a novel cell system. *Nature Communications, 2*(1), 281. doi:10.1038/ncomms1282

Gordon, W. S. (1946). Advances in veterinary research. Louping-ill, tick-borne fever and scrapie. *Veterinary Record, 58*, 516-520.

Grassi, D., Plonka, F. B., Oksdath, M., Guil, A. N., Sosa, L. J., & Quiroga, S. (2015). Selected SNARE proteins are essential for the polarized membrane insertion of igf-1 receptor and the regulation of initial axonal outgrowth in neurons. *Cell Discovery, 1*. doi:10.1038/celldisc.2015.23

Griffith, J. S. (1967). Self-replication and scrapie. *Nature, 215*(5105), 1043-1044. doi:10.1038/2151043a0

Grizenkova, J., Akhtar, S., Brandner, S., Collinge, J., & Lloyd, S. E. (2014). Microglial Cx3cr1 knockout reduces prion disease incubation time in mice. *BMC Neurosci, 15*, 44. doi:10.1186/1471-2202-15-44

Grizenkova, J., Akhtar, S., Hummerich, H., Tomlinson, A., Asante, E. A., Wenborn, A., . . . Lloyd, S. E. (2012). Overexpression of the Hspa13 (Stch) gene reduces prion disease incubation time in mice. *Proc Natl Acad Sci U S A, 109*(34), 13722-13727. doi:10.1073/pnas.1208917109

Groveman, B. R., Ferreira, N. C., Foliaki, S. T., Walters, R. O., Winkler, C. W., Race, B., . . . Haigh, C. L. (2021). Human cerebral organoids as a therapeutic drug screening model for Creutzfeldt-Jakob disease. *Sci Rep, 11*(1), 5165. doi:10.1038/s41598-021-84689-6

Groveman, B. R., Foliaki, S. T., Orru, C. D., Zanusso, G., Carroll, J. A., Race, B., & Haigh, C. L. (2019). Sporadic Creutzfeldt-Jakob disease prion infection of human cerebral organoids. *Acta Neuropathol Commun, 7*(1), 90. doi:10.1186/s40478-019-0742-2

Grundberg, E., Small, K. S., Hedman, A. K., Nica, A. C., Buil, A., Keildson, S., . . . Consortium, M. T. H. E. R. (2012). Mapping cis- and trans-regulatory effects across multiple tissues in twins. *Nat Genet, 44*(10), 1084-1089. doi:10.1038/ng.2394

GTEx Consortium. (2015). Human genomics. The Genotype-Tissue Expression (GTEx) pilot analysis: multitissue gene regulation in humans. *Science, 348*(6235), 648-660. doi:10.1126/science.1262110

Gu, Y., Princely Abudu, Y., Kumar, S., Bissa, B., Choi, S. W., Jia, J., . . . Deretic, V. (2019). Mammalian Atg8 proteins regulate lysosome and autolysosome biogenesis through SNAREs. *EMBO J, 38*(22), e101994. doi:10.15252/embj.2019101994

Haas, L. T., Salazar, S. V., Kostylev, M. A., Um, J. W., Kaufman, A. C., & Strittmatter, S. M. (2016). Metabotropic glutamate receptor 5 couples cellular prion protein to intracellular signalling in Alzheimer's disease. *Brain, 139*(Pt 2), 526-546. doi:10.1093/brain/awv356

Haase, B., Doherr, M. G., Seuberlich, T., Drogemuller, C., Dolf, G., Nicken, P., . . . Leeb, T. (2007). PRNP promoter polymorphisms are associated with BSE susceptibility in Swiss and German cattle. *BMC Genet, 8*, 15. doi:10.1186/1471-2156-8-15

Hadlow, W. J. (1959). Scrapie and Kuru. *The Lancet, 274*(7097), 289-290. doi:10.1016/s0140-6736(59)92081-1

Haigh, C. L., & Collins, S. J. (2016). Endoproteolytic cleavage as a molecular switch regulating and diversifying prion protein function. *Neural Regen Res, 11*(2), 238-239. doi:10.4103/1673-5374.177726

Hannaoui, S., Gougerot, A., Privat, N., Levavasseur, E., Bizat, N., Hauw, J. J., . . . Haik, S. (2014). Cycline efficacy on the propagation of human prions in primary cultured neurons is strain-specific. *J Infect Dis, 209*(7), 1144-1148. doi:10.1093/infdis/jit623

Harrison, P. M., Khachane, A., & Kumar, M. (2010). Genomic assessment of the evolution of the prion protein gene family in vertebrates. *Genomics, 95*(5), 268-277. doi:10.1016/j.ygeno.2010.02.008

Hatakeyama, H., & Kanzaki, M. (2011). Molecular Basis of Insulin-Responsive GLUT4 Trafficking Systems Revealed by Single Molecule Imaging. *Traffic, 12*(12), 1805--1820. doi:10.1111/j.1600-0854.2011.01279.x

Heath, C. A., Cooper, S. A., Murray, K., Lowman, A., Henry, C., MacLeod, M. A., . . . Will, R. G. (2010). Validation of diagnostic criteria for variant Creutzfeldt-Jakob disease. *Annals of Neurology, 67*(6), n/a--n/a. doi:10.1002/ana.21987

Heiseke, A., Schobel, S., Lichtenthaler, S. F., Vorberg, I., Groschup, M. H., Kretzschmar, H., . . . Nunziante, M. (2008). The novel sorting nexin SNX33 interferes with cellular PrP formation by modulation of PrP shedding. *Traffic, 9*(7), 1116-1129. doi:10.1111/j.1600-0854.2008.00750.x

Heisler, F. F., Pechmann, Y., Wieser, I., Altmeppen, H. C., Veenendaal, L., Muhia, M., . . . Kneussel, M. (2018). Muskelin Coordinates PrPC Lysosome versus Exosome Targeting and Impacts Prion Disease Progression. *Neuron, 0*(0). doi:10.1016/j.neuron.2018.08.010

Hernandez-Zimbron, L. F., & Rivas-Arancibia, S. (2016). Syntaxin 5 Overexpression and beta-Amyloid 1-42 Accumulation in Endoplasmic Reticulum of Hippocampal Cells in Rat Brain Induced by Ozone Exposure. *Biomed Res Int, 2016*, 2125643. doi:10.1155/2016/2125643

Hill, A. F., Desbruslais, M., Joiner, S., Sidle, K. C., Gowland, I., Collinge, J., . . . Lantos, P. (1997). The same prion strain causes vCJD and BSE. *Nature, 389*(6650), 448-450, 526. doi:10.1038/38925

Hill, A. F., Joiner, S., Wadsworth, J. D., Sidle, K. C., Bell, J. E., Budka, H., . . . Collinge, J. (2003). Molecular classification of sporadic Creutzfeldt-Jakob disease. *Brain, 126*(Pt 6), 1333-1346. doi:10.1093/brain/awg125

Hnisz, D., Abraham, B. J., Lee, T. I., Lau, A., Saint-Andre, V., Sigova, A. A., . . . Young, R. A. (2013). Super-enhancers in the control of cell identity and disease. *Cell, 155*(4), 934-947. doi:10.1016/j.cell.2013.09.053

Hodge, R. D., Bakken, T. E., Miller, J. A., Smith, K. A., Barkan, E. R., Graybuck, L. T., . . . Lein, E. S. (2019). Conserved cell types with divergent features in human versus mouse cortex. *Nature, 573*(7772), 61-68. doi:10.1038/s41586-019-1506-7

Hoglinger, G. U., Melhem, N. M., Dickson, D. W., Sleiman, P. M., Wang, L. S., Klei, L., . . . Schellenberg, G. D. (2011). Identification of common variants influencing risk of the tauopathy progressive supranuclear palsy. *Nat Genet, 43*(7), 699-705. doi:10.1038/ng.859

Hohenstein, A. C., & Roche, P. A. (2001). SNAP-29 is a promiscuous syntaxin-binding SNARE. *Biochem Biophys Res Commun, 285*(2), 167-171. doi:10.1006/bbrc.2001.5141

Holmes, B. B., Furman, J. L., Mahan, T. E., Yamasaki, T. R., Mirbaha, H., Eades, W. C., . . . Diamond, M. I. (2014). Proteopathic tau seeding predicts tauopathy in vivo. *Proc Natl Acad Sci U S A, 111*(41), E4376-4385. doi:10.1073/pnas.1411649111

Homma, T., Ishibashi, D., Nakagaki, T., Satoh, K., Sano, K., Atarashi, R., & Nishida, N. (2014). Increased expression of p62/SQSTM1 in prion diseases and its association with pathogenic prion protein. *Sci Rep, 4*, 4504. doi:10.1038/srep04504

Hong, Y. J., & Do, J. T. (2019). Neural Lineage Differentiation From Pluripotent Stem Cells to Mimic Human Brain Tissues. *Front Bioeng Biotechnol, 7*, 400. doi:10.3389/fbioe.2019.00400

Hoopmann, P., Punge, A., Barysch, S. V., Westphal, V., Buckers, J., Opazo, F., . . . Rizzoli, S. O. (2010). Endosomal sorting of readily releasable synaptic vesicles. *Proc Natl Acad Sci U S A, 107*(44), 19055-19060. doi:10.1073/pnas.1007037107

Hormozdiari, F., Kostem, E., Kang, E. Y., Pasaniuc, B., & Eskin, E. (2014). Identifying causal variants at loci with multiple signals of association. *Genetics, 198*(2), 497--508. doi:10.1534/genetics.114.167908

Hormozdiari, F., van de Bunt, M., & Segr. (2016). Colocalization of GWAS and eQTL Signals Detects Target Genes. *American Journal of Human Genetics, 99*(6), 1245--1260. doi:10.1016/j.ajhg.2016.10.003

Hornemann, S., & Glockshuber, R. (1998). A scrapie-like unfolding intermediate of the prion protein domain PrP(121-231) induced by acidic pH. *Proceedings of the National Academy of Sciences of the United States of America, 95*(11), 6010--6014. doi:10.1073/pnas.95.11.6010

Hulce, J. J., Cognetta, A. B., Niphakis, M. J., Tully, S. E., & Cravatt, B. F. (2013). Proteome-wide mapping of cholesterol-interacting proteins in mammalian cells. *Nature Methods, 10*(3), 259--264. doi:10.1038/nmeth.2368

International HapMap Consortium. (2005). A haplotype map of the human genome. *Nature, 437*(7063), 1299-1320. doi:10.1038/nature04226

International Human Genome Sequencing Consortium. (2004). Finishing the euchromatic sequence of the human genome. *Nature, 431*(7011), 931-945. doi:10.1038/nature03001

Ivanova, L., Barmada, S., Kummer, T., & Harris, D. A. (2001). Mutant prion proteins are partially retained in the endoplasmic reticulum. *J Biol Chem, 276*(45), 42409-42421. doi:10.1074/jbc.M106928200

Jabbari, E., Tan, M. M. X., Reynolds, R. H., Mok, K. Y., Ferrari, R., Murphy, D. P., . . . Morris, H. R. (2020). Common variation at the LRRK2 locus is associated with survival in the primary tauopathy progressive supranuclear palsy. *bioRxiv*.

Jackson, G. S., Hill, A. F., Joseph, C., Hosszu, L., Power, A., Waltho, J. P., . . . Collinge, J. (1999). Multiple folding pathways for heterologously expressed human prion protein. *Biochim Biophys Acta, 1431*(1), 1-13. doi:10.1016/s0167-4838(99)00038-2

Jaffe, A. E., Straub, R. E., Shin, J. H., Tao, R., Gao, Y., Collado-Torres, L., . . . Weinberger, D. R. (2018). Developmental and genetic regulation of the human cortex transcriptome illuminate schizophrenia pathogenesis. *Nat Neurosci, 21*(8), 1117-1125. doi:10.1038/s41593-018-0197-y

Jakob, A. (1921). Über eigenartige erkrankungen des zentralnervensystems mit bemerkenswertem anatomischen befunde. *Zeitschrift für die gesamte Neurologie und Psychiatrie, 64*(1), 147-228. doi:10.1007/BF02870932

James, D., Levine, A. J., Besser, D., & Hemmati-Brivanlou, A. (2005). TGFbeta/activin/nodal signaling is necessary for the maintenance of pluripotency in human embryonic stem cells. *Development, 132*(6), 1273-1282. doi:10.1242/dev.01706

Jarosz-Griffiths, H. H., Corbett, N. J., Rowland, H. A., Fisher, K., Jones, A. C., Baron, J., . . . Hooper, N. M. (2019). Proteolytic shedding of the prion protein via activation of metallopeptidase ADAM10 reduces cellular binding and toxicity of amyloid-beta oligomers. *J Biol Chem, 294*(17), 7085-7097. doi:10.1074/jbc.RA118.005364

Jaunmuktane, Z., & Brandner, S. (2020). Invited Review: The role of prion-like mechanisms in neurodegenerative diseases. *Neuropathol Appl Neurobiol, 46*(6), 522-545. doi:10.1111/nan.12592

Jaunmuktane, Z., Mead, S., Ellis, M., Wadsworth, J. D., Nicoll, A. J., Kenny, J., . . . Brandner, S. (2015). Evidence for human transmission of amyloid-beta pathology and cerebral amyloid angiopathy. *Nature, 525*(7568), 247-250. doi:10.1038/nature15369

Jeffrey, M., Scott, J. R., Williams, A., & Fraser, H. (1992). Ultrastructural features of spongiform encephalopathy transmitted to mice from three species of bovidae. *Acta Neuropathol, 84*(5), 559-569. doi:10.1007/BF00304476

Jen, A., Parkyn, C. J., Mootoosamy, R. C., Ford, M. J., Warley, A., Liu, Q., . . . Morris, R. J. (2010). Neuronal low-density lipoprotein receptor-related protein 1 binds and endocytoses prion fibrils via receptor cluster 4. *Journal of Cell Science, 123*(2), 246--255. doi:10.1242/jcs.058099

Jinek, M., Chylinski, K., Fonfara, I., Hauer, M., Doudna, J. A., & Charpentier, E. (2012). A programmable dual-RNA-guided DNA endonuclease in adaptive bacterial immunity. *Science, 337*(6096), 816-821. doi:10.1126/science.1225829

Jones, E., Hummerich, H., Vire, E., Uphill, J., Dimitriadis, A., Speedy, H., . . . Mead, S. (2020). Identification of novel risk loci and causal insights for sporadic Creutzfeldt-Jakob disease: a genome-wide association study. *Lancet Neurol, 19*(10), 840-848. doi:10.1016/S1474-4422(20)30273-8

Jones, E., & Mead, S. (2020). Genetic risk factors for Creutzfeldt-Jakob disease. *Neurobiol Dis, 142*, 104973. doi:10.1016/j.nbd.2020.104973

Jost, M., Jacobson, A. N., Hussmann, J. A., Cirolia, G., Fischbach, M. A., & Weissman, J. S. (2021). CRISPR-based functional genomics in human dendritic cells. *Elife, 10*. doi:10.7554/eLife.65856

Julius, C., Heikenwalder, M., Schwarz, P., Marcel, A., Karin, M., Prinz, M., . . . Aguzzi, A. (2008). Prion propagation in mice lacking central nervous system NF-kappaB signalling. *J Gen Virol, 89*(Pt 6), 1545-1550. doi:10.1099/vir.0.83622-0

Jumper, J., Evans, R., Pritzel, A., Green, T., Figurnov, M., Ronneberger, O., . . . Hassabis, D. (2021). Highly accurate protein structure prediction with AlphaFold. *Nature, 596*(7873), 583-589. doi:10.1038/s41586-021-03819-2

Jung, J. J., Inamdar, Shivangi M., Tiwari, A., & Choudhury, A. (2012). Regulation of intracellular membrane trafficking and cell dynamics by syntaxin-6. *Bioscience Reports*. doi:10.1042/BSR20120006

Kabayama, H., Tokushige, N., Takeuchi, M., & Mikoshiba, K. (2008). Syntaxin 6 regulates nerve growth factor-dependent neurite outgrowth. *Neuroscience Letters, 436*(3), 340--344. doi:10.1016/j.neulet.2008.03.061

Kabeiseman, E. J., Cichos, K. H., & Moore, E. R. (2014). The eukaryotic signal sequence, YGRL, targets the chlamydial inclusion. *Front Cell Infect Microbiol, 4*, 129. doi:10.3389/fcimb.2014.00129

Kang, S. W., Rane, N. S., Kim, S. J., Garrison, J. L., Taunton, J., & Hegde, R. S. (2006). Substrate-Specific Translocational Attenuation during ER Stress Defines a Pre-Emptive Quality Control Pathway. *Cell, 127*(5), 999--1013. doi:10.1016/j.cell.2006.10.032

Kang, Y. S., Zhao, X., Lovaas, J., Eisenberg, E., & Greene, L. E. (2009). Clathrin-independent internalization of normal cellular prion protein in neuroblastoma cells is associated with the Arf6 pathway. *Journal of Cell Science, 122*(22), 4062--4069. doi:10.1242/jcs.046292

Karczewski, K. J., Francioli, L. C., Tiao, G., Cummings, B. B., Alfoldi, J., Wang, Q., . . . MacArthur, D. G. (2020). The mutational constraint spectrum quantified from variation in 141,456 humans. *Nature, 581*(7809), 434-443. doi:10.1038/s41586-020-2308-7

Kaski, D., Mead, S., Hyare, H., Cooper, S., Jampana, R., Overell, J., . . . Rudge, P. (2009). Variant CJD in an individual heterozygous for PRNP codon 129. *Lancet, 374*(9707), 2128. doi:10.1016/S0140-6736(09)61568-3

Kichaev, G., Yang, W. Y., Lindstrom, S., Hormozdiari, F., Eskin, E., Price, A. L., . . . Pasaniuc, B. (2014). Integrating functional data to prioritize causal variants in statistical fine-mapping studies. *PLoS Genet, 10*(10), e1004722. doi:10.1371/journal.pgen.1004722

Kim, K., Doi, A., Wen, B., Ng, K., Zhao, R., Cahan, P., . . . Daley, G. Q. (2010). Epigenetic memory in induced pluripotent stem cells. *Nature, 467*(7313), 285-290. doi:10.1038/nature09342

Kim, S., Sato, Y., Mohan, P. S., Peterhoff, C., Pensalfini, A., Rigoglioso, A., . . . Nixon, R. A. (2016). Evidence that the rab5 effector APPL1 mediates APP-betaCTF-induced dysfunction of endosomes in Down syndrome and Alzheimer's disease. *Mol Psychiatry, 21*(5), 707-716. doi:10.1038/mp.2015.97

Kimberlin, R. H., Cole, S., & Walker, C. A. (1987). Temporary and permanent modifications to a single strain of mouse scrapie on transmission to rats and hamsters. *J Gen Virol, 68 (Pt 7)*, 1875-1881. doi:10.1099/0022-1317-68-7-1875

Kimberlin, R. H., & Walker, C. A. (1986). Pathogenesis of scrapie (strain 263K) in hamsters infected intracerebrally, intraperitoneally or intraocularly. *J Gen Virol, 67 (Pt 2)*, 255-263. doi:10.1099/0022-1317-67-2-255

Kimberlin, R. H., Walker, C. A., & Fraser, H. (1989). The genomic identity of different strains of mouse scrapie is expressed in hamsters and preserved on reisolation in mice. *J Gen Virol, 70 (Pt 8)*, 2017-2025. doi:10.1099/0022-1317-70-8-2017

Kircher, M., Witten, D. M., Jain, P., O'Roak, B. J., Cooper, G. M., & Shendure, J. (2014). A general framework for estimating the relative pathogenicity of human genetic variants. *Nat Genet, 46*(3), 310-315. doi:10.1038/ng.2892

Kirkwood, J. K., & Cunningham, A. A. (1994). Epidemiological observations on spongiform encephalopathies in captive wild animals in the British Isles. *Vet Rec, 135*(13), 296-303. doi:10.1136/vr.135.13.296

Klatzo, I., Gajdusek, D. C., & Zigas, V. (1959). Pathology of kuru. *Lab. Invest, 8*, 799-847.

Klohn, P. C., Stoltze, L., Flechsig, E., Enari, M., & Weissmann, C. (2003). A quantitative, highly sensitive cell-based infectivity assay for mouse scrapie prions. *Proc Natl Acad Sci U S A, 100*(20), 11666-11671. doi:10.1073/pnas.1834432100

Klumperman, J., Kuliawat, R., Griffith, J. M., Geuze, H. J., & Arvan, P. (1998). Mannose 6-phosphate receptors are sorted from immature secretory granules via adaptor protein AP-1, clathrin, and syntaxin 6-positive vesicles. *J Cell Biol, 141*(2), 359-371. doi:10.1083/jcb.141.2.359

Knaus, K. J., Morillas, M., Swietnicki, W., Malone, M., Surewicz, W. K., & Yee, V. C. (2001). Crystal structure of the human prion protein reveals a mechanism for oligomerization. *Nat Struct Biol, 8*(9), 770-774. doi:10.1038/nsb0901-770

Knupp, A., Mishra, S., Martinez, R., Braggin, J. E., Szabo, M., Kinoshita, C., . . . Young, J. E. (2020). Depletion of the AD Risk Gene SORL1 Selectively Impairs Neuronal Endosomal Traffic Independent of Amyloidogenic APP Processing. *Cell Rep, 31*(9), 107719. doi:10.1016/j.celrep.2020.107719

Kobayashi, A., Qi, Z., Shimazaki, T., Munesue, Y., Miyamoto, T., Isoda, N., . . . Miyoshi, I. (2019). Ganglioside Synthase Knockout Reduces Prion Disease Incubation Time in Mouse Models. *Am J Pathol, 189*(3), 677-686. doi:10.1016/j.ajpath.2018.11.009

Kocisko, D. A., Come, J. H., Priola, S. A., Chesebro, B., Raymond, G. J., Lansbury, P. T., & Caughey, B. (1994). Cell-free formation of protease-resistant prion protein. *Nature, 370*(6489), 471-474. doi:10.1038/370471a0

Koike, S., & Jahn, R. (2019). SNAREs define targeting specificity of trafficking vesicles by combinatorial interaction with tethering factors. *Nature Communications, 10*(1). doi:10.1038/s41467-019-09617-9

Kolay, S., & Diamond, M. I. (2020). Alzheimer's disease risk modifier genes do not affect tau aggregate uptake, seeding or maintenance in cell models. *FEBS Open Bio, 10*(9), 1912-1920. doi:10.1002/2211-5463.12928

Koldamova, R., Schug, J., Lefterova, M., Cronican, A. A., Fitz, N. F., Davenport, F. A., . . . Lefterov, I. (2014). Genome-wide approaches reveal EGR1-controlled regulatory networks associated with neurodegeneration. *Neurobiology of Disease, 63*, 107--114. doi:10.1016/j.nbd.2013.11.005

Kong, Q., Huang, S., Zou, W., Vanegas, D., Wang, M., Wu, D., . . . Gambetti, P. (2005). Chronic wasting disease of elk: transmissibility to humans examined by transgenic mouse models. *J Neurosci, 25*(35), 7944-7949. doi:10.1523/JNEUROSCI.2467-05.2005

Kouri, N., Murray, M. E., Reddy, J. S., Serie, D. J., Soto-Beasley, A., Allen, M., . . . Dickson, D. W. (2021). Latent trait modeling of tau neuropathology in progressive supranuclear palsy. *Acta Neuropathol, 141*(5), 667-680. doi:10.1007/s00401-021-02289-0

Kovacs, G. G., Gelpi, E., Strobel, T., Ricken, G., Nyengaard, J. R., Bernheimer, H., & Budka, H. (2007). Involvement of the endosomal-lysosomal system correlates with regional pathology in Creutzfeldt-Jakob disease. *J Neuropathol Exp Neurol, 66*(7), 628-636. doi:10.1097/nen.0b013e318093ecc7

Kovacs, G. G., Puopolo, M., Ladogana, A., Pocchiari, M., Budka, H., van Duijn, C., . . . Eurocjd. (2005). Genetic prion disease: the EUROCJD experience. *Hum Genet, 118*(2), 166-174. doi:10.1007/s00439-005-0020-1

Krance, S. H., Luke, R., Shenouda, M., Israwi, A. R., Colpitts, S. J., Darwish, L., . . . Watts, J. C. (2020). Cellular models for discovering prion disease therapeutics: Progress and challenges. *J Neurochem, 153*(2), 150-172. doi:10.1111/jnc.14956

Kranich, J., Krautler, N. J., Falsig, J., Ballmer, B., Li, S., Hutter, G., . . . Aguzzi, A. (2010). Engulfment of cerebral apoptotic bodies controls the course of prion disease in a mouse strain-dependent manner. *J Exp Med, 207*(10), 2271-2281. doi:10.1084/jem.20092401

Kraus, A., Hoyt, F., Schwartz, C. L., Hansen, B., Artikis, E., Hughson, A. G., . . . Caughey, B. (2021). High-resolution structure and strain comparison of infectious mammalian prions. *Mol Cell*. doi:10.1016/j.molcel.2021.08.011

Krejciova, Z., Alibhai, J., Zhao, C., Krencik, R., Rzechorzek, N. M., Ullian, E. M., . . . Chandran, S. (2017). Human stem cell-derived astrocytes replicate human prions in a PRNP genotype-dependent manner. *J Exp Med, 214*(12), 3481-3495. doi:10.1084/jem.20161547

Kresojevic, N., Mandic-Stojmenovic, G., Dobricic, V., Petrovic, I., Brajkovic, L., Stefanova, E., . . . Kostic, V. (2020). Very Late-Onset Niemann Pick Type C Disease: Example of Progressive Supranuclear Palsy Look-Alike Disorder. *Mov Disord Clin Pract, 7*(2), 211-214. doi:10.1002/mdc3.12892

Kreykenbohm, V., Wenzel, D., Antonin, W., & Atlachkine, V. a. (2002). The SNAREs vti1a and vti1b have distinct localization and SNARE complex partners. *European Journal of Cell Biology, 81*(5), 273--280. doi:10.1078/0171-9335-00247

Kuffer, A., Lakkaraju, A. K., Mogha, A., Petersen, S. C., Airich, K., Doucerain, C., . . . Aguzzi, A. (2016). The prion protein is an agonistic ligand of the G protein-coupled receptor Adgrg6. *Nature, 536*(7617), 464-468. doi:10.1038/nature19312

Kuliawat, R., Kalinina, E., Bock, J., Fricker, L., McGraw, T. E., Kim, S. R., . . . Arvan, P. (2004). Syntaxin-6 SNARE involvement in secretory and endocytic pathways of cultured pancreatic beta-cells. *Molecular Biology of the Cell, 15*(4), 1690--1701. doi:10.1091/mbc.e03-08-0554

Kumudu, H., Perera, I., Clarke, M., Morris, N. J., Hong, W., Chamberlain, L. H., & Gould, G. W. (2003). Syntaxin 6 Regulates Glut4 Trafficking in 3T3-L1 Adipocytes. *Molecular Biology of the Cell, 14*, 2946--2958. doi:10.1091/mbcE02-11-0722

Kurt, T. D., Telling, G. C., Zabel, M. D., & Hoover, E. A. (2009). Trans-species amplification of PrP(CWD) and correlation with rigid loop 170N. *Virology, 387*(1), 235-243. doi:10.1016/j.virol.2009.02.025

Ladogana, A., & Kovacs, G. G. (2018). Chapter 13 - Genetic Creutzfeldt–Jakob disease. In M. Pocchiari & J. Manson (Eds.), *Handbook of Clinical Neurology* (Vol. 153, pp. 219-242): Elsevier.

Ladogana, A., Puopolo, M., Croes, E. A., Budka, H., Jarius, C., Collins, S., . . . Zerr, I. (2005). Mortality from Creutzfeldt-Jakob disease and related disorders in Europe, Australia, and Canada. *Neurology, 64*(9), 1586-1591. doi:10.1212/01.WNL.0000160117.56690.B2

Lasmezas, C. I., Deslys, J. P., Demaimay, R., Adjou, K. T., Lamoury, F., Dormont, D., . . . Hauw, J. J. (1996). BSE transmission to macaques. *Nature, 381*(6585), 743-744. doi:10.1038/381743a0

Laufman, O., Hong, W., & Lev, S. (2011). The COG complex interacts directly with Syntaxin 6 and positively regulates endosome-to-TGN retrograde transport. *The Journal of Cell Biology, 194*(3), 459--472. doi:10.1083/jcb.201102045

Lauren, J., Gimbel, D. A., Nygaard, H. B., Gilbert, J. W., & Strittmatter, S. M. (2009). Cellular prion protein mediates impairment of synaptic plasticity by amyloid-beta oligomers. *Nature, 457*(7233), 1128-1132. doi:10.1038/nature07761

Lee, J. J., Wedow, R., Okbay, A., Kong, E., Maghzian, O., Zacher, M., . . . Cesarini, D. (2018). Gene discovery and polygenic prediction from a genome-wide association study of educational attainment in 1.1 million individuals. *Nat Genet, 50*(8), 1112-1121. doi:10.1038/s41588-018-0147-3

Lee, S., Antony, L., Hartmann, R., Knaus, K. J., Surewicz, K., Surewicz, W. K., & Yee, V. C. (2010). Conformational diversity in prion protein variants influences intermolecular beta-sheet formation. *EMBO J, 29*(1), 251-262. doi:10.1038/emboj.2009.333

Lee, W. S., Tan, D. C., Deng, Y., van Hummel, A., Ippati, S., Stevens, C., . . . Ittner, L. M. (2021). Syntaxins 6 and 8 facilitate tau into secretory pathways. *Biochem J, 478*(7), 1471-1484. doi:10.1042/BCJ20200664

Legname, G., & Scialo, C. (2020). On the role of the cellular prion protein in the uptake and signaling of pathological aggregates in neurodegenerative diseases. *Prion, 14*(1), 257-270. doi:10.1080/19336896.2020.1854034

Lewis, V., Johanssen, V. A., Crouch, P. J., Klug, G. M., Hooper, N. M., & Collins, S. J. (2016). Prion protein "gamma-cleavage": characterizing a novel endoproteolytic processing event. *Cell Mol Life Sci, 73*(3), 667-683. doi:10.1007/s00018-015-2022-z

Li, H., Yang, Y., Hong, W., Huang, M., Wu, M., & Zhao, X. (2020). Applications of genome editing technology in the targeted therapy of human diseases: mechanisms, advances and prospects. *Signal Transduct Target Ther, 5*(1), 1. doi:10.1038/s41392-019-0089-y

Liberzon, A., Subramanian, A., Pinchback, R., Thorvaldsdottir, H., Tamayo, P., & Mesirov, J. P. (2011). Molecular signatures database (MSigDB) 3.0. *Bioinformatics, 27*(12), 1739-1740. doi:10.1093/bioinformatics/btr260

Lieu, Z. Z., Derby, M. C., Teasdale, R. D., Hart, C., Gunn, P., & Gleeson, P. A. (2007). The Golgin GCC88 Is Required for Efficient Retrograde Transport of Cargo from the Early Endosomes to the Trans-Golgi Network. *Molecular Biology of the Cell, 18*(12), 4979--4991. doi:10.1091/mbc.E07-06-0622

Lin, Y. T., Seo, J., Gao, F., Feldman, H. M., Wen, H. L., Penney, J., . . . Tsai, L. H. (2018). APOE4 Causes Widespread Molecular and Cellular Alterations Associated with Alzheimer's Disease Phenotypes in Human iPSC-Derived Brain Cell Types. *Neuron, 98*(6), 1141-1154 e1147. doi:10.1016/j.neuron.2018.05.008

Litvan, I., Proudfoot, J. A., Martin, E. R., Standaert, D., Riley, D., Hall, D., . . . Jankovic, J. (2021). Gene-Environment Interactions in Progressive Supranuclear Palsy. *Front Neurol, 12*, 664796. doi:10.3389/fneur.2021.664796

Liu, A., & Niswander, L. A. (2005). Bone morphogenetic protein signalling and vertebrate nervous system development. *Nat Rev Neurosci, 6*(12), 945-954. doi:10.1038/nrn1805

Llewelyn, C. A., Hewitt, P. E., Knight, R. S. G., Amar, K., Cousens, S., MacKenzie, J., & Will, R. G. (2004). Possible transmission of variant Creutzfeldt-Jakob disease by blood transfusion. *Lancet, 363*(9407), 417--421. doi:10.1016/S0140-6736(04)15486-X

Lloyd, S. E., Maytham, E. G., Grizenkova, J., Hummerich, H., & Collinge, J. (2010). A Copine family member, Cpne8, is a candidate quantitative trait gene for prion disease incubation time in mouse. *Neurogenetics, 11*(2), 185--191. doi:10.1007/s10048-009-0219-8

Lloyd, S. E., Maytham, E. G., Pota, H., Grizenkova, J., Molou, E., Uphill, J., . . . Collinge, J. (2009). HECTD2 Is Associated with Susceptibility to Mouse and Human Prion Disease. doi:10.1371/journal.pgen.1000383

Luhken, G., Buschmann, A., Brandt, H., Eiden, M., Groschup, M. H., & Erhardt, G. (2007). Epidemiological and genetical differences between classical and atypical scrapie cases. *Vet Res, 38*(1), 65-80. doi:10.1051/vetres:2006046

Ma, J., & Lindquist, S. (2002). Conversion of PrP to a Self-Perpetuating PrPSc-like Conformation in the Cytosol. *Science, 298*(5599), 1785--1788. doi:10.1126/science.1073619

Madeira, F., Park, Y. M., Lee, J., Buso, N., Gur, T., Madhusoodanan, N., . . . Lopez, R. (2019). The EMBL-EBI search and sequence analysis tools APIs in 2019. *Nucleic Acids Res, 47*(W1), W636-W641. doi:10.1093/nar/gkz268

Magalhes, A. C., Baron, G. S., Lee, K. S., Steele-Mortimer, O., Dorward, D., Prado, M. A. M., & Caughey, B. (2005). Uptake and neuritic transport of scrapie prion protein coincident with infection of neuronal cells. *Journal of Neuroscience, 25*(21), 5207--5216. doi:10.1523/JNEUROSCI.0653-05.2005

Mahal, S. P., Baker, C. A., Demczyk, C. A., Smith, E. W., Julius, C., & Weissmann, C. (2007). Prion strain discrimination in cell culture: the cell panel assay. *Proc Natl Acad Sci U S A, 104*(52), 20908-20913. doi:10.1073/pnas.0710054104

Makarava, N., Chang, J. C., Kushwaha, R., & Baskakov, I. V. (2019). Region-Specific Response of Astrocytes to Prion Infection. *Front Neurosci, 13*, 1048. doi:10.3389/fnins.2019.01048

Mallard, F., Tang, B. L., Galli, T., Tenza, D., Saint-Pol, A., Yue, X., . . . Johannes, L. (2002). Early/recycling endosomes-to-TGN transport involves two SNARE complexes and a Rab6 isoform. *The Journal of Cell Biology, 156*(4), 653--664. doi:10.1083/jcb.200110081

Mallucci, G. R., Ratte, S., Asante, E. A., Linehan, J., Gowland, I., Jefferys, J. G., & Collinge, J. (2002). Post-natal knockout of prion protein alters hippocampal CA1 properties, but does not result in neurodegeneration. *EMBO J, 21*(3), 202-210. doi:10.1093/emboj/21.3.202

Manickam, V., Tiwari, A., Jung, J. J., Bhattacharya, R., Goel, A., Mukhopadhyay, D., & Choudhury, A. (2011). Regulation of vascular endothelial growth factor receptor 2 trafficking and angiogenesis by Golgi localized t-SNARE syntaxin 6. *Blood*. doi:10.1182/blood-2010-06-291690

Marella, M., Lehmann, S., Grassi, J., & Chabry, J. (2002). Filipin prevents pathological prion protein accumulation by reducing endocytosis and inducing cellular PrP release. *Journal of Biological Chemistry, 277*(28), 25457--25464. doi:10.1074/jbc.M203248200

Margiotta, A. (2021). Role of SNAREs in Neurodegenerative Diseases. *Cells, 10*(5). doi:10.3390/cells10050991

Marijanovic, Z., Caputo, A., Campana, V., & Zurzolo, C. (2009). Identification of an Intracellular Site of Prion Conversion. *PLOS Pathogens, 5*(5), e1000426. doi:10.1371/journal.ppat.1000426

Marin-Moreno, A., Espinosa, J. C., & Torres, J. M. (2020). Transgenic mouse models for the study of prion diseases. *Prog Mol Biol Transl Sci, 175*, 147-177. doi:10.1016/bs.pmbts.2020.08.007

Markopoulou, K., Chase, B. A., Premkumar, A. P., Schoneburg, B., Kartha, N., Wei, J., . . . Maraganore, D. (2021). Variable Effects of PD-Risk Associated SNPs and Variants in Parkinsonism-Associated Genes on Disease Phenotype in a Community-Based Cohort. *Front Neurol, 12*, 662278. doi:10.3389/fneur.2021.662278

Marsh, R. F., & Hadlow, W. J. (1992). Transmissible mink encephalopathy. *Rev Sci Tech, 11*(2), 539-550. doi:10.20506/rst.11.2.606

Martin-Martin, B., Nabokina, S. M., Blasi, J., Lazo, P. A., & Mollinedo, F. (2000). Involvement of SNAP-23 and syntaxin 6 in human neutrophil exocytosis. *Blood, 96*(7), 2574-2583.

Massignan, T., Biasini, E., Lauranzano, E., Veglianese, P., Pignataro, M., Fioriti, L., . . . Bonetto, V. (2010). Mutant prion protein expression is associated with an alteration of the Rab GDP dissociation inhibitor alpha (GDI)/Rab11 pathway. *Mol Cell Proteomics, 9*(4), 611-622. doi:10.1074/mcp.M900271-MCP200

Mastrianni, J. A., Nixon, R., Layzer, R., Telling, G. C., Han, D., DeArmond, S. J., & Prusiner, S. B. (1999). Prion protein conformation in a patient with sporadic fatal insomnia. *N Engl J Med, 340*(21), 1630-1638. doi:10.1056/NEJM199905273402104

Matamoros-Angles, A., Gayosso, L. M., Richaud-Patin, Y., di Domenico, A., Vergara, C., Hervera, A., . . . Del Rio, J. A. (2018). iPS Cell Cultures from a Gerstmann-Straussler-Scheinker Patient with the Y218N PRNP Mutation Recapitulate tau Pathology. *Mol Neurobiol, 55*(4), 3033-3048. doi:10.1007/s12035-017-0506-6

Matej, R., Olejar, T., Janouskova, O., & Holada, K. (2012). Deletion of protease-activated receptor 2 prolongs survival of scrapie-inoculated mice. *J Gen Virol, 93*(Pt 9), 2057-2061. doi:10.1099/vir.0.043877-0

Maurano, M. T., Humbert, R., Rynes, E., Thurman, R. E., Haugen, E., Wang, H., . . . Stamatoyannopoulos, J. A. (2012). Systematic localization of common disease-associated variation in regulatory DNA. *Science, 337*(6099), 1190-1195. doi:10.1126/science.1222794

Mays, C. E., Armijo, E., Morales, R., Kramm, C., Flores, A., Tiwari, A., . . . Soto, C. (2019). Prion disease is accelerated in mice lacking stress-induced heat shock protein 70 (HSP70). *Journal of Biological Chemistry*, jbc.RA118.006186. doi:10.1074/jbc.ra118.006186

McGowan, J. P. (1922). Scrapie in sheep. *Scott. J. Agric, 5*, 365-375.

McLaren, W., Pritchard, B., Rios, D., Chen, Y., Flicek, P., & Cunningham, F. (2010). Deriving the consequences of genomic variants with the Ensembl API and SNP Effect Predictor. *Bioinformatics, 26*(16), 2069-2070. doi:10.1093/bioinformatics/btq330

McLelland, G. L., Lee, S. A., McBride, H. M., & Fon, E. A. (2016). Syntaxin-17 delivers PINK1/parkin-dependent mitochondrial vesicles to the endolysosomal system. *J Cell Biol, 214*(3), 275-291. doi:10.1083/jcb.201603105

Mead, S., Gandhi, S., Beck, J., Caine, D., Gallujipali, D., Carswell, C., . . . Collinge, J. (2013). A novel prion disease associated with diarrhea and autonomic neuropathy. *N Engl J Med, 369*(20), 1904-1914. doi:10.1056/NEJMoa1214747

Mead, S., Lloyd, S., & Collinge, J. (2019). Genetic Factors in Mammalian Prion Diseases. *Annu Rev Genet, 53*(1), 117-147. doi:10.1146/annurev-genet-120213-092352

Mead, S., Mahal, S. P., Beck, J., Campbell, T., Farrall, M., Fisher, E., & Collinge, J. (2001). Sporadic-But not variant-Creutzfeldt-Jakob disease is associated with polymorphisms upstream of PRNP exon 1. *American Journal of Human Genetics, 69*(6), 1225--1235. doi:10.1086/324710

Mead, S., Poulter, M., Uphill, J., Beck, J., Whitfield, J., Webb, T. E., . . . Collinge, J. (2009). Genetic risk factors for variant Creutzfeldt-Jakob disease: a genome-wide association study. *Lancet Neurol, 8*(1), 57-66. doi:10.1016/S1474-4422(08)70265-5

Mead, S., Uphill, J., Beck, J., Poulter, M., Campbell, T., Lowe, J., . . . Collinge, J. (2012). Genome-wide association study in multiple human prion diseases suggests genetic risk factors additional to PRNP. *Hum Mol Genet, 21*(8), 1897-1906. doi:10.1093/hmg/ddr607

Mead, S., Whitfield, J., Poulter, M., Shah, P., Uphill, J., Campbell, T., . . . Collinge, J. (2009). A novel protective prion protein variant that colocalizes with kuru exposure. *N Engl J Med, 361*(21), 2056-2065. doi:10.1056/NEJMoa0809716

Medori, R., Tritschler, H. J., LeBlanc, A., Villare, F., Manetto, V., Chen, H. Y., . . . et al. (1992). Fatal familial insomnia, a prion disease with a mutation at codon 178 of the prion protein gene. *N Engl J Med, 326*(7), 444-449. doi:10.1056/NEJM199202133260704

Mehrabian, M., Brethour, D., Wang, H., Xi, Z., Rogaeva, E., & Schmitt-Ulms, G. (2015). The Prion Protein Controls Polysialylation of Neural Cell Adhesion Molecule 1 during Cellular Morphogenesis. *PLoS ONE, 10*(8), e0133741. doi:10.1371/journal.pone.0133741

Meissner, B., Kallenberg, K., Sanchez-Juan, P., Ramljak, S., Krasnianski, A., Heinemann, U., . . . Zerr, I. (2009). MRI and clinical syndrome in dura mater-related Creutzfeldt-Jakob disease. *J Neurol, 256*(3), 355-363. doi:10.1007/s00415-009-0026-z

Merz, P. A., Somerville, R. A., Wisniewski, H. M., & Iqbal, K. (1981). Abnormal fibrils from scrapie-infected brain. *Acta Neuropathol, 54*(1), 63-74. doi:10.1007/BF00691333

Messina, D., Cerasa, A., Condino, F., Arabia, G., Novellino, F., Nicoletti, G., . . . Quattrone, A. (2011). Patterns of brain atrophy in Parkinson's disease, progressive supranuclear palsy and multiple system atrophy. *Parkinsonism Relat Disord, 17*(3), 172-176. doi:10.1016/j.parkreldis.2010.12.010

Mills, I. G., Urbe, S., & Clague, M. J. (2001). Relationships between EEA1 binding partners and their role in endosome fusion. *Journal of Cell Science, 114*(10), 1959.

Mills, M. C., & Rahal, C. (2019). A scientometric review of genome-wide association studies. In (Vol. 2).

Minami, S., Yokota, N., & Kawahara, H. (2020). BAG6 contributes to glucose uptake by supporting the cell surface translocation of the glucose transporter GLUT4. *Biology Open, 9*(1), bio047324. doi:10.1242/bio.047324

Miranzadeh Mahabadi, H., & Taghibiglou, C. (2020). Cellular Prion Protein (PrPc): Putative Interacting Partners and Consequences of the Interaction. *Int J Mol Sci, 21*(19). doi:10.3390/ijms21197058

Mironov, A., Jr., Latawiec, D., Wille, H., Bouzamondo-Bernstein, E., Legname, G., Williamson, R. A., . . . Peters, P. J. (2003). Cytosolic prion protein in neurons. *J Neurosci, 23*(18), 7183-7193.

Misura, K. M. S., Bock, J. B., Gonzalez, L. C., Scheller, R. H., & Weis, W. I. (2002). Three-dimensional structure of the amino-terminal domain of syntaxin 6, a SNAP-25 C homolog. *Proceedings of the National Academy of Sciences, 99*(14), 9184--9189. doi:10.1073/pnas.132274599

Mobley, W. C., Neve, R. L., Prusiner, S. B., & McKinley, M. P. (1988). Nerve growth factor increases mRNA levels for the prion protein and the beta-amyloid protein precursor in developing hamster brain. *Proc Natl Acad Sci U S A, 85*(24), 9811-9815. doi:10.1073/pnas.85.24.9811

Mok, T., Jaunmuktane, Z., Joiner, S., Campbell, T., Morgan, C., Wakerley, B., . . . Collinge, J. (2017). Variant Creutzfeldt-Jakob Disease in a Patient with Heterozygosity at PRNP Codon 129. *N Engl J Med, 376*(3), 292-294. doi:10.1056/NEJMc1610003

Mookherjee, D., Majumder, P., Mukherjee, R., Chatterjee, D., Kaul, Z., Das, S., . . . Chakrabarti, O. (2019). Cytosolic aggregates in presence of non-translocated proteins perturb endoplasmic reticulum structure and dynamics. *Traffic*. doi:10.1111/tra.12694

Moore, E. R., Mead, D. J., Dooley, C. A., Sager, J., & Hackstadt, T. (2011). The trans-Golgi SNARE syntaxin 6 is recruited to the chlamydial inclusion membrane. *Microbiology*. doi:10.1099/mic.0.045856-0

Moreno, C. R., Moazami-Goudarzi, K., Briand, S., Robert-Granie, C., Weisbecker, J. L., Laurent, P., . . . Pong-Wong, R. (2010). Mapping of quantitative trait loci affecting classical scrapie incubation time in a population comprising several generations of scrapie-infected sheep. *J Gen Virol, 91*(Pt 2), 575-579. doi:10.1099/vir.0.014134-0

Morizane, A., Doi, D., Kikuchi, T., Nishimura, K., & Takahashi, J. (2011). Small-molecule inhibitors of bone morphogenic protein and activin/nodal signals promote highly efficient neural induction from human pluripotent stem cells. *J Neurosci Res, 89*(2), 117-126. doi:10.1002/jnr.22547

Munch, C., O'Brien, J., & Bertolotti, A. (2011). Prion-like propagation of mutant superoxide dismutase-1 misfolding in neuronal cells. *Proc Natl Acad Sci U S A, 108*(9), 3548-3553. doi:10.1073/pnas.1017275108

Murray, R. Z., Wylie, F. G., Khromykh, T., Hume, D. A., & Stow, J. L. (2005). Syntaxin 6 and Vti1b form a novel SNARE complex, which is up-regulated in activated macrophages to facilitate exocytosis of tumor necrosis Factor-alpha. *The Journal of Biological Chemistry, 280*(11), 10478--10483. doi:10.1074/jbc.M414420200

Nakamura, N. (2005). MARCH-II Is a Syntaxin-6-binding Protein Involved in Endosomal Trafficking. *Molecular Biology of the Cell, 16*(4), 1696--1710. doi:10.1091/mbc.E04-03-0216

Nalls, M. A., Blauwendraat, C., Vallerga, C. L., Heilbron, K., Bandres-Ciga, S., Chang, D., . . . International Parkinson's Disease Genomics, C. (2019). Identification of novel risk loci, causal insights, and heritable risk for Parkinson's disease: a meta-analysis of genome-wide association studies. *Lancet Neurol, 18*(12), 1091-1102. doi:10.1016/S1474-4422(19)30320-5

Naslavsky, N., Stein, R., Yanai, A., Friedlander, G., & Taraboulos, A. (1997). Characterization of detergent-insoluble complexes containing the cellular prion protein and its scrapie isoform. *J Biol Chem, 272*(10), 6324-6331. doi:10.1074/jbc.272.10.6324

Nedelec, Y., Sanz, J., Baharian, G., Szpiech, Z. A., Pacis, A., Dumaine, A., . . . Barreiro, L. B. (2016). Genetic Ancestry and Natural Selection Drive Population Differences in Immune Responses to Pathogens. *Cell, 167*(3), 657-669 e621. doi:10.1016/j.cell.2016.09.025

Ng, B., White, C. C., Klein, H. U., Sieberts, S. K., McCabe, C., Patrick, E., . . . De Jager, P. L. (2017). An xQTL map integrates the genetic architecture of the human brain's transcriptome and epigenome. *Nat Neurosci, 20*(10), 1418-1426. doi:10.1038/nn.4632

NHGRI-EBI. (2021, 16th August). GWAS Catalog. Retrieved from https://www.ebi.ac.uk/gwas/home

Nixon, R. A. (2017). Amyloid precursor protein and endosomal-lysosomal dysfunction in Alzheimer's disease: inseparable partners in a multifactorial disease. *FASEB J, 31*(7), 2729-2743. doi:10.1096/fj.201700359

Nonno, R., Di Bari, M. A., Cardone, F., Vaccari, G., Fazzi, P., Dell'Omo, G., . . . Agrimi, U. (2006). Efficient transmission and characterization of Creutzfeldt-Jakob disease strains in bank voles. *PLoS Pathog, 2*(2), e12. doi:10.1371/journal.ppat.0020012

Nozawa, T., Minowa-Nozawa, A., Aikawa, C., & Nakagawa, I. (2017). The STX6-VTI1B-VAMP3 complex facilitates xenophagy by regulating the fusion between recycling endosomes and autophagosomes. *Autophagy, 13*(1), 57--69. doi:10.1080/15548627.2016.1241924

Nunziante, M., Ackermann, K., Dietrich, K., Wolf, H., Gadtke, L., Gilch, S., . . . Schatzl, H. M. (2011). Proteasomal dysfunction and endoplasmic reticulum stress enhance trafficking of prion protein aggregates through the secretory pathway and increase accumulation of pathologic prion protein. *J Biol Chem, 286*(39), 33942-33953. doi:10.1074/jbc.M111.272617

Nunziante, M., Gilch, S., & Schatzl, H. M. (2003). Essential role of the prion protein N terminus in subcellular trafficking and half-life of cellular prion protein. *J Biol Chem, 278*(6), 3726-3734. doi:10.1074/jbc.M206313200

O'Rourke, K. I., Besser, T. E., Miller, M. W., Cline, T. F., Spraker, T. R., Jenny, A. L., . . . Williams, E. S. (1999). PrP genotypes of captive and free-ranging Rocky Mountain elk (Cervus elaphus nelsoni) with chronic wasting disease. *J Gen Virol, 80 (Pt 10)*, 2765-2679. doi:10.1099/0022-1317-80-10-2765

O'Shea, M., Maytham, E. G., Linehan, J. M., Brandner, S., Collinge, J., & Lloyd, S. E. (2008). Investigation of Mcp1 as a Quantitative Trait Gene for Prion Disease Incubation Time in Mouse. *Genetics, 180*(1), 559-566. doi:10.1534/genetics.108.090894 %J Genetics

Oesch, B., Westaway, D., Walchli, M., McKinley, M. P., Kent, S. B., Aebersold, R., . . . et al. (1985). A cellular gene encodes scrapie PrP 27-30 protein. *Cell, 40*(4), 735-746. doi:10.1016/0092-8674(85)90333-2

Ondrejcak, T., Klyubin, I., Corbett, G. T., Fraser, G., Hong, W., Mably, A. J., . . . Rowan, M. J. (2018). Cellular Prion Protein Mediates the Disruption of Hippocampal Synaptic Plasticity by Soluble Tau In Vivo. *J Neurosci, 38*(50), 10595-10606. doi:10.1523/JNEUROSCI.1700-18.2018

Otero, A., Betancor, M., Erana, H., Fernandez Borges, N., Lucas, J. J., Badiola, J. J., . . . Bolea, R. (2021). Prion-Associated Neurodegeneration Causes Both Endoplasmic Reticulum Stress and Proteasome Impairment in a Murine Model of Spontaneous Disease. *Int J Mol Sci, 22*(1). doi:10.3390/ijms22010465

Otto, G. P., Razi, M., Morvan, J., Stenner, F., & Tooze, S. A. (2010). A Novel Syntaxin 6-Interacting protein, SHIP164, regulates Syntaxin 6-Dependent sorting from early endosomes. *Traffic, 11*(5), 688--705. doi:10.1111/j.1600-0854.2010.01049.x

Palade, G. (1975). Intracellular aspects of the process of protein synthesis. *Science, 189*(4206), 867. doi:10.1126/science.189.4206.867-b

Palmer, M. S., Dryden, A. J., Hughes, J. T., & Collinge, J. (1991). Homozygous prion protein genotype predisposes to sporadic Creutzfeldt-Jakob disease. *Nature, 352*(6333), 340--342. doi:10.1038/352340a0

Pan, K. M., Baldwin, M., Nguyen, J., Gasset, M., Serban, A., Groth, D., . . . et al. (1993). Conversion of alpha-helices into beta-sheets features in the formation of the scrapie prion proteins. *Proc Natl Acad Sci U S A, 90*(23), 10962-10966. doi:10.1073/pnas.90.23.10962

Pan, L., Meng, L., He, M., & Zhang, Z. (2021). Tau in the Pathophysiology of Parkinson's Disease. *J Mol Neurosci*. doi:10.1007/s12031-020-01776-5

Parkin, E. T., Watt, N. T., Turner, A. J., & Hooper, N. M. (2004). Dual mechanisms for shedding of the cellular prion protein. *J Biol Chem, 279*(12), 11170-11178. doi:10.1074/jbc.M312105200

Parkyn, C. J., Vermeulen, E. G. M., Mootoosamy, R. C., Sunyach, C., Jacobsen, C., Oxvig, C., . . . Morris, R. J. (2008). LRP1 controls biosynthetic and endocytic trafficking of neuronal prion protein. *Journal of Cell Science, 121*(6), 773--783. doi:10.1242/jcs.021816

Pattison, I. H., & Millson, G. C. (1961). Scrapie produced experimentally in goats with special reference to the clinical syndrome. *J Comp Pathol, 71*, 101-109. doi:10.1016/s0368-1742(61)80013-1

Pauly, P. C., & Harris, D. A. (1998). Copper stimulates endocytosis of the prion protein. *J Biol Chem, 273*(50), 33107-33110. doi:10.1074/jbc.273.50.33107

Peak, T. C., Panigrahi, G. K., Praharaj, P. P., Su, Y., Shi, L., Chyr, J., . . . Singh, R. a. (2019). Syntaxin 6-mediated exosome secretion regulates enzalutamide resistance in prostate cancer. *Molecular Carcinogenesis*. doi:10.1002/mc.23129

Peak, T. C., Su, Y., Chapple, A. G., Chyr, J., & Deep, G. (2019). Syntaxin 6: A novel predictive and prognostic biomarker in papillary renal cell carcinoma. *Scientific Reports, 9*(1). doi:10.1038/s41598-019-39305-z

Pease, D., Scheckel, C., Schaper, E., Eckhardt, V., Emmenegger, M., Xenarios, I., & Aguzzi, A. (2019). Genome-wide identification of microRNAs regulating the human prion protein. *Brain Pathol, 29*(2), 232-244. doi:10.1111/bpa.12679

Peggion, C., Stella, R., Chemello, F., Massimino, M. L., Arrigoni, G., Cagnin, S., . . . Bertoli, A. (2018). The Prion Protein Regulates Synaptic Transmission by Controlling the Expression of Proteins Key to Synaptic Vesicle Recycling and Exocytosis. *Molecular Neurobiology*, 1--17. doi:10.1007/s12035-018-1293-4

Pensalfini, A., Kim, S., Subbanna, S., Bleiwas, C., Goulbourne, C. N., Stavrides, P. H., . . . Nixon, R. A. (2020). Endosomal Dysfunction Induced by Directly Overactivating Rab5 Recapitulates Prodromal and Neurodegenerative Features of Alzheimer's Disease. *Cell Rep, 33*(8), 108420. doi:10.1016/j.celrep.2020.108420

Perez-Victoria, F. J., & Bonifacino, J. S. (2009). Dual Roles of the Mammalian GARP Complex in Tethering and SNARE Complex Assembly at the trans-Golgi Network. *Molecular and Cellular Biology, 29*(19), 5251--5263. doi:10.1128/MCB.00495-09

Perez-Victoria, F. J., Schindler, C., Magadan, J. G., Mardones, G. A., Delevoye, C., Romao, M., . . . Bonifacino, J. S. (2010). Ang2/fat-free is a conserved subunit of the Golgi-associated retrograde protein complex. *Mol Biol Cell, 21*(19), 3386-3395. doi:10.1091/mbc.E10-05-0392

Peters, P. J., Mironov, A., & Peretz, D. a. (2003). Trafficking of prion proteins through a caveolae-mediated endosomal pathway. *Journal of Cell Biology, 162*(4), 703--717. doi:10.1083/jcb.200304140

Pflanz, H., Vana, K., Mitteregger, G., Renner-Muller, I., Pace, C., Kuchenhoff, H., . . . Weiss, S. (2009). Scrapie-infected transgenic mice expressing a laminin receptor decoy mutant reveal a prolonged incubation time associated with low levels of PrPres. *J Mol Biol, 388*(4), 721-729. doi:10.1016/j.jmb.2009.03.045

Phadwal, K., Kurian, D., Salamat, M. K. F., MacRae, V. E., Diack, A. B., & Manson, J. C. (2018). Spermine increases acetylation of tubulins and facilitates autophagic degradation of prion aggregates. *Scientific Reports, 8*(1). doi:10.1038/s41598-018-28296-y

Pham, E., Crews, L., Ubhi, K., Hansen, L., Adame, A., Cartier, A., . . . Masliah, E. (2010). Progressive accumulation of amyloid-beta oligomers in Alzheimer's disease and in amyloid precursor protein transgenic mice is accompanied by selective alterations in synaptic scaffold proteins. *FEBS J, 277*(14), 3051-3067. doi:10.1111/j.1742-4658.2010.07719.x

Pickering-Brown, S. M., Mann, D. M. A., Owen, F., Ironside, J. W., de Silva, R., Roberts, D. A., . . . Cooper, P. N. (1995). Allelic variations in apolipoprotein E and prion protein genotype related to plaque formation and age of onset in sporadic Creutzfeldt-Jakob disease. *Neuroscience Letters, 187*(2), 127--129. doi:10.1016/0304-3940(95)11353-3

Pillai-Kastoori, L., Schutz-Geschwender, A. R., & Harford, J. A. (2020). A systematic approach to quantitative Western blot analysis. *Anal Biochem, 593*, 113608. doi:10.1016/j.ab.2020.113608

Pilliod, J., Desjardins, A., Pernegre, C., Jamann, H., Larochelle, C., Fon, E. A., & Leclerc, N. (2020). Clearance of intracellular tau protein from neuronal cells via VAMP8-induced secretion. *J Biol Chem, 295*(51), 17827-17841. doi:10.1074/jbc.RA120.013553

Pineau, H., & Sim, V. L. (2021). From Cell Culture to Organoids-Model Systems for Investigating Prion Strain Characteristics. *Biomolecules, 11*(1). doi:10.3390/biom11010106

Pocchiari, M., Puopolo, M., Croes, E. A., Budka, H., Gelpi, E., Collins, S., . . . Will, R. G. (2004). Predictors of survival in sporadic Creutzfeldt-Jakob disease and other human transmissible spongiform encephalopathies. *Brain, 127*(Pt 10), 2348-2359. doi:10.1093/brain/awh249

Poleggi, A., van der Lee, S., Capellari, S., Puopolo, M., Ladogana, A., De Pascali, E., . . . Pocchiari, M. (2018). Age at onset of genetic (E200K) and sporadic Creutzfeldt-Jakob diseases is modulated by the CYP4X1 gene. *J Neurol Neurosurg Psychiatry, 89*(12), 1243-1249. doi:10.1136/jnnp-2018-318756

Polymenidou, M., Stoeck, K., Glatzel, M., Vey, M., Bellon, A., & Aguzzi, A. (2005). Coexistence of multiple PrPSc types in individuals with Creutzfeldt-Jakob disease. *Lancet Neurol, 4*(12), 805-814. doi:10.1016/S1474-4422(05)70225-8

Prodromidou, K., Papastefanaki, F., Sklaviadis, T., & Matsas, R. (2014). Functional cross-talk between the cellular prion protein and the neural cell adhesion molecule is critical for

neuronal differentiation of neural stem/precursor cells. *Stem Cells, 32*(6), 1674-1687. doi:10.1002/stem.1663

Prusiner, S. B. (1982). Novel proteinaceous infectious particles cause scrapie. *Science, 216*(4542), 136-144. doi:10.1126/science.6801762

Prusiner, S. B. (1991). Molecular biology of prion diseases. *Science, 252*(5012), 1515-1522. doi:10.1126/science.1675487

Prusiner, S. B., Bolton, D. C., Groth, D. F., Bowman, K. A., Cochran, S. P., & McKinley, M. P. (1982). Further purification and characterization of scrapie prions. *Biochemistry, 21*(26), 6942-6950. doi:10.1021/bi00269a050

Prusiner, S. B., Cochran, S. P., Groth, D. F., Downey, D. E., Bowman, K. A., & Martinez, H. M. (1982). Measurement of the scrapie agent using an incubation time interval assay. *Ann Neurol, 11*(4), 353-358. doi:10.1002/ana.410110406

Prusiner, S. B., Groth, D. F., Bolton, D. C., Kent, S. B., & Hood, L. E. (1984). Purification and structural studies of a major scrapie prion protein. *Cell, 38*(1), 127-134. doi:10.1016/0092-8674(84)90533-6

Prusiner, S. B., Scott, M., Foster, D., Pan, K. M., Groth, D., Mirenda, C., . . . et al. (1990). Transgenetic studies implicate interactions between homologous PrP isoforms in scrapie prion replication. *Cell, 63*(4), 673-686. doi:10.1016/0092-8674(90)90134-z

Puig, B., Altmeppen, H. C., Linsenmeier, L., Chakroun, K., Wegwitz, F., Piontek, U. K., . . . Glatzel, M. (2019). GPI-anchor signal sequence influences PrP C sorting, shedding and signalling, and impacts on different pathomechanistic aspects of prion disease in mice. *PLOS Pathogens, 15*(1). doi:10.1371/journal.ppat.1007520

Purcell, S., Neale, B., Todd-Brown, K., Thomas, L., Ferreira, M. A., Bender, D., . . . Sham, P. C. (2007). PLINK: a tool set for whole-genome association and population-based linkage analyses. *Am J Hum Genet, 81*(3), 559-575. doi:10.1086/519795

Purro, S. A., Farrow, M. A., Linehan, J., Nazari, T., Thomas, D. X., Chen, Z., . . . Collinge, J. (2018). Transmission of amyloid-beta protein pathology from cadaveric pituitary growth hormone. *Nature, 564*(7736), 415-419. doi:10.1038/s41586-018-0790-y

Qi, L. S., Larson, M. H., Gilbert, L. A., Doudna, J. A., Weissman, J. S., Arkin, A. P., & Lim, W. A. (2013). Repurposing CRISPR as an RNA-guided platform for sequence-specific control of gene expression. *Cell, 152*(5), 1173-1183. doi:10.1016/j.cell.2013.02.022

Qi, X., Moore, R. A., & McGuirl, M. A. (2012). Dissociation of Recombinant Prion Protein Fibrils into Short Protofilaments: Implications for the Endocytic Pathway and Involvement of the N-Terminal Domain. *Biochemistry, 51*(22), 4600--4608. doi:10.1021/bi300201e

Qina, T., Sanjo, N., Hizume, M., Higuma, M., Tomita, M., Atarashi, R., . . . Mizusawa, H. (2014). Clinical features of genetic Creutzfeldt-Jakob disease with V180I mutation in the prion protein gene. *BMJ Open, 4*(5). doi:10.1136/bmjopen-2014-004968

Quach, H., Rotival, M., Pothlichet, J., Loh, Y. E., Dannemann, M., Zidane, N., . . . Quintana-Murci, L. (2016). Genetic Adaptation and Neandertal Admixture Shaped the Immune System of Human Populations. *Cell, 167*(3), 643-656 e617. doi:10.1016/j.cell.2016.09.024

Race, B., Meade-White, K. D., Miller, M. W., Barbian, K. D., Rubenstein, R., LaFauci, G., . . . Chesebro, B. (2009). Susceptibilities of nonhuman primates to chronic wasting disease. *Emerg Infect Dis, 15*(9), 1366-1376. doi:10.3201/eid1509.090253

Ramasamy, A., Trabzuni, D., Guelfi, S., Varghese, V., Smith, C., Walker, R., . . . Weale, M. E. (2014). Genetic variability in the regulation of gene expression in ten regions of the human brain. *Nat Neurosci, 17*(10), 1418-1428. doi:10.1038/nn.3801

Ramirez, D. M., Khvotchev, M., Trauterman, B., & Kavalali, E. T. (2012). Vti1a identifies a vesicle pool that preferentially recycles at rest and maintains spontaneous neurotransmission. *Neuron, 73*(1), 121-134. doi:10.1016/j.neuron.2011.10.034

Ren, K., Gao, C., Zhang, J., Wang, K., Xu, Y., Wang, S. B., . . . Dong, X. P. (2013). Flotillin-1 mediates PrPC endocytosis in the cultured cells during Cu2+ stimulation through molecular interaction. In (Vol. 48, pp. 631--646).

Ren, P. H., Lauckner, J. E., Kachirskaia, I., Heuser, J. E., Melki, R., & Kopito, R. R. (2009). Cytoplasmic penetration and persistent infection of mammalian cells by polyglutamine aggregates. *Nat Cell Biol, 11*(2), 219-225. doi:10.1038/ncb1830

Restelli, E., Capone, V., Pozzoli, M., Ortolan, D., Quaglio, E., Corbelli, A., . . . Chiesa, R. (2021). Activation of Src family kinase ameliorates secretory trafficking in mutant prion protein cells. *J Biol Chem, 296*, 100490. doi:10.1016/j.jbc.2021.100490

Reverter, M., Rentero, C., Garcia-Melero, A., & Hoque, M. a. (2014). Cholesterol Regulates Syntaxin 6 Trafficking at trans-Golgi Network Endosomal Boundaries. *Cell Reports*. doi:10.1016/j.celrep.2014.03.043

Richt, J. A., & Hall, S. M. (2008). BSE case associated with prion protein gene mutation. *PLoS Pathog, 4*(9), e1000156. doi:10.1371/journal.ppat.1000156

Riedel, M., Straube, A., Schwarz, M. J., Wilske, B., & Mller, N. (1998). Protective prion protein polymorphisms against sporadic Creutzfeldt-Jakob disease. *Lancet, 351*(9100), 419. doi:10.1016/s0140-6736(05)78358-6

Riek, R., Hornemann, S., Wider, G., Glockshuber, R., & Wuthrich, K. (1997). NMR characterization of the full-length recombinant murine prion protein, mPrP(23-231). *FEBS Lett, 413*(2), 282-288. doi:10.1016/s0014-5793(97)00920-4

Riemer, C., Schultz, J., Burwinkel, M., Schwarz, A., Mok, S. W., Gultner, S., . . . Baier, M. (2008). Accelerated prion replication in, but prolonged survival times of, prion-infected CXCR3-/- mice. *J Virol, 82*(24), 12464-12471. doi:10.1128/JVI.01371-08

Riggs, K. A., Hasan, N., Humphrey, D., Raleigh, C., Nevitt, C., Corbin, D., & Hu, C. (2012). Regulation of integrin endocytic recycling and chemotactic cell migration by syntaxin 6 and VAMP3 interaction. *Journal of Cell Science, 125*(16), 3827--3839. doi:10.1242/jcs.102566

Rizo, J., & Sudhof, T. C. (2002). Snares and Munc18 in synaptic vesicle fusion. *Nat Rev Neurosci, 3*(8), 641-653. doi:10.1038/nrn898

Rizzoli, S. O., Bethani, I., Zwilling, D., Wenzel, D., Siddiqui, T. J., Brandhorst, D., & Jahn, R. (2006). Evidence for early endosome-like fusion of recently endocytosed synaptic vesicles. *Traffic, 7*(9), 1163-1176. doi:10.1111/j.1600-0854.2006.00466.x

Roadmap Epigenomics Consortium, Kundaje, A., Meuleman, W., Ernst, J., Bilenky, M., Yen, A., . . . Kellis, M. (2015). Integrative analysis of 111 reference human epigenomes. *Nature, 518*(7539), 317-330. doi:10.1038/nature14248

Rogaeva, E., Meng, Y., Lee, J. H., Gu, Y., Kawarai, T., Zou, F., . . . St George-Hyslop, P. (2007). The neuronal sortilin-related receptor SORL1 is genetically associated with Alzheimer disease. *Nat Genet, 39*(2), 168-177. doi:10.1038/ng1943

Rogers, M. A., Chang, C. C. Y., Maue, R. A., Melton, E. M., Peden, A. A., Garver, W. S., . . . Chang, T.-Y. (2020). Acat1 gene KO restores TGN cholesterol deficiency in mutant NPC1 cells and expands mutant Npc1 mouse lifespan. *bioRxiv*.

Root, J., Merino, P., Nuckols, A., Johnson, M., & Kukar, T. (2021). Lysosome dysfunction as a cause of neurodegenerative diseases: Lessons from frontotemporal dementia and amyotrophic lateral sclerosis. *Neurobiol Dis, 154*, 105360. doi:10.1016/j.nbd.2021.105360

Roucou, X., Guo, Q., Zhang, Y., Goodyer, C. G., & LeBlanc, A. C. (2003). Cytosolic Prion Protein Is Not Toxic and Protects against Bax-mediated Cell Death in Human Primary Neurons. *Journal of Biological Chemistry, 278*(42), 40877--40881. doi:10.1074/jbc.M306177200

Rouvinski, A., Karniely, S., Kounin, M., Moussa, S., Goldberg, M. D., Warburg, G., . . . Taraboulos, A. (2014). Live imaging of prions reveals nascent PrPSc in cellsurface, raft-associated amyloid strings and webs. *Journal of Cell Biology, 204*(3), 423--441. doi:10.1083/jcb.201308028

Rudge, P., Jaunmuktane, Z., Adlard, P., Bjurstrom, N., Caine, D., Lowe, J., . . . Collinge, J. (2015). Iatrogenic CJD due to pituitary-derived growth hormone with genetically determined incubation times of up to 40 years. *Brain, 138*(Pt 11), 3386-3399. doi:10.1093/brain/awv235

Rydbirk, R., Folke, J., Winge, K., Aznar, S., Pakkenberg, B., & Brudek, T. (2016). Assessment of brain reference genes for RT-qPCR studies in neurodegenerative diseases. *Sci Rep, 6*, 37116. doi:10.1038/srep37116

Saborio, G. P., Permanne, B., & Soto, C. (2001). Sensitive detection of pathological prion protein by cyclic amplification of protein misfolding. *Nature, 411*(6839), 810-813. doi:10.1038/35081095

Safar, J., Wille, H., Itri, V., Groth, D., Serban, H., Torchia, M., . . . Prusiner, S. B. (1998). Eight prion strains have PrP(Sc) molecules with different conformations. *Nat Med, 4*(10), 1157-1165. doi:10.1038/2654

Salamat, M. K., Dron, M., Chapuis, J., Langevin, C., & Laude, H. (2011). Prion Propagation in Cells Expressing PrP Glycosylation Mutants. *Journal of Virology, 85*(7), 3077--3085. doi:10.1128/jvi.02257-10

Salvatore, M., Seeber, A. C., Nacmias, B., Petraroli, R., D'Alessandro, M., Sorbi, S., & Pocchiari, M. (1995). Apolipoprotein E in sporadic and familial Creutzfeldt-Jakob disease. *Neuroscience Letters, 199*(2), 95--98. doi:10.1016/0304-3940(95)12030-8

Salvesen, O., Espenes, A., Reiten, M. R., Vuong, T. T., Malachin, G., Tran, L., . . . Ersdal, C. (2020). Goats naturally devoid of PrP(C) are resistant to scrapie. *Vet Res, 51*(1), 1. doi:10.1186/s13567-019-0731-2

Sanchez-Contreras, M. Y., Kouri, N., Cook, C. N., Serie, D. J., Heckman, M. G., Finch, N. A., . . . Ross, O. A. (2018). Replication of progressive supranuclear palsy genome-wide association study identifies SLCO1A2 and DUSP10 as new susceptibility loci. *Molecular Neurodegeneration, 13*(1). doi:10.1186/s13024-018-0267-3

Sanchez-Juan, P., Bishop, M. T., Aulchenko, Y. S., Brandel, J. P., Rivadeneira, F., Struchalin, M., . . . van Duijn, C. M. (2012). Genome-wide study links MTMR7 gene to variant Creutzfeldt-Jakob risk. *Neurobiol Aging, 33*(7), 1487 e1421-1488. doi:10.1016/j.neurobiolaging.2011.10.011

Sanchez-Juan, P., Bishop, M. T., Kovacs, G. G., Calero, M., Aulchenko, Y. S., Ladogana, A., . . . van Duijn, C. M. (2014). A genome wide association study links glutamate receptor

pathway to sporadic Creutzfeldt-Jakob disease risk. *PLoS ONE, 10*(4), e0123654. doi:10.1371/journal.pone.0123654

Sandberg, M. K., Al-Doujaily, H., Sharps, B., Clarke, A. R., & Collinge, J. (2011). Prion propagation and toxicity in vivo occur in two distinct mechanistic phases. *Nature, 470*(7335), 540-542. doi:10.1038/nature09768

Sandberg, M. K., Al-Doujaily, H., Sharps, B., De Oliveira, M. W., Schmidt, C., Richard-Londt, A., . . . Collinge, J. (2014). Prion neuropathology follows the accumulation of alternate prion protein isoforms after infective titre has peaked. *Nat Commun, 5*(May), 4347. doi:10.1038/ncomms5347

Sandberg, M. K., Al-Doujaily, H., Sigurdson, C. J., Glatzel, M., O'Malley, C., Powell, C., . . . Collinge, J. (2010). Chronic wasting disease prions are not transmissible to transgenic mice overexpressing human prion protein. *J Gen Virol, 91*(Pt 10), 2651-2657. doi:10.1099/vir.0.024380-0

Santuccione, A., Sytnyk, V., Leshchyns'ka, I., & Schachner, M. (2005). Prion protein recruits its neuronal receptor NCAM to lipid rafts to activate p59fyn and to enhance neurite outgrowth. *J Cell Biol, 169*(2), 341-354. doi:10.1083/jcb.200409127

Sarnataro, D., Campana, V., Paladino, S., Stornaiuolo, M., Nitsch, L., & Zurzolo, C. (2004). PrP(C) association with lipid rafts in the early secretory pathway stabilizes its cellular conformation. *Mol Biol Cell, 15*(9), 4031-4042. doi:10.1091/mbc.e03-05-0271

Sarnataro, D., Caputo, A., Casanova, P., Puri, C., Paladino, S., Tivodar, S. S., . . . Zurzolo, C. (2009). Lipid rafts and clathrin cooperate in the internalization of PrP in epithelial FRT cells. *PLoS ONE, 4*(6), e5829. doi:10.1371/journal.pone.0005829

Sarnataro, D., Paladino, S., Campana, V., Grassi, J., Nitsch, L., & Zurzolo, C. (2002). PrPC is sorted to the basolateral membrane of epithelial cells independently of its association with rafts. *Traffic, 3*(11), 810-821. doi:10.1034/j.1600-0854.2002.31106.x

Sarnataro, D., Pepe, A., & Zurzolo, C. (2017). Cell Biology of Prion Protein. *Prog Mol Biol Transl Sci, 150*, 57-82. doi:10.1016/bs.pmbts.2017.06.018

Satpute-Krishnan, P., Ajinkya, M., Bhat, S., Itakura, E., Hegde, R. S., & Lippincott-Schwartz, J. (2014). ER stress-induced clearance of misfolded GPI-anchored proteins via the secretory pathway. *Cell, 158*(3), 522-533. doi:10.1016/j.cell.2014.06.026

Schaid, D. J., Chen, W., & Larson, N. B. (2018). From genome-wide associations to candidate causal variants by statistical fine-mapping. *Nat Rev Genet, 19*(8), 491-504. doi:10.1038/s41576-018-0016-z

Schindler, C., Chen, Y., Pu, J., Guo, X., & Bonifacino, J. S. (2015). EARP is a multisubunit tethering complex involved in endocytic recycling. *Nature Cell Biology, 17*(5), 639--650. doi:10.1038/ncb3129

Schmiedel, B. J., Singh, D., Madrigal, A., Valdovino-Gonzalez, A. G., White, B. M., Zapardiel-Gonzalo, J., . . . Vijayanand, P. (2018). Impact of Genetic Polymorphisms on Human Immune Cell Gene Expression. *Cell, 175*(6), 1701-1715 e1716. doi:10.1016/j.cell.2018.10.022

Schmitt-Ulms, G., Ehsani, S., Watts, J. C., Westaway, D., & Wille, H. (2009). Evolutionary Descent of Prion Genes from the ZIP Family of Metal Ion Transporters. *PLoS ONE, 4*(9), e7208. doi:10.1371/journal.pone.0007208

Schneider, B., Mutel, V., Pietri, M., Ermonval, M., Mouillet-Richard, S., & Kellermann, O. (2003). NADPH oxidase and extracellular regulated kinases 1/2 are targets of prion protein

signaling in neuronal and nonneuronal cells. *Proc Natl Acad Sci U S A, 100*(23), 13326-13331. doi:10.1073/pnas.2235648100

Scialo, C., Celauro, L., Zattoni, M., Tran, T. H., Bistaffa, E., Moda, F., . . . Legname, G. (2021). The Cellular Prion Protein Increases the Uptake and Toxicity of TDP-43 Fibrils. *Viruses, 13*(8). doi:10.3390/v13081625

Scott-McKean, J. J., Surewicz, K., Choi, J. K., Ruffin, V. A., Salameh, A. I., Nieznanski, K., . . . Surewicz, W. K. (2016). Soluble prion protein and its N-terminal fragment prevent impairment of synaptic plasticity by Abeta oligomers: Implications for novel therapeutic strategy in Alzheimer's disease. *Neurobiol Dis, 91*, 124-131. doi:10.1016/j.nbd.2016.03.001

Shaimardanova, A. A., Chulpanova, D. S., Solovyeva, V. V., Mullagulova, A. I., Kitaeva, K. V., Allegrucci, C., & Rizvanov, A. A. (2020). Metachromatic Leukodystrophy: Diagnosis, Modeling, and Treatment Approaches. *Front Med (Lausanne), 7*, 576221. doi:10.3389/fmed.2020.576221

Shi, Y., Kirwan, P., & Livesey, F. J. (2012). Directed differentiation of human pluripotent stem cells to cerebral cortex neurons and neural networks. *Nat Protoc, 7*(10), 1836-1846. doi:10.1038/nprot.2012.116

Shim, S. Y., Karri, S., Law, S., Schatzl, H. M., & Gilch, S. (2016). Prion infection impairs lysosomal degradation capacity by interfering with rab7 membrane attachment in neuronal cells. *Scientific Reports, 6*(1), 21658. doi:10.1038/srep21658

Shitara, A., Shibui, T., Okayama, M., Arakawa, T., Mizoguchi, I., Shakakura, Y., & Takuma, T. (2013). VAMP4 is required to maintain the ribbon structure of the Golgi apparatus. *Molecular and Cellular Biochemistry, 380*(1-2), 11--21. doi:10.1007/s11010-013-1652-4

Shou, Y., Liang, F., Xu, S., & Li, X. (2020). The Application of Brain Organoids: From Neuronal Development to Neurological Diseases. *Front Cell Dev Biol, 8*, 579659. doi:10.3389/fcell.2020.579659

Shyng, S. L., Heuser, J. E., & Harris, D. A. (1994). A glycolipid-anchored prion protein is endocytosed via clathrin-coated pits. *Journal of Cell Biology, 125*(6), 1239--1250. doi:10.1083/jcb.125.6.1239

Shyng, S. L., Huber, M. T., & Harris, D. A. (1993). A prion protein cycles between the cell surface and an endocytic compartment in cultured neuroblastoma cells. *The Journal of Biological Chemistry, 268*(21), 15922--15928.

Sigurdsson, B. (1954). RIDA, A Chronic Encephalitis of Sheep: With General Remarks on Infections Which Develop Slowly and Some of Their Special Characteristics. *British Veterinary Journal, 110*(9), 341-354. doi:https://doi.org/10.1016/S0007-1935(17)50172-4

Simonsen, A., Gaullier, J. M., D'Arrigo, A., & Stenmark, H. (1999). The Rab5 effector EEA1 interacts directly with syntaxin-6. *Journal of Biological Chemistry, 274*(41), 28857--28860. doi:10.1074/jbc.274.41.28857

Skedsmo, F. S., Malachin, G., Vage, D. I., Hammervold, M. M., Salvesen, O., Ersdal, C., . . . Tranulis, M. A. (2020). Demyelinating polyneuropathy in goats lacking prion protein. *FASEB J, 34*(2), 2359-2375. doi:10.1096/fj.201902588R

Skibinski, G., Parkinson, N. J., Brown, J. M., Chakrabarti, L., Lloyd, S. L., Hummerich, H., . . . Collinge, J. (2005). Mutations in the endosomal ESCRTIII-complex subunit CHMP2B in frontotemporal dementia. *Nat Genet, 37*(8), 806-808. doi:10.1038/ng1609

Slapsak, U., Salzano, G., Amin, L., Abskharon, R. N., Ilc, G., Zupancic, B., . . . Legname, G. (2016). The N Terminus of the Prion Protein Mediates Functional Interactions with the

Neuronal Cell Adhesion Molecule (NCAM) Fibronectin Domain. *J Biol Chem, 291*(42), 21857-21868. doi:10.1074/jbc.M116.743435

Smolders, S., & Van Broeckhoven, C. (2020). Genetic perspective on the synergistic connection between vesicular transport, lysosomal and mitochondrial pathways associated with Parkinson's disease pathogenesis. *Acta Neuropathol Commun, 8*(1), 63. doi:10.1186/s40478-020-00935-4

Sollner, T., Whiteheart, S. W., Brunner, M., Erdjument-Bromage, H., Geromanos, S., Tempst, P., & Rothman, J. E. (1993). SNAP receptors implicated in vesicle targeting and fusion. *Nature, 362*(6418), 318-324. doi:10.1038/362318a0

Spain, S. L., & Barrett, J. C. (2015). Strategies for fine-mapping complex traits. *Hum Mol Genet, 24*(R1), R111-119. doi:10.1093/hmg/ddv260

Stahl, N., Borchelt, D. R., Hsiao, K., & Prusiner, S. B. (1987). Scrapie prion protein contains a phosphatidylinositol glycolipid. *Cell, 51*(2), 229--240.

Steegmaier, M., Klumperman, J., Foletti, D. L., Yoo, J. S., & Scheller, R. H. (1999). Vesicle-associated membrane protein 4 is implicated in trans-Golgi network vesicle trafficking. *Molecular Biology of the Cell, 10*(6), 1957--1972.

Stockman, S. (1913). Scrapie: an obscure disease of sheep. *Journal of Comparative Pathology and Therapeutics, 26*, 317-327.

Strang, K. H., Golde, T. E., & Giasson, B. I. (2019). MAPT mutations, tauopathy, and mechanisms of neurodegeneration. *Lab Invest, 99*(7), 912-928. doi:10.1038/s41374-019-0197-x

Studer, L., Vera, E., & Cornacchia, D. (2015). Programming and Reprogramming Cellular Age in the Era of Induced Pluripotency. *Cell Stem Cell, 16*(6), 591-600. doi:10.1016/j.stem.2015.05.004

Suga, K., Saito, A., Mishima, T., & Akagawa, K. (2015). ER and Golgi stresses increase ER-Golgi SNARE Syntaxin5: Implications for organelle stress and betaAPP processing. *Neurosci Lett, 604*, 30-35. doi:10.1016/j.neulet.2015.07.017

Sunyach, C., Jen, A., Deng, J., Fitzgerald, K. T., Frobert, Y., Grassi, J., . . . Morris, R. (2003). The mechanism of internalization of glycosylphosphatidylinositol-anchored prion protein. *EMBO Journal, 22*(14), 3591--3601. doi:10.1093/emboj/cdg344

Takahashi, K., Tanabe, K., Ohnuki, M., Narita, M., Ichisaka, T., Tomoda, K., & Yamanaka, S. (2007). Induction of pluripotent stem cells from adult human fibroblasts by defined factors. *Cell, 131*(5), 861-872. doi:10.1016/j.cell.2007.11.019

Takahashi, K., & Yamanaka, S. (2006). Induction of pluripotent stem cells from mouse embryonic and adult fibroblast cultures by defined factors. *Cell, 126*(4), 663-676. doi:10.1016/j.cell.2006.07.024

Tam, V., Patel, N., Turcotte, M., & Boss. (2019). Benefits and limitations of genome-wide association studies. *Nature Reviews Genetics, 20*(8), 467--484. doi:10.1038/s41576-019-0127-1

Tamgney, G., Giles, K., Glidden, D. V., Lessard, P., Wille, H., Tremblay, P., . . . Prusiner, S. B. (2008). Genes contributing to prion pathogenesis. *Journal of General Virology, 89*(7), 1777--1778. doi:10.1099/vir.0.2008/001255-0

Taraboulos, A., Scott, M., Semenov, A., Avrahami, D., Laszlo, L., & Prusiner, S. B. (1995). Cholesterol depletion and modification of COOH-terminal targeting sequence of the prion protein inhibit formation of the scrapie isoform. *J Cell Biol, 129*(1), 121-132. doi:10.1083/jcb.129.1.121

Taraboulos, A., Serban, D., & Prusiner, S. B. (1990). Scrapie prion proteins accumulate in the cytoplasm of persistently infected cultured cells. *J Cell Biol, 110*(6), 2117-2132. doi:10.1083/jcb.110.6.2117

Terry, C., Harniman, R. L., Sells, J., Wenborn, A., Joiner, S., Saibil, H. R., . . . Wadsworth, J. D. F. (2019). Structural features distinguishing infectious ex vivo mammalian prions from non-infectious fibrillar assemblies generated in vitro. *Sci Rep, 9*(1), 376. doi:10.1038/s41598-018-36700-w

Terry, C., & Wadsworth, J. D. F. (2019). Recent Advances in Understanding Mammalian Prion Structure: A Mini Review. *Front Mol Neurosci, 12*, 169. doi:10.3389/fnmol.2019.00169

Terry, C., Wenborn, A., Gros, N., Sells, J., Joiner, S., Hosszu, L. L., . . . Wadsworth, J. D. (2016). Ex vivo mammalian prions are formed of paired double helical prion protein fibrils. *Open Biol, 6*(5). doi:10.1098/rsob.160035

Thackray, A. M., Hopkins, L., Klein, M. A., & Bujdoso, R. (2007). Mouse-adapted ovine scrapie prion strains are characterized by different conformers of PrPSc. *J Virol, 81*(22), 12119-12127. doi:10.1128/JVI.01434-07

Thackray, A. M., McKenzie, A. N., Klein, M. A., Lauder, A., & Bujdoso, R. (2004). Accelerated prion disease in the absence of interleukin-10. *J Virol, 78*(24), 13697-13707. doi:10.1128/JVI.78.24.13697-13707.2004

Thellung, S., Scoti, B., Corsaro, A., Villa, V., Nizzari, M., Gagliani, M. C., . . . Florio, T. (2018). Pharmacological activation of autophagy favors the clearing of intracellular aggregates of misfolded prion protein peptide to prevent neuronal death. *Cell Death Dis, 9*(2), 166. doi:10.1038/s41419-017-0252-8

Thompson, a. G. B., Uphill, J., Lowe, J., Porter, M. C., Lukic, a., Carswell, C., . . . Mead, S. (2015). Genome-wide association study of behavioural and psychiatric features in human prion disease. *Translational psychiatry, 5*(4), e552. doi:10.1038/tp.2015.42

Tiwari, A., Jung, J. J., Inamdar, S. M., Brown, C. O., Goel, A., & Choudhury, A. (2011). Endothelial cell migration on fibronectin is regulated by syntaxin 6-mediated alpha5beta1 integrin recycling. *J Biol Chem, 286*(42), 36749-36761. doi:10.1074/jbc.M111.260828

Torres, M., Medinas, D. B., Matamala, J. M., Woehlbier, U., Cornejo, V. H., Solda, T., . . . Hetz, C. (2015). The Protein-disulfide Isomerase ERp57 Regulates the Steady-state Levels of the Prion Protein. *J Biol Chem, 290*(39), 23631-23645. doi:10.1074/jbc.M114.635565

Tremblay, P., Bouzamondo-Bernstein, E., Heinrich, C., Prusiner, S. B., & DeArmond, S. J. (2007). Developmental expression of PrP in the post-implantation embryo. *Brain Res, 1139*, 60-67. doi:10.1016/j.brainres.2006.12.055

Tribouillard-Tanvier, D., Race, B., Striebel, J. F., Carroll, J. A., Phillips, K., & Chesebro, B. (2012). Early cytokine elevation, PrPres deposition, and gliosis in mouse scrapie: no effect on disease by deletion of cytokine genes IL-12p40 and IL-12p35. *J Virol, 86*(19), 10377-10383. doi:10.1128/JVI.01340-12

Tsangaras, K., Kolokotronis, S. O., Ulrich, R. G., Morand, S., Michaux, J., & Greenwood, A. D. (2014). Negative purifying selection drives prion and doppel protein evolution. *J Mol Evol, 79*(1-2), 12-20. doi:10.1007/s00239-014-9632-1

Uchiyama, K., Muramatsu, N., Yano, M., Usui, T., Miyata, H., & Sakaguchi, S. (2013). Prions disturb post-Golgi trafficking of membrane proteins. *Nature Communications, 4*(1), 1846. doi:10.1038/ncomms2873

Uchiyama, K., Tomita, M., Yano, M., Chida, J., Hara, H., Das, N. R., . . . Sakaguchi, S. (2017). Prions amplify through degradation of the VPS10P sorting receptor sortilin. *PLOS Pathogens, 13*(6), e1006470. doi:10.1371/journal.ppat.1006470

Uffelmann, E., Huang, Q. Q., Munung, N. S., de Vries, J., Okada, Y., Martin, A. R., . . . Posthuma, D. (2021). Genome-wide association studies. *Nature Reviews Methods Primers, 1*(1), 59. doi:10.1038/s43586-021-00056-9

Urano, Y., Watanabe, H., Murphy, S. R., Shibuya, Y., Geng, Y., Peden, A. A., . . . Chang, T. Y. (2008). Transport of LDL-derived cholesterol from the NPC1 compartment to the ER involves the trans-Golgi network and the SNARE protein complex. *Proceedings of the National Academy of Sciences, 105*(43), 16513--16518. doi:10.1073/pnas.0807450105

Van Deerlin, V. M., Sleiman, P. M., Martinez-Lage, M., Chen-Plotkin, A., Wang, L. S., Graff-Radford, N. R., . . . Lee, V. M. (2010). Common variants at 7p21 are associated with frontotemporal lobar degeneration with TDP-43 inclusions. *Nat Genet, 42*(3), 234-239. doi:10.1038/ng.536

Vaquer-Alicea, J., Diamond, M. I., & Joachimiak, L. A. (2021). Tau strains shape disease. *Acta Neuropathol, 142*(1), 57-71. doi:10.1007/s00401-021-02301-7

Varkey, J., Isas, J. M., Mizuno, N., Jensen, M. B., Bhatia, V. K., Jao, C. C., . . . Langen, R. (2010). Membrane curvature induction and tubulation are common features of synucleins and apolipoproteins. *J Biol Chem, 285*(42), 32486-32493. doi:10.1074/jbc.M110.139576

Veith, N. M., Plattner, H., Stuermer, C. A., Schulz-Schaeffer, W. J., & Burkle, A. (2009). Immunolocalisation of PrPSc in scrapie-infected N2a mouse neuroblastoma cells by light and electron microscopy. *Eur J Cell Biol, 88*(1), 45-63. doi:10.1016/j.ejcb.2008.08.001

Vella, L. J., Hill, A. F., & Cheng, L. (2016). Focus on Extracellular Vesicles: Exosomes and Their Role in Protein Trafficking and Biomarker Potential in Alzheimer's and Parkinson's Disease. *Int J Mol Sci, 17*(2), 173. doi:10.3390/ijms17020173

Vey, M., Pilkuhn, S., Wille, H., Nixon, R., DeArmond, S. J., Smart, E. J., . . . Prusiner, S. B. (1996). Subcellular colocalization of the cellular and scrapie prion proteins in caveolae-like membranous domains. *Proceedings of the National Academy of Sciences of the United States of America, 93*(25), 14945--14949. doi:10.1073/pnas.93.25.14945

Victoria, G. S., & Zurzolo, C. (2017). The spread of prion-like proteins by lysosomes and tunneling nanotubes: Implications for neurodegenerative diseases. *The Journal of Cell Biology*, jcb.201701047. doi:10.1083/jcb.201701047

Vilarino-Guell, C., Wider, C., Ross, O. A., Dachsel, J. C., Kachergus, J. M., Lincoln, S. J., . . . Farrer, M. J. (2011). VPS35 mutations in Parkinson disease. *Am J Hum Genet, 89*(1), 162-167. doi:10.1016/j.ajhg.2011.06.001

Vilette, D., Andreoletti, O., Archer, F., Madelaine, M. F., Vilotte, J. L., Lehmann, S., & Laude, H. (2001). Ex vivo propagation of infectious sheep scrapie agent in heterologous epithelial cells expressing ovine prion protein. *Proc Natl Acad Sci U S A, 98*(7), 4055-4059. doi:10.1073/pnas.061337998

Võsa, U., Claringbould, A., Westra, H.-J., Bonder, M. J., Deelen, P., Zeng, B., . . . Franke, L. (2018). Unraveling the polygenic architecture of complex traits using blood eQTL metaanalysis. *bioRxiv*.

Wadsworth, J. D. F., Asante, E. A., Desbruslais, M., Linehan, J. M., Joiner, S., Gowland, I., . . . Collinge, J. (2004). Human prion protein with valine 129 prevents expression of variant CJD phenotype. *Science, 306*(5702), 1793-1796. doi:10.1126/science.1103932

Wadsworth, J. D. F., Joiner, S., Linehan, J. M., Jack, K., Al-Doujaily, H., Costa, H., . . . Collinge, J. (2021). Humanised transgenic mice are resistant to chronic wasting disease prions from Norwegian reindeer and moose. *J Infect Dis*. doi:10.1093/infdis/jiab033

Walmsley, A. R., Zeng, F., & Hooper, N. M. (2001). Membrane topology influences N-glycosylation of the prion protein. *EMBO J, 20*(4), 703-712. doi:10.1093/emboj/20.4.703

Wang, D., Liu, S., Warrell, J., Won, H., Shi, X., Navarro, F. C. P., . . . Gerstein, M. B. (2018). Comprehensive functional genomic resource and integrative model for the human brain. *Science, 362*(6420). doi:10.1126/science.aat8464

Wang, G., Zhou, X., Bai, Y., Zhang, Z., & Zhao, D. (2010). Cellular prion protein released on exosomes from macrophages binds to Hsp70. *Acta Biochim Biophys Sin (Shanghai), 42*(5), 345-350. doi:10.1093/abbs/gmq028

Wang, G. H., Zhou, X. M., Bai, Y., Yin, X. M., Yang, L. F., & Zhao, D. (2011). Hsp70 binds to PrPC in the process of PrPC release via exosomes from THP-1 monocytes. *Cell Biol Int, 35*(6), 553-558. doi:10.1042/CBI20090391

Wang, K., Li, M., & Hakonarson, H. (2010). ANNOVAR: functional annotation of genetic variants from high-throughput sequencing data. *Nucleic Acids Res, 38*(16), e164. doi:10.1093/nar/gkq603

Wang, X., Huang, T., Bu, G., & Xu, H. (2014). Dysregulation of protein trafficking in neurodegeneration. *Mol Neurodegener, 9*, 31. doi:10.1186/1750-1326-9-31

Watanabe, K., Taskesen, E., van Bochoven, A., & Posthuma, D. (2017). Functional mapping and annotation of genetic associations with FUMA. *Nat Commun, 8*(1), 1826. doi:10.1038/s41467-017-01261-5

Watson, R. T., Hou, J. C., & Pessin, J. E. (2008). Recycling of IRAP from the plasma membrane back to the insulin-responsive compartment requires the Q-SNARE syntaxin 6 but not the GGA clathrin adaptors. *J Cell Sci, 121*(Pt 8), 1243-1251. doi:10.1242/jcs.017517

Watson, R. T., & Pessin, J. E. (2000). Functional cooperation of two independent targeting domains in syntaxin 6 is required for its efficient localization in the trans-golgi network of 3T3L1 adipocytes. *The Journal of Biological Chemistry, 275*(2), 1261--1268. doi:10.1074/JBC.275.2.1261

Watts, J. C., Bourkas, M. E. C., & Arshad, H. (2018). The function of the cellular prion protein in health and disease. *Acta Neuropathol, 135*(2), 159-178. doi:10.1007/s00401-017-1790-y

Watts, J. C., Giles, K., Bourkas, M. E., Patel, S., Oehler, A., Gavidia, M., . . . Prusiner, S. B. (2016). Towards authentic transgenic mouse models of heritable PrP prion diseases. *Acta Neuropathol, 132*(4), 593-610. doi:10.1007/s00401-016-1585-6

Watts, J. C., Huo, H., Bai, Y., Ehsani, S., Jeon, A. H., Shi, T., . . . Schmitt-Ulms, G. (2009). Interactome analyses identify ties of PrP and its mammalian paralogs to oligomannosidic N-glycans and endoplasmic reticulum-derived chaperones. *PLoS Pathog, 5*(10), e1000608. doi:10.1371/journal.ppat.1000608

Weimbs, T., Low, S. H., Chapin, S. J., Mostov, K. E., Bucher, P., & Hofmann, K. (1997). A conserved domain is present in different families of vesicular fusion proteins: a new superfamily. *Proc Natl Acad Sci U S A, 94*(7), 3046-3051. doi:10.1073/pnas.94.7.3046

Weissmann, C., & Aguzzi, A. (1999). Perspectives: neurobiology. PrP's double causes trouble. *Science, 286*(5441), 914-915. doi:10.1126/science.286.5441.914

Wenborn, A., Terry, C., Gros, N., Joiner, S., D'Castro, L., Panico, S., . . . Wadsworth, J. D. (2015). A novel and rapid method for obtaining high titre intact prion strains from mammalian brain. *Sci Rep, 5*(1), 10062. doi:10.1038/srep10062

Wendler, F., Page, L., & Urb. (2001). Homotypic Fusion of Immature Secretory Granules During Maturation Requires Syntaxin 6. *Molecular Biology of the Cell*. doi:10.1091/mbc.12.6.1699

Westaway, D., Goodman, P. A., Mirenda, C. A., McKinley, M. P., Carlson, G. A., & Prusiner, S. B. (1987). Distinct prion proteins in short and long scrapie incubation period mice. *Cell, 51*(4), 651-662. doi:10.1016/0092-8674(87)90134-6

Westra, H. J., Peters, M. J., Esko, T., Yaghootkar, H., Schurmann, C., Kettunen, J., . . . Franke, L. (2013). Systematic identification of trans eQTLs as putative drivers of known disease associations. *Nat Genet, 45*(10), 1238-1243. doi:10.1038/ng.2756

Wilesmith, J. W., Wells, G. A., Cranwell, M. P., & Ryan, J. B. (1988). Bovine spongiform encephalopathy: epidemiological studies. *Vet Rec, 123*(25), 638-644.

Wilhelm, B. G., Mandad, S., Truckenbrodt, S., Krohnert, K., Schafer, C., Rammner, B., . . . Rizzoli, S. O. (2014). Composition of isolated synaptic boutons reveals the amounts of vesicle trafficking proteins. *Science, 344*(6187), 1023-1028. doi:10.1126/science.1252884

Will, R. G., Ironside, J. W., Zeidler, M., Cousens, S. N., Estibeiro, K., Alperovitch, A., . . . Smith, P. G. (1996). A new variant of Creutzfeldt-Jakob disease in the UK. *Lancet, 347*(9006), 921--925. doi:10.1016/S0140-6736(96)91412-9

Willett, R., Kudlyk, T., Pokrovskaya, I., Schnherr, R., Ungar, D., Duden, R., & Lupashin, V. (2013). COG complexes form spatial landmarks for distinct SNARE complexes. *Nature Communications, 4*. doi:10.1038/ncomms2535

Williams, E. S., & Young, S. (1980). Chronic wasting disease of captive mule deer: a spongiform encephalopathy. *J Wildl Dis, 16*(1), 89-98. doi:10.7589/0090-3558-16.1.89

Wingo, A. P., Liu, Y., Gerasimov, E. S., Gockley, J., Logsdon, B. A., Duong, D. M., . . . Wingo, T. S. (2021). Integrating human brain proteomes with genome-wide association data implicates new proteins in Alzheimer's disease pathogenesis. *Nat Genet, 53*(2), 143-146. doi:10.1038/s41588-020-00773-z

Wopfner, F., Weidenhofer, G., Schneider, R., von Brunn, A., Gilch, S., Schwarz, T. F., . . . Schatzl, H. M. (1999). Analysis of 27 mammalian and 9 avian PrPs reveals high conservation of flexible regions of the prion protein. *J Mol Biol, 289*(5), 1163-1178. doi:10.1006/jmbi.1999.2831

Xiang, W., Windl, O., Wunsch, G., Dugas, M., Kohlmann, A., Dierkes, N., . . . Kretzschmar, H. A. (2004). Identification of differentially expressed genes in scrapie-infected mouse brains by using global gene expression technology. *J Virol, 78*(20), 11051-11060. doi:10.1128/JVI.78.20.11051-11060.2004

Xu, Y., Wong, S. H., Tang, B. L., Subramaniam, V. N., Zhang, T., & Hong, W. (1998). A 29-kilodalton Golgi soluble N-ethylmaleimide-sensitive factor attachment protein receptor (Vti1-rp2) implicated in protein trafficking in the secretory pathway. *J Biol Chem, 273*(34), 21783-21789. doi:10.1074/jbc.273.34.21783

Yamasaki, T., Baron, G. S., Suzuki, A., Hasebe, R., & Horiuchi, M. (2014). Characterization of intracellular dynamics of inoculated PrP-res and newly generated PrPSc during early stage prion infection in Neuro2a cells. *Virology, 450-451*, 324--335. doi:10.1016/j.virol.2013.11.007

Yamasaki, T., Suzuki, A., Hasebe, R., & Horiuchi, M. (2018). Retrograde Transport by Clathrin-Coated Vesicles is Involved in Intracellular Transport of PrPSc in Persistently Prion-Infected Cells. *Scientific Reports, 8*(1), 12241. doi:10.1038/s41598-018-30775-1

Yamasaki, T., Suzuki, A., Shimizu, T., Watarai, M., Hasebe, R., & Horiuchi, M. (2012). Characterization of intracellular localization of PrP Sc in prion-infected cells using a mAb that recognizes the region consisting of aa 119-127 of mouse PrP. *Journal of General Virology, 93*(3), 668--680. doi:10.1099/vir.0.037101-0

Yang, Y., Kim, J., Kim, H. Y., Ryoo, N., Lee, S., Kim, Y., . . . Shin, Y. K. (2015). Amyloid-beta Oligomers May Impair SNARE-Mediated Exocytosis by Direct Binding to Syntaxin 1a. *Cell Rep, 12*(8), 1244-1251. doi:10.1016/j.celrep.2015.07.044

Yim, Y.-I., Park, B.-C., Yadavalli, R., Zhao, X., Eisenberg, E., & Greene, L. E. (2015). The multivesicular body is the major internal site of prion conversion. *Journal of Cell Science, 128*(7), 1434--1443. doi:10.1242/jcs.165472

Zafar, S., von Ahsen, N., Oellerich, M., Zerr, I., Schulz-Schaeffer, W. J., Armstrong, V. W., & Asif, A. R. (2011). Proteomics approach to identify the interacting partners of cellular prion protein and characterization of Rab7a interaction in neuronal cells. *J Proteome Res, 10*(7), 3123-3135. doi:10.1021/pr2001989

Zafar, S., Younas, N., Correia, S., Shafiq, M., Tahir, W., Schmitz, M., . . . Zerr, I. (2017). Strain-Specific Altered Regulatory Response of Rab7a and Tau in Creutzfeldt-Jakob Disease and Alzheimer's Disease. *Mol Neurobiol, 54*(1), 697-709. doi:10.1007/s12035-016-9694-8

Zahn, R., Liu, A., Luhrs, T., Riek, R., von Schroetter, C., Lopez Garcia, F., . . . Wuthrich, K. (2000). NMR solution structure of the human prion protein. *Proc Natl Acad Sci U S A, 97*(1), 145-150. doi:10.1073/pnas.97.1.145

Zavodszky, E., & Hegde, R. S. (2019). Misfolded GPI-anchored proteins are escorted through the secretory pathway by ER-derived factors. *Elife, 8*. doi:10.7554/eLife.46740

Zerr, I., Giese, A., Windl, O., Kropp, S., Schulz-Schaeffer, W., Riedemann, C., . . . Poser, S. (1998). Phenotypic variability in fatal familial insomnia (D178N-129M) genotype. *Neurology, 51*(5), 1398--1405. doi:10.1212/WNL.51.5.1398

Zerr, I., Kallenberg, K., Summers, D. M., Romero, C., Taratuto, A., Heinemann, U., . . . Sanchez-Juan, P. (2009). Updated clinical diagnostic criteria for sporadic Creutzfeldt-Jakob disease. *Brain, 132*(10), 2659--2668. doi:10.1093/brain/awp191

Zhang, C., De Koning, D. J., Hernandez-Sanchez, J., Haley, C. S., Williams, J. L., & Wiener, P. (2004). Mapping of multiple quantitative trait loci affecting bovine spongiform encephalopathy. *Genetics, 167*(4), 1863-1872. doi:10.1534/genetics.104.026401

Zhang, H., Therriault, J., Kang, M. S., Ng, K. P., Pascoal, T. A., Rosa-Neto, P., . . . Alzheimer's Disease Neuroimaging, I. (2018). Cerebrospinal fluid synaptosomal-associated protein 25 is a key player in synaptic degeneration in mild cognitive impairment and Alzheimer's disease. *Alzheimers Res Ther, 10*(1), 80. doi:10.1186/s13195-018-0407-6

Zhang, Y., Shu, L., & Chen, X. (2008). Syntaxin 6, a regulator of the protein trafficking machinery and a target of the p53 family, is required for cell adhesion and survival. *The Journal of Biological Chemistry, 283*(45), 30689--30698. doi:10.1074/jbc.M801711200

Zhao, B., Luo, T., Li, T., Li, Y., Zhang, J., Shan, Y., . . . Zhu, H. (2019). Genome-wide association analysis of 19,629 individuals identifies variants influencing regional brain volumes and refines their genetic co-architecture with cognitive and mental health traits. *Nat Genet, 51*(11), 1637-1644. doi:10.1038/s41588-019-0516-6

Zhernakova, D. V., Deelen, P., Vermaat, M., van Iterson, M., van Galen, M., Arindrarto, W., . . . Franke, L. (2017). Identification of context-dependent expression quantitative trait loci in whole blood. *Nat Genet, 49*(1), 139-145. doi:10.1038/ng.3737

Zhou, X., Fu, A. K., & Ip, N. Y. (2021). APOE signaling in neurodegenerative diseases: an integrative approach targeting APOE coding and noncoding variants for disease intervention. *Curr Opin Neurobiol, 69*, 58-67. doi:10.1016/j.conb.2021.02.001

Zhu, L., Xiong, X., Kim, Y., Okada, N., Lu, F., Zhang, H., & Sun, H. (2016). Acid sphingomyelinase is required for cell surface presentation of Met receptor tyrosine kinase in cancer cells. *J Cell Sci, 129*(22), 4238-4251. doi:10.1242/jcs.191684

Zimprich, A., Biskup, S., Leitner, P., Lichtner, P., Farrer, M., Lincoln, S., . . . Gasser, T. (2004). Mutations in LRRK2 cause autosomal-dominant parkinsonism with pleomorphic pathology. *Neuron, 44*(4), 601-607. doi:10.1016/j.neuron.2004.11.005

Zlotnik, I., & Rennie, J. C. (1963). Further observations on the experimental transmission of scrapie from sheep and goats to laboratory mice. *J Comp Pathol, 73*, 150-162. doi:10.1016/s0368-1742(63)80018-1